Gina Bjerkan

Master's thesis

NTNU
Norwegian University of Science and Technology
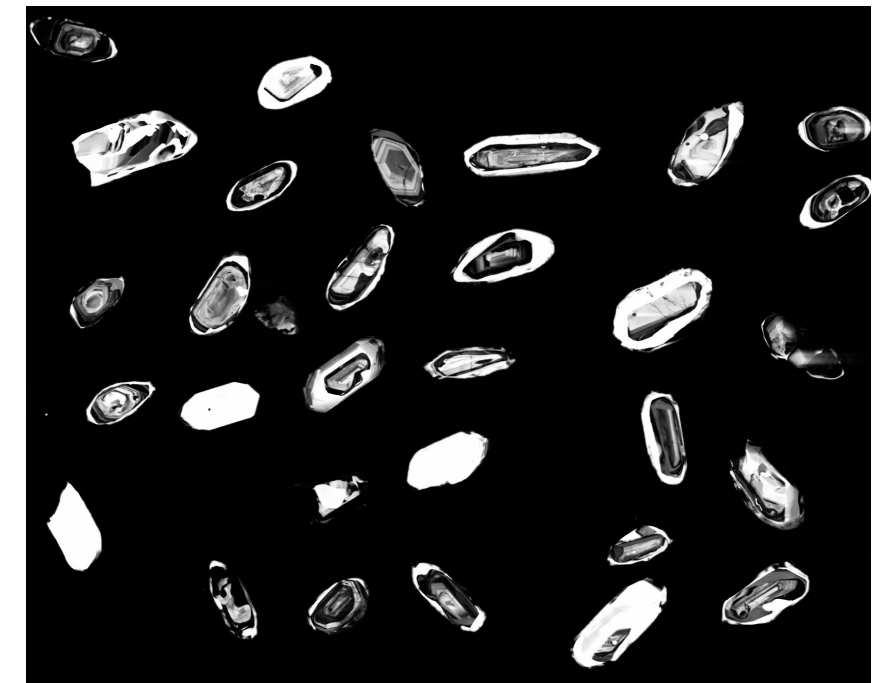Faculty of Engineering
Department of Geoscience and Petroleum

Gina Bjerkan

Zircon U-Pb geochronology and whole-rock geochemistry of migmatitic gneisses reveal the late Paleoproterozoic through Devonian history of the Western Gneiss Region

Master's thesis in Geology
Supervisor: Trond Slagstad & Allan Krill
May 2020

Cathodoluminescence image of zircons from sample 127878L

NTNU
Kunnskap for en bedre verden

NTNU
Kunnskap for en bedre verden

Gina Bjerkan

Zircon U-Pb geochronology and whole-rock geochemistry of migmatitic gneisses reveal the late Paleoproterozoic through Devonian history of the Western Gneiss Region

Master's thesis in Geology
Supervisor: Trond Slagstad & Allan Krill
May 2020

Norwegian University of Science and Technology
Faculty of Engineering
Department of Geoscience and Petroleum

NTNU
Norwegian University of
Science and Technology

Abstract

The study area is located on the north-western coast of Norway in the exposed basement window known as the Western Gneiss Region, (WGR). The WGR is an approximately 50 000 km^2 region of Proterozoic gneisses, known as one of the world's largest exposed ultra-high pressure (UHP) terrains. The area comprises mainly granodiorites- tonalites dated at 1.7 Ga to 1.6 Ga, as well as some mafic intrusions dated at 1.4 and 1.2 Ga. Later, the Sveconorwegian orogeny at ca. 1.0 Ga to 0.9 Ga resulted in a granulite facies overprint accompanied by dike and pluton emplacement and migmatisation which affected the southern part of the WGR. UHP metamorphism during the Caledonian orogeny affected the WGR from ca. 420 Ma to 385 Ma, resulting from subduction of the Baltic margin below Laurentia, and the juxtaposition of several nappes on to the Baltic margin. In the final stages of the orogen, the UHP terrain underwent rapid exhumation. Later extensional deformation has resulted in folding and thrust imbrication affecting most of the overall structural features.

Through detailed geological mapping and sample collection in a field area of 10 x 10 km located in Nordmøre, together with additional samples collected throughout the WGR, this study aims at getting a better understanding of the magmatic, metamorphic and deformational processes that have affected this area from its formation in Paleoproterozoic to the Devonian. The focus has been on dating the migmatisation of the Proterozoic basement gneisses in this region. U-Pb zircon ages were obtained from 27 samples, whereof 18 were leucosomes, using the LA-ICP-MS lab at NGU, Trondheim. Whole rock geochemical analysis was performed at the ALS Chemex laboratories in Sweden.

The geochemical and geochronological data suggest that the protoliths to the migmatites formed in a magmatic arc system between 1691 ± 22 and 1589 ± 19 Ma. The leucosome zircons have a distinct core and mantle morphology, which is interpreted to reflect the inheritance from the protoliths (core) and subsequent migmatisation (mantle). This interpretation is supported by the obtained U/Pb geochronological data from the zircons. The zircons record both Sveconorwegian, ~ 1.0 Ga, and Caledonian, ~ 400 Ma, migmatisation. Sveconorwegian migmatisation of the basement gneisses is confirmed for the southern WGR, but has yet to be identified in the northern WGR. Based on the geochemistry and the obtained protolith and Sveconorwegian metamorphic ages, a correlation between the exposed basement in the WGR and the Sveconorwegian Eastern Segment in Sweden is proposed. The Caledonian ages in the leucosomes indicate that migmatisation took place during the 423 ± 10 to 392 ± 3 Ma time interval. These dates combined with structural top-to-east thrusting observations made in some leucosomes indicate that the migmatisation was mostly active during prograde subduction of the Baltic margin below Laurentia. Based on available pressure-temperature estimates from the WGR, partial melting was most likely hydrous fluid-present, and the lack of significant melting during exhumation may have been prevented by prograde partial dehydration. Partial melting would have altered the rheology of the subducted continental crust, and may have facilitated rapid exhumation. These interpretations are in line with previously published work. Suggestions are made for further research, that would give increased insight into the evolution of the rocks and the region.

Sammendrag

Studieområdet ligger på den nord-vestlige kysten av Norge, i det eksponerte grunnfjellsvinduet kjent som den vestre gneisregionen, (VGR). VGR er et område på omtrent 50 000 km^2 med eksponerte gneiser av tidligproterozoisk alder, og er kjent for å inneholde et av verdens største eksponerte terreng med metamorfe bergarter utsatt for høye til svært høye trykk. Området omfatter hovedsakelig granodioritter og tonalitter med en alder fra 1.7 til 1.6 Ga, samt noen mafiske intrusjoner fra 1.4 til 1.2 Ga. Senere svenskonorvegisk orogenese, fra ca. 1.0 Ga til 0.9 Ga resulterte i en granulittfacies metamorfose, intruderende årer og plutoner, samt migmatisering i de sørlige delene av regionen. Den kaledonske orogenesen påvirket VGR fra ca. 420 til 385 Ma. Den kaledonske orogenesen var en følge av at Baltika og Leurentia kolliderte, noe som resulterte i en dyp subdukjon av den Baltiske skorpen under Leurentia. Den subduserte skorpen ble så utsatt for en hurtig ekshumering under den påfølgende ekstensjonen. Dette resulterte i dannelse av høytrykksmetamorfose bergarter, deriblant eklogitt, som området er mest kjent for i dag. Den senere ekstensjonen resulterte i storskala folding og strekning, som i dag preger store deler av områdets strukturelle geologi.

Den geologiske kartleggingen og prøvetakingen ble gjort i et feltområde på 10 x 10 km lokalisert på Nordmøre, samt en rekke tilleggsprøver samlet fra større deler av regionen. Datering av leukosomer av grunnfjellet i VGR har vært hovedfokuset i denne oppgaven. Målet er å oppnå en bedre forståelse av de magmatiske, metamorfe og strukturelle prosessene som har påvirket dette området fra dets dannelse i tidlig proterozoisk tid til devon. Zirkon har blitt separert ut av et sett på 27 prøver, hvorav 18 er leukosomer. Zirkonene er datert ved bruk av LA-ICP-MS laboratoriet på NGU, Trondheim. De geokjemiske analysene er blitt utført ved ALS Chemex-laboratoriet i Sverige.

De geokjemiske analysene har blitt brukt til å tolke den tektoniske settingen til protolittene til de migmattitiske gneisene, og indikerer at de ble dannet i en vulkansk øybue mellom 1691 ± 22 og 1589 ± 19 Ma. Zirkonene fra leukosom-prøvene har en distinkt struktur, med en omliggende rand rundt en tydelig kjerne. Kjernen er tolket til å reflektere dannelsen av den originale protolitten, mens randen representerer senere migmatisering. Denne tolkningen bekreftes av de geokronologiske analysene av zirkonene, som gir både svekonorvegiske, ~ 1.0 Ga, og kaledonske, ~ 400 Ma, aldre for randene. Svekonorvegiske aldre på migmatiseringen ble bare funnet i de sørlige delene av gneissregionen. Det foreslås en sammenheng mellom VGR i Norge og det svekonorvegiske Eastern Segment i Sverige basert på lik geokjemi og protolitt aldre, samt svekonorvegiske metamorfosealdre i de to områdene. De kaledonske aldrene indikerer at migmatiseringen i VGR skjedde i løpet av tidsintervallet 423 ± 10 og 392 ± 3 Ma. Disse aldrene kombinert med observasjoner av topp-mot-øst strukturer i noen leukosomer indikerer at migmatiseringen var aktiv under den prograderende subduksjonen. Partiell oppsmelting ser ut til å ha funnet sted pga tilstedeverelse av hydrøse fluider og det diskuteres hvilke følger partiell oppsmelting under den prograde subduksjonen vil ha på reologien og den påfølgende ekshumeringen av den subduserte skorpen. Dataene presentert i denne oppgaven er i tråd med tidligere publisert arbeid og det fremmes forslag til mulige videre studier som kan gi en utvidet forståelse for bergartenes og regionens utvikling.

Acknowledgement

Table of contents

Figures

Tables

Equations

Abbreviations/symbols

ASI	Alumina Saturation Indices
BSE	Backscattered electron
BS	Backscatter
Cl	Cathodoluminescence
COLG	Collision Granites
Ga	A billion years, (Giga-annum)
HFS	High Field Strength
HP	High Pressure
ICP-AES	Inductively Coupled Plasma Atomic Emission Spectroscopy
LA-ICP-MS	Laser Ablation Inductively Coupled Plasma Mass Spectrometry
LiDAR	Light Detecting and Ranging
LILE	Large Ion Lithophile Elements
Ma	A million years, (Mega-annum)
MORB	Mid Ocean Ridge Basalt
MSWD	Mean Square Weighted Deviation
MTFC	Møre-Trøndelag Fault Complex
MZ	Mylonite Zone
NGU	Norges Geologiske Undersøkelse
NTNU	Norwegian University of Science and Technology
ORG	Ocean Ridge Granite
Pbc	Common lead
REE	Rare Earth Elements

SEM	Scanning Electron Microscope
SGU	Svensk Geologisk Undersökning
TIB	Transscandinavian Igneous Belt
TSI	Total alkalis versus Silica Index
TW-plot	Tera-Wasserburg plot
UHP	Ultra-High Pressure
VAG	Volcanic Arc Granite
VGR	Vestlig gneisregion
WGR	Western Gneiss Region
WPG	Within Plate Granites
XRF	X-ray Fluorescence
xσ	Standard deviation
λ_x	Isotope half-life
σ_x	Stress, indicate direction of either σ_1 or σ_3
X	Magnetic susceptibility

1 Introduction

1.1 Background and aim of study

This thesis is a regional geological study of the exposed basement gneisses on the western coast of Norway, and the migmatisation that has occurred in this area. The aim is to get a better understanding of the magmatic, metamorphic and deformational processes that have affected this area from its formation in the late Paleoproterozoic to the Devonian. Geological mapping, U-Pb zircon geochronology in both rock and the migmatitic leucosomes, together with whole-rock geochemistry forms the foundation of this study.

The study area is located on the north-western coast of Norway in the exposed basement window known as the Western Gneiss Region (WGR). The WGR is an approximately 50 000 km^2 region of Proterozoic gneisses, known for containing one of the world's largest exposed high- to ultra-high pressure (HP to UHP) terrains (Walsh et al., 2007). The area comprises mainly granodiorites- tonalites with ages between 1.7 and 1.6 Ga. as well as some mafic intrusions at ca. 1.4 and 1.2 Ga. Later the Sveconorwegian orogeny at ca. 1.0 Ga to 0.9 Ga resulted in a granulite facies overprint accompanied by dike and pluton emplacement and migmatisation which affected the southern part of the WGR (DesOrmeau et al., 2015). The Caledonian orogeny affected the WGR from ca. 420 to 385 Ma (DesOrmeau et al., 2015, Gee et al., 2008), resulting in subduction of the Baltic margin below Laurentia and subsequent exhumation. This prosses resulted in the HP-UHP eclogites which the area is best known for. Later extensional deformation has resulted in folding and thrust imbrication affecting most of the overall structural features.

The field work was done in a 10 x 10 km area in Nordmøre, including the Raudsand and Eidsvåg villages, together with a large section of the mountain area in between, see Figure 1.1. The lithologies in this area are described and differentiated and presented in a geological map, see section *5.1.1 Geological map*. Samples collected in this area went through whole-rock chemical analysis, performed at the ALS Chemex laboratories in Sweden, and zircon geochronology using the LA-ICP-MS lab at NGU. Additionally, the study of thin sections prepared at NTNU should have been included, but due to the outbreak of the corona pandemic, this last stage was halted to a significant degree. Leucosome samples distributed throughout the WGR have been included in order to obtain a better regional understanding for the variations in the metamorphic evolution.

The isotopic and geochemical data are first used to interpret the initial formation of the protoliths. Then, the extent of the first migmatisation event in relation to the Sveconorwegian orogeny is explored. These data are used to interpret the relationship between the WGR, and other Proterozoic basement exposed on the Baltic shield, aiming to construct a better regional understanding of the tectonic development in the Proterozoic. This study then aims to discuss the second generation of migmatisation

within the framework of the Caledonian subduction model. The obtained dataset can be used to further explore and substantiate already existing theories and reveals plenty of opportunities for further studies.

1.2 Description of the study area

The field work was focused on a 10 x 10 km area, including Raudsand, Eidsvåg and a large section of the mountain area in-between, see Figure 1.1 below. The mapping has mainly been done along roads and paths with exposed outcrops and a selection of traverses across the mountain area to better extrapolate the geological boundaries. A map with precise location of the field study area is supplied in section *5.1.1 Geological map,* with a smaller scale-map given in Figure 1.1. In addition to field work and sampling within this 10 x 10 km area, samples from a larger area within the WGR are also included; the precise locations of these samples are shown in Figure 5.28. Figure 2.1 on the following page is a simplified tectonic map of the Baltic Shield, illustrating the geographical location of the main tectonic domains. The approximate location of the study area is marked in red.
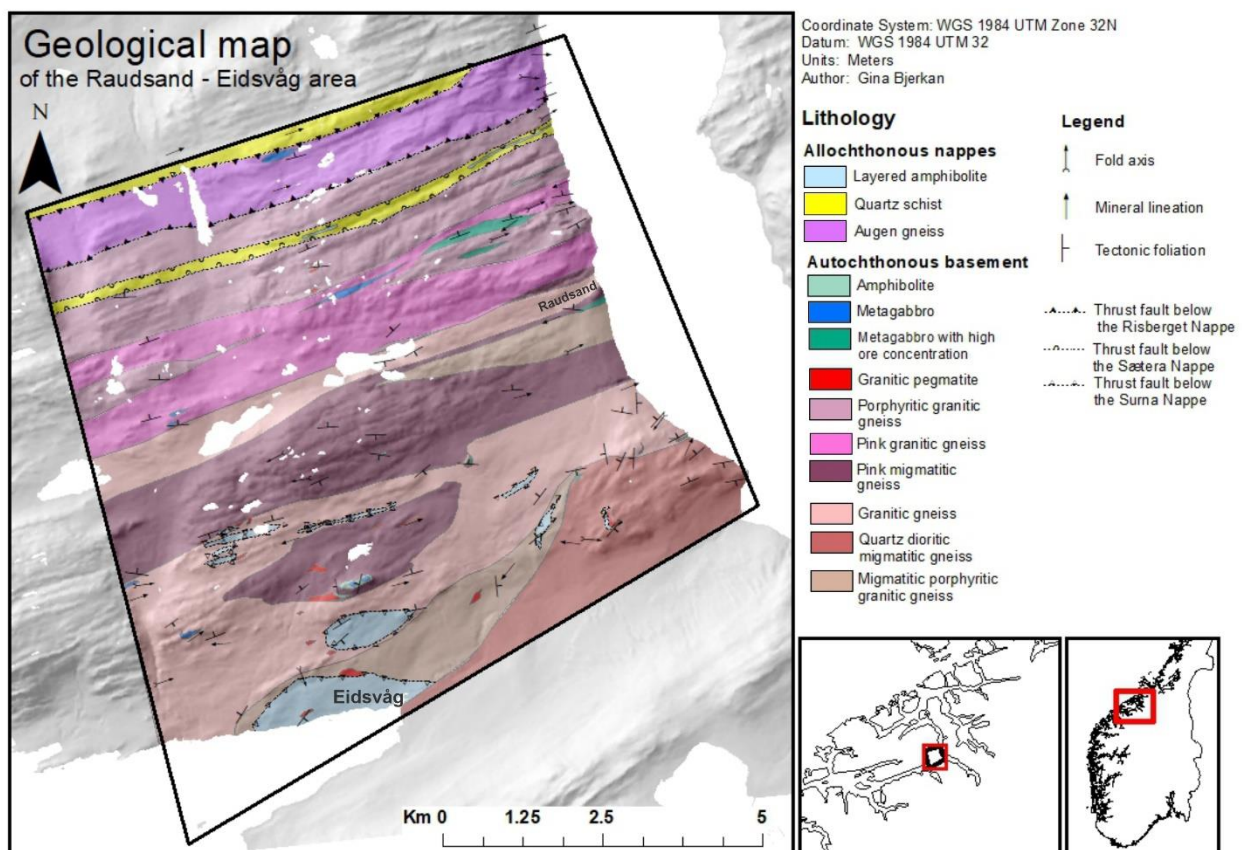
Figure 1.1: Geological map of the field work area within the WGR.

2 Regional geology

This study incorporates events from the origin of the Proterozoic protoliths to the Caledonian exhumation in Early Devonian, which includes covering a large amount of Norwegian geological history. The following section, *2.1 The evolution of the Fennoscandian Shield and 2.2 The Caledonian Orogeny,* gives a brief overview of the tectonic development and the geological background which is relevant to the field area and the discussion given in section *6*.
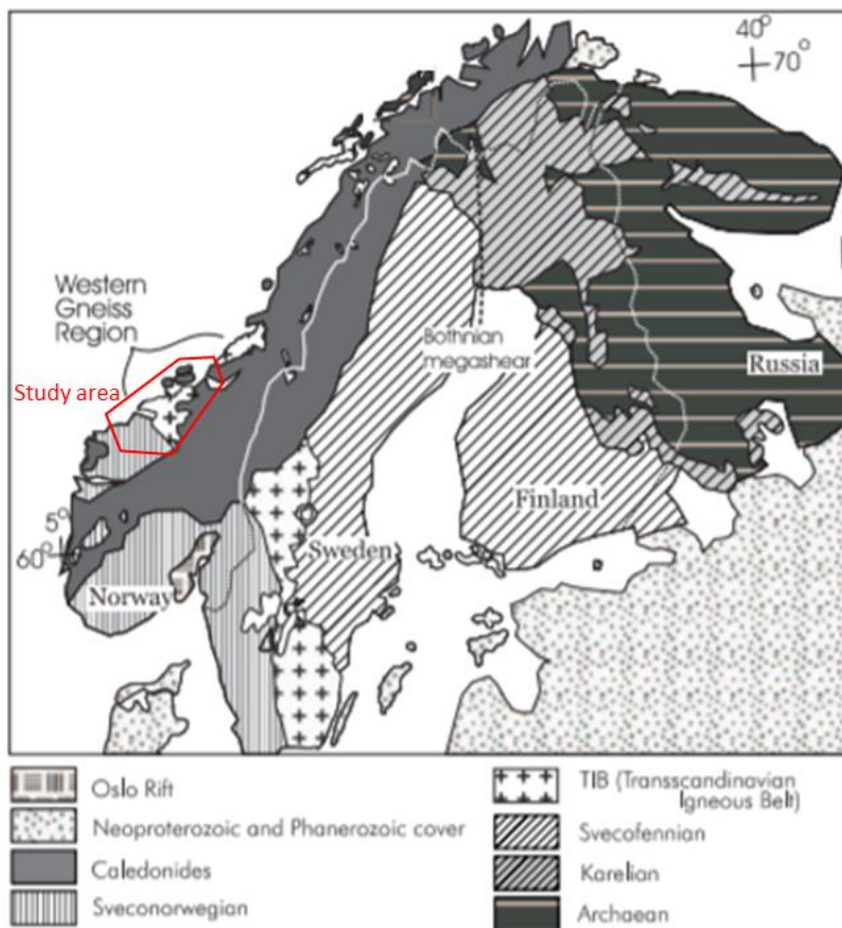
Figure 2.1: *Simplified tectonic map of the Fennoscandian Shield. The approximate location of the field area within the WGR is marked in red. The figure is modified after Corfu et al. (2003) fig 1.*

2.1 The evolution of the Fennoscandian Shield

The tectonostratigraphic history of the late Paleoproterozoic era until the Neoproterozoic is dominated by the formation and later breakup of the supercontinent Colombia, and the later re-agglomeration of the next supercontinent, Rodinia.

The Fennoscandian Shield (also known as simply Fennoscandia) is a craton formed by the merging of several fragments of Archean and Proterozoic age. Figure 2.2, upper inset, illustrates the amalgamation of the Fennoscandian craton with the eastern Sarmatia and Volgo-Uralia cratons. The amalgamation was followed by subsequent accretion of younger Paleoproterozoic continental crust. These processes formed the proto-Fennoscandian craton. This craton amalgamation marks the end of the 'Svecofennian' period, which generally refers to the period from 2.0 to 1.8 Ga and overlaps with the merging and continuous growth of the Colombian supercontinent, at 1.9 to 1.85 Ga (Roberts and Slagstad, 2014). The present-day south-west margin of the Fennoscandian Shield is perceived to have been located on the outer edge of the Colombian supercontinent, Figure 2.2, lower inset.
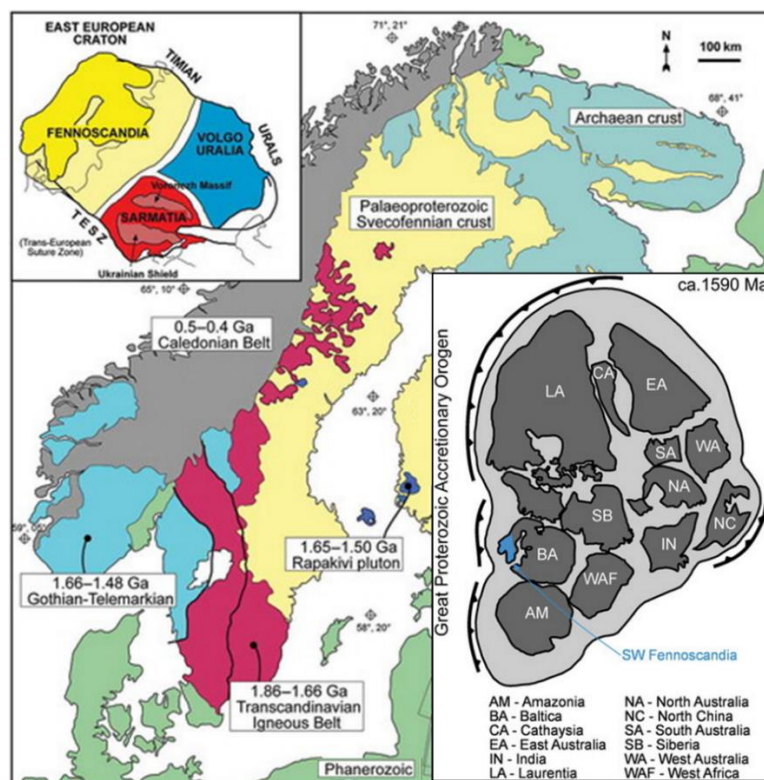
Figure 2.2: *Sketch map of Fennoscandia showing the major geological domains, top inset shows Fennoscandia within the East European craton (Roberts and Slagstad, 2014, fig 1). Modified after (Bingen et al., 2008, Korja et al., 2006 & Bogdanova et al., 2008). The bottom inset shows the Columbia supercontinent at ca. 1590 Ma (Roberts and Slagstad, 2014, fig 9. Modified after Zhang et al., 2012) SW Fennoscandia is marked in blue showing its location on the southwestern margin of the Fennoscandian Shield.*

2.1.1 The Transscandinavian Igneous Belt (1.86 – 1.66 Ga)

After the earlier formation of the proto-Fennoscandian Shield, accretionary growth started at the SW margin at 1.86 – 1.66 Ga. This suite of plutonic and associated volcanic rocks is known as the Transscandinavian Igneous Belt (TIB) and stretch from the NW coast of Norway to the SE coast of Sweden. According to Högdahl et al. (2004) the TIB refers to a series of similar rocks that are mapped on the basis of geological and petrological background, rather than on region, tectonic setting or time period. Though the definition has changed over time and different interpretations have been proposed by different authors, the consensus is that the TIB can broadly be divided into three units, TIB-0-, TIB-1- and TIB-2/3. Each unit reflects the different ages of the rocks involved, where the two earlier units are thought to overlap with the later stages of the Svecofennian deformation. All units in the sequence are interpreted to be related to a convergent margin setting (Roberts and Slagstad, 2014, Åhäll and Connelly, 2008, and references therein).

The TIB granitoids are generally alkali-calcic and of either I or A- type. Geochemically and isotopically, the majority of the rocks are compatible with a reworking of Svecofennian sources, with some accretion of more juvenile arc material (Roberts and Slagstad, 2014, and references therein). The TIB rocks are mostly undeformed, and the few deformational zones are thought to relate to transpressional, and compressional geodynamic forces, related to the tectonic activity during the 1.86 to 1.66 evolution of the area.

2.1.2 The Gothian – Telemarkian domain (1.66 – 1.48 Ga)

The Gothian lasted from 1.66 to 1.52 Ga. The Gothian crust is comprised of granitoids and orthogneisses, resembling remnants of volcanic arc complexes, all deformed to variable degrees. New U – Pb data has been used to provide a framework of for different time periods within the Gothian domain (Åhäll and Connelly, 2008), all of these reflect stages of westward continental growth away from the Fennoscandian craton in an arc setting environment. The Telemarkian lasted between 1.52 and 1.48 Ga (Roberts and Slagstad, 2014). As with TIB and the Gothian domain, this period is dominated by continental growth of the Fennoscandian Shield. The tectonic setting found to dominate in this period is a mature island- or continental arc setting (Åhäll and Connelly, 2008, and references therein)

For both the Gothian and the Telemarkian the transitions are a bit blurred, and the domains have overlapping protolith ages with both older (TIB) and younger Hallandian – Danoplonian domains, see next section. The origin, specifically for the Telemarkian crust, is also a subject for discussion. Arguments are made that any distinction, except for the geographical, is unnecessary for the two units. Not going into further detail, the Gothian – Telemarkian domain is here interpreted to be formed in an accretionary orogen as a single convergent margin (Roberts and Slagstad, 2014).

2.1.3 The Hallandian – Danopolian Orogeny (1.47 – 1.38 Ga)

The Halladian – Danopolian is a broad term used to define the tectonic and geothermal activity in the period between 1.47 to 1.38 Ga. This activity includes felsic intrusion in southernmost Sweden and scattered mafic intrusions in central Sweden between 1.47 to 1.44 Ga, and metamorphism in the Eastern Segment (Roberts and Slagstad, 2014). The events are thought to relate to a back-arc setting in today's central Sweden and a subduction zone further south (Lundmark and Lamminen, 2016).

2.1.4 Accretionary orogenesis, inboard events from 1.65 – 1.15 Ga

The period between the Telemarkian and the initiation of the Sveconorwegian orogenesis at ~1.15 Ga has been referenced by (Åhäll and Connelly, 1998) and other authors as an interorogenic period, due to the lack of metamorphic and deformational events. Though this is mostly reflected in the Idefjorden domain and should not be interpreted as 'no activity at all' in this period. During the proposed accretion of the Fennoscandian Shield, magmatism of Gothian and Telemarkian age occurred within the craton, away from the supposed continental margin. In southern Norway and southwest Sweden was in the form of various granitic rapakivi suites. The pattern with westwards-younging emplacement of intrusive bodies suggests a link between the accretionary arc magmatism and this episodic inboard magmatism (Roberts and Slagstad, 2014). Episodes of magmatism and sedimentation from the Hallandian – Danopolian Orogeny can also be observed in numerous features. The primary domains for this period are the Eastern segment, the Idefjorden-, the Bamle-Kongsberg- and the Telemarkian- domain.

2.1.5 Sveconorwegian orogeny 1.15 – 0.9 Ga.

The tectonic setting and evolution of the Sveconorwegian orogeny is still a matter of discussion. It has traditionally been viewed as a continent – continent collision zone, linked to the Grenville Province in Canada (Roberts and Slagstad, 2014, and references therein), though recent studies shift to an accretionary orogenesis model. This latter hypothesis uses modern-style plate tectonic processes as a basis. The basis for this latter interpretation is presented by e.g. (Slagstad et al., 2013) and is based on observations and data from the central and western part of the orogen in the Kongsberg- Telemark- Bamble domains. The apparent major tectonic and metamorphic features from the later stages of this period is associated with an end of the long-lived accretionary orogen in this area. After the Sveconorwegian, subduction either continued, but jumped outboard, or ceased altogether leaving a passive margin. Such a large-scale change in the geodynamics reflects a significant change in the plate motion, which in turn can relate to the merging of the supercontinent Rodina, which occurred at this approximate time, ca. 0.9 Ga.

The following figure is a simplified cartoon from Roberts and Slagstad, (2014), which encompasses the stages of evolution related to the Fennoscandia Shield introduced above. The later Sveconorwegian stage in this figure follows the interpretation of a long-lived accretionary arc system.
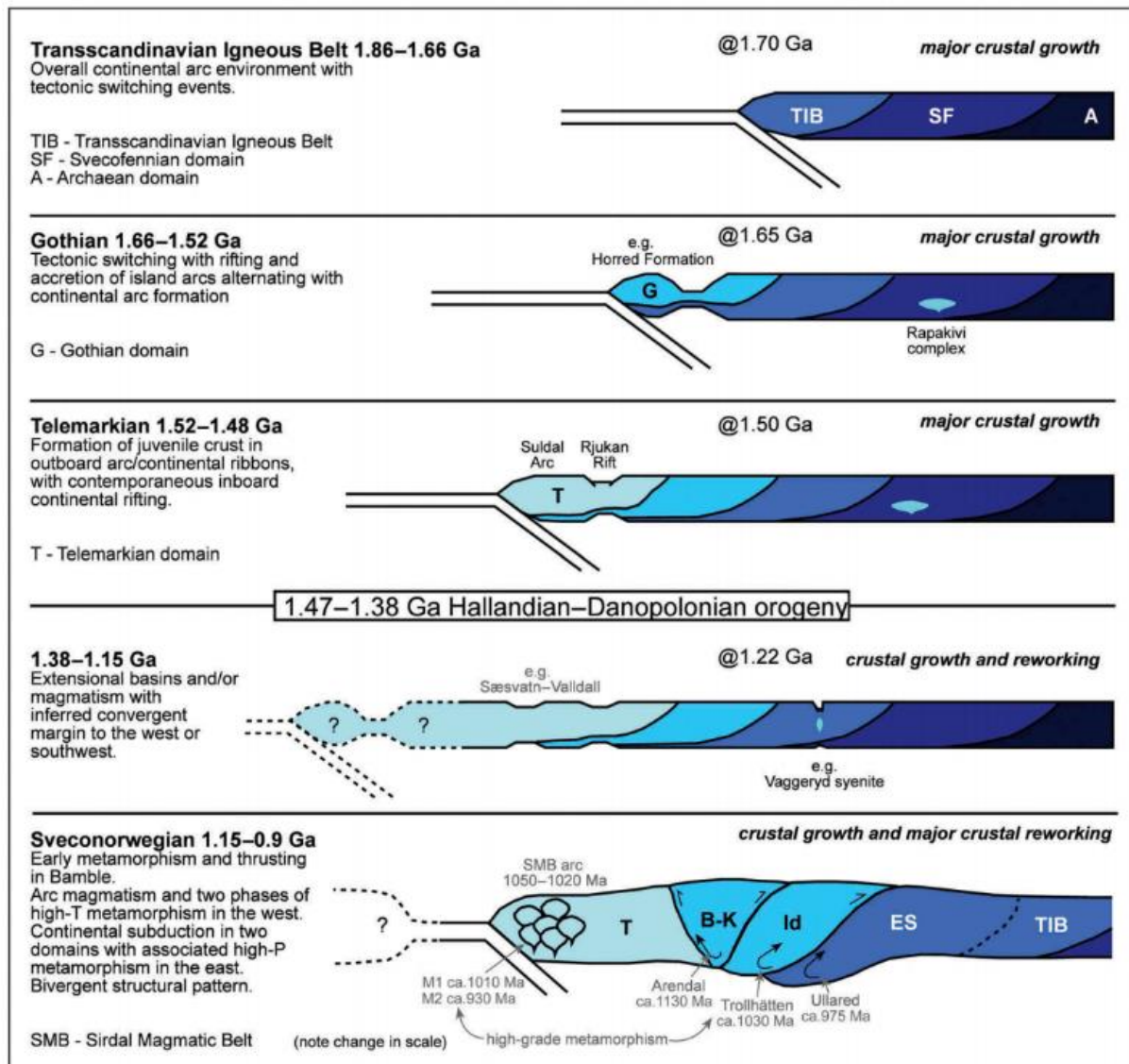
Figure 2.3: *Cartoon tectonic cross-sections of southwest Fennoscandia at various time periods, highlighting the westward younging of crustal domains, formed along an accretionary convergent margin. For simplicity, a single subduction zone with consistent polarity is maintained, and along-margin movement between domains is ignored. The final Sveconorwegian period is a composite of major diachronous events shown in one section, with the geometry of crustal boundaries being largely inferred from the metamorphic gradients. Diagram and figure text from Roberts and Slagstad, (2014), fig 8.*

2.1.6 Sveconorwegian influence within the Western Gneiss Region

A limited Sveconorwegian influence in the Western Gneiss Region was first suggested by Tucker et al. (1990). He restricts the influence of the Sveconorwegian to the southern parts of the region by dating crosscutting granodiorite and pegmatite dykes in the area. Later studies by Skar and Pedersen (2003) found that this overprint also could be found in granite intrusion and migmatisation, by the use of U-Pb dating of both zircon and titanite in the southern part of the region. Concordant monazite ages from Hisarøya and Bårdsholmen, located at the southern end of the Western Gneiss Region, also indicate a Sveconorwegian impact (Røhr et al., 2004).

2.1.7 Continental growth and Sveconorwegian influence in the Idefjorden Terrane and the Eastern Segment.

The Idefjorden lithotectonic unit in the south-western part of Sweden is an approximately 400 km long and 140 km wide segment trending approximately north- south, and extends north-westward into Norway, where it can be observed on both sides of the Oslo Rift. Further potential extent is covered by later Caledonian nappes. The unit is dominated by crust formed during accretionary orogeny during the Gothian period, 1.66 to 1.49 Ga, and later features related to crustal extension. The crustal extension occurred in four segments: 1.51 – 1.49 Ga, 1.46 Ga, 1.34 – 1.30 Ga and after 1.33 Ga (Bergström et al., 2020), and consist mainly of orthogneiss, paragneiss and granite suites, with some extrusive rocks. Isotopic information indicates juvenile sources, further indicative of an accreted juvenile arc setting. The unit is heterogeneously affected by later Sveconorwegian metamorphism, which ranges from greenschist to locally granulite facies (Petersson et al., 2015).

The Eastern Segment is generally interpreted to be a reworked part of the TIB (Røhr, T.S, et al., 2013). Further detail on the geochemical and isotopic characteristics are thus given in section *2.1.1 The Transscandinavian Igneous Belt*. The segment is a 50 to 100 km wide belt which generally is composed of orthogneisses, with protoliths ages of 1.81 to 1.66 Ga, assumed to be equal to granitic to monzonitic intrusions to the east of the Sveconorwegian front (Möller et al., 2015). The Eastern Segment is divided it three based on the structural relationships and the metamorphic grades within the region. Metamorphism related to the Sveconorwegian orogeny grades from greenschist to amphibolite facies towards west.

Separating the higher-grade Idefjorden lithotectonic unit to the west and the lower-grade Eastern Segment to the east is the 'Mylonite Zone', (MZ) (Law et al., 2010, Bergström et al., 2020). The MZ is a ductile high-strain belt with transpressive and later extensional components of deformation (Bergström et al., 2020). The exact nature of the MZ is, however, still a matter of debate, and whether it is an accretionary suture of a proximal arc segment onto Fennoscandia, or simply a shear zone related to the Sveconorwegian

orogeny remains unknown (Bergström et al., 2020, Hynes and Rivers, 2010, Åhäll and Connelly, 2008, and references therein)

2.2 The Caledonian Orogeny

During the Proterozoic the supercontinent Rodinia broke up and then amalgamated into the new supercontinent Pangea during the Paleozioc (Murphy et al., 2009). During the amalgamation, the two continents Baltica and Laurentia played a big part in the tectonic history in Scandinavia in determining the shape of the Caledonian Orogen. The orogeny was active from the Ordovician to the Devonian and dominates a vast part of the exposed Norwegian geology. The nappes expose fragments of a complex history of oceanic opening, closure, followed by continent-continent collision and subsequently extension and the formation of a new ocean, the Atlantic. A short summary of the regional geological history of the Caledonian orogeny will be given below highlighting the main outline of the events, followed by a section with primary focus on the related exposures in the Western Gneiss Region.

During the late Palaeozoic, at about 600 Ma Baltica and Laurentia began drifting apart, forming the Iapetus Ocean between them, see Figure 2.4 below (Torsvik et al., 1996). The Iapetus Ocean would subsequently close, resulting in the initiation of the what is called the Scandian event (Gee, 1975), an oblique collision between Laurentia and Baltica at about 435 Ma (Walsh et al., 2007, Roberts, 2003). Figure 2.4 below illustrate the outline of the Caledonian Orogen at ca. 60 Ma, prior to opening of the North Atlantic (Gee et al., 2010). Today evidence of the Caledonian orogeny can be found on both sides of the Atlantic Ocean.
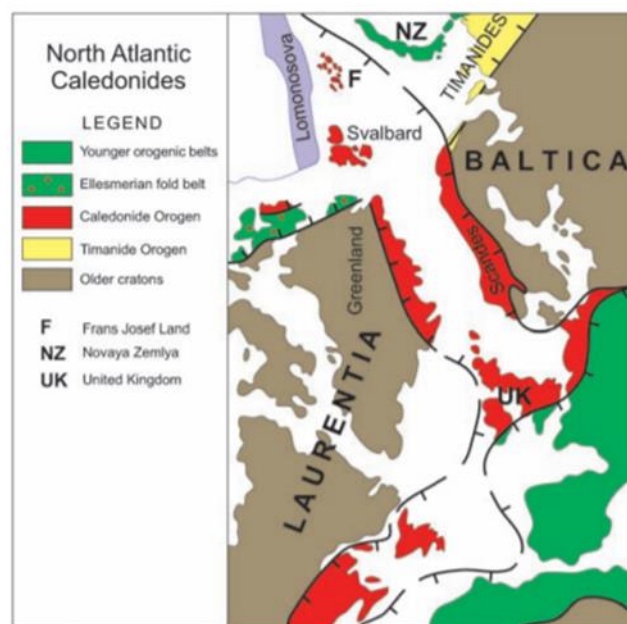
Figure 2.4: *Outline of the North Atlantic Caledonides and relationship between Laurentia and Baltica. Figure and text from (Gee et al., 2008, fig 1.)*

The closure of the Iapetus Ocean resulted in thrusting of oceanic and continental allochthons, or nappes, onto the Baltic margin up until ca. 415 Ma (Tucker et al., 2004, Roberts, 2003, DesOrmeau et al., 2015) These allochthonous units are traditionally divided into the Uppermost, Upper, Middle, and Lower allochthon, see Figure 2.5 below. In tectonostratigraphically descending order these include the eastern margin of Laurentia, Iapetus ophiolites, the western margin of Baltica and allochthonous slivers of the Baltic Shield and its sedimentary cover (Roberts and Gee, 1985).
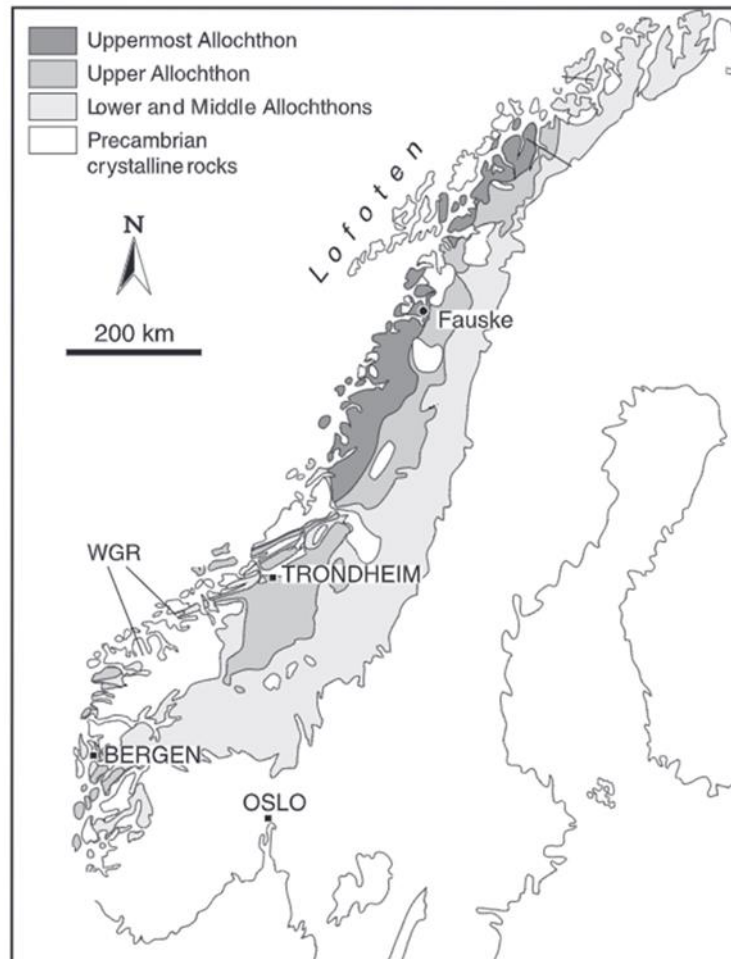
Figure 2.5: *Simplified tectonostratigraphic subdivisions of the Scandinavian Caledonides, altered figure and text from (Roberts, 2003, fig 1).*

The continent-continent collision resulted in a simultaneous continental subduction of the Baltic margin (WGR) under the overlying allochthons. The WGR subducted below Laurentia during the Silurian from ca. 420 to 400 Ma. Exhumation and near isothermal decompression of the subducted slab from the mantle to shallow crustal depths, took place from ca. 400 to 385 Ma (DesOrmeau et al., 2015, Gee et al., 2008). The exhumation of the HP and UHP orogenic hinterland was followed by deformation related to the late Scandian collapse. The Old Red Sandstone deposits in Devonian extensional basin marking the end of the Caledonian Orogeny.

2.2.1 The Western Gneiss Region

The WGR consists primarily of autochthonous orthogneisses from the Baltic Shield, overlain by the allochthonous units emplaced onto the eastern foreland. Through the work of (Krill et al., 1985, Robinson, 1995, Terry et al., 2000) the less deformed allochthonous units in the east have been correlated with similar units in the western UHP part of the orogen. The allochthonous units overlying the Baltic basement in the WGR are given by four tectonostratigraphic units, the Risberget Nappe, the Sætra Nappe, the Blåhø-Surna Nappe, and the Støren Nappe (Robinson, 1995, and references therein) but for the purpose of this thesis, these units will all be referred to simply as allochthonous nappes or undifferentiated Caledonian nappes. Many of the structures in the WGR are interpreted to be late extensional deformation. Folding and thrust imbrication has resulted in juxtaposition of tight interfolding of basement rock and the allochthonous nappes (Gordon, 2016, Krill, 1980).
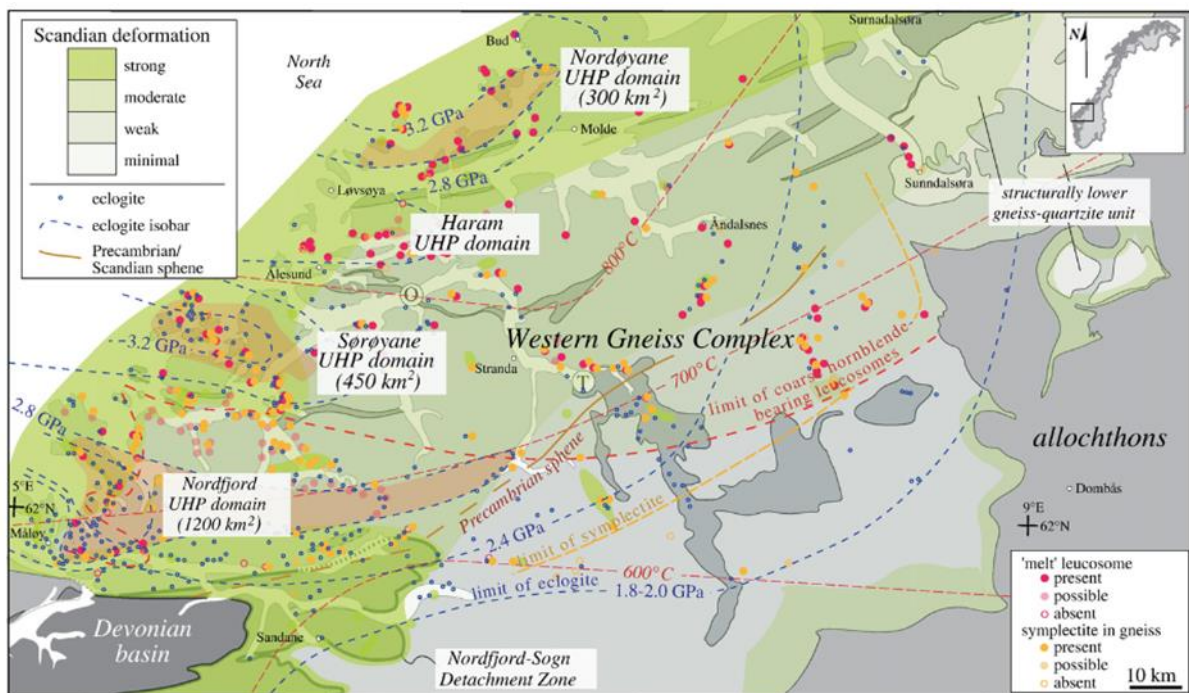
Figure 2.6: *Basement gneisses overlain by allochthonous nappes are given in shades of grey after (Lutro and Tveten, 1998 & Tveten et al., 1998). The green shading illustrates the intensity of Scandian deformation. Eclogite pressure illustrated by blue isobars (poorly constrained) and the peak metamorphic temperatures after (Kylander-Clark et al., 2008). The abundance of hornblende-bearing leucosomes; and the presence of symplectite-bearing gneiss are marked. Sphene has Scandian ages in the northwest and Precambrian ages in the southeast (Kylander-Clark et al., 2008, Tucker et al., 1990) The NE boundary of Nordøyane UHP domain is set after (Vrijmoed et al., 2006). All contacts shown are faults, except the NW edge of the Devonian basin. Figure and caption modified from (Hacker et al., 2010, fig 1).*

The WGR is known for its large exposure of UHP and HP domains. On the western edge of the WGR there are three distinct zones with UHP eclogites. These are known as the Nordfjord, Sørøyane and Nordøyane domains, which are illustrated in Figure 2.6 above. The UHP domains are identified by the presence of the UHP quartz pseudomorph coesite, or the residual quartz, which is mostly found within the eclogite outcrops (Root et al., 2005). The Nordøyane domain records maximum temperatures of 850 °C and pressures between 3.2 to 3.6 GPa. Whilst the southern Nordfjord domain records temperatures from 700 °C and pressures of ~ 2.8 GPa (Hacker, 2006, Cuthbert et al., 2000, Krogh Ravna and Terry, 2004, Young et al., 2007).

The increase of peak temperature and pressure from southeast towards northwest, has been interpreted to indicate a westward-facing subduction of the Baltic margin below Laurentia. Using zircon U-Pb geochronology these eclogites have been interpreted to reflect subduction of both the autochthonous basement and the allochthonous nappes in the WGR. This implies that that the nappes were emplaced before the subduction (Walsh et al., 2007). The UHP metamorphism is proposed to have occurred from about 425 Ma to 400 Ma, followed by an amphibolite facies overprint related to the exhumation, proposed to have lasted from 400 Ma to 385 Ma (DesOrmeau et al., 2015, Hacker et al., 2015, Walsh et al., 2007, Holder et al., 2015, Kylander-Clark et al., 2007, Kylander-Clark et al., 2008, Terry et al., 2000). Several datasets show a westwards younging of exhumation related mineralisation. Monazite (Hacker et al., 2015) titianite, rutile (Kylander-Clark et al., 2008) and mica (Walsh et al., 2007), which is interpreted to reflect a westward progression of the exhumation and unroofing of the WGR as a coherent slab.

3 Theory

3.1 Geochronology

Geochronology is a branch of geological studies focused on age determination of geological events or features. The developing relationship between parent and daughter isotopes in radioactive decay is used as a tool to measure the elapsed time. This is possible due to the constant decay factor in radiogenic nuclei. The decay of unstable parent isotopes leads to the formation of a selection of stable daughter isotopes. The decay time of a radiogenic isotope is referred to as the isotope half-life, λ, whereof λ daughter < λ parent. The principle of secular equilibrium is an essential concept for geochronology. The simplest equations assume secular equilibrium, where one daughter isotope is created from every parent that decays. Events such as partial melting, or a disruption during crystallization will affect the equilibrium state and by consequence the age calculations for relevant isotopes (Schoene, B., 2014). The general formula for isochron calculations is given as

$$D^* = D_0 + N(e^{\lambda t}-1) \tag{I}$$

Where λ is the decay constant for the isotope, t is the time since system closure, N is the abundance of the radioactive parent, D^* is the initial isotope daughter abundance, and D_0 is the isotope abundance already present in the sample (White, 2015).

3.1.1 Uranium lead geochronology

Uranium, (U), and thorium, (Th), are both rather incompatible elements, and usually occur as trace elements in major phases, or are concentrated in accessory minerals, such as zircon, ($ZrSiO_4$) (White, 2015). The U – Th – Pb system consists of three naturally occurring decay systems, ^{238}U, ^{235}U and ^{232}Th, each having a half-life of respectively λ_{238} =$1,55125e^{-10}$, $\lambda_{235} = 9,8485e^{-10}$ and $\lambda =4,9475e^{-11}$ (Schoene, 2014). The decay of uranium and thorium can go in several stages and will all result in different stable lead isotopes, see Figure 3.1 below (Schoene, 2014).
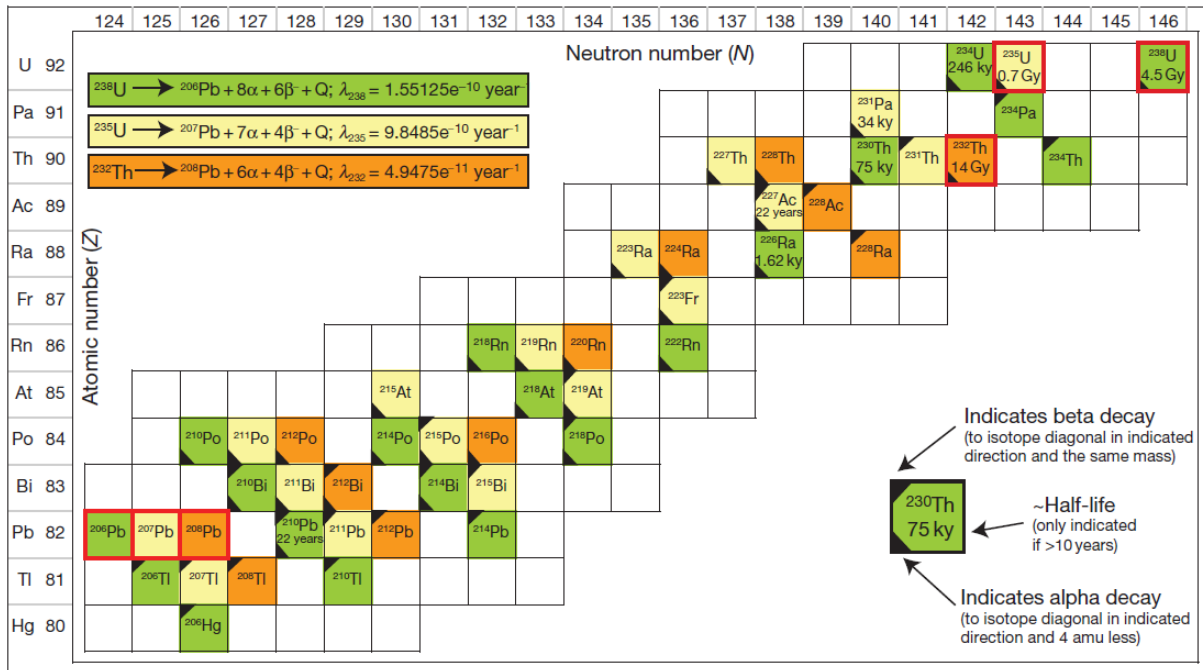
Figure 3.1: *Illustration of the U–Th–Pb decay chains. Each isotope occurring in a given decay chain is color-coded to its parent isotope, which are outlined in red, as are the stable daughter isotopes of Pb. See inset for description of symbols used in each box. Figure and description from (Schoene, 2014, fig 2).*

The complete reaction from parent to daughter in uranium and thorium is given in equation II to IV below.

$$^{238}U \rightarrow {}^{206}\text{Pb} + 8\alpha + 6\beta + Q \tag{II}$$

$$^{235}U \rightarrow {}^{207}\text{Pb} + 7\alpha + 4\beta + Q \tag{III}$$

$$^{232}Th \rightarrow {}^{208}\text{Pb} + 6\alpha + 4\beta + Q \tag{IV}$$

The stable lead isotopes are ^{206}Pb, ^{207}Pb and ^{208}Pb, corresponding to, ^{238}U, ^{235}U and ^{232}Th respectively, α is the alpha particle, β is the beta particle and Q is the energy released during decay (Schoene, 2014). All the systems given in equation II – IV above can be used independently, but their strength is enhanced when they are combined. By combining the ^{238}U/^{206}Pb and the ^{235}U/^{207}Pb one can control the fidelity, and even eliminate error related to common lead, the none-radiogenic isotope, ^{204}Pb (Schoene, 2014, White, 2015).

3.1.2 Zircon

Zircon is a common accessory mineral in the crust and can occur in igneous, metamorphic, and sedimentary rocks, as well as unconsolidated deposits. This is due to its characteristically robust properties, making it able to withstand an array of different P-T environment and subsequent erosion and deposition, whilst still containing chemical

14

and isotopic information. The mineral is most likely to grow in felsic to intermediate rock but can also occur in mafic rocks. Zircon can incorporate both radiogenic ions and rare earth elements (REE) into its crystal structure. The abundance of these elements can be used to investigate the evolution of both the earth's crust and mantle (Hoskin, 2003). Cathodoluminescence (CL) and Backscattered electron (BSE) -imaging can be used to observe growth pattern, inclusions and cracks that are present in the zircon crystals. The patters are visible due to the heterogeneous distribution of elements within the grains. Zircon can cease and restart growth on the same crystal, making it possible for one crystal to reflect more than a singular geological event. The distinct patterns can be used to identify the growth environment and be used as a supplement to make more precise age measurements.

3.1.3 Dating techniques

LA-ICP-MS: Laser Ablation Inductively Coupled Plasma Mass Spectrometry

LA-ICP-MS analysis first started up during the 1990s and is a relatively new analytical method. The method is based on creating aerosols by directing a laser beam at the sample surface. A carrier gas will go through the chamber at the same time, carrying the fumes to the plasma torch camber where the carrier gas with the incorporated fumes are analysed by a mass spectrometer. The resulting analysis has relatively good spatial resolution, and yield an useful age solution between 2 – 3% (Schaltegger et al., 2015). The sample analysis time is by far the most effective at =< 2min (Schoene, 2014). However, the in-situ analysis is invasive, and leaves a "beam - crater" during sampling. Figure 3.2 below illustrates a simple schematic illustration of how the LA-ICP-MS system operates.
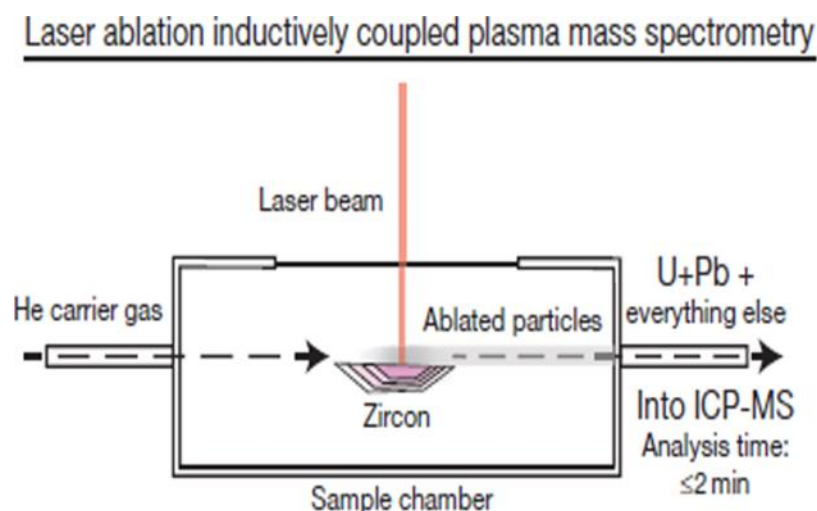
Figure 3.2: *Laser ablation inductively coupled plasma mass spectrometry (LA-ICPMS), Figure and text from (Schoene, 2014, fig 8).*

3.1.4 Plots

There are several different techniques that can be applied to geochronologically date zircon, and by a continuous technological development, the amount of data that can be collected is increasing. Geochronological data is usually presented in plots to give a visual interpretation of the age. The plots are tailored to visualize the information one wants to convey. The two most usual plot are the Wetherill concordia plot, and the Tera–Wasserburg plot.

Wetherill concordia plot

The Wetherill concordia plot is based on the calculated values of time, t, using the base equation (I) for each isotope, plotting $^{206}Pb/^{238}U$ versus $^{207}Pb/^{235}U$ from the same analysis. The concordia form, where t overlaps for both isotopes. ^{238}U and ^{235}U having different half-lives, λ, resulting in a curved line. For a closed system, all values will fall along the concordia, but where the system has experienced some open behaviour the analysis data will fall along the discordia. These dates can in turn be interpreted as a geological age. Figure 3.3 below illustrate two examples of different open system behaviours, and two different events can be observed.
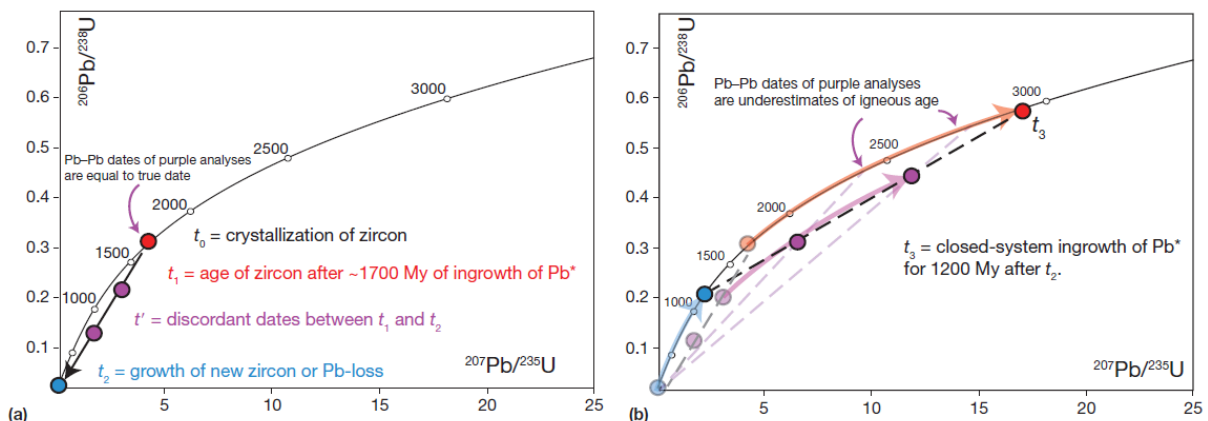
Figure 3.3: *(a) Example of a 1700 Ma zircon losing Pb or mixing with metamorphic overgrowth. t_0 is the crystallization age of the zircons; after 1700 Ma of closed-system ingrowth of Pb, the zircons appears on concordia at t_1; at t_2 the zircon suffers Pb loss or growth of new zircon around old core; t_0 represents zircons that are discordant following partial Pb loss or mineral overgrowth at t_2. (b) The same data after the system has closed again and continues to evolve up the concordia curve. The discordia line defined by purple analyses now has an upper intercept with concordia representing the original igneous crystallization event at t_1, and a lower intercept age representing t_2, the time before the present at which Pb loss or overgrowth occurred. Image and description from (Schoene, 2014, fig 4).*

Tera–Wasserburg diagram

The Tera-Wasserburg plot, (TW-plot), plots the $^{238}U/^{206}Pb$ versus $^{207}Pb/^{206}Pb$. As with the Wetherill plot the data in the TW-plot falls along the concordia in closed systems and along the discordia on open systems. The principles of the two systems are rather similar but in cases where the concordia and discordia in the Wetherill concordia plot are not easily distinguished, the TW-plot can be used. The increased precision, and the accountability of inherited common lead (Pb_C), make the TW diagram the preferred diagram for some. The normal TW-plot cannot account for Pb_C occurring due to mixing or multiple age domain. However, by additionally plotting $^{204}Pb/^{206}Pb$ in the third dimension this Pb loss can be accounted for. Se Figure 3.4 below for an example of a TW-diagram.
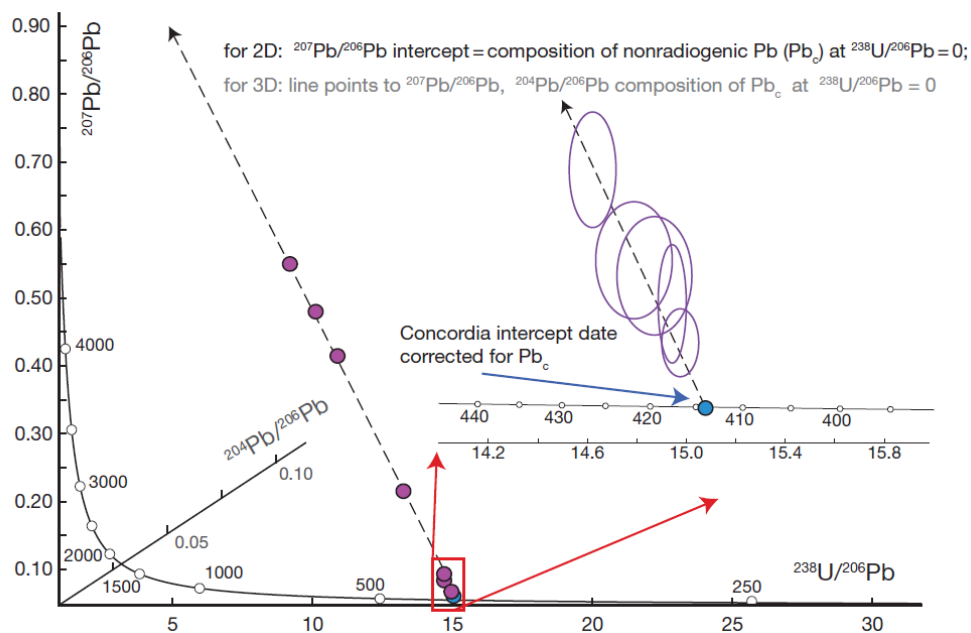
Figure 3.4: *Tera–Wasserburg (TW) concordia diagram shown in 2D and 3D. Note that if discordance is caused by mixture with initial Pb_c, the resulting. Image and text from (Schoene ,2014, fig 5).*

3.1.5 Potential errors

There are a lot of possible pitfalls related to geochronological studies. Schoene, B., (2014) defined some terminology related to potential uncertainties, dividing the uncertainties into random or systematic, where random errors are caused by randomly occurring factors and systematic errors are predictable uncertainties relevant for every measurement (Schoene, B., 2014). Natural causes of discordance in U – Th – Pb systems can be classified as both and errors are often related to the system not being completely closed. Systematic errors are usually related to external factors, such as errors in analytical method or equipment.

Uncertainty related to the calculated U and Th decay constants are a pure systematic error. Though not going into further detail on the matter here both Schoene (2014) and Schaltegger et al. (2015) go through a selection of typical statistical models used and how incorrect use, or bad samples systematically can lead to grossly incorrect age estimations.

Age mixing, loss of Pb and system that are not in secular equilibrium are examples of natural features that might cause error in a potential analysis. In a natural system several of these factors may be influencing the mineral simultaneously. Previously mentioned spectroscopic methods, such as CL and BSE, can be used to identify distinct growth areas within the zircon. And calculations can be made to correct the effect of intermediate daughter products and common lead. Both methods reduce the potential error.

3.2 Geochemistry

Geochemistry is the study of the chemical compositions in nature, mainly focused on parts of the geosphere. The geosphere is not an isolated system and it can interact with the surrounding environment, such the atmosphere, hydrosphere, and biosphere. The distribution, movement, and chemical characteristics of elements in the earth can be studied, and in turn be used to construct the story of the geological evolution.

3.2.1 Whole rock geochemistry

Geochemistry can be done at different levels, from an entire rock sample, to one singular grain. For whole rock geochemistry, a representative sample of the rock is selected, and crushed. The larger grains in the rock to be analysed, the lager the sample needs to be in order to be a representative. The crushed sample is then split to get a smaller sample for analysis. The fully detailed process is given in the methods section *4 Methods*. The analytical data that is obtained can be plotted in a selection of diagrams, and the relative abundance and distribution of elements can be compared to each other, or a standardized norm. Magma series are defined by adding the analytical data into a set of different plots categorizing the chemical distribution by a standardized definition. The plots aid the chemical classification which in turn can be used to characterize the source environment.

3.2.2 Major and minor elements

All elements that have a weight percent (oxide wt.%) higher that 1 count as a major element, while those below 1 and greater than 0.1 are classified as minor elements (Winter, 2001). The major elements compromise a larger part of the rock and will therefore have a greater impact on the properties related to the mineralogical composition. The minor elements often serve as substitutions for major elements, and can if concentrated, form accessory minerals.

When presenting data from a chemical analysis the result is often presented as wt. % of the most common oxides. When presented in a table the total wt. % of the combined oxides are < or ≈100. To better analyse the data and get an understanding of the geological system it is common to use graphic plots. Examples of common plots are given below.

Harker diagram

A simple bivariate diagram is the Harker diagram, most often plotting the wt. % of silica oxide (SiO_2), against the wt. % of the other major oxides (TiO_2, Al_2O_3, Fe_2O_3, FeO, MnO, MgO, CaO, Na2O, K_2O, H2O+). This is because SiO_2 is the most variable constituent in most mafic magmas. In a more basaltic environment, the Fenner diagram might be more useful. The principle is the same, but with magnesium oxide, (MgO), on the x axis instead of silica. The plots can then be used to identify if there are any apparent trends in the systems where the samples were collected. By studying the chemical characteristics of several samples one can get insight to how the system might have developed though time. Figure 3.5 illustrate 8 different Harker diagrams plotted with sample data from Crater Lake.
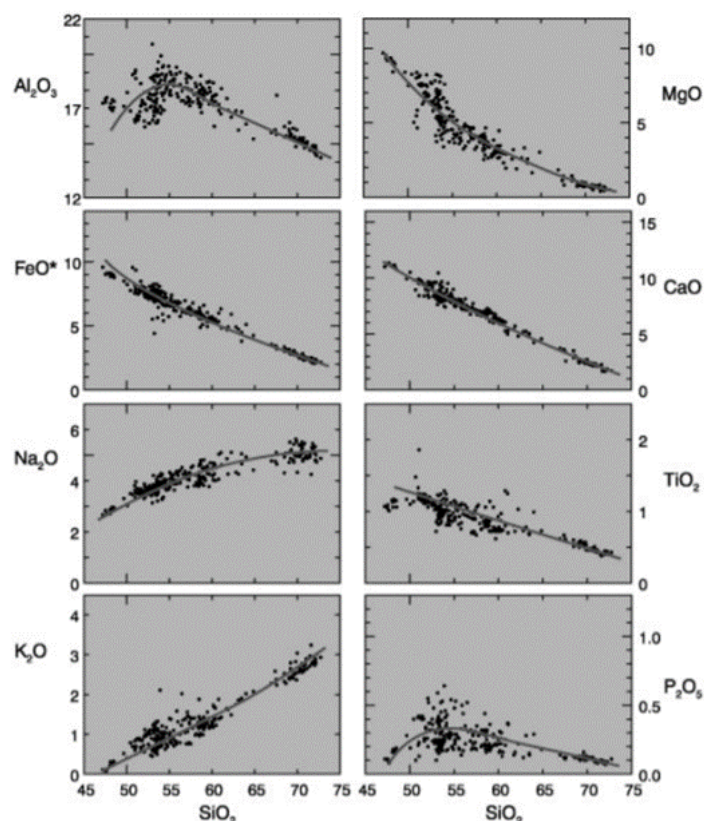
Figure 3.5: *Harker variation diagram for 310 analysed volcanic rocks from Crater Lake (Mt. Mazama), Oregon Cascades. Data compiled by Rick Conrey. Figure and text from (Winter, 2001).*

Alumina saturation indices (ASI)

The alumina saturation indices are another bivariate plot based on the molar content of alkali metals versus the molar content of alumina. The ASI is a molecular ratio that can give information on the magma source, and the conditions under which it was melted (FROST et al., 2001). The ASI is given by

$$ASI = \frac{molar\,(Al)}{molar\,(Ca+Na+K)} \qquad\qquad (V)$$

If the ASI is < 1 the rock can be either peralkaline or metaluminous depending on the relative content of K + Na vs Al. With a high content of Al the ASI will be > 1, and the rock is thus termed as peraluminous. The amount of Al in the rock exceed the amount that can be incorporated into the feldspars and will thus enter other mineral phases. This is common in rocks with a sedimentary protolith. Figure 3.6 below, having of an ASI > 1, is one such example.
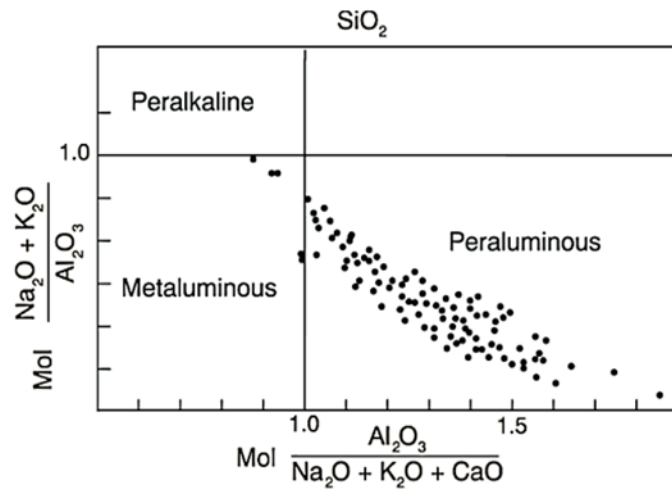
Figure 3.6: *Alumina saturation indices with analysis from the peraluimonous granitic rock from the Alchala Batholith, Argentina. Figure and text from (Winter, 2001).*

Total alkalis vs. silica index (TSI)

The total alkalis versus silica index is used to differentiate between the alkaline and the subalkaline magma series. The bivariate plot the wt. % silica oxide, SiO_2, vs. the combined wt % of sodium and potassium oxides ($Na_2O + K_2O$). The division can be used to indicate the tectonic environment, where subalkaline magmas are typical for different arc setting, whereas the alkaline is more typical for continental rift setting or hot spots. Figure 3.7 below a TSI diagram with sample data from Hawaii.
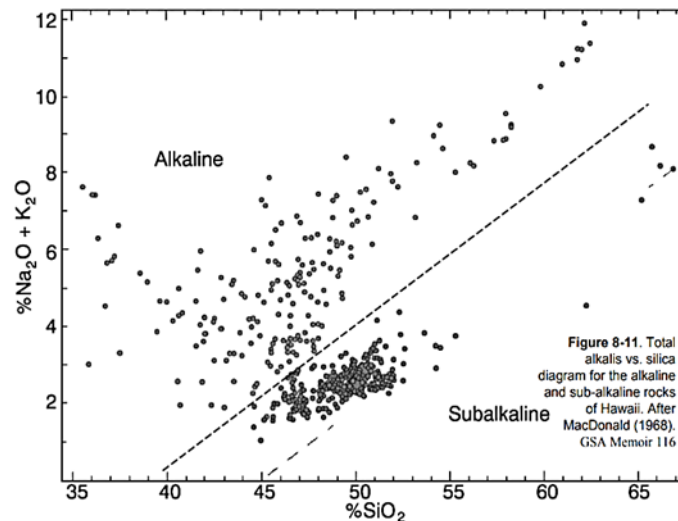
Figure 3.7*: Total alkalis vs. silica diagram for the alkaline and subalkaline rocks of Hawaii. Figure and text from (Winter, 2001).*

AFM diagram

Of the trivariate diagrams the AFM diagram is one of the most used. It characterizes the magmatic trend by plotting the magnesium oxides (MgO) against the alkali oxides (K_2O + Na_2O) and the calculated total of the iron oxides (FeO + Fe_2O_3). The main strength of the plot is to illustrate trends in the development, which in turn can be used to define the magma series. The plot illustrated in Figure 3.8 below is used to differentiate two subalkaline subdivisions, the tholeiitic and the calc-alkaline magma series, where the Skaergård samples represent the former and the Crater Lake samples represents the latter.
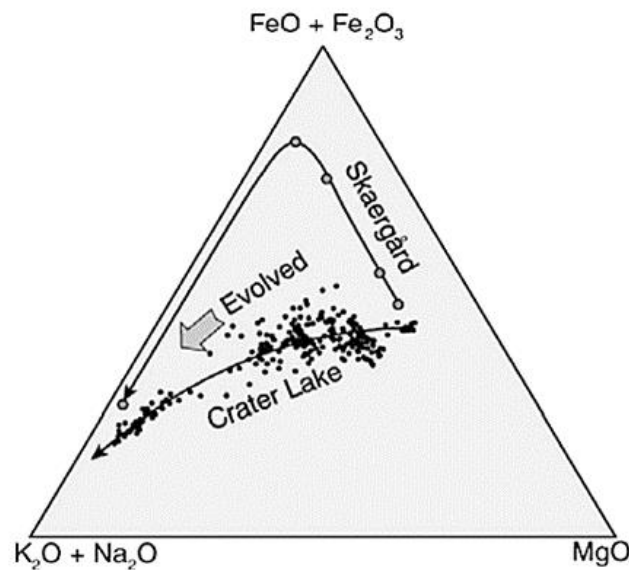
Figure 3.8: *AFM diagram from Crater Lake volcanic and the Skaergård intrusion. The arrow illustrates the leftwards direction of the magma evolution, from more primitive to evolved (Winter, 2001).*

3.2.3 Trace elements

Trace elements are elements that comprise < 0.1 wt. % of a sample (Winter, 2001). The elements are classified on the basis of their geochemical behaviour where the most useful are the transition metals, and the rare earth elements, (REE). Where small cations with a high charge are known as high field strength (HFS) cations, and large cations with a small charge known as large ion lithophile elements (LILE). An important characteristic of the trace elements is whether the elements in the melt are compatible or incompatible. If an element is compatible it would prefer to stay in a crystal phase, whereas the incompatible will remain in the melt if possible. These properties can be related to the ionic radii and charge, often referred to as the "field strength". Small cations with a relatively low charge usually are more compatible. The partition coefficient, D, is given by

$$D = \frac{C_S}{C_L} \qquad \text{(VI)}$$

Where Cs and CL is the concentration of trace elements in the solid and liquid phase respectively, given as either ppm or wt. % (Winter, 2001). The partition coefficient can be affected not only by internal factors in the elements themselves, but also external factors such as composition, temperature, pressure, and water content in the melt (Rollinson, 1993). This variation can lead to the formation of distinct patterns unique for each tectonic setting, making trace element geochemistry a preferred method for petrographic research.

REE diagrams

The REE include the fifteen elements between Lanthanum (La) and Lutetium (Lu) in the periodic table. The elements are placed together due to their similar chemical and physical properties causing them to behave as a coherent series. When plotting the REE the atomic number are on the x-axis against the concentration on the y-axis. The atomic number are arranged with increasing compatibility toward the righthand side. The plots are commonly standardized against chondrite, which eliminates the Oddo-Harkins effect and makes it possible to compare the REE directly with primordial Earth values (Winter, 2001). The pattern and shape of the REE anomalies can be used to interpret events in the magmatic evolution. One such example is the Europium (Eu) anomaly illustrated in Figure 3.9 below, indicating crystallization of plagioclase. It is worth noting that the patter will get more complicated as a magma evolves. Rocks with granitic compositions, which can contain several different accessory minerals with high partition coefficients, will complicate the RRE pattern.
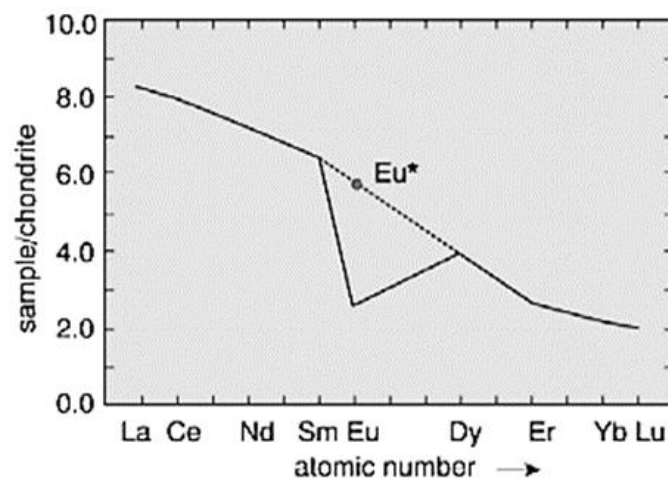
Figure 3.9: *REE diagram with 10% batch melting of a hypothetical Iherzolite with 20% plagioclase. Because Eu^{+2} is retained in the plagioclase of the source, the extracted melt is depleted in Eu, resulting in a pronounced negative Eu anomaly. Text and figure from (Winter, 2001)*

Spider diagram

Spider diagram are based on the same principles as the REE diagram discussed above and are essentially the same. They differ in that they incorporate a larger selection of trace elements. The selected elements can vary in different literature, as there is no set norm. The system is also flexible as to which normalization schemes is being used, chondrite, Mid Ocean Ridge Basalt (MORB) and primitive mantle are some examples. Figure 3.10 below gives an example of two spiders plots with different normalization schemes.
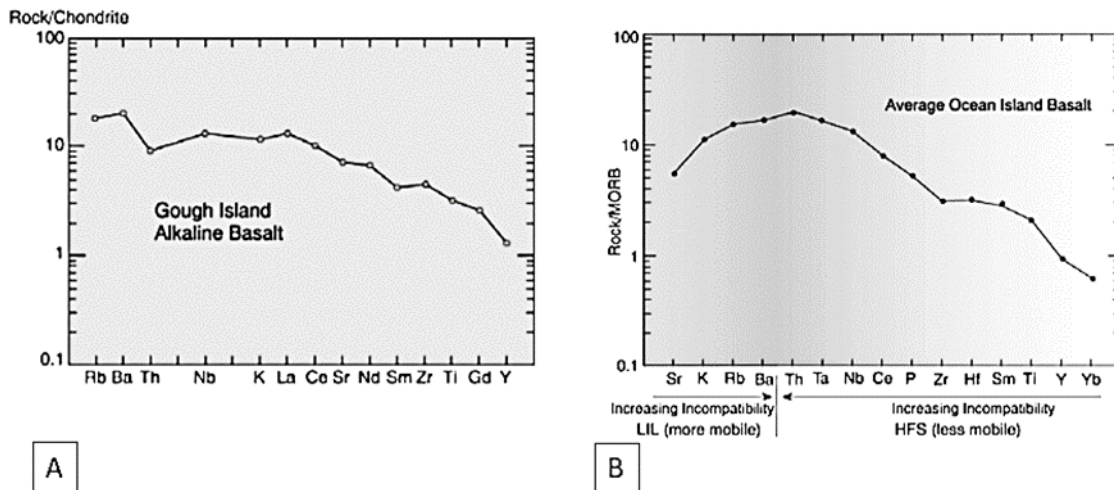
Figure 3.10: A) Chondorite-normalized spider diagram showing the trace patterns of an alkaline island basalt B) MORB normalized diagram showing the pattern of an ocean island basalt. Figures and text from (Winter, 2001).

Trace element discrimination

Trace element discrimination diagrams are plots used to fingerprint the geological setting of a rock, though most used on basaltic rock. Methods have been developed to try and implement the same method on rocks with a granitic composition. Granites, being more complex, are not best suited for such a classification, but as noted by Winter (2001) when working with old rocks they may not be in their original setting, making the trace element discrimination diagrams a method that can indicate the former geodynamic conditions. Figure 3.11 below illustrates an example of a trace element discrimination plot, plotting ppm Rubidium (Rb) against Yttrium and Niobium (Y + Nb) (Pearce et al., 1984).
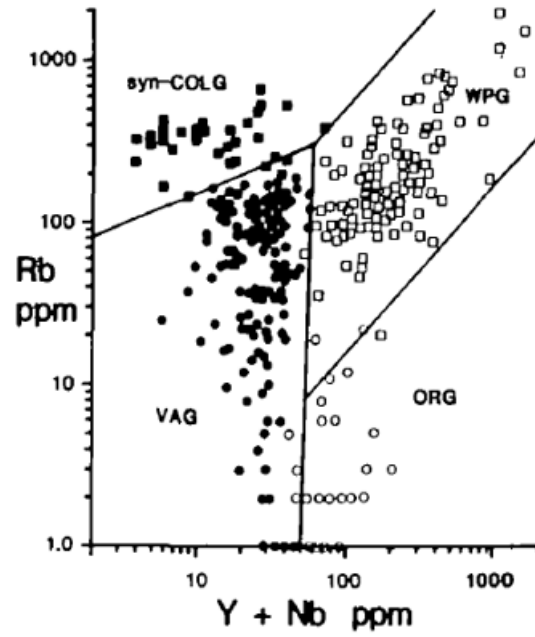
Figure 3.11: *Example of granitoid element discrimination plot, Rb – (Y + Nb) The granites are divided into four main groups based on origin, ocean ridge granite (ORG), volcanic arc granite (VAG), within plate granites (WPG) and collision granites (COLG) (Pearce et al., 1984).*

4 Methods

4.1 Fieldwork

The field area was first visited on a two-day trip during the fall 2018. The main bulk of the field work was done over a period of 30 days divided into two separate periods the next year. The first session of seven days early summer 2019 was used to assess the area and prepare for the return later the same summer. In addition, one daytrip was made to the area to visit key locations for further observation during the fall of the same year.

The field area covers approximately 100 km^2 in Nordmøre, a region in Møre og Romsdal. The field area compromises two populated areas, Rausand and Eidsvåg, and a large section of mountain area located in between.

The mapping was done with the use of both modern and more traditional methods. Maps printed on A3 paper, at a 1:100 000 scale, were used to map the geological features. In total 12 maps where used all together. The maps illustrated the terrain outline by contours and distinct features such as ponds, settlements, roads, and marshlands. Supplemental digital maps were used to locate less vegetated areas. The traditional geological mapping was done by using colour to mark the outcrops, marks made to fit the outcrop actual size. Additional information for each outcrop, such as measured magnetic susceptibility, were noted in the field notebook. Where features are small to make any distinguishable map feature additional notes were made, and a marker added on the map. The digital mapping was done with the use of a windows tables with the software ArcPad v-10.2. Structural features, measured with a geological compass, and other notable field observation were marked on the pad to get precise UTM coordinates. The same procedure was used to mark the location of the collected field samples. Registered data from both the analogue and the digital maps where combined to create the finalized geological map.

Supplement maps and data images supplied by NGU and Allan Krill was used to aid the mapping and locate areas of potential interest. Of most importance is the geophysical mapping done in the area, which has been used to indicate the location of highly magnetic ore bodies. Previous geological maps made in the region made available via NGUs open map system, and published LiDAR images were also used.

4.2 Samples

A collection of 30 samples from the field area were selected for further analysis. The samples were selected to give an insight of the region, with both geographical and petrological variation in mind. The samples can be roughly divided into three groups: basement gneisses, mafic intrusions, and allochthonous rocks from the nappes. Each sample was cut into pieces to suitable size for further analysis. A section was taken out of each sample to be used as a reference sample.

In addition to the 30 samples collected in the field area, and additional 16 samples from the Western Gneiss Region were used for geochronological analyses, and 38 additional samples for the geochemistry, all provided by Trond Slagstad. The additional geochronological samples are leucosome from selected gneisses from the basement, where the zircon in the leucosomes were to be dated. Two thin sections made from rock collected during the first reconnaissance trip in 2018 fall within the set field area and will be used as well. Figure 4.1 below illustrates the sample distribution. A summarised list of the 30 samples from within the field work area, with associated information of location, lithology, and preformed analysis is given in Appendix A.
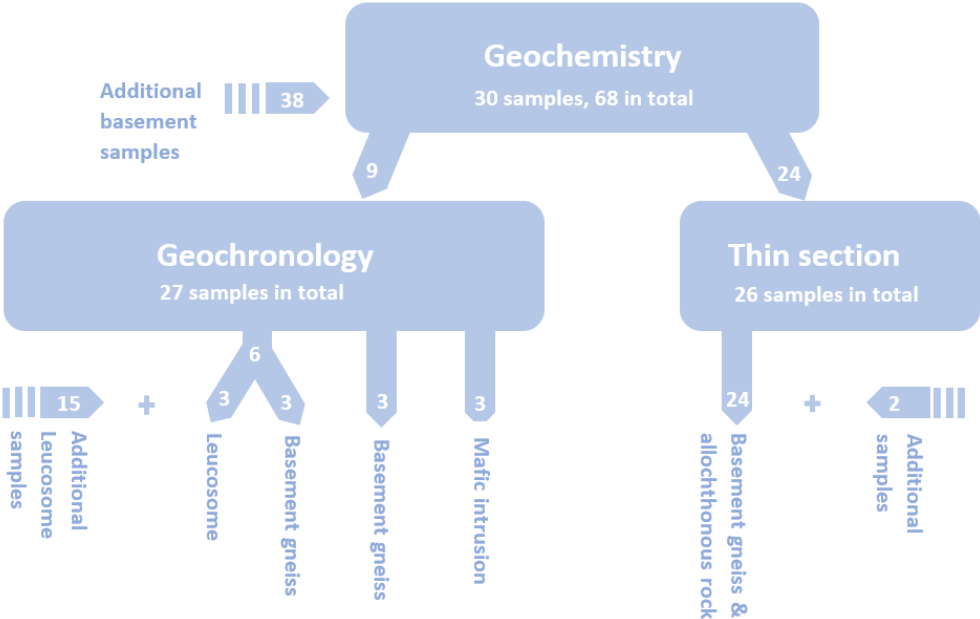
Figure 4.1: *Simple diagram illustrating the sample distribution for analytical work*

Figure 4.2 below illustrates a workflow diagram for the performed sample analysis. Further details of the analysis process are given in the following sections.

Figure 4.2: *Workflow diagram for sample analysis*

4.3 Geochronology

In total 9 samples from the field, and an additional 15 samples were analysed. The additional samples were collected leucosomes from elsewhere in the Western Gneiss Region and are to be used as supplement to give a broader geographical perspective. Three leucosomes were cut out of their host rock for individual analysis, resulting in a total of 27 samples for further geochronological study. The work process and equipment used will be given in further detail in the subsections below. Appendix D3 lists the complete analysis results. Appendix D1 and D2 illustrate the BS- and CL images respectively, of the selected zircons, each sample marked with its corresponding analysis number.

4.3.1 Fracturing

SelFrag

The SelFrag Lab is a machine that uses high voltage pulse power technology to fracture rock samples. The technology is based on the principle of introduction of energy via electrical discharges into solids immersed in water which are situated near two electrodes. The induced energy produces a shock wave that fractures the material (Kaeppeler and Morach, 2016). The method fractures the samples without any loss of material, but the container can only fit samples of approximately 200g and is thus only used for smaller samples. Due to the smaller sample size of the leucosomes these three samples where fractured using the SelFrag Lab at NTNU. The samples were divided into smaller portions and placed in the lowermost part of the container, which in turn was filled with water and placed in the lab machine, as can be seen in Figure 4.3 below. The SelFrag Lab was set to complete 100 pulses with a frequency (Hz) of 5.0 at a voltage of 200kV. After each subsequent fracturing, the container was dismantled and cleaned to avoid contamination between samples and limit wear and tear on the machine.

Figure 4.3: *SelFrag Lab at NTNU. The sample container can be seen on the green holder in the machine.*

Jaw crusher

The remaining nine samples were crushed using the jaw crusher at NGU, as the larger sample sizes allowed for more material loss during the fracturing prosses. The jaw crusher works by the simple principle of feeding the sample material into the cruncher, where the one plate subsequently applies mechanical force onto a stationary plate, fracturing the input material. Each sample was fed though the machine twice to get enough material in the desired fraction. The jaw crusher was dismantled and cleaned before each sample was crushed.

4.3.2 Splitting and sifting

After fracturing, the samples were split using the splitter at NGU. Splitting the samples serves to get a statistically valid sample for further processing, dividing the sample in too randomly distributed parts. The splitting was conducted in several turns for each sample to get appropriate sample size for further chemical analysis. One part was sent to the ALS Chemex laboratories in Sweden, one part of similar proportion was kept as a backup reference sample. Further processing of the geochemistry samples is given in the geochemistry section below. The remaining samples were sifted continuously with the crushing and splitting. The sifting process separates the crushed material into two fractions, >250 µm and <250 µm, respectively. The former was kept aside in case of further need of the sample, the latter put aside for further use in mineral separation. Before each sample, the splitter was cleaned with alcohol and an airbrush to avoid sample contamination. The used sifts were cleaned with alcohol and visually inspected with a lightboard to control that no remaining grains where stuck in the filters. The sifts with smaller grids were place in an ultrasound bath to better release the smaller grains before the visual inspection.

4.3.3 Water table

The remaining part of each sample with a grain size of <250 µm was taken to the mineral separation lab at NGU. The water table consists of an approximate 100x50 cm plate with groves and a slight tilt. Mounted pipes distribute water equally over the plate before running over at the end corner, allowing the lighter minerals to be washed off first, and the heavier to remain last. An image of the water table is given in Figure 4.4 below. For each sample, a small portion of the material was placed on top of the water table, first letting the lighter material rinse off, before collecting the heavy material at the end, this way segregating the material by relative density. This procedure was repeated for each sample for the number of times needed to separate the entirety of the <250 µm portion of the sample. The water table was rinsed off and dried over before each separate sample to avoid any contamination. The resulting material was dried, heavy material put in plastic containers for further separation, the light material bagged and stored.
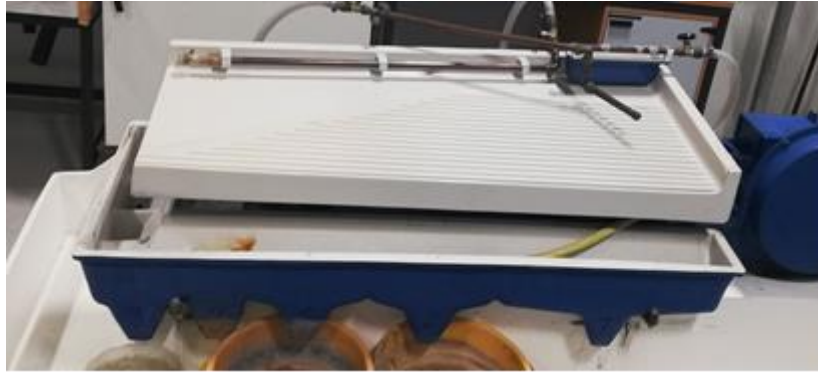
Figure 4.4: *Water table used for wet separation of heavy minerals*

4.3.4 Magnetic separation

Separation of magnetic material from the heavy samples were done in two stages, first using a magnetic stick, and then the vertical Franz separator.

Magnetic stick

Each plastic container was filled approximately 2/3 with alcohol. A small magnet stick was then held over the sample to remove magnetic material from the remaining sample. The magnet was covered in plastic wrap that was removed and changed between each sample. The magnetic material removed was thrown away with the covering plastic.

Vertical Franz

When dried the samples were further separated using the vertical Franz, see Figure 4.5 below. The procedure consisted of making a paper tube, taping it to the magnets and dropping the sample though the tube with the magnets activated. Thus, the magnetic material would stick within the tube, whereas the nonmagnetic material would fall straight through. Each sample was dropped twice with an applied field induced with 1V. The separated material was collected when the magnetic field was turned off and placed in a separate plastic container. The paper tube and prepping paper were changed between each sample. The vertical Franz was cleaned with an airbrush to remove any potential residue before each sample.
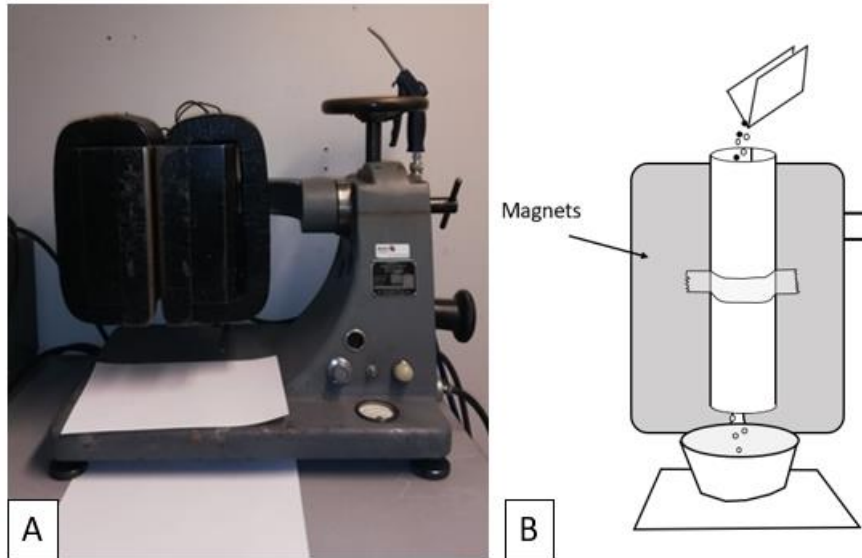
Figure 4.5: *A) Image of vertical Franz separator at NGU. B) Illustrative sketch of assembly during separation, black and white circles illustrate magnetic and nonmagnetic material, respectively.*

4.3.5 Heavy liquid separation

Out of the zircon samples only 4 were deemed to be of adequate sorting to not undergo this last step. These samples would proceed directly to the next step of the process. The remaining samples either contained too much residual material to sufficiently pick out the zircons or contained "zircon like" material that would be hard to distinguish in a microscope. This separation was performed at NGU under supervision.

Figure 4.6 below illustrates the four main segments of the heavy liquid separation process. First, the 250 ml separation funnel was mounted on a ring stand together with two funnels with filters. The heavy liquid with a density of 3.3 g/cm^3 was poured in. The mineral material was then poured into the separatory funnel and left to segregate. The separatory funnel can be rotated slightly to get all the material into the liquid. Due to the density contrast the heavier minerals such as zircon, apatite and pyrite will fall to the bottom and can be drained out separately, see Figure 4.6 C. Removing the filter containing the heavy material, and changing to a new clean funnel, the rest of the heavy liquid can be drained out and be poured back into its original storing container. The residual light material can then be cleaned out of the separatory funnel with acetone, as seen in Figure 4.6 D. As the heavy liquid contains hazardous chemicals all equipment and filters are cleaned with acetone after use. The contaminated acetone is stored in a separated container. The separated material was then dried and put in separate containers for further use. This process was performed on each sample separately.
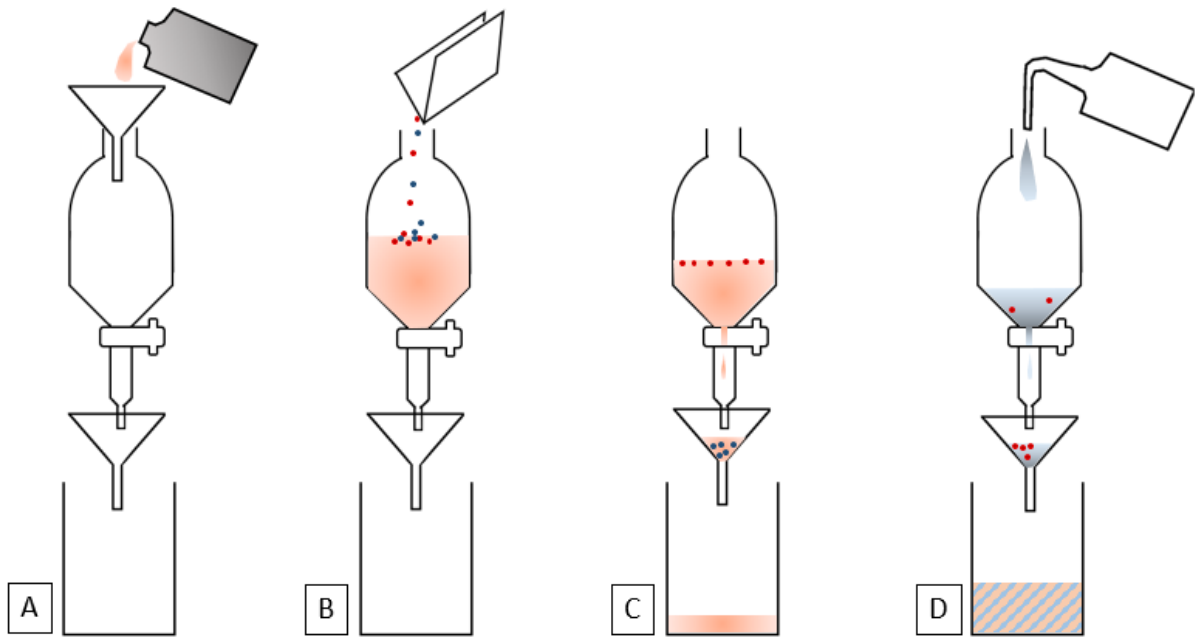
Figure 4.6: *A) Separatory funnel is filled with heavy liquid, a funnel with a filter placed on top to ensure no contamination between samples. B) Sample material is poured into the separatory funnel. Red circles marking light material, blue heavy. C) After the material gets some time to settle the funnels is drained slightly to remove the heavy material at the bottom. D) Having changed the bottom funnel with a new filter the remaining heavy liquid is drained out, the bottom beaker is replaced, and the separatory funnel is clean with acetone to remove any residual material and clean the funnel.*

4.3.6 Picking and assembly

The plastic container was first filled approximately 2/3 with alcohol, then 50 grains were separated out from the remaining material with needle tweezers. After the alcohol was drained and dried, these grains were moved over on tape. The selected grains were primarily zircon, but for some of the samples a few grains of possible monazite were also picked out. The grains were placed on the tape in separated areas, each area designated to one sample. All equipment in contact with the samples was either changed or cleaned before each sample to avoid contamination. When the tape was sufficiently filled with samples it was covered with a plastic form which was then filled with epoxy. When the epoxy dried the plastic-form was then removed from the tape, leaving a piece with mounted zircons ready for polishing. The epoxy piece was polished down to get a cut approximately in the middle of the zircons, which normally is about 10th μm. The samples were mounted on two separate bricks.

4.3.7 Imaging

The two bricks were both carbon-coated at NTNU before cathodoluminescence, (CL), and backscatter, (BS), -imaging with the scanning electron microscope, (SEM), at NGU. The carbon coat was meant to create a conductive layer on the brick surface so that any charge would not be collected on the surface during CL scanning. While mounting the bricks carbon tapes were placed on the brick's sides to further lead away any charge from the brick surface.

The SEM was run over several days to get CL and BS images of all the mounted samples. One BS image was needed for each sample. The BS images were correlated with images of the mounted grains to ensure that the images were branded with the correct sample number. The CL images had to be taken in two turns for a selected number of samples, one with high and one with low brightness exposure. This was due to high light contrast making one image insufficient to display both the inner and outer structure of the grains. The CL images were to be used as a reference during the U-Th-Pb analysis to place the laser-beam on the zircon grains. Making it possible to differentiate between the zircons outer-rim and the inner-core. And to separate which mineral grains that in fact were not zircon. These grains would have had zircon like properties and appearance that would have made them indistinguishable during earlier separation. The BS and Cl images combined made it simpler to identify these grains, which were important as they were not to be used in further analysis. Overview images of the mounted samples are provided in Appendix D.

4.3.8 LA – ICP - MS

The bricks were cleaned of carbon with nitric acid, to ensure a completely clean surface, and separately placed into the laser ablation inductively coupled plasma mass spectrometry (LA-ICP-MS) at NGU. Twenty-four shots were done on each sample, where possible. The laser shoots with a spot size of 15 μm in diameter over a up to $60\mu m$-long line a repetition rate of 10 Hz and an energy corresponding to a fluence of 3 J/cm^2 for each grain. Five different standards were used for calibrating during shooting, GJ, Z6412, 9500, SJONA, and NIST. The last standard, Tomari, was only used one of the two bricks. In total the shooting was performed over five sessions, dividing the samples between the time available for each session. With an exception for the first shooting, where the shooting and calibration was done in turns, the sessions where fully calibrated before shooting was initiated.

4.3.9 Ur -Pb dating

The obtained result data was transferred to excel files and imported into the program GLITTER® (Van Achterbergh et al. 2001) for data reduction which was executed by Trond Slagstad. Complete dataset and CL images with marked shooting location and number is given in Appendix D2. Further plotting and age calculation were performed with Isoplot (Ludwig 2003). The resulting U – Pb isotopic data is presented in TW-plots. The age is set individually for each sample, further description for each sample is given in section *5.2 Geochronological data.*

4.4 Geochemistry

All the selected samples were sent to geochemical analysis. First 20 samples were sent to ALS Chemex laboratories in Sweden. The remaining 10 were sent later to the same laboratory, as 9 of the samples first had to be crushed and separated to be used in geochronological studies. All samples used for geochronological studies were crushed before being sent, as described in the section above. The first 20 samples were sent in cut pieces, and were crushed in the ALS Chemex laboratory with the following description provided on the laboratory web page; sample crushed to 70% less than 2 mm, then riffle split off 250 g and pulverize split to better than 85% passing 75 microns. It is to be noted that for all migmatitic basement samples the leucosomes were cut out so as not to be part of the geochemical analysis.

In the ALS Chemex laboratory, the samples went through a whole-rock geochemistry analysis. The samples were analysed by the method code ME-MS81d, which entails a combination of Rare Earth & Trace Elements from method ME-MS81™, plus whole-rock package by method ME-ICP06. ME-MS81™ is a code for Trace Elements analysis by Li Borate Fusion, and ME-ICP06 as a code for both XRF (x-ray fluorescence) and ICP-AES (Inductively coupled plasma atomic emission spectroscopy) analysis. Full descriptions and analysis method can be found on ALS Chemex webpage, alsglobal.com/. Specific whole-rock analysis procedures are in the free ALS Geochemistry brochure available on the webpage given above. The returned data were given in an excel file, which in turn were inserted into the plotting program Igpet for graphical representation.

4.5 Thin sections and petrography

Twenty-four samples collected during the field work summer 2019 were sent to the thin section laboratories at NTNU for preparation. The samples were polished to 25micrometres thick thin sections of 28x40 mm in size. All thin sections were polished. Two thin sections made from samples collected in 2018 from a nearby field area.

Due to the Convoid-19 Pandemic complete petrographic description and scanning of all Thin sections where not feasible. All thin sections were when possible studied in a transmitting light microscope to identify the mineral composition and to characterize structures and textures within the rock samples. For the mafic samples with opaque minerals, a reflecting light microscope were used to identify the magnetic mineralization. Twelve thin sections were scanned at NTNU, two at TTU. Scans and images of the thin sections are given in Appendix E. Complete petrographic description are given for two samples both prepared in the manner described above at the same lab at NTNU. Both of which were collected during the field work, fall 2018.

4.6 Sources of error

For this project there were three main analytical methods applied in the lab; whole-rock geochemistry, U – Th - Pb geochronology, and thin section petrography. As the geochemistry was mostly performed at an external lab full control over the process is not given. Potential errors would then mostly be limited to later interpretation of the data. The same goes for thin-section petrography, where the most likely source of error would be interpreter mistakes. In the section below a potential source of error related to the U-Pb geochronology is given in more detail. The final remark made related to analytical and statistical errors below, can apply to not only the U-Pb geochronology but also the geochemistry and petrography.

Though the U – Th – Pb dating systems can give high precision results, they are far from perfect, and there are a lot of possible pitfalls related to geochronological studies. Natural causes of discordance in U – Th – Pb systems can be classified as both random and systematic and are often related to the system not being completely closed. One geological feature that might lead to this is mixing of age domains within the mineral. E.g. where inclusion within a zircon might have an older age than the rim, thus a bulk analysis would lead to a wrongly set age. Spectroscopic methods, such as CL and BSE, can be used to identify distinct growth areas within the zircon, thus making it possible to date different growth areas separately with a directed laser beam. Another essential feature is the loss of Pb from the mineral. In zircon this can occur from an array of processes: volume diffusion, loss due to radiation damage of the crystal, plastic deformation generating fast diffusion flow tracks, and reprecipitation of dissolution at low-T hydrothermal conditions (Schoene, 2014). In a natural system several factors may be affecting the mineral simultaneously. The final factor would be that the system is not in secular equilibrium, due to some intermediate daughter products. Calculations can be

made to try and correct this factor, and though such calculations can help, they do not render true results. The same is true for the correction of initial Pb percent in the mineral prior to radiogenic decay. A purely systematic error is the uncertainty related to the calculated U and Th decay constants.

Analytical errors are an external uncertainty. Examples of such errors would be any errors with the measurement instruments, or any contamination of the samples during the preparation procedures. To ensure that this latter problem is minimized all equipment is cleaned before use, during the zirconium dating a reference sample is used during the laser ablation. Though not going into more depth in the subject, note is made of the effect correct use of statistics has on the results. Schoene (2014) and Schaltegger et al. (2015) go through selection of typical statistical models used and how incorrect use, or bad samples can lead to grossly incorrect age estimations when dating zircons. For the whole rock geochemistry, it is important to note what normalization model has been used when correlating data with, or from different publications.

5 Results

5.1 Field observations

Observed geological and structural features within the field area will here be described. The first section will be presenting the constructed geological map, followed by an introduction to the rock description made in the field of which the map is based. Then an introduction to some of the structural features within the field area. Finally, a note will be made on the observed migmatites in the area.

5.1.1 Geological map

The study area is set the central part of the Western Gneiss Region located on the north-western coast of Norway. The field work area is a 10 x 10 km area, including Raudsand, Eidsvåg and a large section of the mountain area in between. The geological mapping has mainly been done along roads and paths with exposed outcrops and a selection of traverses across the mountain area to better extrapolate the geological boundaries. A geophysical map of the area is used as a supplement to the mapping and is of special use due to the magnetic ore present. The 1:50 000 geological map available by the NGU has also been used and found to mostly coincide with observations made in the field, with some slight alterations.

The resulting geological map is presented in Figure 5.1 on the following page. Further detail on the mapping procedure is given in the method chapter under section *4.1. Fieldwor*k.
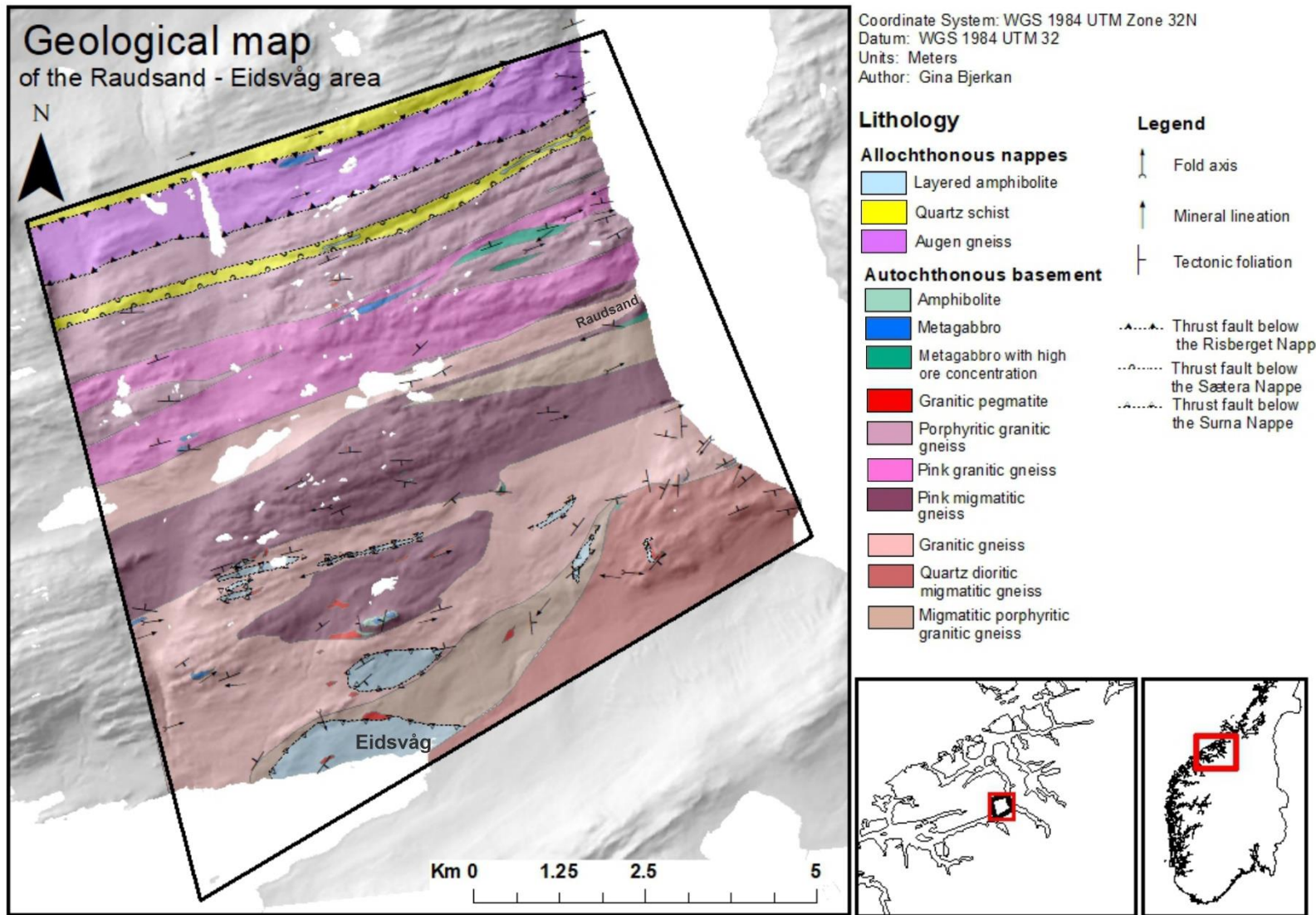
Figure 5.1: *Geological map of field area*

5.1.2 Rock description

A description on the mapped units in the presented geological map in section *5.1.1. Geological Map* above, is given in this section. The descriptions are based on field observation made during mapping. Later thin sections have not been taken into consideration.

Porphyritic granitic gneiss

Granitic composition with high proportions of plagioclase and quartz, mafic minerals consist mainly of biotite and amphibole, all heterogeneously distributed along the lineation, with a medium to fine grain size, see Figure 5.2. It is characterised by lineated phenocrysts of K-feldspar, 2 - 10 mm in size. Some veins are observable, occurring alone, or in sets situated a few metres apart. The veins are leucocratic, with similar grains size as surrounding rock, and are 1 - 2 cm in thickness. The lack of an apparent melanosome suggest that the interpretation of these leucocratic areas represent fluid injections. The magnetic susceptibility (χ) is low, with χ less than or equal to 0. The colour is light grey, some variations can appear slightly pink. The mode of biotite, though mostly consistent, can be variable.
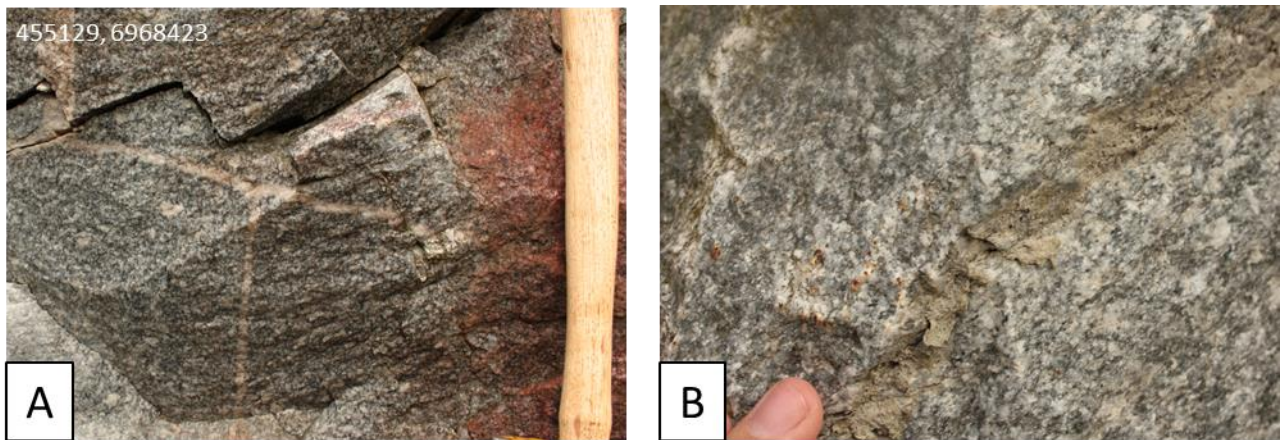
Figure 5.2: *A) Porphyritic granitic gneiss, geological hammer for scale B) Porphyritic granitic gneiss, fingertip for scale. Both images are form the same approximate location.*

Augen gneiss

The rock has a granitic composition, with abundant biotite and oxides, which can be observed as millimetre-sized grains. It is characterised by feldspar megacrysts of 0.5 – 2 cm in diameter that are heterogeneously distributed within the rock. Al megacrysts are elongated along with the lineation. The surrounding rock is of medium grainsize, and is has a homogenous distribution of biotite, giving the rock a dark grey colour, with the light pink megacrysts giving a spotted appearance when viewed perpendicular to the lineation, see Figure 5.3A. The magmatic megacrysts are assumed K-feldspar porphyroclast that has been reduced under the deformation forming the Augen gneiss. The magnetic susceptibility is intermediate, with χ values varying from 10 – 30.
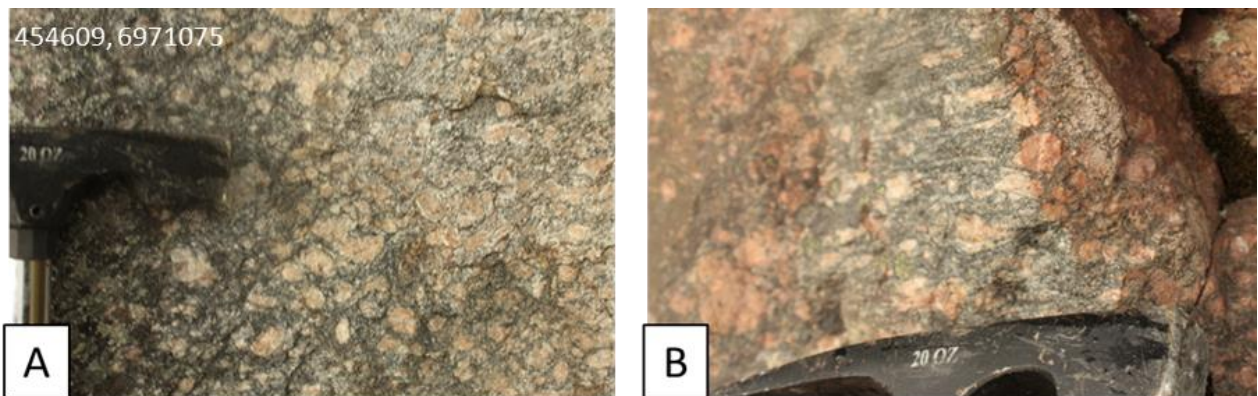
Figure 5.3: *A) Augen gneiss with hammer for scare B) Augen gneiss with hammerhead for scale. Note the lineation is visible when viewed parallel to the strike. Both images are from the same approximate location.*

Quartz dioritic migmatitic gneiss

The rocks light minerals consist of mainly plagioclase and quarts, see Figure 5.4. High content of amphibole, with additional biotite, give the rock a dark colour. Garnet can be observed. The rock has medium grainsize and a coarse surface texture. Migmatite leucosomes are aligned with the foliation and occur with an even distribution from decimetre to centimetre distance, appearing heterogeneously distributed within the rock. Two separate distinctions can be made of the migmatite appearances. In the first, leucosomes have a similar grain size with the surrounding rock, appear as even continuous layers of 1 – 2 cm in thickness and have a distinct mafic melanosome of 1 -2 mm. In the second, leucosomes appears as thicker elongated pegmatite lenses elongated with the foliation, with a decimetre scale elongation, with no apparent melanosome. These leucosomes may have migrated away from possible melanosomes. Amphiboles can be observed within the leucosomes in both types, but mainly occur on the pegmatitic migmatites. The magnetic susceptibility is low, χ < 5.
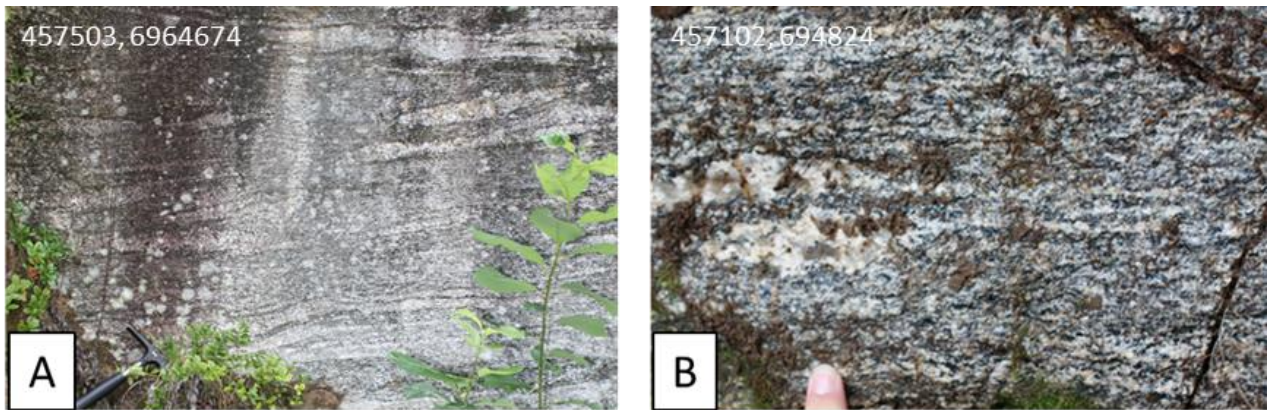
Figure 5.4: *A) Quarts dioritic gneiss with hammer in left-hand corner for scale. B) Quarts diotitic gneiss with finger for scale. Note the leucosomes in both figures.*

Granitic gneiss

In the granitic rock gneiss biotite and amphibole represent the main mafic minerals, oxides can be observed, see Figure 5.5. The rock is fine to medium grained, with a heterogeneous mineral distribution, aligned with the foliation. The amphibole can be observed in lager millimetre scale grains. The migmatite in this rock suite can be observed as a compositional layering of alternating decimetre scale layers with variable biotite content. The rock is observed with layers of intruding amphibolite, interfingering the granite in heterogeneous centimetre to decimetre thick layers. The magnetic susceptibility is variable, intermediate, χ between 20-30 in some locations, whereas it appears low, $\chi < 5$, in others.
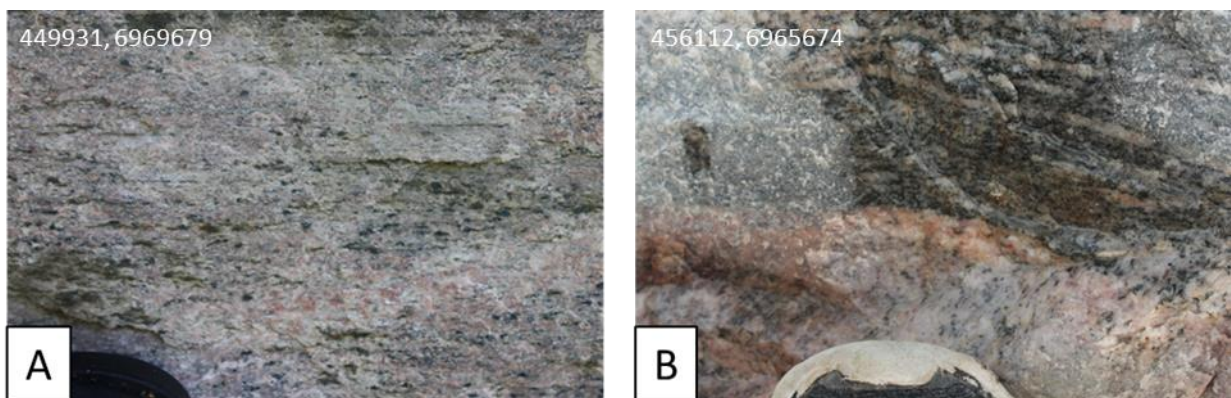
Figure 5.5: *Granitic gneiss, with a shoe tip on the lower left-hand former for scale. H) Granitic gneiss with shoe tip for scale. Note the compositional layering interpreted to be part of the migmatisation.*

Pink granitic gneiss

The rock has a granitic composition, with a distinct "salmon pink" colour, that appears homogeneously in the medium grained rock, see Figure 5.6. The mafic minerals consist of mainly fine-grained biotite, amphibole and in some places medium grained oxides. The biotite is heterogeneously dispersed along the foliation, resulting in a gneissic texture. Pegmatitic leucosomes, with the same distinct colouring as the host rock, are observed in decimetre scale elongated lenses, crossing the foliation at a low angle. In the right cut the leucosomes can indicate a sinistral sense of shear. The leucosomes show no distinct melanosome but have cm scale amphiboles within the pegmatitic areas. The susceptibility is generally low, 0-5, but has been observed with intermediate values between 20-30 in more oxide rich areas.
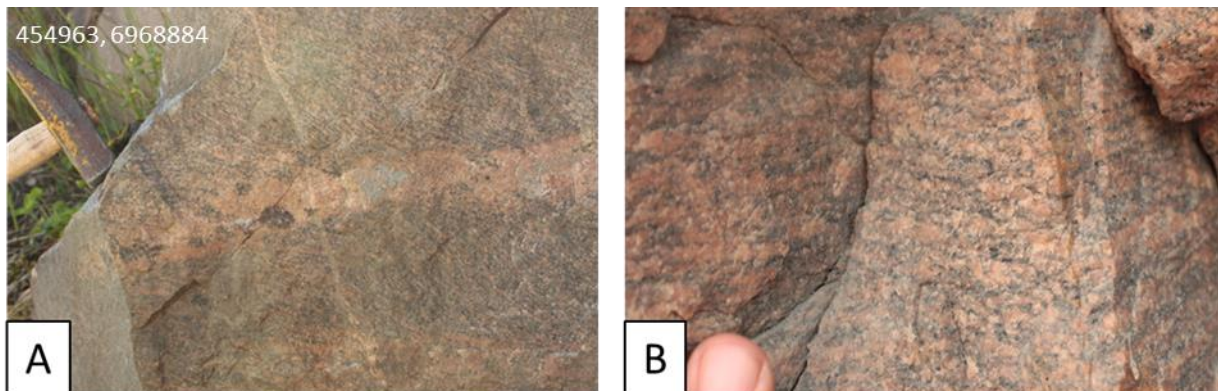
Figure 5.6: A) Pink granitic gneiss with geological hammer for scale. The leucosome cutting the foliation is distinctive for this rock suite and is only observed at a few locations along the roadcut. B) Closer image of the pink granitic gneiss, with fingertip for scale. Both images are from the same approximate location.

Migmatitic pink granitic gneiss

The rock has a granitic composition, with pink feldspars, see Figure 5.7. Biotite and amphibole represent the main mafic minerals. Varying grain size, mainly of fine to medium size, but with up to decimetre scale, pegmatitic layers. Two separate distinctions can be made of the migmatite appearances. The first, and mainly occurring type, has a similar grain size with the surrounding rock, appears as even continuous layers of 1 – 2 cm in thickness and has a distinct mafic melanosome of 1 -2mm. It appears with centimetres distance apart, in heterogeneous layers. The second type is a pegmatitic migmatite with varying thickness from centimetre to decimetre scale and is seldom occurring. The medium grained leucosomes appears with even thickness and grainsize along with the foliation, even in folded areas. The pegmatitic layers, though undulating in thickness, do not cross the foliation. The susceptibility is variable, but generally low, χ 0 – 5.
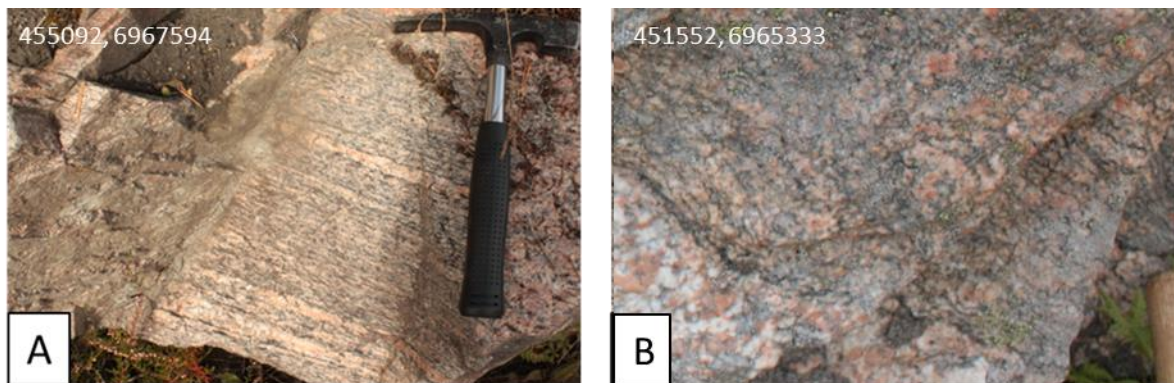
Figure 5.7: *A) Migmatitic granitic gneiss, with hammer for scale. B) Migmatitic granitic gneiss with hammer handle-tip on the lower right-hand former for scale. Not the distinct leucosomes with a mm tick melanosome.*

Migmatitic porphyritic granitic gneiss

The rock has a granitic composition, with a high content of biotite, see Figure 5.8. The rock is medium grained, with course to medium grained felsic migmatites lying along the foliation. Elongated, centimetre scale, phenocrysts can be observed within the host rock. The migmatites consist of leucocratic leucosomes, 1 – 5 cm in thickness, and biotite rich granitic layers in-between. The thinner leucosomes have a distinct 1 – 2 mm melanosome, whereas the larger leucosomes are observed with larger, millimetre scale, amphiboles. The magnetic susceptibility is relatively low, $\chi < 5$.
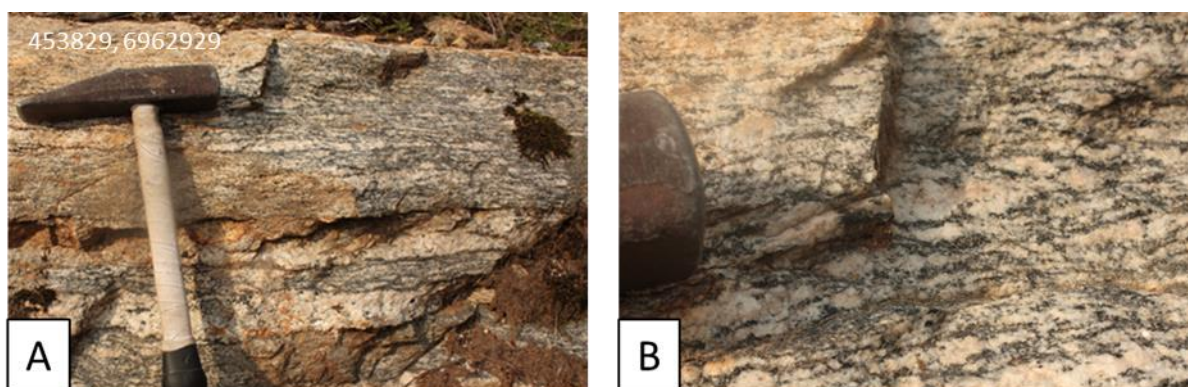
Figure 5.8: *Migmatitic phenocrystic biotite rich granitic gneiss with geological hammer for scale. B) Close shoot of same outcrop as in A, tip of hammer head for scale. Both images are from the same location.*

Layered amphibolite

Fine to medium grained amphibolite is observed with alternating mode of felsic minerals, giving a layered impression, See Figure 5.9. Quarts occur in both thin continuous layers, and lenses of 1 - 5mm thickness along the foliation. Elongated clasts of ~1cm can also be observed. Biotite is often observed as part of the foliation. Porphyroblastic garnets, 2 – 5 mm, and sulphides can occur. Magnetic susceptibility is low, usually with $\chi < 5$.
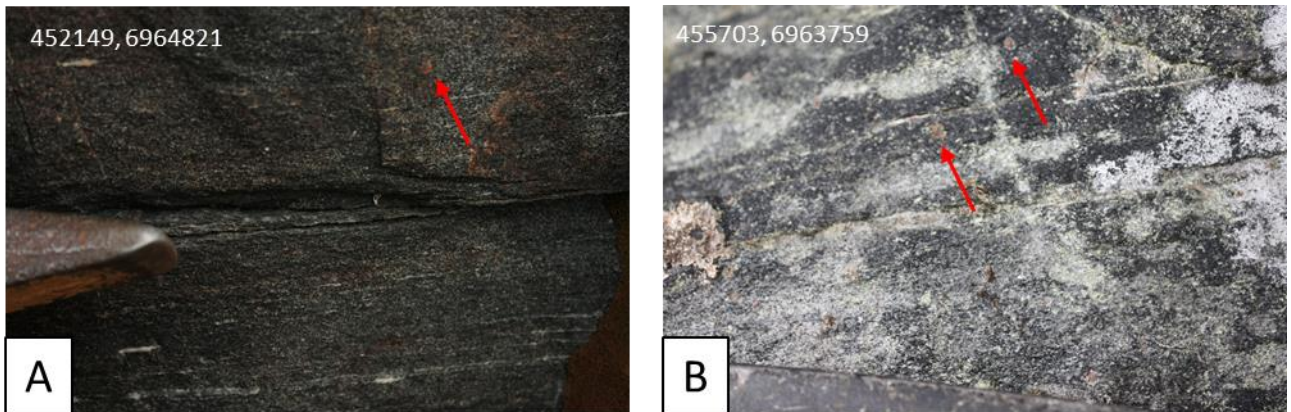
Figure 5.9: A) Layered amphibolite, with hammer tip for scale. B) Layered amphibolite with a more weathered surface, top of geological hammer for scale on lower left-hand side. Red arrows point towards visible garnets in both figures.

Metagabbro

Gabbroic bodies are mostly metagabbro with alternating compositional variation of mainly amphibole and plagioclase and heterogeneous variation giving a subtle layered appearance. Grain size varies from fine grained to pegmatitic, whereof the latter has a clear lineation. Finer layers with higher plagioclase content show clear sign of foliation. In other areas the metagabbro appears coarse grained and less affected by surrounding shear. The magnetic susceptibility of the metagabbro is generally low. The ore mineralization in the area is all centred in the metagabbro. The ore has little to no felsic minerals, observed as both fine grained and with larger magnetite crystals, in compositional layers in the metagabbro. The ore has a distinctly high magnetic susceptibility, measured as high as, $\chi = 800$. Figure 5.10 A to C below illustrates some examples of the observed metagabbro.

Amphibolite

Amphibole is fine to medium grained, occurring both as larger packages and as intruding layers. It is fine grained, with little to no felsic materials. The content of biotite can vary from moderate to high. It is clearly foliated and observed with cm scale crenulation folds. The magnetic susceptibility is low, $\chi < 5$. Figure 5.10 D to F below illustrates some examples of the observed amphibolite.
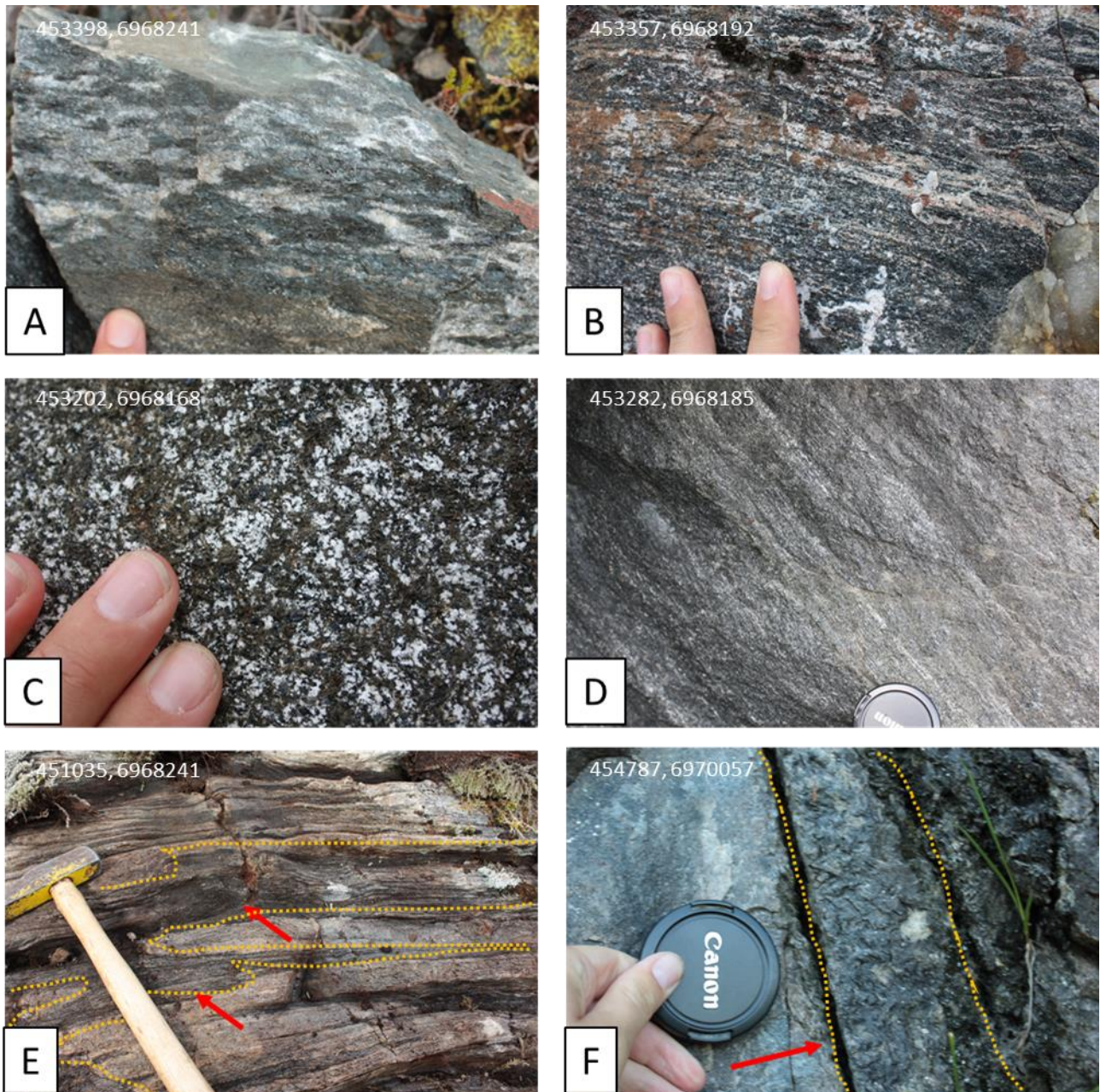
Figure 5.10: *A) Pegmatitic metagabbro. B) Foliated metagabbro C) Metagabbro with remanence of the original gabbroic texture intact D) Fine grained amphibolite, possible further alteration of metagabbro with little felsic material. E) Intruding amphibolite, marked with red arrows, in granitic gneiss which later has been folded. F) Intruding amphibolite in quartz schist, marked with a red arrow. The intrusion is interpreted to be altered, resulting in a high content of biotite forming crenulated folds.*

Biotitite

"Biotitite" layers have >90% biotite, observed with a thickness varying from a few mm to several cm. These layers are assumed to be altered mafic intrusions. The mica is aligned with the surrounding foliation. The magnetic susceptibility is low, $\chi < 5$. Note that these features are not marked on the geological map in section 5.1.1, due to its small-scale appearance.

Granitic pegmatite

Pegmatite with granitic composition, with large flakes of biotite observed. There is little to no foliation in the rock. The magnetic susceptibility is low, $\chi < 0$. Figure 5.11 A and B below illustrates some examples of the observed granitic pegmatite.

Quarts schist

Quarts schist is composed of fine-grained quarts and mica, mainly muscovite. A slight colour difference in 2 – 3 cm thick layers could indicate primary layering but is most likely an effect of later metamorphism. The magnetic susceptibility is low, $\chi \sim 0$. Figure 5.11 C and D below illustrates some examples of the observed quarts schist.
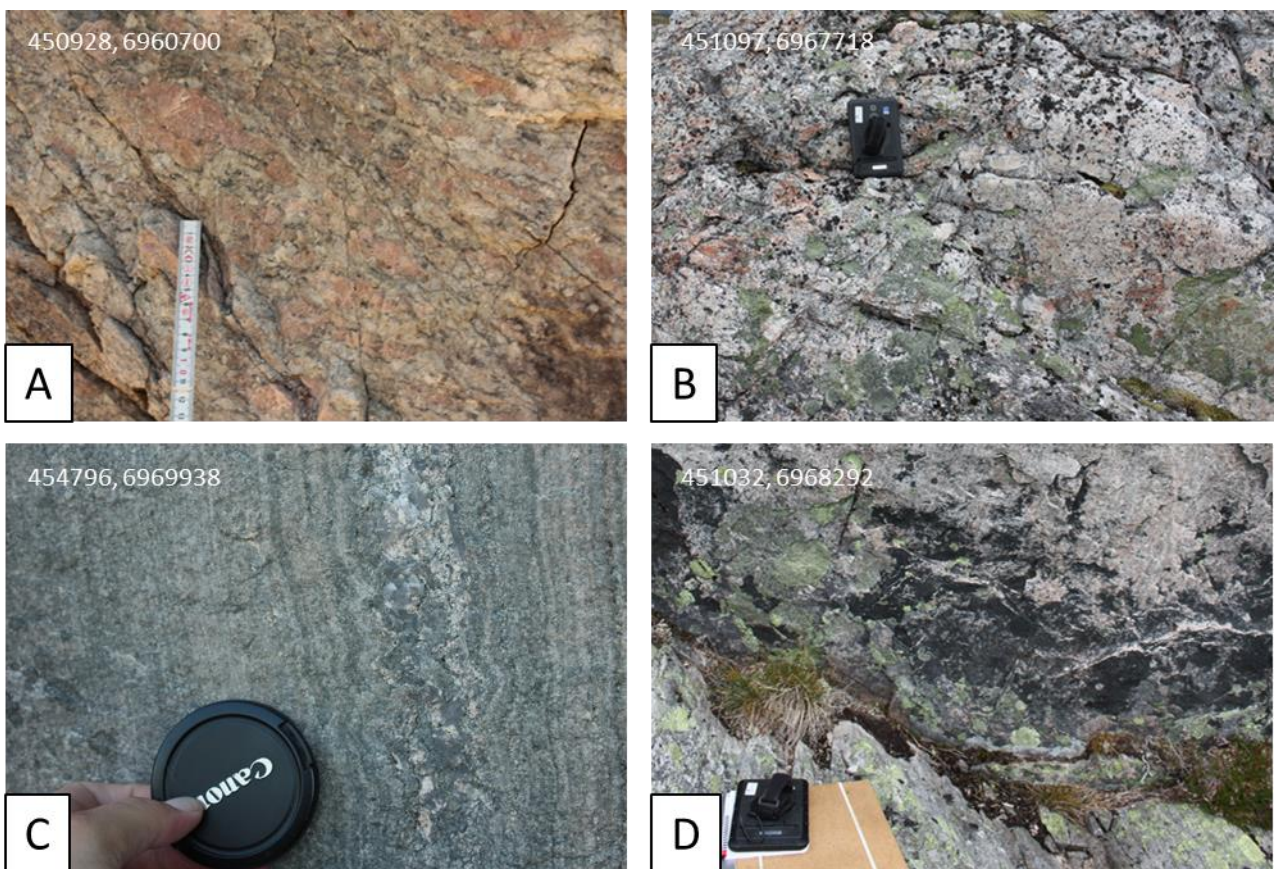
Figure 5.11: *A) Pegmatite with a slight lineation in the mafic minerals. B) Large outcrop with seemingly unaltered pegmatite, mapping pad for scale. C) Small folds observed in the quartz schist. D) Outcrop of quarts schist.*

5.1.3 Structural features

The Wester Gneiss Region is strongly affected by the Caledonian orogeny, see *section 2.2 The Caledonian Orogeny*. Given the size of the field area not all features will be discussed, only a selection will be given as examples, either to give an idea of the general nature of the area, or to highlight features of special interest.

All structural features are measured made a geological compass provided by NGU. Structural data is plotted using Stereonet 10.2.9. A software based on the original Stereonet and SteroWin by Richard Allmendinger; interface follows that of OSXStereonet by Nestor Cardozo and Richard Allmendinger. All contours are plotted with a Kamb contouring, with a spacing interval of 2, and a significance level of 3σ. For tectonic foliation, the measurements are made as dip/dip-direction and the complete selection of samples are plotted as poles on planes.

Boudins

Prominent extensional features are boudins. These features can be observed in different areas with variable lithological compositions and scales, varying from decimetre to metre scale. The occurrence of this feature in the different nappes serves as an indicator of the how the extensional strain has affected all nappes and basement present in this area during the late Caledonian extension.

The main requirement needed to create boudins is a variation in relative composition strength at the time of extension. In Figure 5.12 below examples are given where the less rigid material is the altered amphibolite. This is an occurring feature observed several places in the designated field area. Unaltered mafic rock has the higher compositional strength than felsic material, which usually for the boudins in an extension area. Seeing the reverse here indicate an alteration of the mafic rock before or during the extension. These mafic bodies are observable in different nappes, and do not necessarily belong to the same source. There are thus many possibilities as to what caused the alteration.
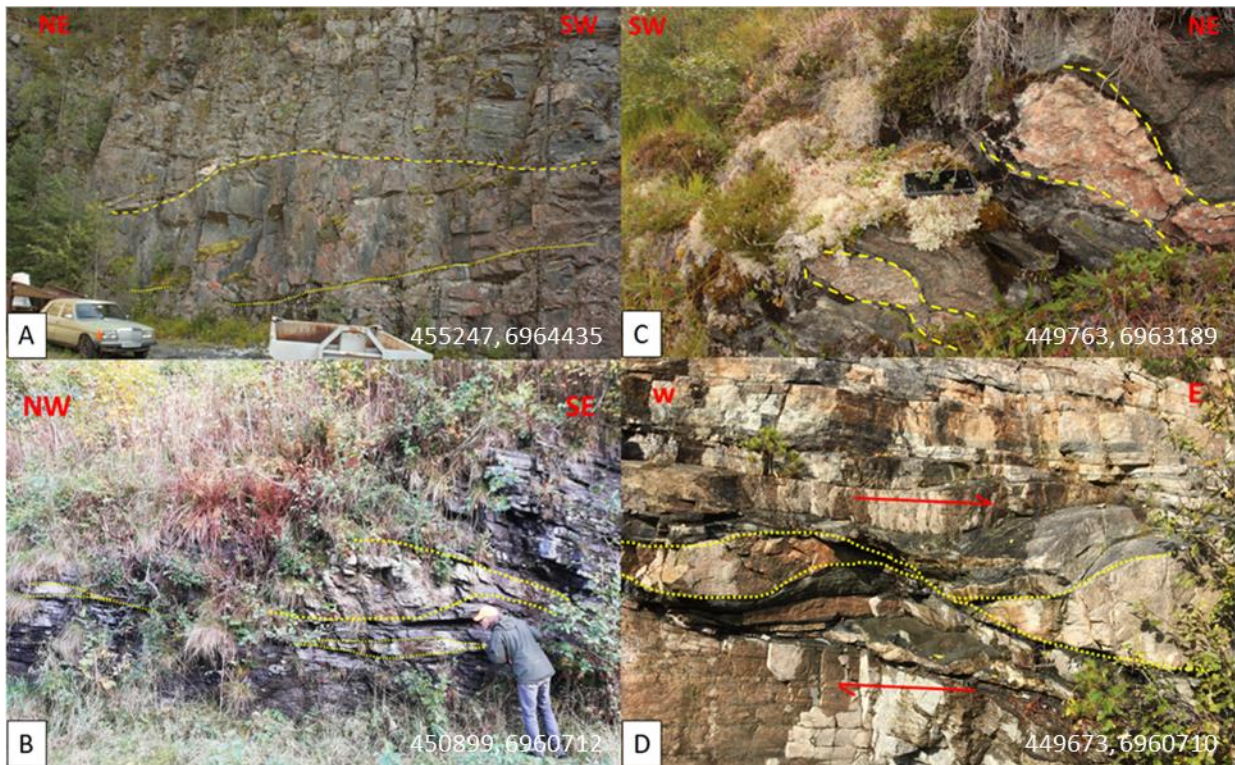
Figure 5.12: *A) Meter scale boudin in old quarry, car in left hand corner for scale. The boudin are in an ore rich mafic rock surrounded by foliated metagabbro. B) Meter scale boudins of pegmatite in layered supracrustal amphibolite, geologist for scale. C) Decimetre scale boudins of pegmatite in altered amphibolite, mapping pad for scale. D) Decimetre scale boudin of layered red granitic gneiss with dykes of altered amphibolite, asymmetry indicate a top to the east direction of movement, branches in righthand corner for scale.*

Folds

Folds are observed in wide ranges in size. The larges fold is in the km scale, these large-scale features are not directly observable but are a distinct Caledonian feature described as large-scale folds with an additional dome feature (Krill & Sturt, 1985)

Observable folds are within the metre to cm scale. The structural appearance is variable, from open to isoclinal folds. In biotitite, amphibolite with biotite rich layers, and in quarts schist cm scale crenulation folds in band of 1 – 5 dm thickness are observed. In Figure 5.13 below, two examples from the migmatite bearing pink granitic gneiss are given. Figure 5.13 B illustrate the dm scale subhorrisontal open folds with a low amplitude depicted in figure 5.13 A. Figure 5.13 D illustrate dm scale closed folds with a high amplitude depicted inn figure 5.13 C. The two examples are from locations proximate to each other by a few metres illustrating the variation that can be observed in areas with adequate exposure. This variation is observable in several locations.

Folding is most easily observed where there are distinct marker layers, of either leucosomes or mafic intrusions. Outcrops without these marker layers are not to be assumed "fold free", as the rock might be severely folded, but rather lacking any distinct visual markers as the ones illustrated in Figure 5.13 and Figure 5.14.
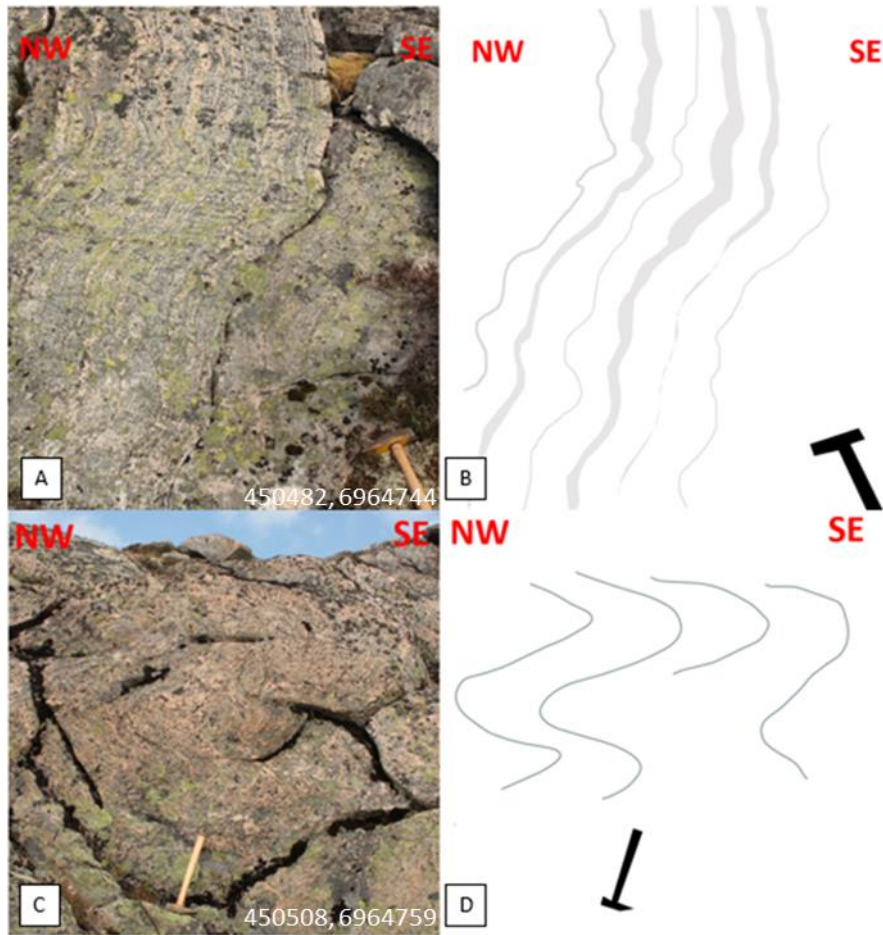
Figure 5.13: A) Sub-horizontal dm scale open folds with a low amplitude in migmatitic pink granitic gneiss B) Sketch of figure 5.13A highlighting the folded leucosomes C) Dm scale closed fold with a high amplitude in migmatitic pink granitic gneiss D) Sketch of figure 5.13C highlighting the folded leucosomes.

Most of the observed folds are symmetrical, showing little to no indication of directional shear in them self. The easiest folds to measure, are open, symmetrical, decimetre scale folds, like those illustrates in Figure 5.13 A. Thus, most of the fold axis measurements have been done the folds that fall under this description. A total of twenty-nine-fold axis measurements indicate a distinct NE-SW lineament of the fold axes. The collective measurements are illustrated in Figure 5.15.

Within the granitic gneiss, areas with visible mafic intrusion show some apparent asymmetrical z- folds. These indicate a direction of shear towards east. This sense of direction is apparent in several features in the same outcrop location, a selected example is given in Figure 5.14 below.

50
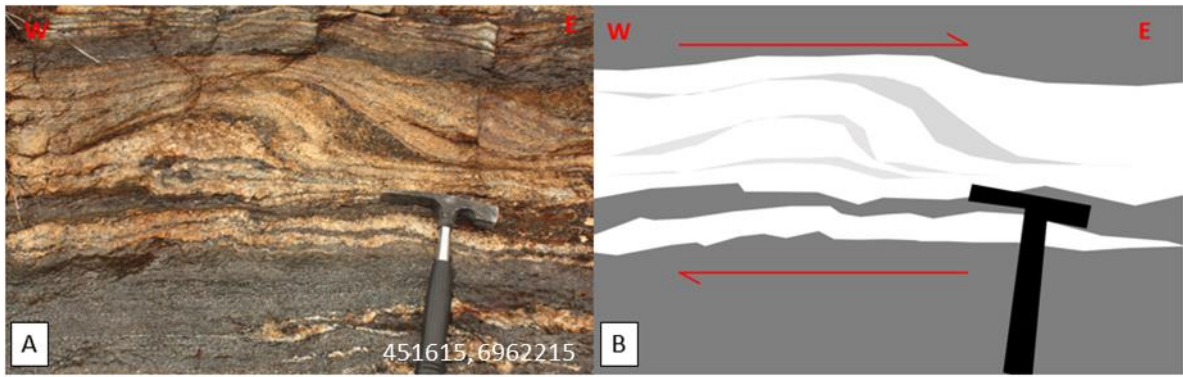
Figure 5.14: A) Image of folded layers of mafic composition and granitic gneiss. The layers are interlocked to a degree that it's not possible to make any assumption as to how the original protolith was structured. B) Sketch of 5.14 A, highlighting the features indicating the sense of shear.
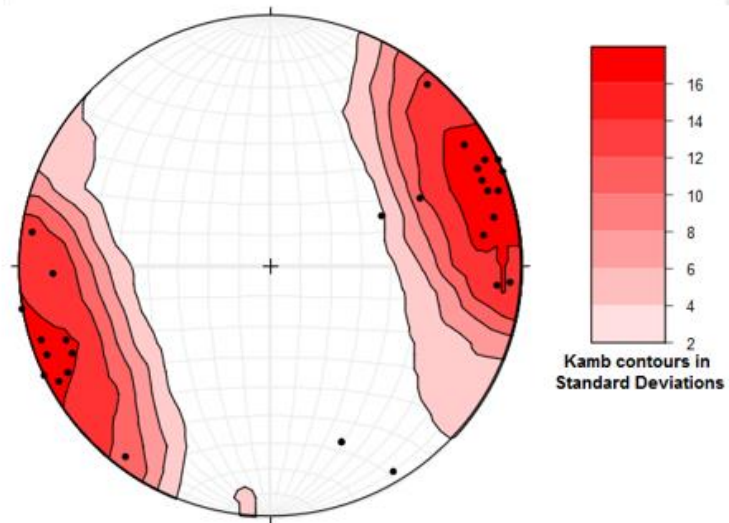
Figure 5.15: Stereoplot of fold axis measured in field area, based on a collective of 29 measurements

Faults

In the WGR the Møre-Trøndelag Fault Complex (MTFC) is by far the largest fault feature. Though not directly visible in the field, the southernmost fault in the complex, the Tjellefonna fault, passes though the field area. The location an description of the fault is given by (Nasuti et al., 2011) and will not be discussed further here.

As with the folding the faults occur within a range of sizes, from kilometre to centimetre-scale dislocations. The location seems not to be restricted by nappe units or rock type. Two examples are given in Figure 5.16 below.
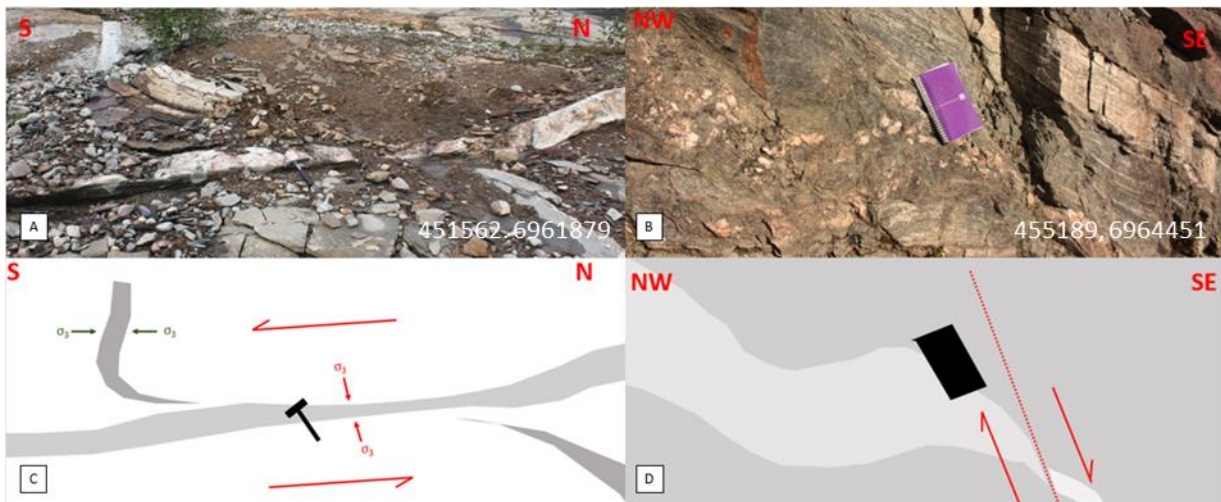
Figure 5.16: C) is an illustrated sketch of the image A, it illustrates a top to the south fault in the supracrustal amphibolite belonging to Surnadekket. What is interesting to note in this location is the two cutting dykes of relatively unaltered pegmatite. The horizontal dyke falls along the fault plane, the cut vertical dyke lies almost perpendicular to the fault plane. The two dykes indicate to different directions of σ_3, but both pegmatites are relatively undeformed. This could indicate a change in the strain distribution in a relatively close time interval at the last stages of the Caledonian exhumation. B) and is corresponding sketch in D) illustrate a normal fault in mafic ore containing rock in the basement rock. The displacement is a few dm, with a marker layer interpreted as brecciated and deformed pegmatite, marked light grey. Though these observations are not relevant to any events prior to the Caledonian but serves as a good example to some of the complexity in the area, and that even in the latter stages there is a variable activity.

Note that the σ_3 for the pegmatitic dykes in the figure above are not measured directly and are illustrated here to give an example to the variable strain distribution.

Rotation

Within the supracrustal bodies porphyroblastic garnets have overgrown the foliation, thus recording some part of the pre deformation foliation. Figure 5.17 below illustrate rotated garnet with a top to the west movement found in the supracrustal amphibolite. The same observation can be made in more several other garnets within the same area.

Figure 5.17: *Sub-grain rotation in amphibolite garnet. Both images are from the approximate same location.*

It is to be noted that some garnets deviate from the top to the west pattern. Though not disproving the initial interpretation of the rotating garnets, it served to illustrate that even though most of the observations tends towards a simple interpretation, the area displays some complexity.

Strain distribution

The field area compromise rocks that from earlier classifications made by Tveten, E. et.al (1998), fall within both the allochthonous and the autochthonous units. The collected mineral lineation measurements show a characteristic alignment having an NE-SW direction parallel to the general strike, which appears to be independent of whether the measurements are made in the allochthonous or the autochthonous rocks. This indicates that the same forces have affected the area at large. The tectonic foliation has the same orientation as the lineament, when plotting the poles to the planes in the tectonic foliation the poles form a kamb contour interval cloud perpendicular to the lineation. The relationship can be seen when comparing the plotted measurements in Figure 5.18 and 5.19. Some deviations to the trend are observed in both figures, but not of any significant number. Note that the values do not represent an equal distribution

throughout all the entire mapping area, but a collective mean from different selected locations.
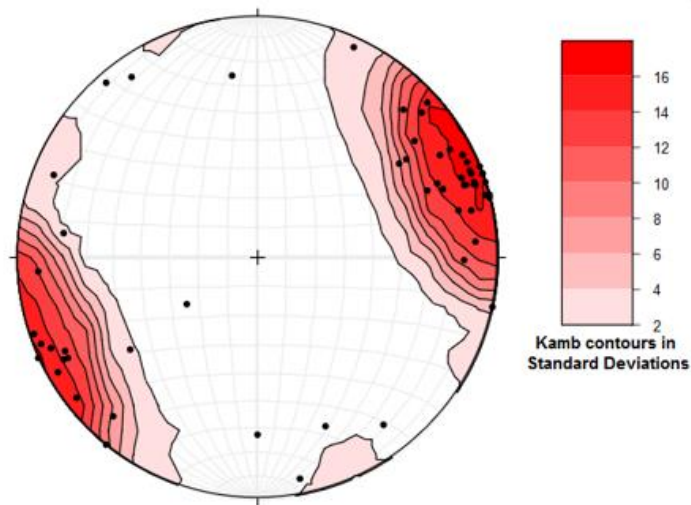
Figure 5.18: *Mineral lineation's, illustrating a collective of 57 measurements made within the field area*
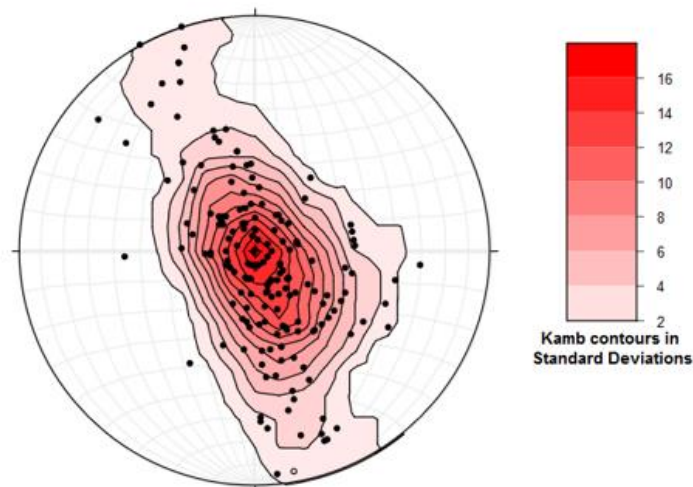
Figure 5.19: *Tectonic foliation, plotted as poles on planes. Illustrating a collective of 175 measurements made within the field area.*

The foliation coincides with structural observations of fractures and planes done with LiDAR and Geophysical observations made in the same area by NGU (Rønning et al., 2019). And both the foliation and lineation fall in line with prior structural observations made in the WGR at large (Harker et al., 2010) and are most likely linked to the subduction and extension of the Caledonian orogeny.

Mafic dykes

One locality that show signs of being relatively less affected by the implemented strain is the old quarry by the road exit to the Rausand mines. The porphyroclastic granitic gneiss in this area is by no way unaffected, and the rock have a strong mineral lineament in porphyroclast of feldspar, though some remnant of the possible phenocryst is still visible. However, the most distinct feature is the observable dike swarm of amphibolitic intrusions. The parallel subvertical dykes vary from 2 dm to 5 m in thickness, and at least seven distinct dykes are observed in the same proximate area.

The dykes have the same lineament at the surrounding host rock, thus indicating their presence during the Caledonian, but can be observed cutting the foliation at a low angle and a chilled margin can be observed in contact with the host rock. Thus, indicating an intrusion in a solidified, colder, host rock under an earlier stress regime. Figure 5.20 below illustrate some of the intruding dikes with a corresponding interpretive sketch.
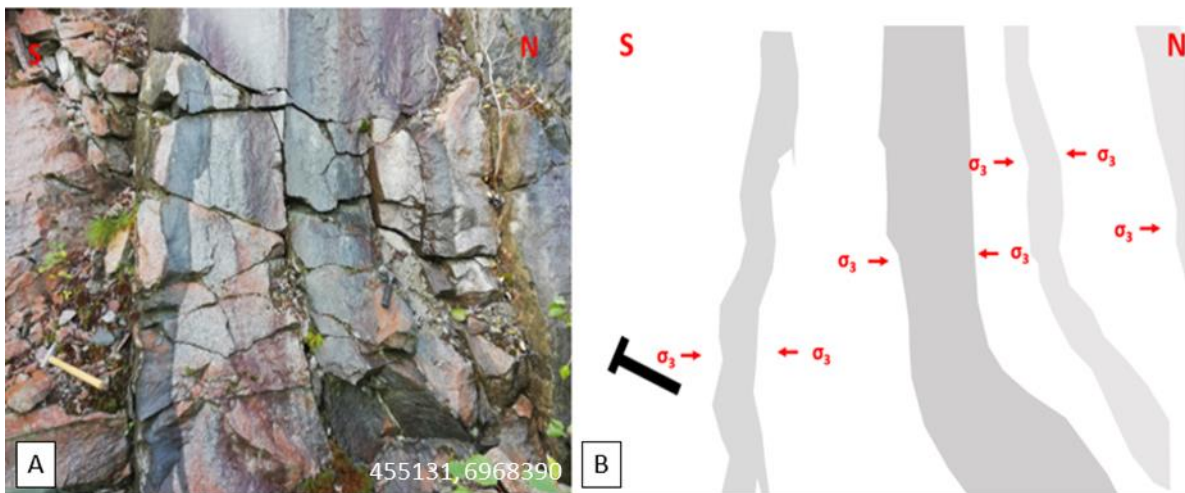
Figure 5.20: *A) Image amphibolite dykes in Porphyritic granitic gneiss, geological hammer for scale. B) Sketch highlighting the intruding dikes with interpreted σ_3 direction, the lineation is perpendicular to the image.*

The large-scale folding in the area might have tilted the host rock form its original direction. The indicated σ_3 measured at 45/145 does not give certain direction of prior stress fields but it can indicate the presence of prior events.

Mafic bodies are observable in several location within the field area. Their placement within the basement gneisses makes it a probable interpretation that these two are remnant of mafic intrusions. Though through time alteration and deformation removes signs for a certain interpretation. It is also not certain that the dykes belong to the same intrusion and would have to be correlated chemically to get a better indication.

The mafic bodies are a central to many of the structural observation. As noted earlier they serve as visible marker layer. Another distinct feature is that the altered layers take up some larger proportion of the strain, as can be seen both in the folds and the boudins.

In general, the texture and mineralogy vary and seem to coincide with the degree of alteration. An illustrated sketch of an observed outcrop is given in Figure 5.21 below, where the initial gabbroic texture is preserved within the body, and the outer edges is altered to biotite rich amphibolite. Intrusions of a smaller scale are observed fully altered, some appearing as pure biotitite.
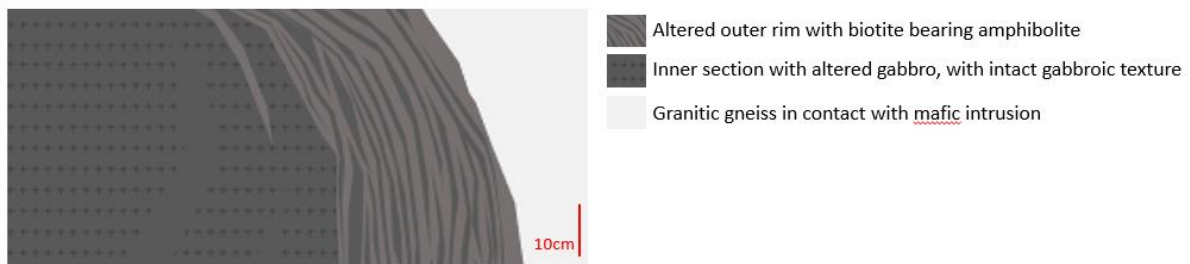
Figure 5.21: Illustrated sketch of outcrop with an relatively unaltered core, where the gabbroic texture still is intact, ant the outer rim which is in contact with the surrounding granitic gneiss is altered to biotite bearing amphibolite. The location is given by the coordinates 449 245, 6 691 979 a thin section sample of the core is given in Appendix E, Sample 200955.

5.1.4 Migmatites

Not all lithologies within the field area appear migmatitic. This can simply be explained by the natural chemical variance in the basement rock, were some compositions would reach the solidus temperature while other compositions would not. Melt migration could also remove visible evidence of migmatisation in the field.

Anatexite is an underused synonym for migmatites and refers to a rock formed by partial melting of the continental crust. The terms diatexsite and metatexsite can be referred to as subdivisions of this definition. Were a diatexsite migmatite is a migmatite with structural features dominated by the leucosomes, and an metatexsite migmatite have mesosomes with preserved structures from pre-partial-melting (Sawyer, 2008). The observed migmatites seem to primarily be metatexsite, with a remnant mesosome. Hence the mesosomes is interpreted to reflect the remnant protoliths of the migmatised gneisses in the area. The leucosome vary in appearance and distribution, but the different field observations can broadly be divided into three groups of apparent features that differentiate from each other. Each one is given with correlation images and field description below.

Stromatic migmatite

The most common type of migmatite in the field area is stromatic leucosomes. It appears in different rock suites, but the general appearance is roughly the same. Thin leucosomes, usually between 1 – 3 cm in thickness with a thin, 1-2 mm melanosome. They appear as continuous layers or lenses parallel to the foliation. Where the leucosome are thicker the grain size increases, and the melanosome can appear more distinct. In outcrops where the rock is folded the leucosomes fall along the fold with an approximately even thickness, which is indicative of subsolidus deformation. Figure 5.22 below shows two examples of different stomatic leucosomes observed in the field.
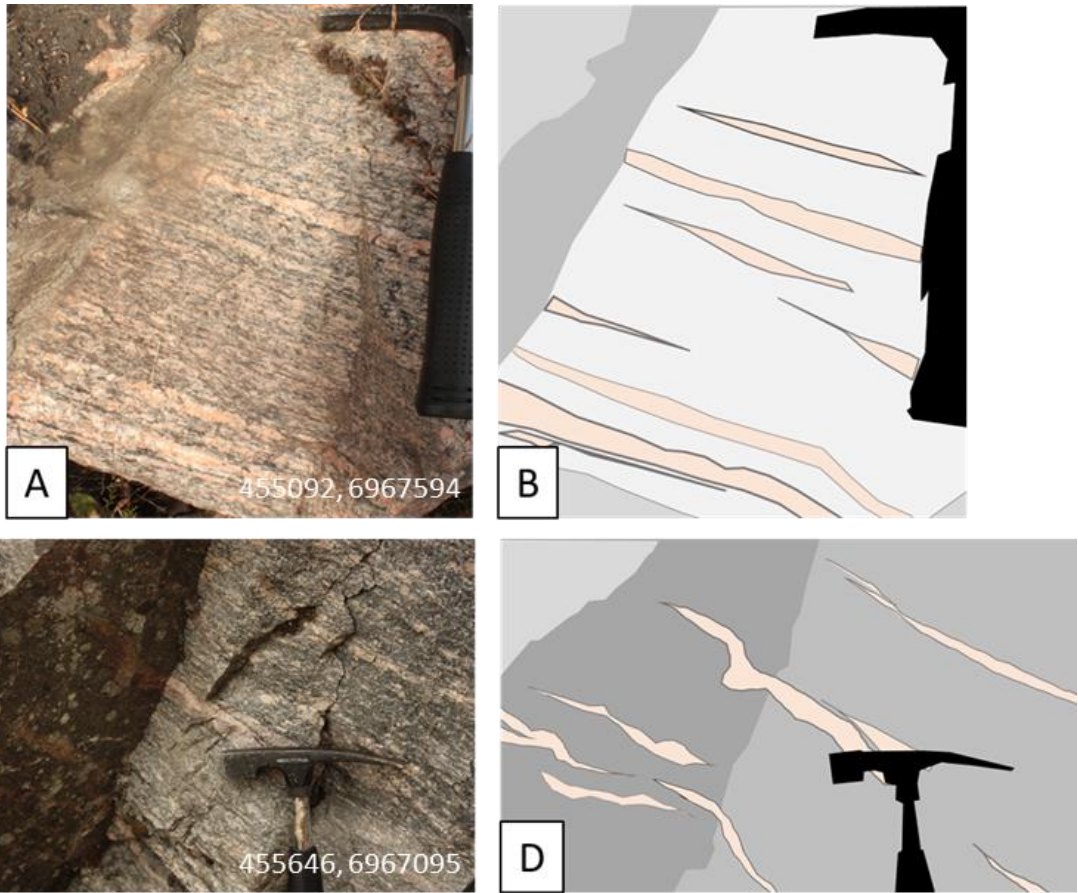
Figure 5.22: *A) Stomatic leucosomes in pink migmatitic granitic gneiss, hammer for scale. B) sketch of figure A. C) Stromatic leucosomes in migmatitic phenocrystic biotite rich granitic gneiss, with hammer for scale. D) Sketch of figure C.*

Compositionally layered migmatite

The second most common migmatite appears in the compositionally layered granitic gneisses. The leucocratic layers consist of thick, usually decimetre scale leucosomes. There is no evident melanosome, except for some more biotite rich layers. This could be due to a diffuse transition between the leucosome and the mesosome. The leucosome appears to compromise a large volume of the bulk rock, resulting in what appears as a compositionally layered migmatite. The layers are parallel to the foliation. Figure 5.23 below, illustrate an example of this.
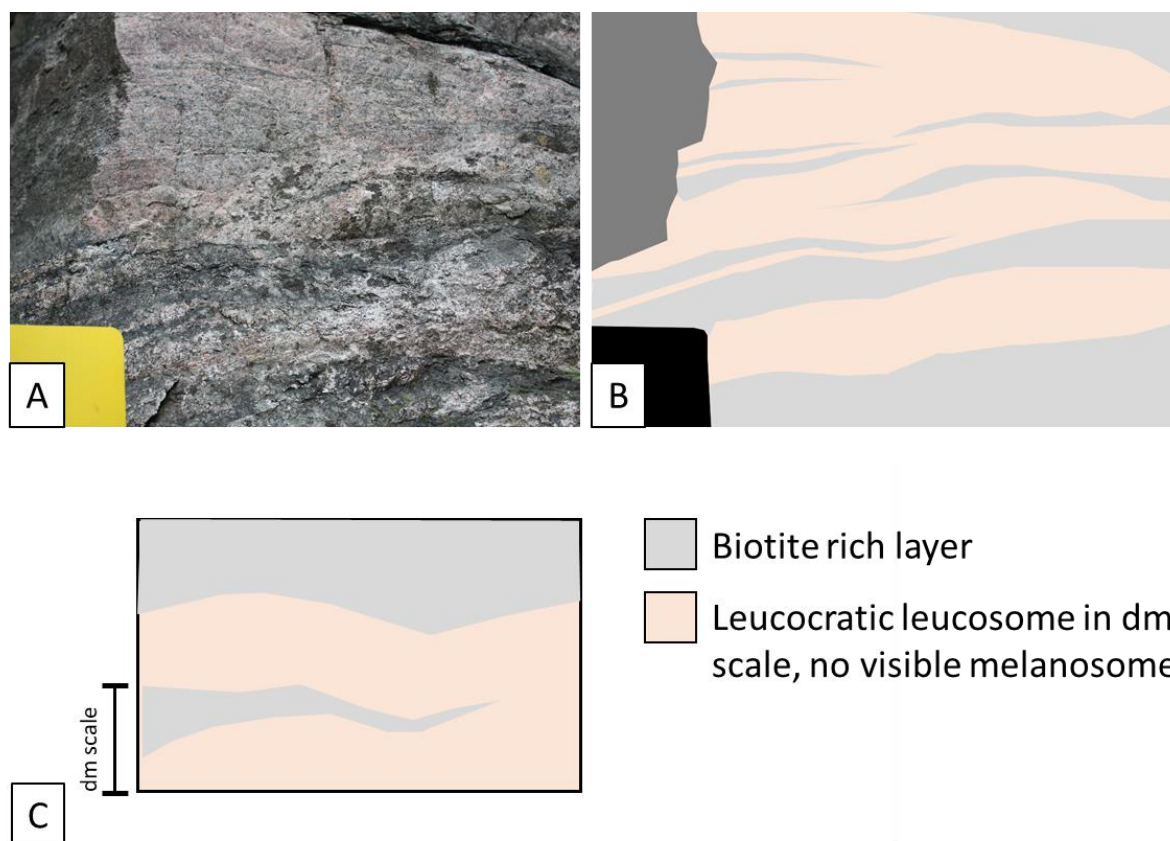
Figure 5.23: *A) Image of a compositionally layered migmatite, with a field book for scale. B) Sketch of Figure 5.23 A. C) Illustrative sketch with corresponding legend to better illustrate the observed layering, and to further explain the sketch given in Figure 5.23 B.*

Cross-cutting migmatite

In the pink granitic gneiss, cross cutting, decimetre scale irregular veins of leucosomes can be observed along the road cuts on the north side of Rausand. The leucosomes have a coarser grainsize than the surrounding host rock, but with the same distinct colouring. The leucosomes cross the foliation at a low angle along small shear bands, suggesting a syn-tectonic relationship with a top-to-SE sense of shear, as illustrated in Figure 5.24 below. The leucosomes show no distinct melanosome but has cm scale amphiboles within the pegmatitic areas.
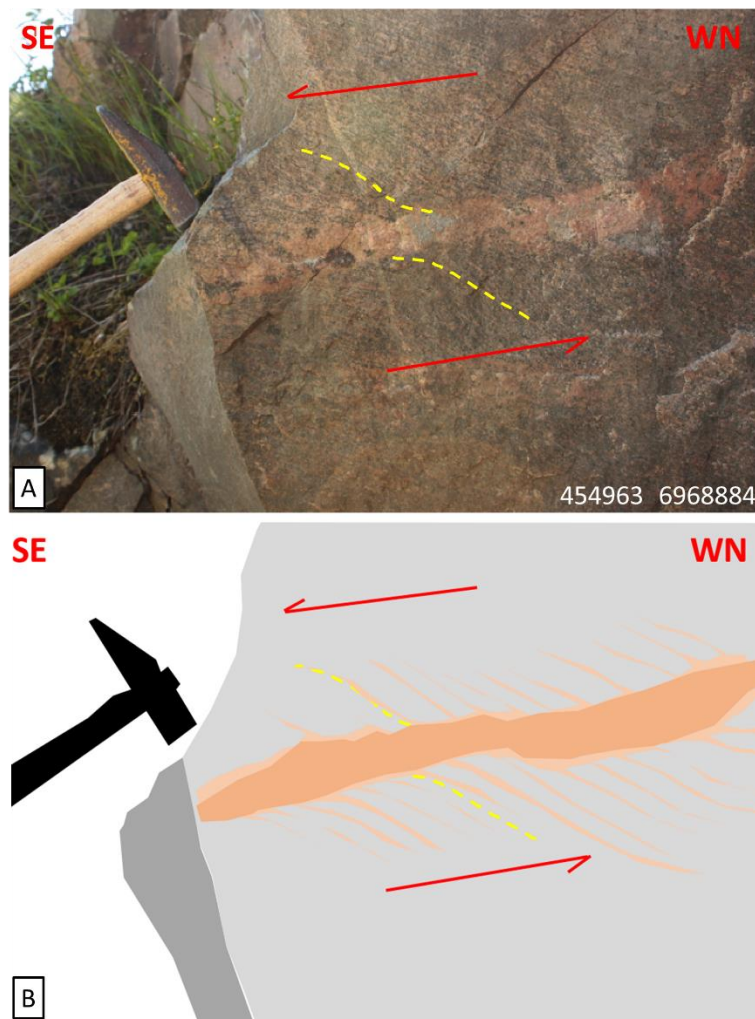
Figure 5.24: *A) Image of the cross cutting leucosome in the pink granitic gneiss, The red arrows illustrate the sense of shear, the yellow dotted lines mark the surrounding foliation. Geological hammer for scale. B) Sketch of the image in A, with the same markers. The dark orange ellipsoid marks the leucosome, while the light orange indicates the foliation.*

5.2 Geochronological data

Table 5.1 below summarize the geochronological data, giving the coordinates, brief sample description, ages with the 2σ variance, and what interpretation the sample is based on. Figure 5.28 mark the sample locations within the WGR. Figure 5.29 – 5.53 illustrates primarily the TW-plots, with additional plots used in the interpretations, for all samples with valid age estimates. A full description for each sample analysis is given in section *5.2.1 Sample 12879L* to section *5.2.24 Sample 200998*. Complete dataset and CL images of analysed samples is given in Appendix D3 and D2. Note that sample 200955, 200976 and 200960 have no further description, as no zircons where found in these samples.

The analysed zircons vary in size and form, some examples are given in Figure 5.25 below. There are some general factors that seem to be consistent overall. Most of the samples have zircons with a distinct core. The cores appear to be dark, usually darker that the surrounding mantles, but there is some exception to this. No younger age (~400 Ma or ~ 1000 Ma) is registered in the cores that fall under these characteristics, and they are thus interpreted to be remnant of the formation of the original photolith. The leucosome, and some of the protoliths samples have zircons with rims or mantles with diffuse irregular features. The relative thickness of these rims wary from each sample and are in instances not possible to analyse separately from the core. The younger age can be correlated for most parts with the surrounding rim or metamorphosed grains, making it a viable interpretation that thy are related to some secondary event.
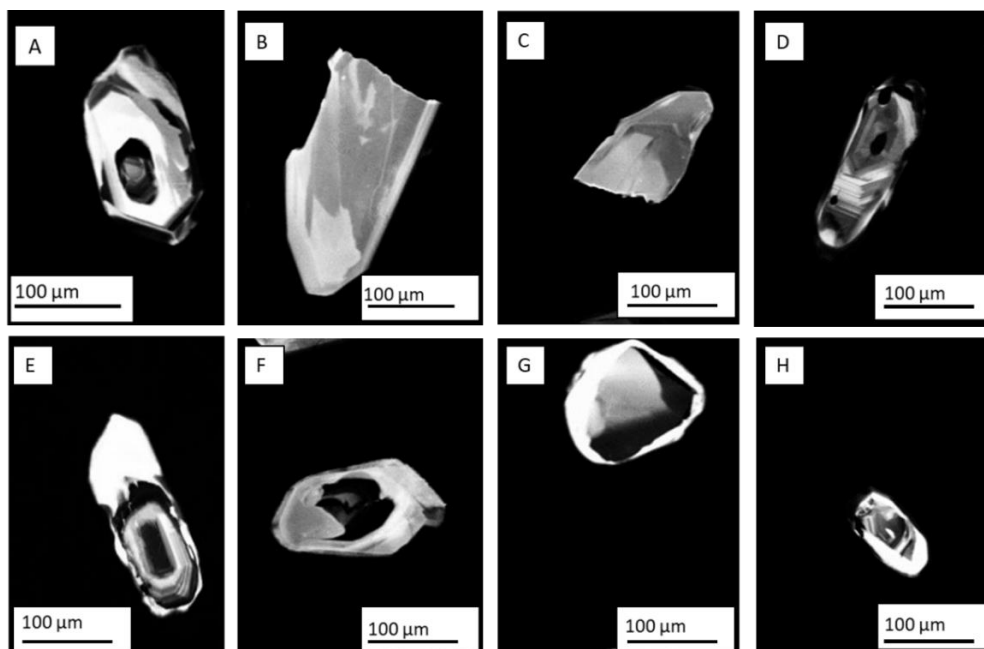
Figure 5.25: *Examples of zircons from this study, the samples are selected to display some of the variability observed in the zircon grains. The grains are from sample A) 127891L B) 127868L C) 127877L D) 197555 E) 127876L F) 127866L G) 127884B H) 197578, respectively.*

For all leucosome samples, and some photoliths, there is a distinct difference in the Uranium content between the core and rim. The Uranium will absorb much of the electron rays, yielding a CL-dark appearance, whereas the Uranium poor rims will reflect a higher proportion, appearing CL-bright. To better get a representative image two CL-images with different contrast were taken for most samples. An example of a CL-image with different brightness contrast is given in figure 5.26 below. In figure 5.26 A, the internal structures in the rims and metamorphic grains can be observed. In figure 5.26 B the internal magmatic structures in the dark cores is visible.
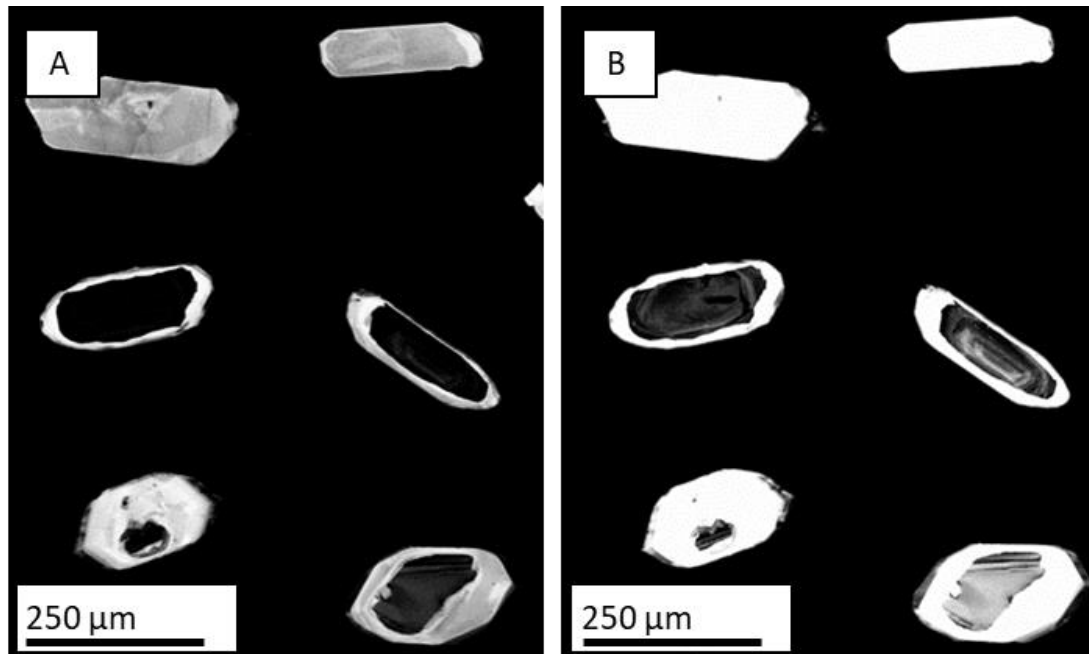
Figure 5.26: *A) CL-dark image of selected zircons from sample 127866L. B) CL- bright image of the same zircons as in A.*

Analysing the U-Pb isotopic data the U/Th ratio is distinctive between the mantles and metamorphosed grains, and the dark magmatic cores. This is recurring in all samples in this study. In figure 5.27 below the TW-plot for sample 197578L illustrates the compliance between the Th/U ratio and the older analyses and the younger. With high ratio cores placing as older analyses and rims and metamorphic grains as younger. The 197578L sample also illustrates well how this ratio decreases when the samples fall down the indicated discordia.
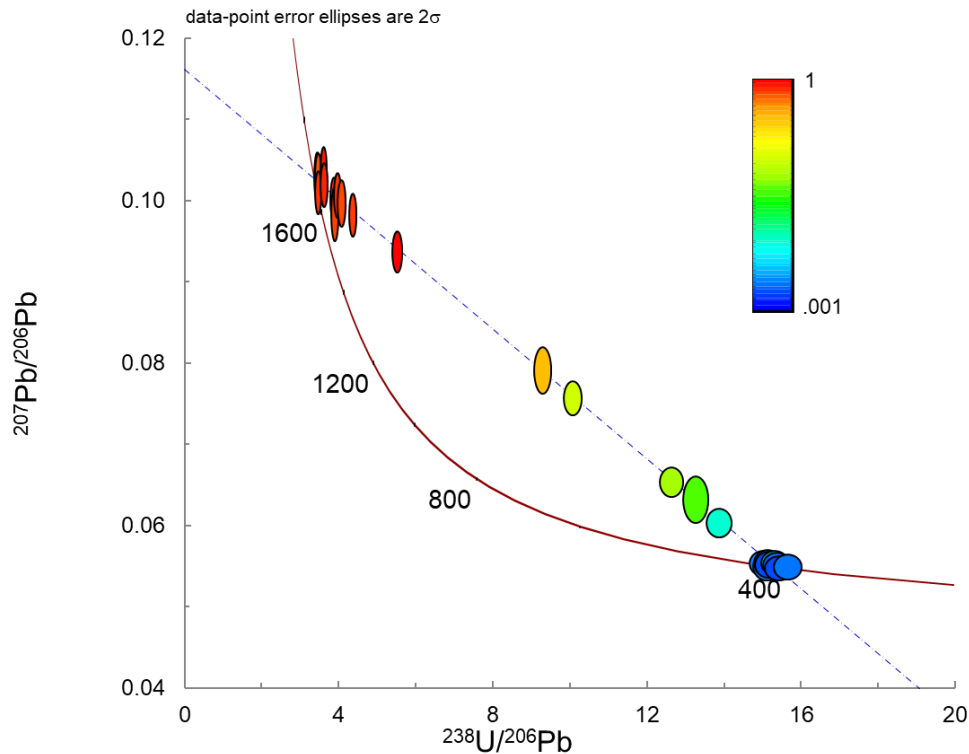
Figure 5.27: *TW-plot of sample 197578L. The colour indications are given with a logarithmic scale based on the Th/U ratio corresponding to each analysis.*

There is however some observation that deviates from the norm. In some instances, the ages seem not to be fitting their placement in the zircon grain, e.g. photolith ages in the rims. An explanation this is that the laser beam cross over two, or more, different age domains in the grain, whereof only one domain made it through the initial data reduction. In other instances, an age is indicated, but there are not enough data points to place a viable age on the concordia. Two such examples are sample 127886L and sample 127879L, both of which place values at that indicate an age of ~ 1000 Ma. For sample 127884B and 200987L however, it is an age of ~ 400 Ma that is indicated.

As given in section *4.3.9 Ur – Pb dating*, the data reduction in the software Glitter, was performed by Trond Slagstad for each sample. Plotting and further U – Pb isotopic data analysis of the samples were done by the respective student. All samples are plotted with a data point ellipse error of 2σ.

For all samples, the ^{207}Pb/^{206}Pb and ^{238}U/^{206}Pb ratios are used to construct a TW plot for each sample. Making any bias of common lead more readily detected. For these samples, any correction has not been necessary. Two main factors come into consideration when selecting the age estimate. Firstly, one wants the age range to be as low as possible, whilst still having a statistical validity. And secondly, one wants to get valid ages, without "contaminating" the sample analysis data with unnecessary data alterations. To the degree possible it has been strived to analyse all samples in the same manner. Alteration have been done where necessary; the chosen method used for each sample is given in

Table 5.1 below. Recurring for much of the sample data are two distinct population, one older in the cores and one younger in the rims and metamorphosed grains. For these analyses, a weighted average is used to set the age estimate. Linear regressions are used where the analyses data in the sample is spread out, indicating a discordia. For these samples the Mean Square Weighted Deviation, (MSWD), value is used as a statistical modifier. Any MSWD value over 2.5 is considered to make the age estimate statistically invalid, an MSWD value ≈ 1 is desired. When either the weighted average $^{207}Pb/^{206}Pb$ age estimate or the weighted average $^{238}U/^{206}Pb$ age estimate is used the MSWD value has been used less strictly as a modifier. Statistical outliers are set if they fall outside the 2σ or the 95% confidence interval set by Isoplot. The calculated discordia is used in two instances, the first where both the WA age estimate of both the $^{207}Pb/^{206}Pb$ and the $^{238}U/^{206}Pb$ ratio is needed to make a reliable estimate. And secondly, in analyses with few analyses at the younger intercept, with no significant $^{207}Pb/^{206}Pb$ anomaly.

Sample data is only removed if they fall as statistical outliers, are reverse discordant, or removal is necessary to get a statistically valid age estimate. Altered samples are indicated with as grey or blue error ellipses in the respective plots, see Figures 5.29 – 5.53.
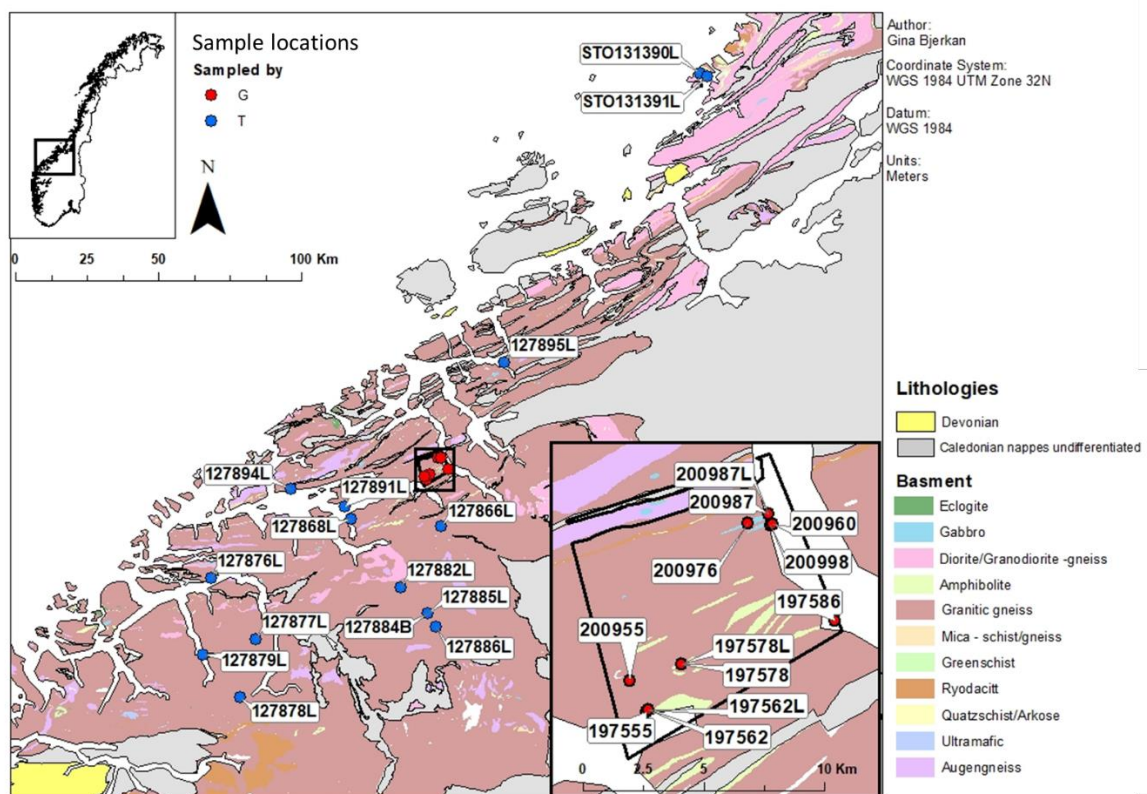
Figure 5.28: *Illustrates the geographic location of the samples given in table 5.1 below.*

Table 5.1: Summarised list of zircon U-Pb analyses, full description for each analysis given in section 5.2.1 to 5.2.14 below, complete dataset given in appendix D.

Sample	UTM E	UTM N	Rock description	Zircon size	Zircon description	Age	Interpretation
127879L	371740	6899564	migmatitic bt gneiss	100 – 300 µm	Tabular to sub-angular in shape	1589 ± 19 Ma (indicated: 1000 Ma) 402 ± 6 Ma	C: Wtd. Avg. ^{207}Pb/^{206}Pb age R: Only indicated. R: Wtd. Avg. ^{238}U/^{206}Pb age
127866L	455362	6944490	leucosome, migmatitic bt hbl gneiss	150 – 400 µm	Prismatic, sub angular, to sub rounded shape in smaller grains	1655 ± 20 Ma 404±5 Ma	C: Wtd. Avg. ^{207}Pb/^{206}Pb age R: Wtd. Avg. ^{238}U/^{206}Pb age
127868L	423601	6946929	migmatitic bt hbl gneiss	150 – 300 µm	Elongated tabular, to sub-rounded shape in smaller grains	1649 ± 20 Ma 396 ± 3 Ma	C: Wtd. Avg. ^{207}Pb/^{206}Pb age R: Wtd. Avg. ^{238}U/^{206}Pb age
127876L	374663	6926464	migmatitic qtz dioritic gneiss	100 – 250 µm	Tabular to sub-rounded in shape	1691 ± 22 Ma 398 ± 3 Ma	C: Regression line all analyses R: Wtd. Avg. ^{238}U/^{206}Pb age
127877L	390390	6905041	migmatitic qz dioritic gneiss	125 – 275 µm	Small sub-rounded grains, with some larger more angular exceptions	1675 ± 28 Ma 880 ± 61 Ma 392 ± 3 Ma	C: One concordant analysis R: Wtd. Avg. ^{207}Pb/^{206}Pb age R: Wtd. Avg. ^{238}U/^{206}Pb age
127878L	384681	6884856	migmatitic bt hbl gneiss	175 – 300 µm	Tabular to sub-angular in shape	1610 ± 43 Ma 398 ± 6 Ma	C: Regression line all analyses R: Wtd. Avg. ^{238}U/^{206}Pb age
127882L	441159	6923212	muscovite rich light grey migmatitic gneiss	250 – 150 µm	Round to elongated, sub-angular, shape	1670 ± 11 Ma 411 ± 24 Ma	C: Wtd. Avg. ^{207}Pb/^{206}Pb age R: Regression line, all analyses
127884B	450513	6914230	two-generation migmatitic gneiss	100 – 200 µm	Tabular, sub-angular shape	1619 ± 10 Ma 962 ± 11 Ma (Indicated: 400 Ma)	C: Wtd. Avg. ^{207}Pb/^{206}Pb age R: Calculated concordia R: Only indicated
127885L	450513	6914230	x-cutting coarse grained leucosome from en echelon array.	150 – 275 µm	Tabular, sub-angular shape	1629 ± 12 Ma 406 ± 26 Ma	C: Wtd. Avg. ^{207}Pb/^{206}Pb age R: Wtd. Avg. ^{238}U/^{206}Pb age
127886L	453428	6909184	stromatic migmatitic bt gneiss	100 – 500 µm	Tabular, sub-angular shape	1625 ± 9 Ma (Indicated: 1000 Ma) 406 ± 7 Ma	C: Wtd. Avg. ^{207}Pb/^{206}Pb age R: Only indicated R: Calculated Concordia

Table 5.1: Table 5.1 continued….

Sample	UTM E	UTM N	Rock description	Zircon size	Zircon description	Age	Interpretation
127891L	421362	6951444	leucosome, (M) migmatitic hbl bt granitic gneiss	100 – 200 µm	larger tabular, sub-angular grains, smaller subangular, diamond shaped grains	1683 ± 11 Ma 401 ± 5 Ma	C: Wtd. Avg. ^{207}Pb/^{206}Pb age R: Wtd. Avg. ^{238}U/^{206}Pb age
127894L	402583	6957475	leucosome, (M) heterogeneous orthogneiss	100 – 175 µm	Tabular, sub-angular to rounded shape	1662 ± 16 Ma 413 ± 4 Ma	C: Wtd. Avg. ^{207}Pb/^{206}Pb age R: Wtd. Avg. ^{238}U/^{206}Pb age
127895L	477272	7001798	migmatitic granitic gneiss	150 – 325 µm	Tabular, sub-angular shape	1690 ± 49 Ma 399 ± 2 Ma	C: Regression line, all analyses R: Wtd. Avg. ^{238}U/^{206}Pb age
STO131390L	545978	7102867	migmatitic orthogneiss	100 – 400 µm	Very heterogenous sample. Larger elongated and subangular grains, smaller subangular diamond- to tabular grains	1637 ± 12 Ma 414 ± 6 Ma	C: Wtd. Avg. ^{207}Pb/^{206}Pb age R: Wtd. Avg. ^{238}U/^{206}Pb age
STO131391L	548505	7101824	migmatitic granitic orthogneiss	150 – 300 µm	Tabular, sub-angular shape	1641 ± 24 Ma 412 ± 4 Ma	C: Regression line, all analyses R: Wtd. Avg. ^{238}U/^{206}Pb age
197555	449940	6960684	Pink granitic gneiss	100 – 225 µm	Tabular, sub-angular shape	1688 ± 8 Ma	C: Wtd. Avg. ^{207}Pb/^{206}Pb age
197562	450011	6960762	Quarts dioritic gneiss	100 – 200 µm	Tabular, sub-angular to rounded shape	1672 ± 8 Ma	C: Wtd. Avg. ^{207}Pb/^{206}Pb age
197578	451403	6962671	Pink granitic gneiss	75 – 150 µm	Tabular, sub-angular to rounded shape	1644 ± 9 Ma 423 ± 10 Ma	C: Wtd. Avg. ^{207}Pb/^{206}Pb age R: Regression line, all analyses
197586	457734	6964449	Quarts dioritic gneiss	100 – 200 µm	Tabular, sub-angular to rounded shape	1652 ± 11 Ma 392 ± 21 Ma	C: Regression line, all analyses R: Regression line, all analyses

Table 5.1: Table 5.1 continued…

Sample	UTM E	UTM N	Rock description	Zircon size	Zircon description	Age	Interpretation
200987	454984	6968894	Pink granitic gneiss	100 – 175 µm	Tabular, sub-angular to rounded shape	1647 ± 9 Ma	C: Wtd. Avg. $^{207}Pb/^{206}Pb$ age
200998	455072	6968397	Granitic gneiss	100 – 200 µm	Tabular, sub-angular shape	1660 ± 9 Ma	C: Wtd. Avg. $^{207}Pb/^{206}Pb$ age
197562L	450011	6960762	Leucosome in quarts dioritic gneiss	100 – 175 µm	Tabular, sub-angular shape	1649 ± 13 Ma 408 ± 2 Ma	C: Wtd. Avg. $^{207}Pb/^{206}Pb$ age R: Wtd. Avg. $^{238}U/^{206}Pb$ age
197578L	451403	6962671	Leucosome in pink granitic gneiss	100 – 175 µm	Tabular to round shape, with sub-angular to rounded edges.	1672 ± 15 Ma 407 ± 4 Ma	C: Regression line, all analyses R: Regression line, all analyses
200987L	454984	6968894	Leucosome in pink granitic gneiss	75 – 200 µm	Tabular, sub-angular to rounded shape	1636 ± 13 Ma (Indicated: 400 Ma)	C: Wtd. Avg. $^{207}Pb/^{206}Pb$ age R: Only indicated
200955	449245	6961979	Gabbro	-	-	-	No valid samples
200976	454129	6968513	Pegmatitic gabbro	-	-	-	No valid samples
200960	455165	6968440	Gabbroic dike	-	-	-	No valid samples

5.2.1 Sample: 127879L

In this sample 24 analyses were made on 23 zircons. The grains are between 100 and 300 μm, all tabular to sub-angular in shape. In CL images, most of the grains display a dark (i.e., U-rich) core, interpreted to be magmatic, transected by CL-bright (i.e., U-poor) rims or mantles with diffuse irregular features. A few grains are CL-bright, with internal features like the rims, but lack cores. The CL-bright rims and grains are interpreted to be metamorphic.

A regression through all 24 analyses from this sample, yield an upper intercept age of 1575 ± 120 Ma, and a lower intercept age of 384±39 Ma, with an MSWD of 13 indicating significant scatter, see Figure 5.29. Most of the data fall in two groups, one at ca. 1600 Ma and another at ca. 400 Ma. The older group consist of seven analyses that target cores with Th/U > 0.3, whereas the younger group consists of thirteen analyses that target the rims and metamorphic grains with Th/U generally <0.05.

Two analyses from the older group are 12-13% discordant; excluding these analyses, the remaining five analyses yield a weighted mean $^{207}Pb/^{206}Pb$ age of 1589 ± 19Ma (Figure 5.29 upper inset, MSWD = 0.59) interpreted to reflect the crystallization age of the protolith to the host gneiss.

As for most of the analyses of U-poor metamorphic rims and grains in this study, the analyses display large errors in$^{207}Pb/^{206}Pb$ ratios. This is most likely related to the very low U concentration in these zircons, typically with only a few tens of ppm U, resulting in very small concentrations of radiogenic ^{207}Pb and therefor large analytical uncertainties. In contrast the $^{206}Pb/^{238}U$ ratios are much better constrained, and preferable for determining the age of the rims and grains. The weighted average $^{206}Pb/^{238}U$ of the thirteen analyses in the younger group is 402 ± 6 Ma, (Figure 5.29 lower inset, MSWD = 3.0), interpreted to reflect the age of the high-grade metamorphism and migmatisation. Two samples were removed as statistical outliers by Isoplot.

The significance of the discordant analyses is unclear. Some of these analyses plot on a trajectory between the older (1589 Ma) and younger (402 Ma) group of analyses, indicative either of Pb loss at 402 Ma or mixed core-rim analyses. Other analyses plot on poorly defined trajectories between ca. 1590 and 1000 Ma, or between 1000 and 400 Ma, which may be interpreted to reflect the effects of an event at ca. 1000 Ma, as observed in some of the other samples discussed below.
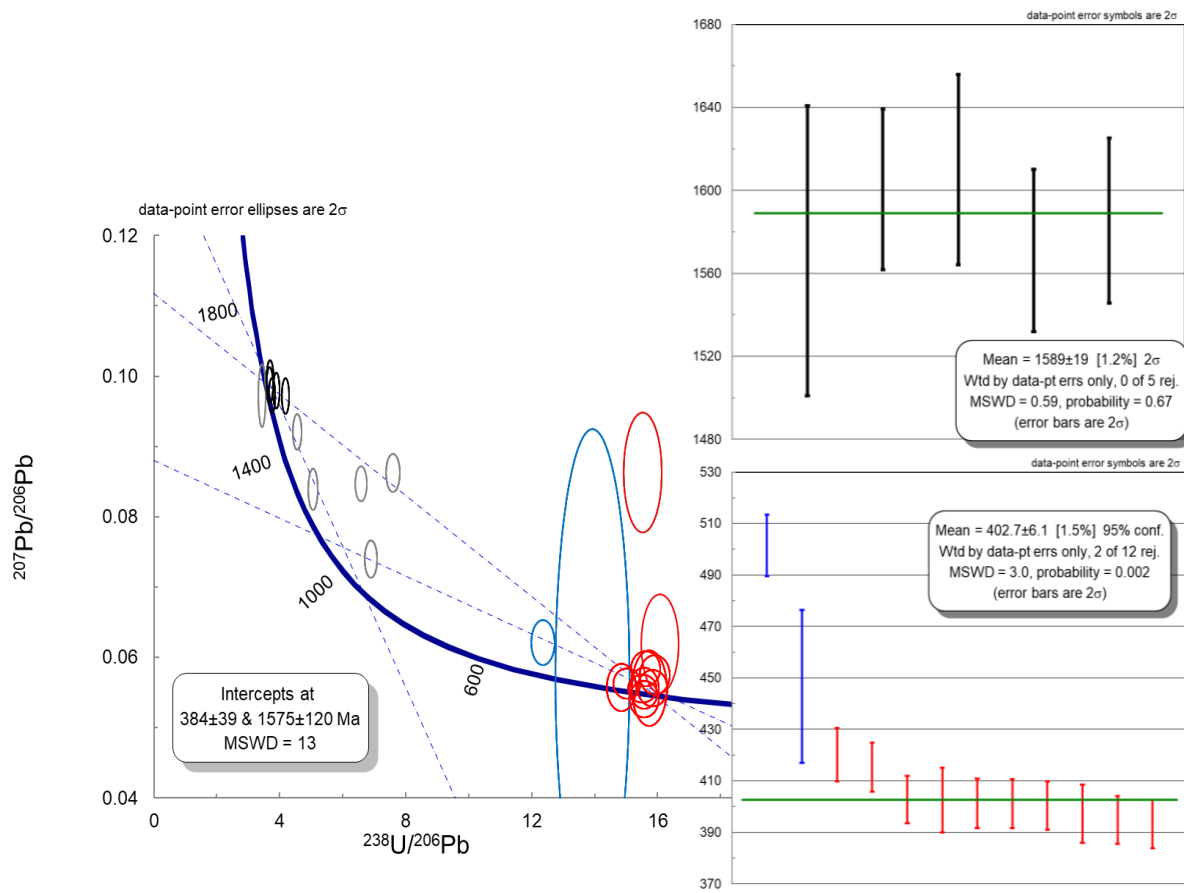
Figure 5.29: *TW plot of U-Pb isotopic data from sample 127879L. Analyses removed from calculations due to discordance are shown as grey ellipses. Analyses removed as statistical outliers in the weighted average 206Pb /238U age are shown as blue error ellipses. Black and red error ellipses indicate the cores and rims analyses, respectively. Two of the regression lines are not calculated but are meant to indicate the possible intersection at ~1000 Ma. The weighted average 206Pb /238U age for the metamorphic rims and grains, and the weighted average 206Pb/207Pb age for the magmatic cores are shown on the right-hand side.*

5.2.2 Sample: 127882L

In this sample 24 analyses were made on 23 zircons. The grains between 250 – and 150 µm in size, with round to elongated, sub-angular shapes. All the grains have cores with oscillatory zoning that are interpreted to be magmatic. Some of the grains have CL-light rims interpreted to be metamorphic. In general, the rims are too thin to analyse.

A regression though all the analyses from this sample yields an upper intercept of 1677 ± 14 Ma and a lower intercept of 411 ± 24 Ma (Figure 5.30, MSWD = 2.0).

Twenty-three of the analyses targeted oscillatory-zoned cores, with Th/U generally well above 0.1, and yield less than 5% discordant dates with a weighted mean $^{207}Pb/^{206}Pb$ age of 1670 ± 11 (MSWD = 1.7), interpreted to reflect the crystallization age of the protolith to the host gneiss. One analysis was identified as a statistical outlier by Isoplot and excluded from the calculation.

The single young analysis targeted at a rim with Th/U = 0.01 that yielded a 5% discordant $^{206}Pb/^{238}U$ age of 410 ± 5 Ma. Unfortunately, the size of the rims hampered additional analyses. Due to the lack of additional analyses the 411 ± 24 Ma age from the resulting regression line with all samples is interpreted to reflect the age of high-grade metamorphism and migmatisation.
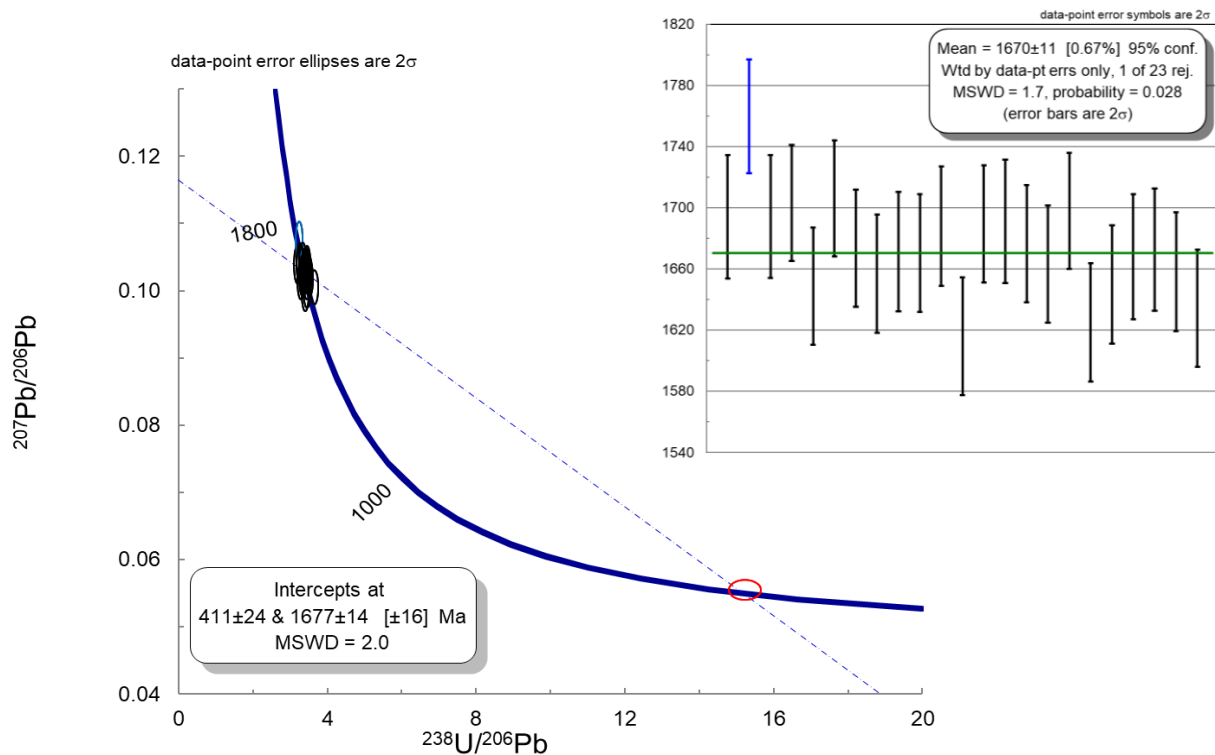
Figure 5.30: *TW plot of analyses U-Pb isotopic data from sample 127882L. Black and red error ellipses represent the magmatic cores and metamorphic rims respectively. The blue error ellipse marks the statistical outlier, corresponding to the weighted average $^{207}Pb/^{206}Pb$ age estimate for the cores is shown on the right-hand side.*

5.2.3 Sample: 127884B

In this sample 24 analyses were made on 23 zircons. The grains vary between 200 and 100µm in size, and most are around 200 µm and have a sub-angular shape. The cores vary and have both zonation, interpreted to be magmatic, and diffuse irregular features of unknown origin. All grains have a CL-light rims interpreted to be metamorphic.

A regression though all the analyses from this samples yields an upper intercept of 1578±89 Ma and a lower intercept age of 512 ± 110 Ma, with an MSWD of 45, indicating significant scatter. Most of the data fall within two groups, one at ca 1600 Ma and another at ca 1000 Ma.

The older group of sixteen analyses yielded a weighted average $^{207}Pb/^{206}Pb$ age of 1619 ± 10 Ma (Figure 5.31 upper inset, MSWD = 1.4), with the youngest analysis identified as a statistical outlier and excluded by Isoplot. The age is interpreted to reflect the crystallization age of the protolith to the host gneiss. Some of these analyses were aimed at CL- light rims, but given that these are very thin, there is a significant potential for mixed analyses, in which case the significantly higher U and Pb concentrations in the cores would result in ages closer to the core than the rim.

Three analyses yield an age around the 1000 Ma, with a calculated Concordia age of 962 ± 11 Ma (Figure 5.31 lower inset, MSWD = 0.98). Two of the analyses are made with in cores and have Th/U ratios > 0.1, whereas the third analysis is made on a CL-bright rim with Th/U < 0.1., thus, the significance of this age results is somewhat ambiguous. Two additional analyses plot on a line between 1619 and 960 Ma.

The two youngest analyses from the rims could indicate the presence of a younger, ~400 Ma event, which is clearly seen in other samples, including from the same outcrop as sample 127884B. Some attempts were made to determine a precise age, but each attempt gave distinctly different ages that could not reconciled.
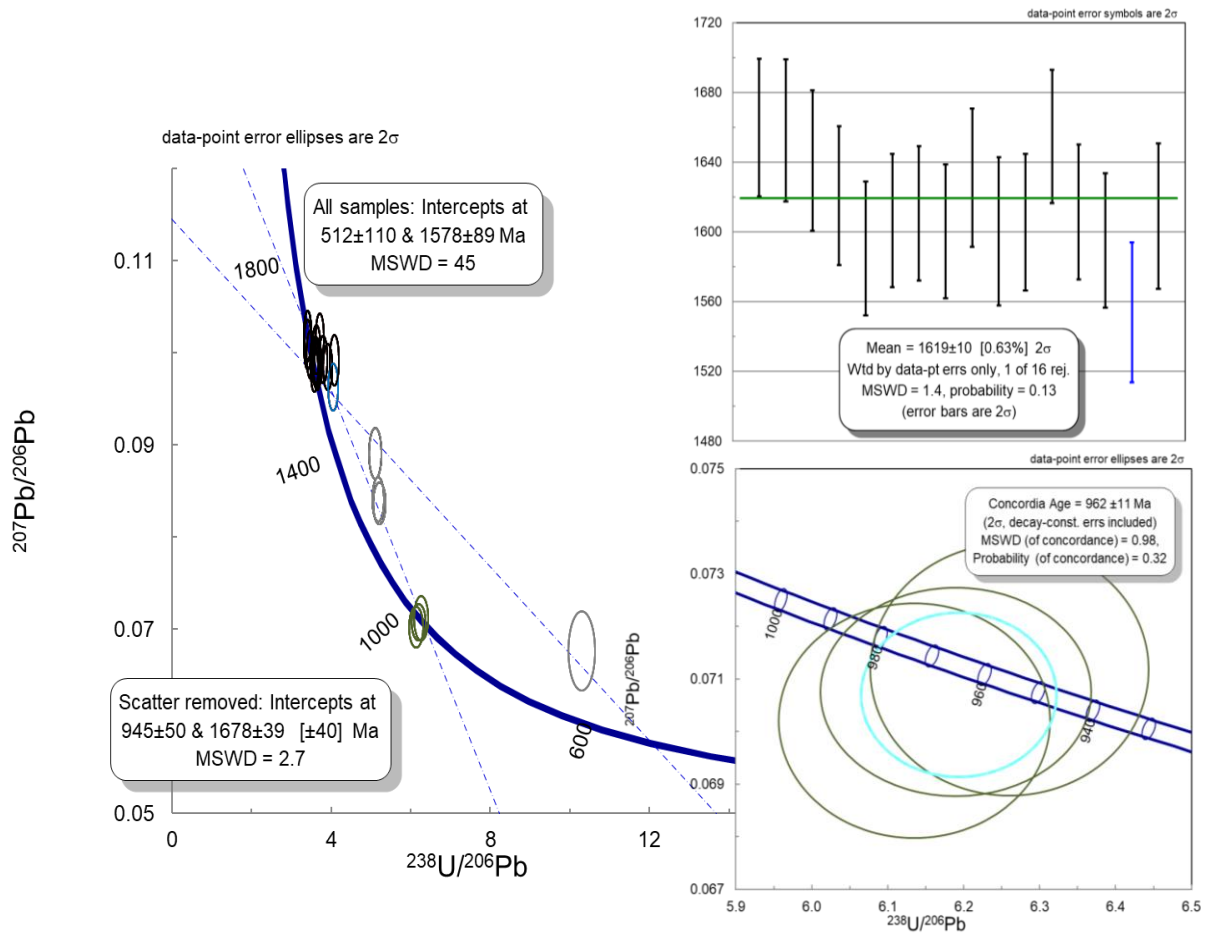
Figure 5.31: *TW plot of U-Pb isotopic data from sample 127884B. Analyses removed from calculations due to discordance are shown with grey error ellipses. Calculations for both regression lines are given in the plot. The first with all U-Pd isotopic data included, the second with selected U-Pb isotopic analytical data. The black error ellipses, and the one blue ellipse, correspond with the weighted average $^{207}Pb/^{206}Pb$ age shown on the upper right-hand side. The green error ellipses mark the rim and metamorphic grain analyses, the light blue error ellipse on the lower right-hand side mark the calculated Concordia age of these analyses.*

5.2.4 Sample: 127885L

In this sample 14 analyses were done on 13 zircons. The grains range in size from 150 to 275 μm and have a tabular, sub-angular shape. In CL-images, all but one grain have dark cores with oscillatory zoning, interpreted to be magmatic. All grains have CL-bright rims, with varying thickness. The one exception has a CL-bright appearance throughout the whole grain, with features much like the rims. The CL-bright rims and one grain are interpreted to be metamorphic.

Apart from one discordant analysis, the data plot in two groups at ca. 1600 and 400 Ma. A regression though all 14 analyses from this sample, yield an upper intercept age of 1626 ± 69 Ma, and a lower intercept age of 374 ± 49 Ma, with an MSWD of 5.8. The one discordant analysis plots well of the regression line. Removing this analysis, the new regression line yields an upper intercept age of 1634 ± 15 Ma, and lower intercept age of 406 ± 13 Ma (MSWD = 0.76). The older group consist of ten analyses that targeted zircon cores with Th/U > 0.2. The younger group target the Cl-bright rims and one grain, all with Th/U ranges < 0.05.

A weighted average $^{207}Pb/^{206}Pb$ age yields an age of 1629 ± 12 Ma (MSWD = 0.58), interpreted to be the crystallization age of the photolith to the host gneiss.

One of the rim analyses displays a large error in the $^{207}Pb/^{206}Pb$ ratio. This is most likely related to a very low U concentration in the analysed rim. As discussed above the low concentration of U will in turn result in low concentrations of radiogenic ^{207}Pb, thus the large uncertainty. The other rim analyses have Th/U ratios ≈ 0.01. and thus, a more constricted range. The $^{206}Pb/^{238}U$ ratio is much better constrained (Figure 5.32, lower inset). The weighted average $^{206}Pb/^{238}U$ age of the three analyses yields an age of 406 ± 26 Ma (MSWD = 3.5). Interpreted to reflect the high-grade metamorphism and migmatisation.
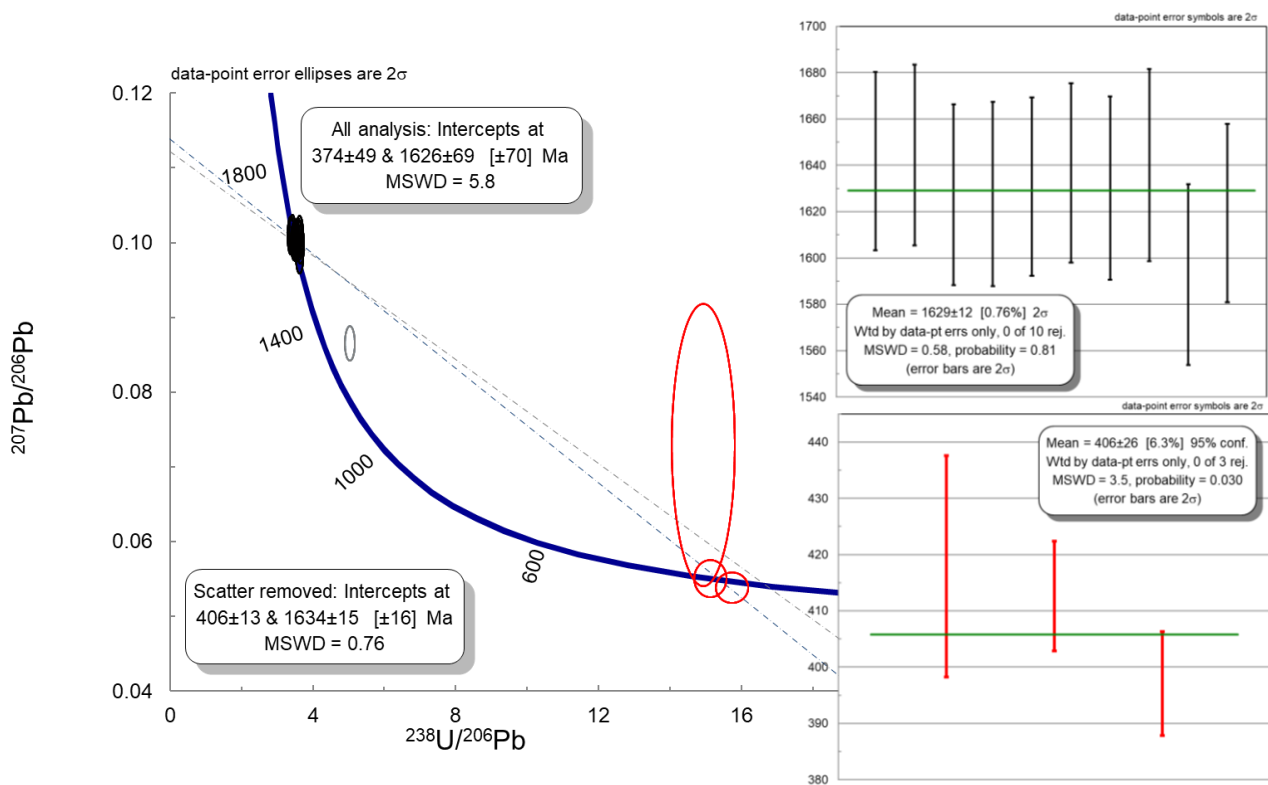
Figure 5.32: *TW plot of analysis U – Pb isotopic data from sample 127885L. Analyses removed from calculations due to discordance is shown with grey error ellipses. Calculations for both regression lines are given in the plot. The uppermost with all sample's analysis data included, the lower with selected data. The black error ellipses mark the core analyses, which correspond with the weighted average $^{207}Pb/^{206}Pb$ age shown on the upper right-hand side. The red error ellipses mark the rim analyses and correspond with the weighted average $^{206}Pb/^{238}U$ age shown on the lower right-hand side.*

5.2.5 Sample: 127886L

In this sample 24 analyses were done on 24 separate zircons. The grains range in size from 100 to 500µm, whereof most are around 200 µm, with a tabular, sub-angular shape. In CL-images all but one analysed grain has dark cores with oscillatory zoning, interpreted to be magmatic. The one exception has a CL-bright appearance throughout the whole grain, with features much like the rims. All grains have CL-bright rims with varying thickness, whereof most are rather thin. The CL-bright rims and the one grain is interpreted to be metamorphic.

A regression line though all 24 analyses in this sample yields an upper intercept age of 1616 ± 42 Ma, and a lower intercept age of 431 ± 48 Ma (MSWD =14). The sample data fall into three groups, an older at ca. 1600Ma, an intermediate at ca. 1000 Ma and a younger at ca. 400 Ma. One of the older analysis is reverse concordant and is excluded from this point on. A regression line though the younger and older analyses, yield an upper interception age of 1629±11 Ma, and a lower interception age of 400 ± 12 Ma (Figure 5.33, MSWD = 0.98). The older group consist of 20 samples, and target CL-dark cores with TH/U ratios > 0.2. Both the intermediate and younger analyses target CL-bright rims with Th/U ratios < 0.02.

The weighted average ^{207}Pb/^{206}Pb age of the older analyses yield an age of 1625 ± 9 Ma, interpreted to reflect the crystallization age of the protolith to the host gneiss. (Figure 5.33, upper inset, MSWD = 1.4)

One analysis place within the intermediate age range. This analysis is concordant yielding a ^{206}Pb/^{238}U age of 956.3 Ma. with a calculated Concordia age of 958 ±20 Ma (MSWD = 0.112). When plotted in a linear regression the age is 971±88 Ma and 929±84 Ma in a regression with the older and younger analyses respectively (Figure 5.33, MSWD = 1.5 & 2 respectively). The one sample cannot give a certain age estimate. The analysis is however interpreted to reflect the presence of high-grade metamorphism and migmatisation at ca. 950 Ma.

The two youngest analyses, within the 400 Ma range, has a calculated Concordia age of 406 ±7 Ma, interpreted to reflect the age of a secondary high-grade metamorphism and migmatisation event (Figure 5.33 lower inset, MSWD = 1.4).
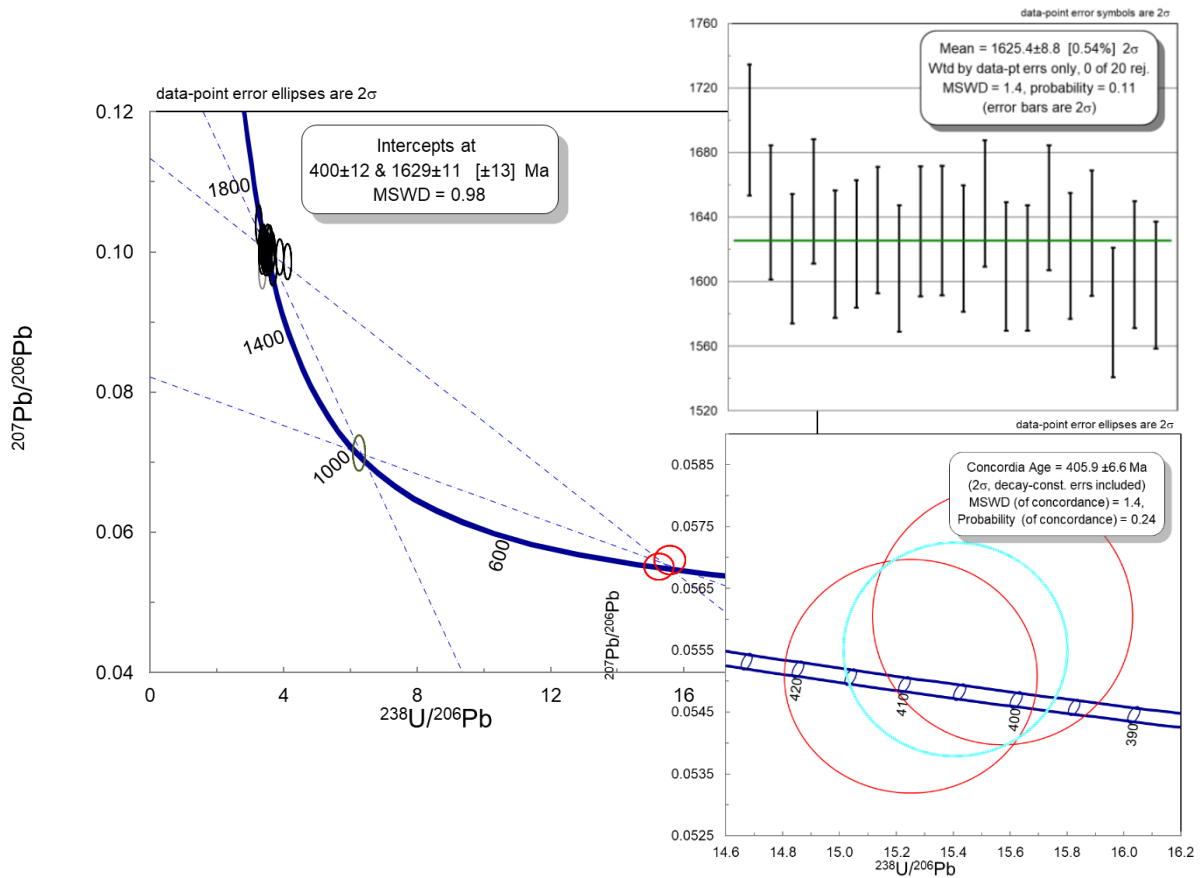
Figure 5.33: *TW plot of analysis U-Pb isotopic data from sample 127886L. Analyses removed from calculations due to discordance are shown with grey error ellipses. Calculations for one regression line, with the older and younger analyses, is shown in the TW plot. Two regression lines are indicated between the older and younger and the intermediate analyses. The black error ellipses correspond with the weighted average $^{207}Pb/^{206}Pb$ age for the cores shown on the upper right-hand side. The green error ellipse marks the intermediate rim analyses. The red error ellipses represent the youngest rim analyses, the light blue error ellipse on the lower right-hand side mark the calculated Concordia age of the youngest rim analyses.*

5.2.6 Sample: 127866L

In this sample 24 analyses were made on 23 zircons. The grains range in size from 150 to 400 μm, whereof most are around 250 μm, and have a prismatic to sub-rounded shape in smaller grains. In CL-images, serval grains have a dark core with oscillating zonation interpreted to be magmatic, transected by a Cl-bright rim. The remaining grains are CL-bright, with diffuse internal features like the rims. The CL-bright rims and grains are interpreted to be metamorphic.

A regression though all 24 analyses in the samples yield an upper intercept age of 1672 ± 24 Ma, and a lower intercept age of 394 ± 9 Ma with an MSWD of 1.2, see Figure 5.34. The analyses are divided into two groups, one older at ca. 1700 Ma and a younger at ca. 400 Ma. The older group consist of five analyses that primarily targets cores, with a Th/U > 0.2. Whereas the younger group of nineteen analyses targets only CL-bright rims and grains with a Th/U < 0.03.

The core analyses yield a weighted average $^{207}Pb/^{206}Pb$ age of 1655 ± 20 Ma, interpreted to reflect the crystallization age of the protolith to the host gneiss (Figure 5.34, upper inset, MSWD = 0.28).

The nineteen rims and metamorphic grains analyses, as for many samples this study, display large errors in the $^{207}Pb/^{206}Pb$ ratios. This is most likely related to the very low U concentration in these zircons, typically with only a few tens of ppm U, resulting in very small concentrations of radiogenic ^{207}Pb, thus the large analytical uncertainties. In contrast the $^{206}Pb/^{238}U$ ratios are much better constrained, and preferable for determining the age of the rims and CL-bright grains. Many of the younger analyses have a high relative percentage of common lead, with the already low amount of radiogenic lead in the grains a small amount of common lead will have a decisive effect, however a correlation between the analyses with high relative wt.% of common lead could however not be found.

The weighted average $^{206}Pb/^{238}U$ age of the nineteen analyses yield an age of 404 ± 5 Ma (Figure 5.34 lower inset, MSWD = 2.4), one analysis excluded as a statistical outlier by Isoplot. The age is interpreted to reflect the high-grade metamorphism and migmatisation.
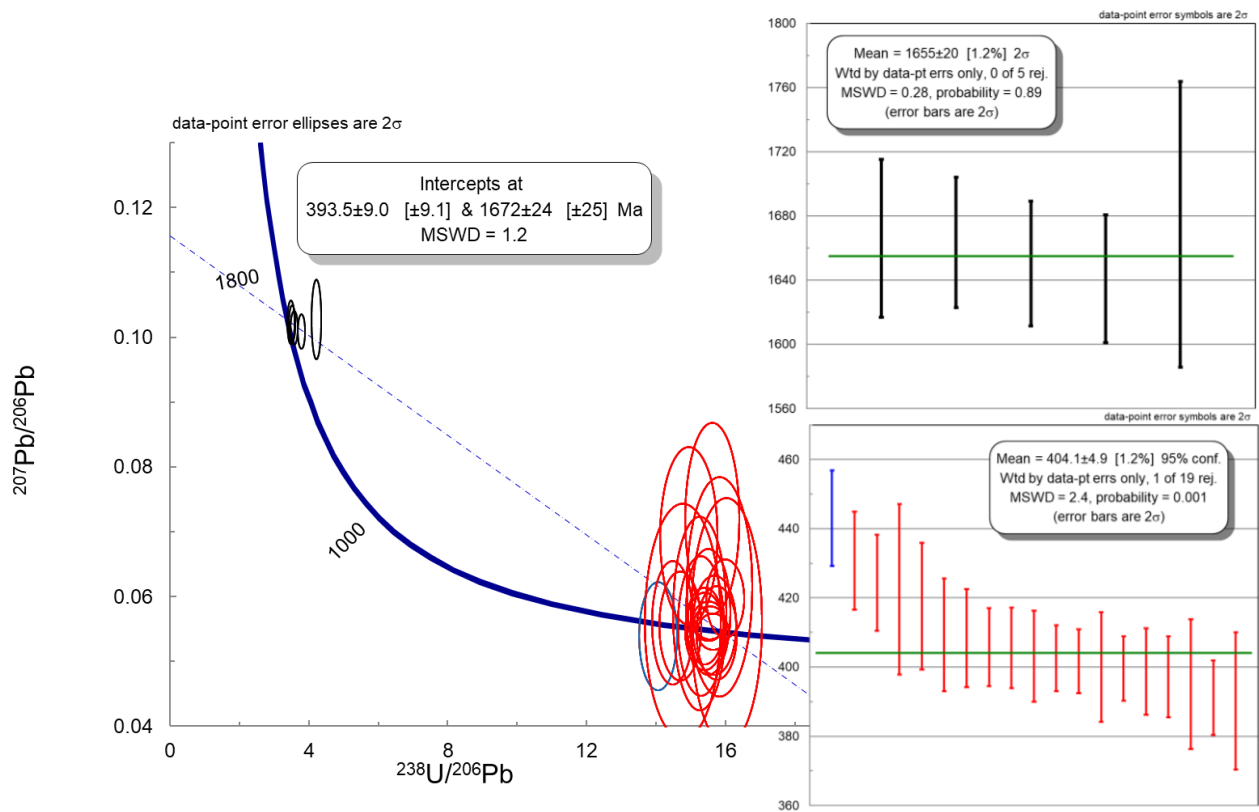
Figure 5.34: *TW plot of U-Pb isotopic data from sample 127866L. The black error ellipses correspond with the weighted average $^{207}Pb/^{206}Pb$ age, shown on the uppermost right-hand side, of the core analyses. The red error ellipses mark the rims and metamorphic grains analyses, the blue error ellipses mark the statistical outlier, corresponding to the weighted average $^{206}Pb/^{238}U$ age shown on the lower right-hand side*

5.2.7 Sample: 127868L

In this sample 24 analyses were made on 23 zircons. The grains are between 150 and 300µm in size, and are varying in shape from elongated tabular, to smaller more sub rounded grains. Several of the grains appear in fractured pieces. In CL-images the grains have dark cores with oscillatory zoning, interpreted to be magmatic, transected by CL-bright rims with diffuse irregular features. Some of the grains are completely CL-bright, with internal features like the rims but lacking a distinct core. The CL-bright rims and grains are interpreted to be metamorphic.

A regression though all 24 analyses in this sample yield an upper intersection age of 3418 ± 1300 Ma, and a lower intersection age of 444 ± 73 Ma, with a MSWD of 17, indicating the presence of strongly discordant analysis data. Two analyses are excluded from this point: one being strongly discordant, and the other being reverse discordant. Note that the former of these analyses are not visible in the plot (Figure 5.35), as its values lies outside the plot constrictions. The regression line thought the remaining twenty-two analyses yield an upper intercept age of 1657 ± 23 Ma, and a lower intercept age of 398 ± 10 Ma (Figure 5.35, MSWD = 1.3). The analysis U – Pb isotopic data fall in two groups, one older at ca. 1650 Ma and a younger at ca. 400 Ma. The older group consist of four analyses that target zircon cores with Th/U > 0.2, whereas the younger group consists of eighteen analyses that target the CL-bright zircon rims or grains with a Th/U generally <0.04.

The four analyses targeting cores yield a weighted average ^{207}Pb/^{206}Pb age of 1649 ± 20 Ma, (Figure 5.35 upper inset, MSWD = 0.39) interpreted to reflect the crystallization age of the protolith to the host gneiss.

The younger analyses targeting the rims and metamorphic grains have the same characteristics as in the former samples, with large errors in the ^{207}Pb/^{206}Pb ratios, and some analyses with a high wt.% of common lead, which have no apparent effect on the analyses distribution. The weighted average ^{206}Pb/^{238}U age yield an age of 396 ± 3 Ma (Figure 5.35 lower inset, MSWD = 0.98), two analyses are excluded as statistical outliers by Isoplot. This age is interpreted to reflect the age of the high-grade metamorphism and memorization
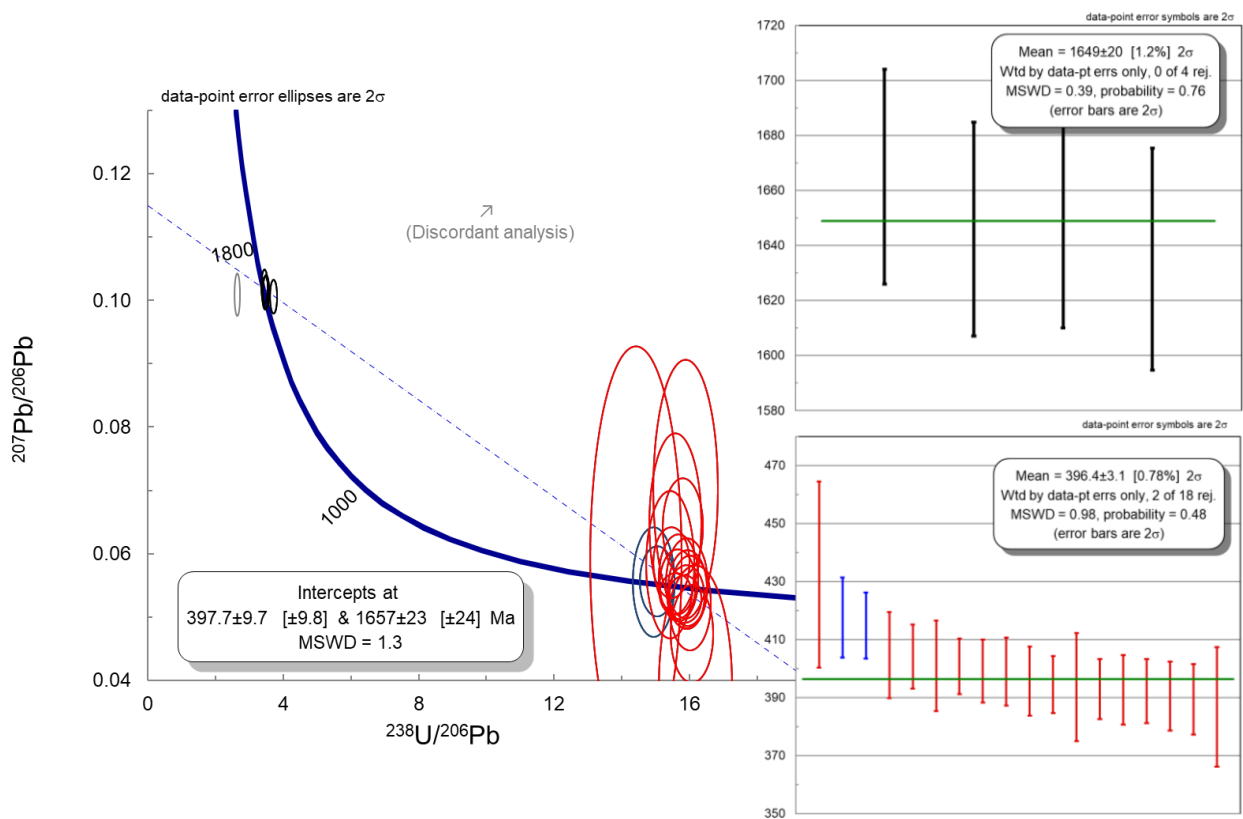
Figure 5.35: *TW plot of U-Pb isotopic data from sample 127868L. Analyses removed from calculations due to discordant are shown with grey error ellipses. The black error ellipses correspond with the core analyses weighted average $^{207}Pb/^{206}Pb$ age, shown on the upper right-hand side. The red error ellipses mark the rims and metamorphic grains analyses, the blue error ellipses mark the statistical outliers, corresponding to the weighted average $^{206}Pb/^{238}U$ age shown on the lower right-hand side.*

5.2.8 Sample: 127876L

In this sample 24 analyses were made on 23 zircons. The grains are between 100 and 250 μm in size, whereof most are around 200 μm, and vary from tabular to more sub rounded in shape. The larger grains appear to be in fractured pieces. In CL-images the grains with cores display a CL-dark core with oscillatory zoning, interpreted to be magmatic, transected by mostly thin CL-bright rims. The thicker mantles are less CL-bright and display diffuse and irregular feature interpreted metamorphic. Some grains display this characterization throughout lacking.

A regression line though all 24 analyses from this sample, yield an upper intersect age of 1691 ± 22 Ma, and a lower intercept age of 394 ± 8 Ma, with an MSWD of 0.85 (Figure 5.36). Most of the U – Pb isotopic data fall within two groups, one at ca. 1700 Ma, and one at ca. 400 Ma. The older group consist of five analyses that target zircon cores with Th/U > 0.5. The core analyses fall along the regression line, which could indicate the discordia. The younger group consist of nineteen analyses that target the Cl-bright rims and grains, with a Th/U < 0.03.

The five core analyses yield a weighted mean $^{207}Pb/^{206}Pb$ age of 1648 ± 19 Ma (MSWD = 1.17). Due to the slight spread in the analyses data the weighted mean could be biased and result in a younger age. Plotting the five analyses in a separate linear regression line the age is to 1677 ± 45 Ma, with a MSWD of 0.69. Which is more within the range of the upper intercept with all analyses plotted. The age 1691 ± 22 Ma is thus interpreted to reflect the crystallization age of the protolith to the host gneiss.

Of the rims and metamorphic grains analyses all nineteen places in a cluster with no evident statistical outliers excluded by Isoplot. Some analyses have a high wt.% ratio of common lead, but this has no apparent effect on the analysis's distribution. The high ratios could be explained the small concentrations of radiogenic ^{207}Pb in the rims, thus little common lead is needed to boost the wt.% ratio. The weighted average $^{206}Pb/^{238}U$ age yield an age of 398 ± 3 Ma, interpreted to reflect the age of the high-grade metamorphism and migmatisation (Figure 5.36 inset, MSWD = 0.63).
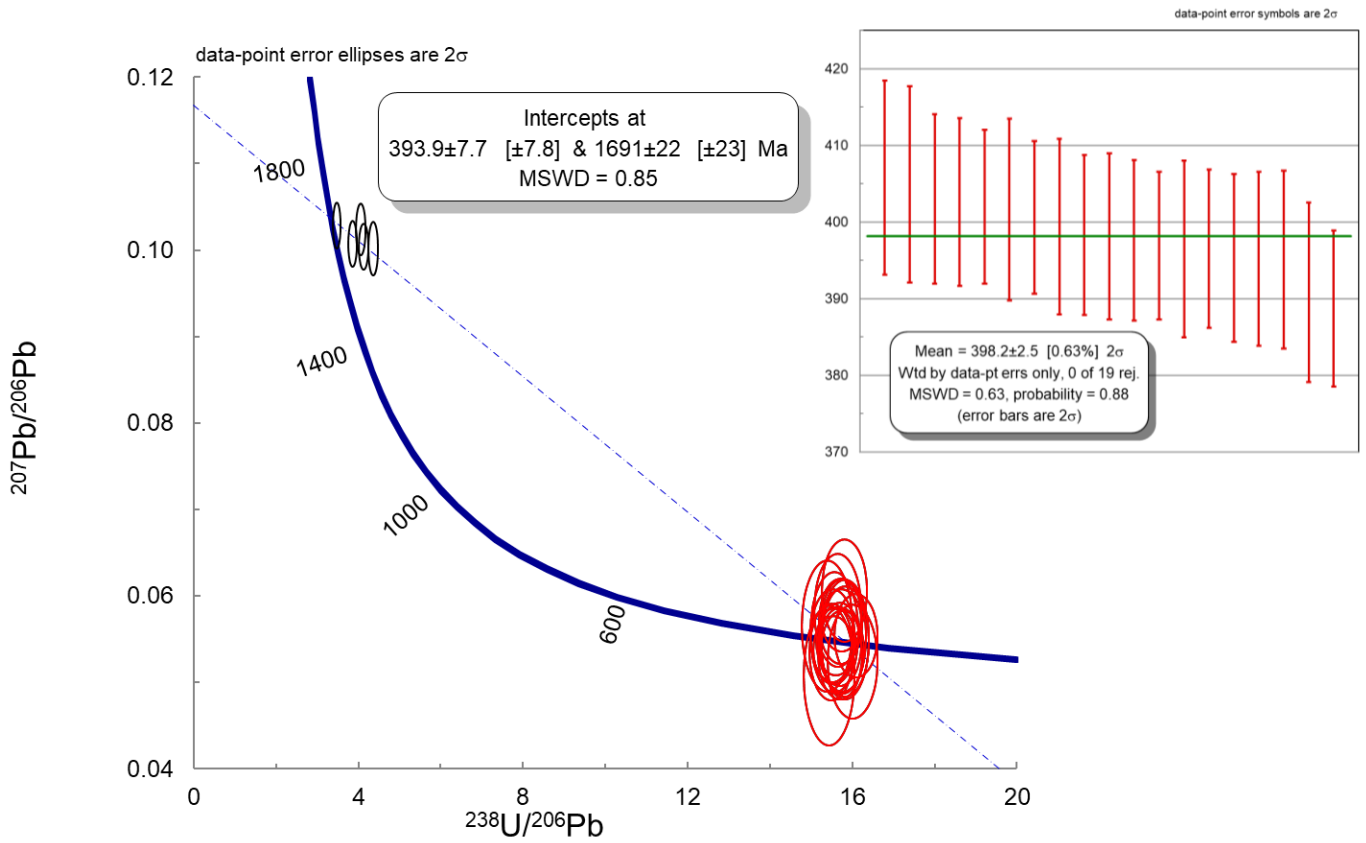
Figure 5.36: *TW plot of U-Pb isotopic data from sample 127876L. The black error ellipses correspond with the core analyses. The red error ellipses mark the rims and metamorphic grains analyses, corresponding to the weighted average $^{206}Pb/^{238}U$ age shown on the right-hand side.*

5.2.9 Sample: 127877L

In this sample 24 analyses were made on 24 separate zircons. The grains range in size from 125 to 275 μm, most being smaller sub-rounded grains, with some larger more angular exceptions. The larger pieces have sharp edges and appear to be fractured pieces of larger grains. In CL-images most of the grains display a dark core, interpreted to be magmatic, transected by CL-bright rims or mantles with diffuse irregular features. A few grains are CL-bright, with internal features like the rims, but lack cores. The CL-bright rims and grains are interpreted to be metamorphic.

A regression through all twenty-four analyses from this sample, yield an upper intercept age of 1443 ± 140 Ma, and a lower intercept age of 404 ±3 1 Ma, with an MSWD of 24, indicating significant scatter (Figure 5.37). Most of the U – Pb isotopic data fall within three groups, one at ca. 1700 Ma, one at ca. 1000 Ma and one at ca. 400 Ma. The older group consist of four analyses, targeting primarily cores with Th/U > 0.2, that fall along an indicated discordia towards the middle intercept. The middle group consist of four analyses targeting primarily rims and metamorphic grains with Th/U > 0.2 and < 0.05. The younger group consist of sixteen analyses targeting rims and metamorphic grains with Th/U < 0.05.

The four core analyses place close to the upper intercept, all within the same Th/U range. The analyses place evenly distributed along an indicated discordia towards the medium age analyses, thus a weighted mean ^{207}Pb/^{206}Pb age would not yield any valid result. A regression though the older and intermediate analyses yield an upper intercept age of 1682 ± 110 Ma (MSWD = 3.6). The same problem occurs when isolation the four analyses separately, the MSDW value falls within an acceptable limit, but the resulting age range is too large to be a good age representation. The one analysis that fall along the concordia has an age of 1675 ± 28 Ma, eliminating much of the statistical error, and is thought to best reflect the crystallization age of the protolith to the host gneiss

Four analyses place in the middle group, but the same problem arises as with the intermediate analyses as with the older. Large age ranges, when using linear regression, with both with the older and younger analyses, yielding ages of 837±60 Ma (MSWD =3.6) and 1020 ± 110 Ma (MSWD = 2.1) respectively (see calculated regression lines in Figure 5.37). The weighted mean ^{207}Pb/^{206}Pb age yields an age of 880 ± 61 Ma (MSWD = 16) and is interpreted to best reflect the age of the first event of high-grade metamorphism and migmatisation.

The weighted average ^{206}Pb/^{238}U age of the sixteen analyses in the younger group yield an age of 392 ± 3 Ma (MSWD of 1.6), one analysis being excluded as a statistical outlier by Isoplot. The age is interpreted to reflect the age of a second high-grade metamorphism and migmatisation. The impact two separate events of high-grade metamorphism and migmatisation has on the analysis samples is evident, but to exactly how and to what degree is unclear.
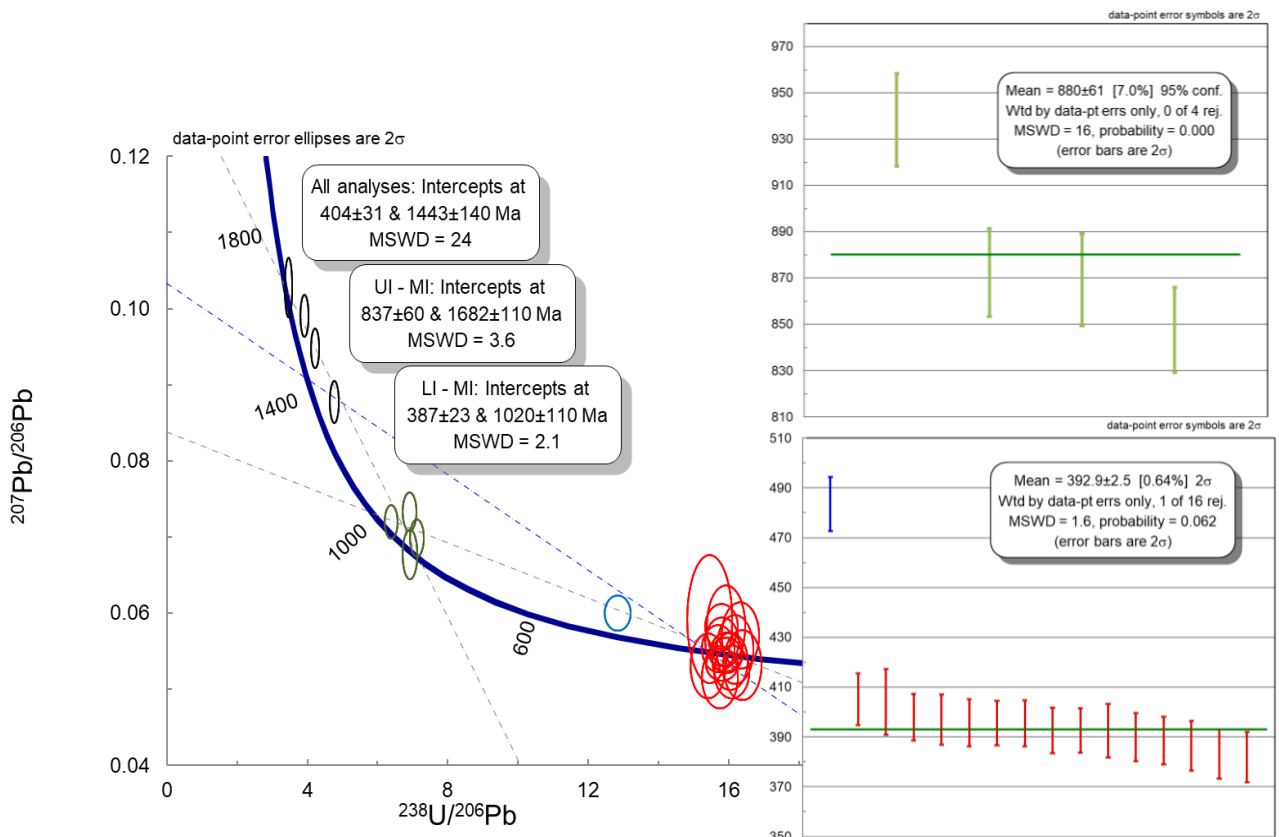
Figure 5.37: *TW plot of U-Pb isotopic data from sample 127877L. The black error ellipses mark the older core analyses. The green error ellipses correspond intermediate rims and metamorphic grains, corresponding with the weighted average $^{207}Pb/^{206}Pb$ age shown on the upper right-hand side. The red error ellipses mark the youngest rims and metamorphic grains analyses, the blue error ellipse marking the statistical outlier, corresponding to the weighted average $^{206}Pb/^{238}U$ age shown on the lower right-hand side.*

5.2.10   Sample: 127878L

In this sample 24 analyses were made on 23 zircons. The grains are between 175 and 300µm in size. And are tabular to sub-angular in shape. In CL-images most of the grains display a dark core, interpreted to be magmatic, transected by CL-bright rims or mantles with diffuse irregular features. The mantles vary in thickness and are in some grains barely visible. A few grains are CL-bright, with internal features like the rims, but lack cores. The CL-bright rims and grains are interpreted to be metamorphic.

A regression though all twenty-four analyses from this sample, yield an upper intercept age of 1610 ± 43 Ma, and a lower intercept age of 391 ± 13 Ma, with an MSWD of 1.6 (Figure 5.38). Most of the U – Pb isotopic data fall within two groups, one at ca. 1600 Ma, and another at ca. 400 Ma. The older group consist of eleven samples that targets primarily zircon cores with Th/U > 0.1. The younger group consist of thirteen analyses that target rims and metamorphic grains with Th/U < 0.02.

The eleven core analyses yield a weighted mean ^{207}Pb/^{206}Pb age of 1585 ± 27 Ma (Figure 3.38 upper inset, MSWD =3.2), one sample is excluded as a statistical outlier by Isoplot. Though the sample lack some analysis data to create a significant discordia the older analyses indicate lead loss towards the lower intercept. The initial linear regression age of 1610 ± 43 Ma is interpreted to reflect the crystallization age of the protolith to the host gneiss.

The rims and metamorphic grains analyses display the same large errors in the ^{207}Pb/^{206}Pb ratios as seen in many of the rims and CL-bright grains in this study. The more constrained weighted average ^{206}Pb/^{238}U age of the thirteen analyses yield an age of 398 ± 6 Ma (Fig 5.38 lower inset, MSWD = 3.5), one analysis excluded as a statistical outlier by Isoplot. This age is interpreted to reflect the age of the high-grade metamorphism and migmatisation.
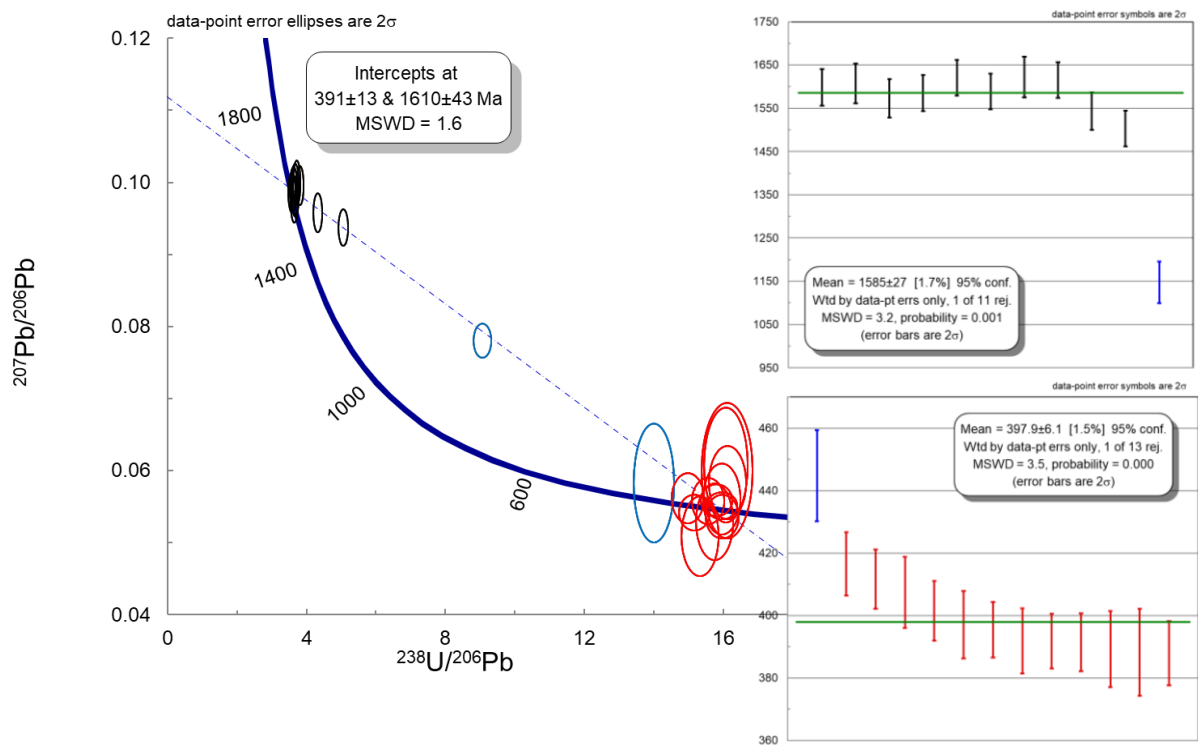
Figure 5.38: *TW plot of U-Pb isotopic data from sample 127878L. The black error ellipses correspond with the core analyses weighted average [207]Pb/[206]Pb age shown on the upper right-hand side. The red error ellipses mark the rims and metamorphic grains analyses corresponding with the weighted average [206]Pb/[238]U age given on the lower right-hand side. The blue error ellipses correspond to the statistical outliers for both plots.*

5.2.11   Sample: 197555

In this sample 24 analyses were made on 23 zircons. The grains between 100 and 225 µm in size, all having a tabular, sub-angular shape. In CL - images, some of the grains display an oscillatory zonation, interpreted to be magmatic, while others have more diffuse irregular features, interpreted to be metamorphic. Both features appear both as CL-bright and CL-dark in the different grains. The grains all lack the distinct CL-bright mantle observed in the prior leucosome samples.

A regression though all 24 analyses from this sample yield an upper intercept age of 1692 ± 12 Ma, and a lower intercept age of 227 ± 410 Ma, with an MSWD of 0.56. All the sample U – Pb isotopic data fall within one group at ca. 1700 Ma. With a lack of distinct mantles all analyses target the cores, which all have a Th/U> 0.1.

One analysis is reverse discordant; excluding this analysis the remaining twenty-three analyses yield a weighted mean ^{207}Pb/^{206}Pb age of 1688 ± 8 Ma (Figure 5.39 inset, MSWD = 0.56) interpreted to reflect the crystallization age of the protolith to the host gneiss.
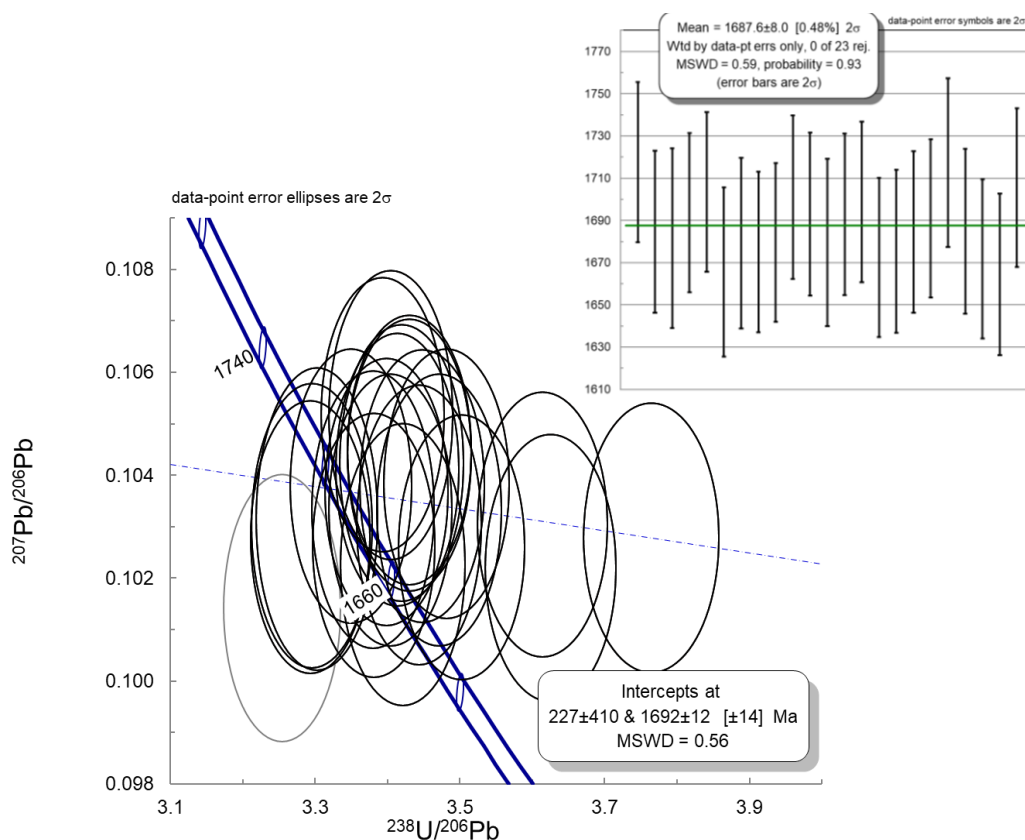
Figure 5.39: *TW plot of U-Pb isotopic data from sample 197555. The black error ellipses correspond with the weighted average ^{207}Pb/^{206}Pb age, shown on the upper right-hand side.*

5.2.12   Sample: 197562

In this sample 24 analyses were made on 24 separate zircons. The grains are between 100 and 200 µm in size, whereof most are around 150 µm. All having a tabular, sub-angular to rounded shape. In CL - images, some of the grains display an oscillatory zoning, interpreted to be magmatic, while most have more diffuse irregular features, interpreted to be metamorphic. There is little variation in the CL-brightness between the grains, and all grains lack the distinct CL-bright mantle observed in the prior leucosome samples.

A regression though all twenty-four analyses in this sample yield an upper intercept age of 1682±16 Ma, and a lower intercept age of 631 ± 410 Ma, with an MSWD of 0.83. All the sample U – Pb isotopic data fall within one group at ca. 1700 Ma. With a lack of distinct mantles all analyses target the cores, which all have a Th/U> 0.3. Four of the analyses have a small amount of common lead, but no visible correlation was found between these analyses.

The weighted average ^{207}Pb/^{206}Pb age yield an age of 1672 ± 8 Ma (Figure 5.40 inset, MSWD = 1.06) interpreted to reflect the crystallization age of the protolith to the host gneiss.
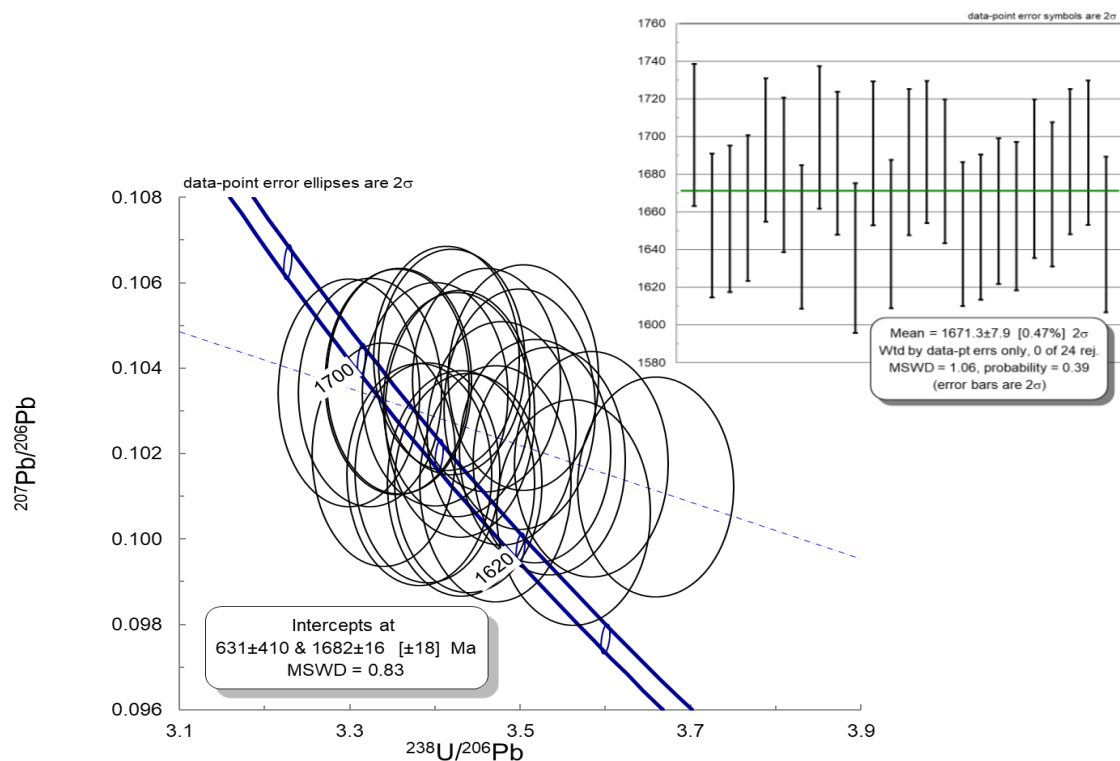
Figure 5.40: *TW plot of U-Pb isotopic data from sample 197562. The black error ellipses correspond with the weighted average ^{207}Pb/^{206}Pb age shown on the upper right-hand side.*

5.2.13   Sample: 197562L

In this sample 24 analyses were made on 24 separate zircons. The grains are between 100 and 175µm in size, all tabular, sub-angular in shape. In CL-images, some of the grains have cores with oscillatory zoning, interpreted to be magmatic. All grains are transected by rims or mantles with diffuse irregular features. The rims vary in thickness, from thin barely visible rims, too almost consuming the core, and are interpreted to be metamorphic. The CL-brightness in both core and mantles is variable.

A regression through all twenty-four analyses from this sample, yield an upper intercept age of 1662 ± 15 Ma, and a lower intercept age of 404 ± 4 Ma, with an MSWD of 1.4 (Figure 5.41). The analyses U – Pb isotopic data fall in two groups, one at ca. 1700 Ma, and another at ca. 400 Ma. The older group consist of ten analyses that target zircon cores with a Th/U > 0.4, whereas the younger group consists of fourteen analyses that target the mantles with a Th/U <0.01.

One analysis is reverse concordant; excluding this analysis, the remaining nine core analyses yield a weighted mean ^{207}Pb/^{206}Pb age of 1649 ± 13 Ma (Fig 5.41 upper inset, MSWD = 0.93) interpreted to reflect the crystallization age of the protolith to the host gneiss.

The weighted average ^{206}Pb/^{238}U age of the fourteen rim analyses yields an age of 408 ± 2 Ma (Figure 5.41 lower inset, MSWD = 1.4), one analysis being excluded as a statistical outlier by Isoplot. The age is interpreted to reflect the age of the high-grade metamorphism and migmatisation.

It is noted that the younger rim analyses have less errors in the ^{207}Pb/^{206}Pb ratios than some of the former samples, and all the data place in a tight cluster at the lower intercept. With the statistical outlier from the weighted average ^{206}Pb/^{238}U age estimate removed, the concordia age can be calculated to 409 ± 3 Ma (MSWD = 6.2), which is a nearly identical to the former age estimate.
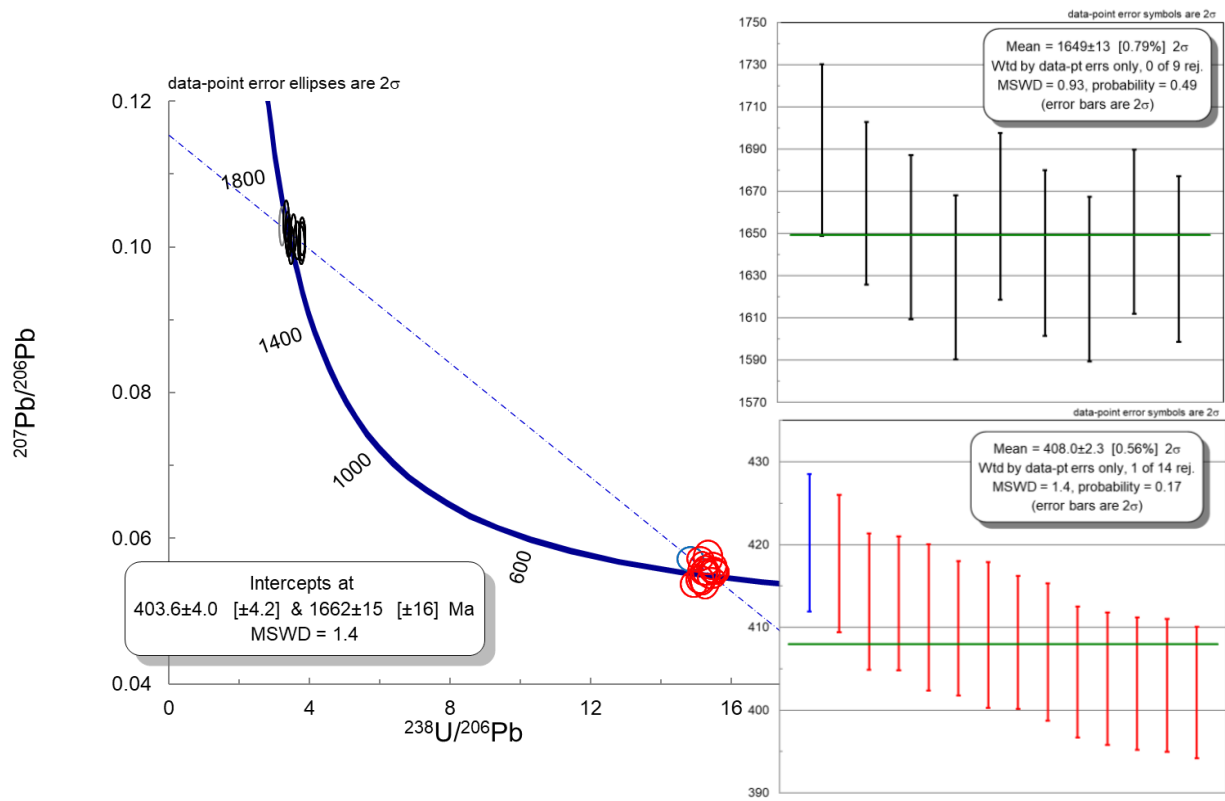
Figure 5.41: *TW plot of U-Pb isotopic data from sample 197562L. The black error ellipses correspond with the core analyses weighted average $^{207}Pb/^{206}Pb$ age, shown on the upper right-hand side. The red error ellipses mark the rim analyses corresponding to the weighted average $^{206}Pb/^{238}U$ age shown on the lower right-hand side. The blue error ellipse corresponds to the statistical outlier shown in the same plot.*

5.2.14   Sample: 197578

In this sample 24 analyses were made on 24 separate zircons. The grains are between 75 and 150 µm in size, all with a tabular, sub-angular to rounded shape. In CL-images, most of the grains display a dark core, interpreted to be magmatic, transected by CL-bright thin rims or mantles with diffuse irregular features. A few grains are CL-bright, with internal features like the rims, but lack cores. The CL-bright rims and grains are interpreted to be metamorphic.

A regression through all twenty-four analyses from this sample, yield an upper intercept age of 1659 ± 11 Ma, and a lower intercept age of 423 ± 10 Ma, with an MSWD of 0.64 (Figure 5.42). The U – Pb isotopic data fall in two groups, one at ca. 1600 Ma and another at c. 400 Ma. The older group consist of twenty-one analyses that target primarily zircon cores with Th/U > 0.2. Whereas the younger group consists of three analyses that target the rims and metamorphic grains, with a Th/U generally <0.05.

The twenty-one core analyses yield a weighted mean ^{207}Pb/^{206}Pb age of 1644 ± 9 Ma (Figure 5.42 inset, MSWD = 0.87) interpreted to reflect the crystallization age of the protolith to the host gneiss.

Of the three rims and metamorphic grain analyses, only one place on the concordia, the two others fall along an indicated discordia towards the older analyses. Due to the spread in the analyses any weighted average would not yield any valid result. A linear regression though the three analyses set the age to 415 ± 18 Ma, with a MSWD of 0.54. The lower intercept age set with all the analyses data, of 423 ± 10 Ma, is interpreted to best reflect the age of the high-grade metamorphism and migmatisation.

The collected sample is of a photolith with the more prominent leucosomes cut out during the sample preparation. The presence of high-grade metamorphism and migmatisation analysis data in the photolith is not unexpected and can be explained by melting occurring in the rock, forming smaller leucosomes in the rock that has not migrated into the larger ones. By studying the sample in thin section sharp angles between grain boundaries can indicate the presence of melt in the rock. If all the melt has subtracted during migmatisation such structures will not be found, but one can still find zircons with altered grains and rims.
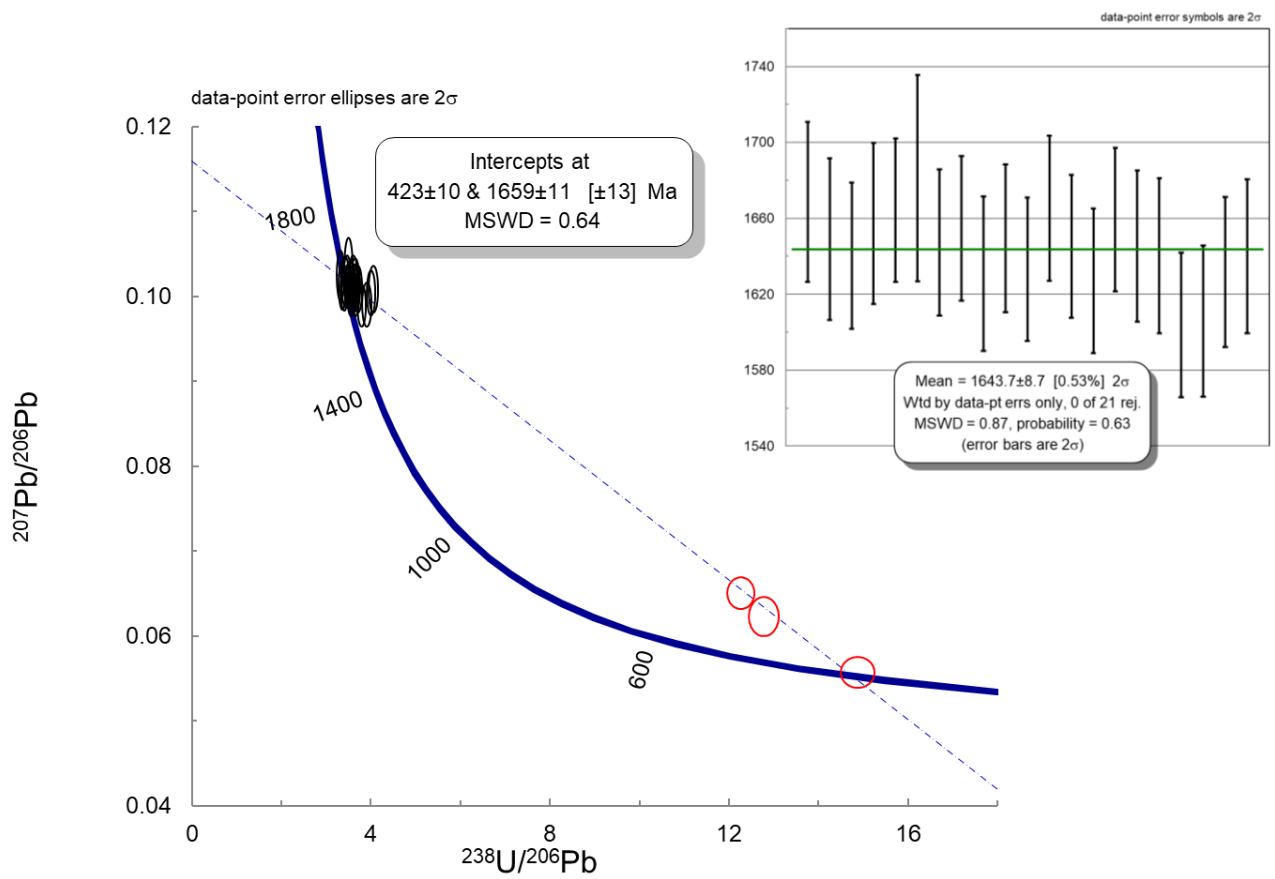
Figure 5.42: *TW plot of U-Pb isotopic data from sample 197578. The analyses marked with black error ellipses, correspond with the weighted average $^{207}Pb/^{206}Pb$ age shown on the right-hand side. The rims and metamorphic grains are shown with red error ellipses.*

5.2.15   Sample: 197586

In this sample 24 analyses were made on 24 separate zircons. The grains are between 100 and 200 µm in size, all have a tabular, sub-angular to rounded shape. In CL-images, the grains display a dark core, interpreted to be magmatic, transected by CL-bright rims or mantles with diffuse irregular features. A few grains are CL-bright, with internal features like the rims, but lack cores. The CL-bright rims and grains are interpreted to be metamorphic.

A regression though all the analyses in this sample yield an age of 1652 ± 11 Ma at the upper intercept, and an age of 392 ± 21 Ma at the lower, with a MSWD of 0.79 (Figure 5.43). The U – Pb isotopic data fall in two groups, one at ca. 1600 Ma and another at ca. 400 Ma. The older group consist of twenty-one analyses that target primarily dark cores, but also some CL-bright areas, all with a Th/U ratio > 0.1, whereas the younger group consists of three analyses that target only the rims and metamorphic grains, where the Th/U ratio is <0.04.

The twenty-one analyses targeting the cores yield a weighted mean $^{207}Pb/^{206}Pb$ age of 1643 ± 9 Ma, with two analyses excluded as statistical outliers by Isoplot (Figure 5.43 inset, MSWD = 1.14). One of the analysis contain common lead, which could affect the analysis age range. The removal of this analysis does however not affect the calculated age to any significant degree. There is however a slight indication of analysis placement along an indicated discordia towards the rim analyses, this could shift the mean age down, giving slightly biased younger age. Thus, the upper intercept age set with all the analyses data of 1652 ± 11 Ma, is interpreted to reflect the crystallization age of the protolith to the host gneiss.

Due to the spread in the analyses any weighted average would not yield any valid result for the younger analyses. Two younger analyses that fall on the concordia both have a discordance > 30%. The last analysis is more concordant and falls along the indicated discordia towards the upper intercept, corresponding with some of the older analyses. The lower intercept age set with a linear regression with all the U – Pb isotopic data, of 392±21 Ma, is thus interpreted to best reflect the age of the high-grade metamorphism and migmatisation.

As with sample 197578 above this sample is a collected photolith with the more prominent leucosomes cut out during the sample preparation. The same case could thus be made again, as of where the younger analysis data hails from.
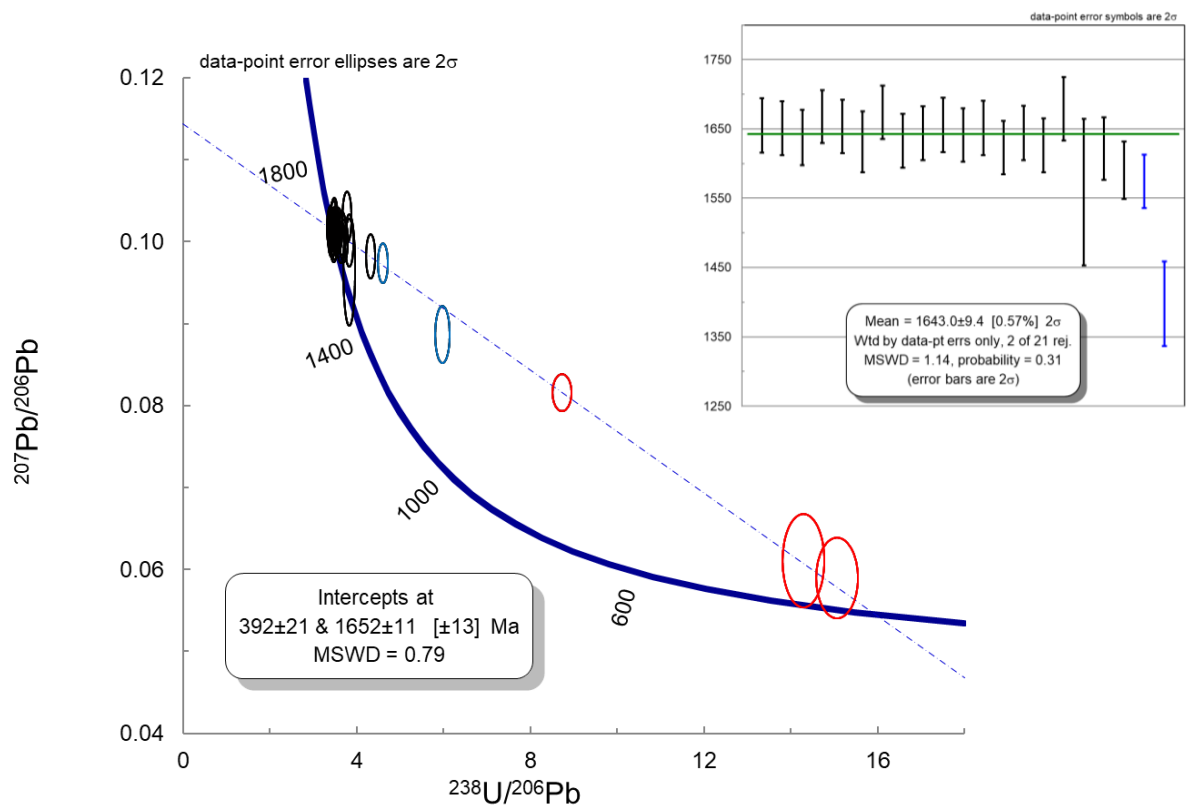
Figure 5.43: TW plot of U-Pb isotopic data from sample 197586. The analyses marked with black error ellipses, correspond with the weighted average $^{207}Pb/^{206}Pb$ age shown to the right-hand side. The analyses targeting the rims and metamorphic grains are market with a red error ellipses.

5.2.16   Sample: 200987

In this sample 24 shots were done on 23 grains. The zircon grains are in between 100 and 175 µm in size, and are tabular, sub-angular to rounded, in shape. In Cl-images, some of the grains display a dark core, interpreted to be magmatic, while the rest of the grains have Cl-bright cores with diffuse irregular features. A thin light CL-right rim can be observed on some grains, but this is not a prominent feature overall. The CL-bright rims and grains are interpreted to be metamorphic.

A regression though all 24 analyses from this sample, yield an upper intercept age of 1656 ± 11 Ma, and a lower intercept age of 265 ± 130 Ma, with a MSWD of 0.56. The analysis U – Pb isotopic data all fall within one group at ca. 1600 Ma. Due to the thin mantles all analysis data target primarily cores, which all have a Th/U> 0.2. Attempts were made to target rims separately but falters due to the small size.

The analyses data yield a weighted mean ^{207}Pb/^{206}Pb age of 1647 ± 9 Ma (Figure 5.44 inset, MSWD = 1.12) interpreted to reflect the crystallization age of the protolith to the host gneiss.
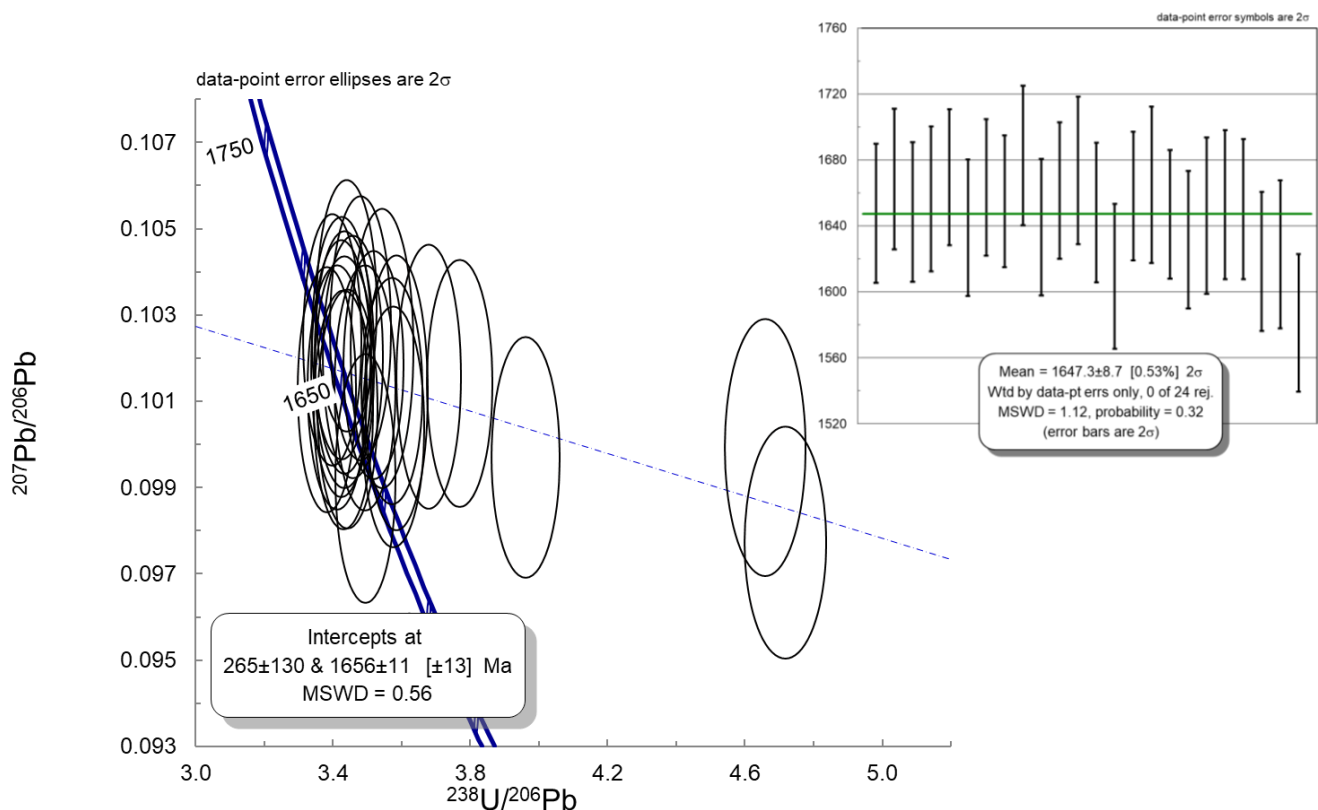
Figure 5.44: *TW plot of U-Pb isotopic data from sample 200987. The black error ellipses correspond with the weighted average ^{207}Pb/^{206}Pb age shown on the upper right-hand side.*

5.2.17 Sample: 200987L

In this sample 24 shots were done on 24 separate zircons. The grains are between 75 and 200 µm in size, mostly around 1500µm. All are tabular, sub-angular to rounded in shape. In CL-images the cores mostly have diffuse characterizations interpreted to be metamorphic. Some oscillatory zoning interpreted to be magmatic can be observed. A thin rim can be observed on some grains but is not a prominent feature overall. There is little contrast in the CL-brightness in this sample.

A regression though all analyses from this sample, yield an upper intercept age of 1650 ± 13 Ma, and a lower intercept age of 459± 110 Ma, with a MSWD of 0.72. The analysis U – Pb isotopic data all fall within one group at ca. 1600 Ma. Due to the thin mantles all analysis data all target primarily cores, which all have a Th/U> 0.4. One analysis is reverse concordant and will be excluded from this point on. The remaining twenty-three analyses yield a weighted mean ^{207}Pb/^{206}Pb age of 1636 ± 13 Ma (Figure 5.46 A, right-hand side, MSWD = 1.9), one analysis is excluded by Isoplot as a statistical outlier. The age is interpreted to reflect the crystallization age of the protolith to the host gneiss.

A second round of data reduction in the program Glitter was performed on this leucosome sample, yielding an indicated young age in one analysis, the remaining analyses data remaining unchanged. Thus, contrary to the initial data reduction it indicates the presence of a high-grade metamorphism and migmatisation event. The younger analysis has a Th/U ratio < 0.01, which corresponds with other rims and metamorphosed grains in this study. It is however extremely discordant, < 50%, and cannot be used to set a precise age estimate. A possible reason for this is that the rims have been too thin to be separately cut by the laser. The distinct difference in uranium content between the cores and rims will result in the core "overpowering" the rims. Figure 5.45 below illustrate a section of the data reduction in Glitter of analysis 200987L_19. The change in reading illustrates how the laser have gotten data from the rim, and then transitioned over to the core.
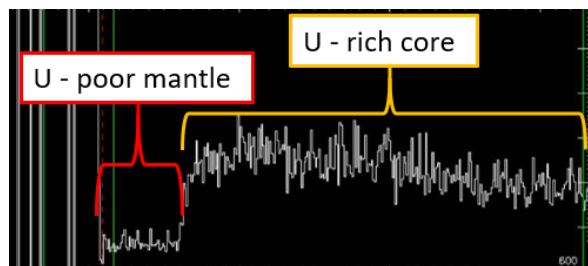
Figure 5.45: Screenshot from Glitter during data reduction of analysis 200987L_19.

In Figure 5.46 A and B the analysis is indicated in orange. It is a statistical outlier in Fig 5.46 A, and as a younger analysis in figure XB. The orange error ellipse marks the specific analysis 200987L_19 and illustrates the change in the resulting TW-plot, a change which depend on selective choices done during the data reduction.
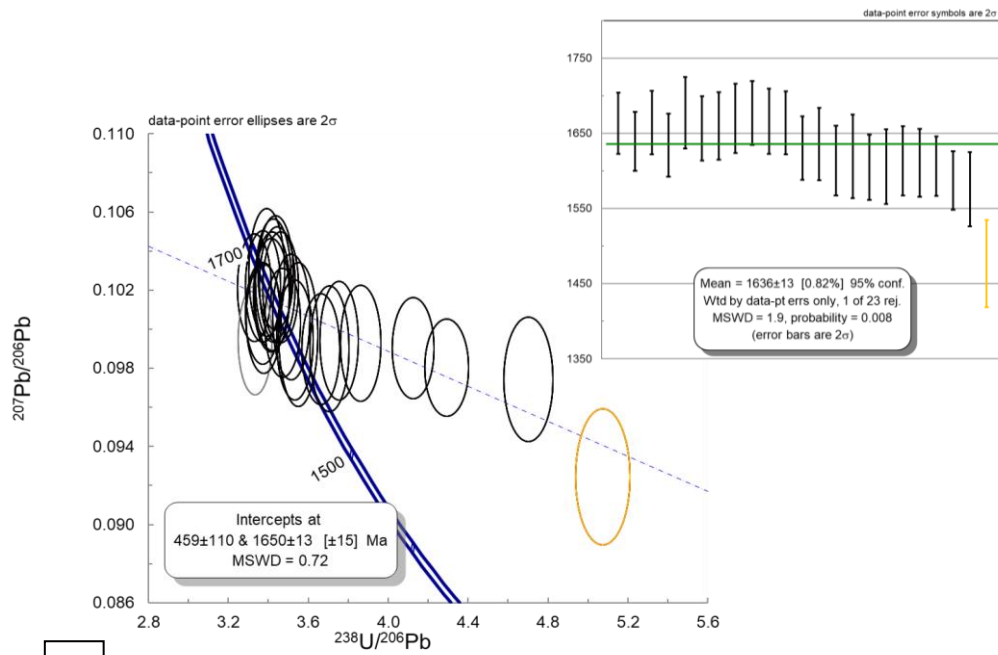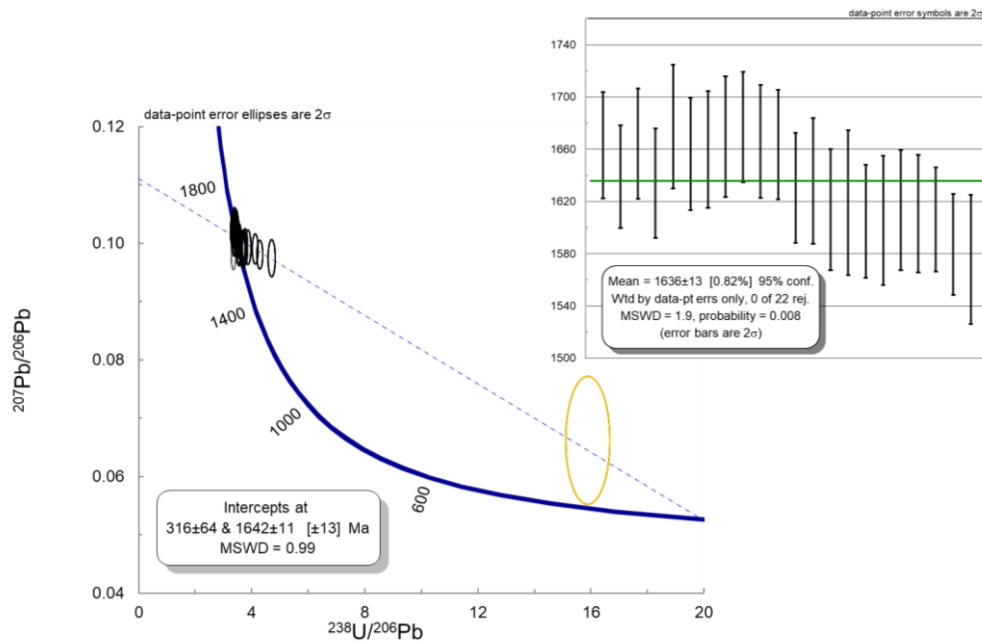
Figure 5.46: A) Initial TW plot of U-Pb isotopic data from sample 200987L. The black and orange error ellipses correspond with the weighted average ^{207}Pb/^{206}Pb age, shown on the upper right-hand side. B) Second TW plot of U-Pb isotopic data from sample 200987L. The black error ellipses correspond with the weighted average ^{207}Pb/^{206}Pb age, shown on the upper right-hand side. The orange error ellipse corresponds to the same colour as in Figure 5.46A and illustrate the altered analysis. Note that the weighted average ^{207}Pb/^{206}Pb age remain unchanged.

5.2.18   Sample: 127891L

In this sample 24 analyses were made on 24 separate zircons. The grains are between 100 and 200 μm in size. The larger grains are a tabular, sub-angular in shape, the smaller are more subangular, diamond shape. In CL-images, most of the grains display a dark core, interpreted to be magmatic, transected by CL-bright rims or mantles with diffuse irregular features. A few grains are CL-bright, with internal features like the rims, but lack cores. The CL-bright rims and grains are interpreted to be metamorphic.

A regression through all twenty-four analyses from this sample, yield an upper intercept age of 1691 ± 24 Ma, and a lower intercept age of 382 ± 9 Ma, with an MSWD of 1.8 (Figure 5.47). Most of the data fall in two groups, one at ca. 1600 Ma and another at c. 400 Ma. The older group consist of thirteen analyses that target cores with Th/U > 0.3, whereas the younger group consists of seven analyses that target the rims or metamorphic grains with Th/U generally <0.01.

The thirteen analyses targeting cores yield a weighted average ^{207}Pb/^{206}Pb age of 1683 ± 11 Ma, with one analysis excluded as statistical outlier by Isoplot (Figure 4.47 upper inset, MSWD = 1.2). The age is interpreted to reflect the crystallization age of the protolith to the host gneiss.

The analyses targeting the rims and metamorphic grains display the same large errors in^{207}Pb/^{206}Pb ratios as seen in many of the samples in this study. The more constrained weighted average ^{206}Pb/^{238}U age of the seven yields an age of 401 ± 5 (Figure 5.47 lower inset, MSWD = 3.6) and interpreted to reflect the age of the high-grade metamorphism and migmatisation.
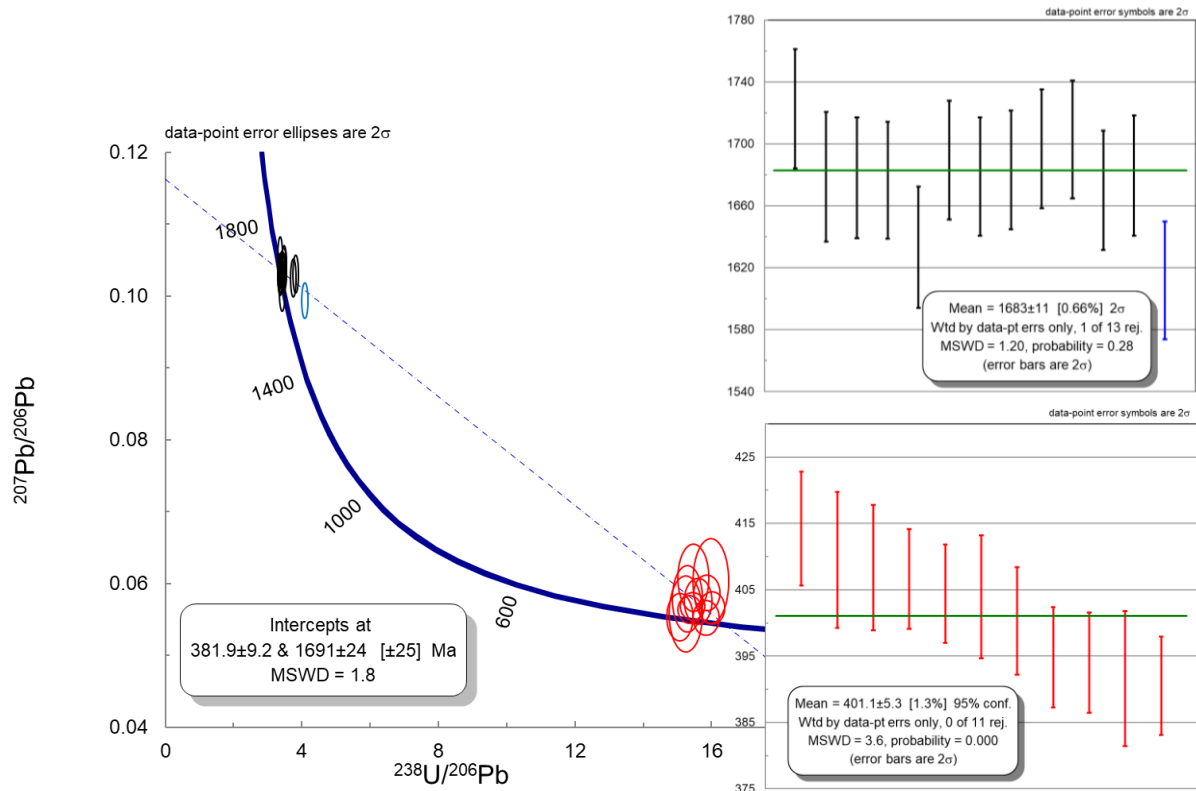
Figure 5.47: *TW plot of U-Pb isotopic data from sample 127891L. The black ellipses correspond with the core analyses weighted average $^{207}Pb/^{206}Pb$ age, and the blue error ellipse correspond with the statistical outlier, both shown on the upper right-hand side. The red error ellipses mark the rims and metamorphic grains corresponding to the weighted average $^{206}Pb/^{238}U$ age shown on the lower right-hand side.*

5.2.19   Sample: STO131390L

In this sample 24 analyses were made on 24 separate zircons. The grains are between 100 and 400 µm in size. The larger grains are elongated and subangular, the smaller are subangular diamond- to tabular in shape. But in general, the grain are very heterogenous in shape in shape. Recurring in all grains are sharp fractured edges. In CL-images some grains have dark cores of CL-bright oscillatory zoning which is interpreted to be magmatic. Irregular CL-bright rims can be observed, as well as CL-dark grains with diffuse and irregular features. Both rims and grains are interpreted to me metamorphic.

A regression though al twenty-four analyses in the sample yields an upper interception age of 1653 ± 17 Ma, and a lower interception age 412 ± 7 Ma, with a MSWD of 2.0 (Figure 5.48). The U – Pb isotopic analyses fall into two groups, one older at ca 1600Ma, and one younger at ca 400Ma. The older group consist of fourteen analyses, targeted primarily on the cores, all with Th/U ratios > 0.05. Two of these analyses are quite discordant but do however fall within the Th/U ratio of the older core analyses and is thus placed in this group. The younger analyses are aimed at the rims and cores interpreted to me metamorphic, all with a Th/U ratio < 0.01.

The two discordant analyses from the older group are excluded, the remaining twelve analyses yield a weighted mean ^{207}Pb/^{206}Pb age of 1637 ± 12 Ma (Figure 5.48 upper inset, MSWD = 1.60) interpreted to reflect the crystallization age of the protolith to the host gneiss.

The weighted average ^{206}Pb/^{238}U age of the ten analyses targeting the rims and metamorphic grains yields an age of 414 ± 6 Ma (Figure 5.48 lower inset, MSWD = 5.2) interpreted to reflect the age of the high-grade metamorphism and migmatisation.
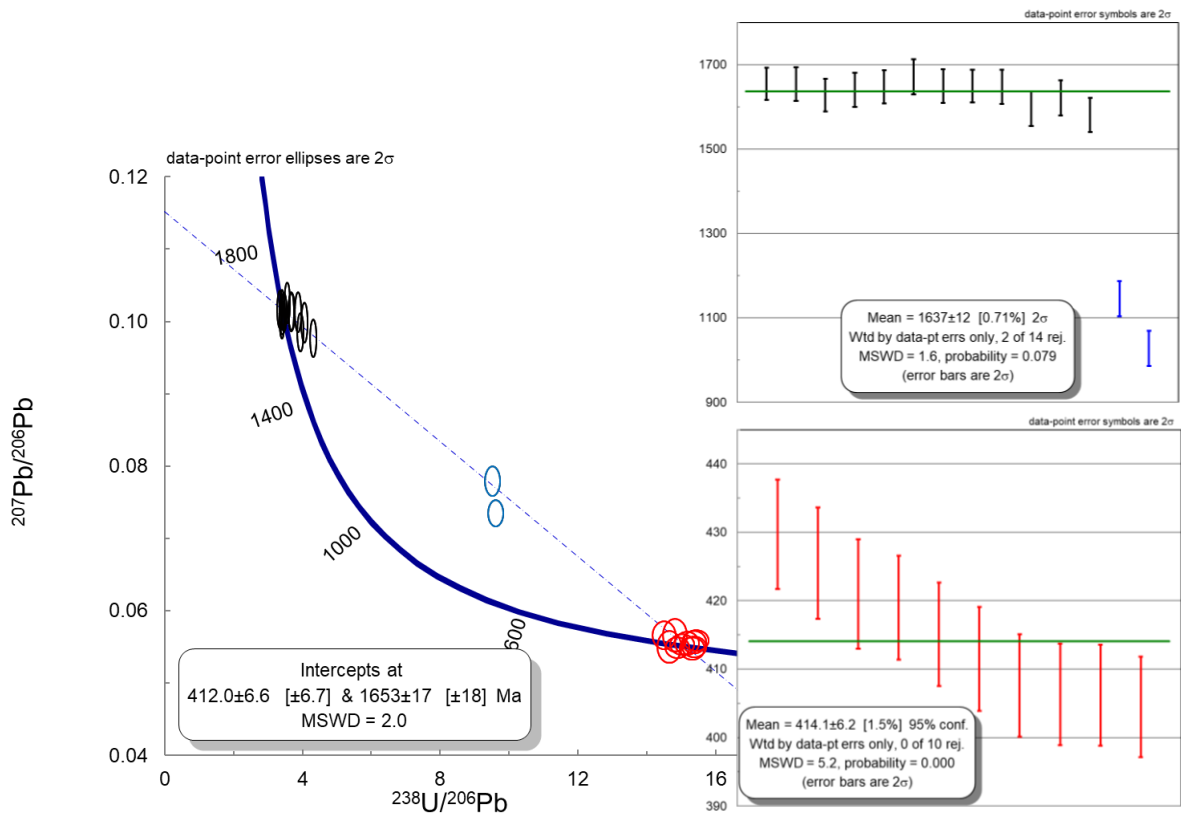
Figure 5.48: TW plot of U-Pb isotopic data from sample STO131390L. The black error ellipses correspond with the core analyses weighted average $^{207}Pb/^{206}Pb$ age. The blue error ellipses correspond with the two discordant analyses, both shown on the upper right-hand side. The red error ellipses mark the rims and metamorphic grains analyses corresponding to the weighted average $^{206}Pb/^{238}U$ age shown on the lower right-hand side.

5.2.20　　　Sample: STO131391L

In this sample 24 analyses were made on 24 separate zircons. The grains are between 150 and 300 μm size, all grains are tabular, sub-angular in shape. In CL-images, the grains display a dark core with visible oscillatory zonation, interpreted to be magmatic. Transected by rims or mantles with diffuse irregular features. The rims are CL-brighter that the cores, but the contrast is not as distinct as in previous samples. The rims and are interpreted to be metamorphic.

A regression through all twenty-four analyses from this sample, yield an upper intercept age of 1641 ± 24 Ma, and a lower intercept age of 407 ± 5 Ma, with an MSWD of 1.7 (Figure 5.49) Most of the data fall in two groups. One younger with an analyses cluster at ca. 400 Ma, targeting rims with Th/U ratios < 0.05. The other group target primarily cores, and the analyses are distributed along the discordia, all with Th/U ratios > 0.05.

The eight analyses targeting the cores have so much scatter that a weighted average $^{207}Pb/^{206}Pb$ age would yield no valid results. The regression line with all samples is thought to be the best representative and the upper intercept age of 1641 ± 24 Ma is interpreted to reflect the crystallization age of the protolith to the host gneiss.

The sixteen analyses targeting the rims all fall within a cluster, though are to spread out to calculate a Concordia age. The weighted average $^{206}Pb/^{238}U$ age of the thirteen analyses, one analysis was excluded as an statistical outlier by Isoplot; resulting in an age of 412 ± 4 Ma (Figure 5.49 inset, MSWD = 4.1) interpreted to reflect the age of the high-grade metamorphism and migmatisation.
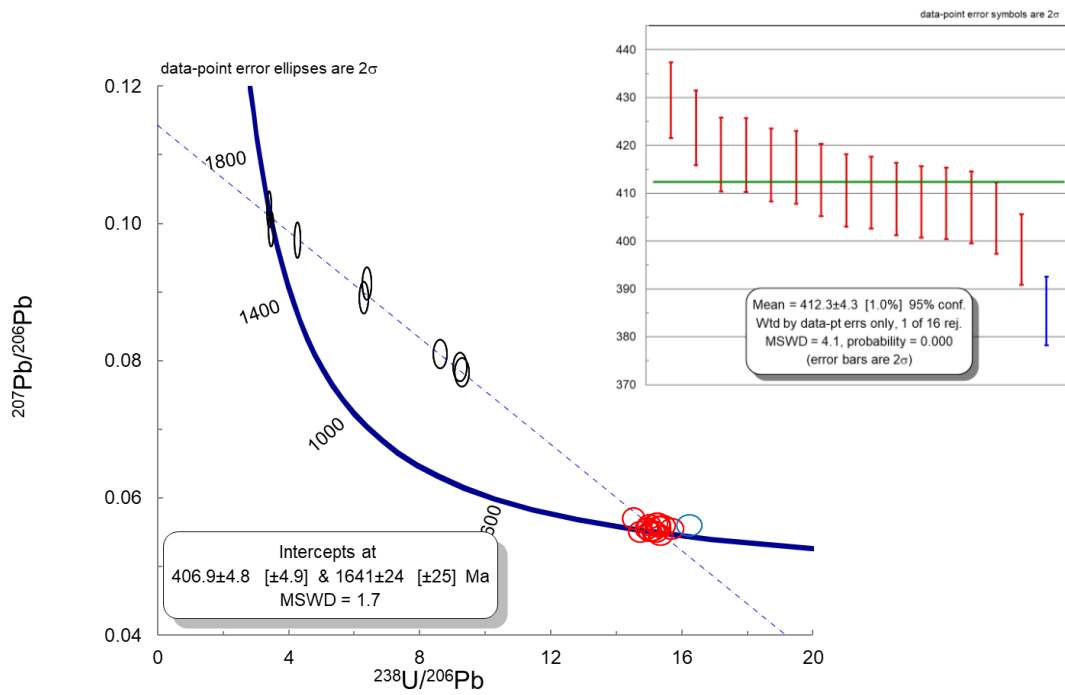
Figure 5.49: *TW plot of U-Pb isotopic data from sample STO131391L. The black error ellipses correspond with the analyses targeting the cores. The red and blue error ellipses mark the rim analyses and statistical outliers respectively, corresponding to the weighted average ²⁰⁶Pb/²³⁸U age shown on the right-hand side.*

5.2.21   Sample: 127894L

In this samples 24 analyses were made on 24 separate zircons. The grains are between 100 and 175 μm in size, and are tabular, sub-angular to rounded in shape. In CL - images, most of the grains display a dark core, with oscillatory zoning, interpreted to be magmatic, transected by rims or mantles with diffuse irregular features. The rims are CL-brighter that the cores, but the contrast is not as distinct as in previous samples. A few grains have with features like the rims but lack cores, these rims and grains are interpreted to be metamorphic.

A regression though all twenty-four analyses, yield an upper intercept age of 1658 ± 33 Ma, and a lower intercept age of 414 ± 9 Ma, with a MSWD of 5.8 (Figure 5.50). The U – Pb isotopic analysis data fall into two groups, one at ca. 1700 Ma, and another at ca. 400 Ma. The older group target primarily cores, all with Th/U ratios > 0.2. The younger analyses target rims and metamorphic grains, where the Th/U is < 0.07.

Two analyses targeting the cores are reverse discordant; excluding these analyses, the remaining six analyses yield a weighted average ^{207}Pb/^{206}Pb age of 1662 ± 16 Ma (Figure 5.50 upper inset, MSWD = 0.57) interpreted to reflect the crystallization age of the protolith to the host gneiss.

One analysis is reverse discordant, and one analysis is deemed as a statistical outlier by Isoplot. Excluding these analyses, the remaining fourteen rim and metamorphic grain analyses yield a weighted average ^{206}Pb/^{238}U age of 413 ± 4 Ma (Figure 5.50 lower inset, MSWD = 0.3.2), interpreted to reflect the age of the high-grade metamorphism and migmatisation.
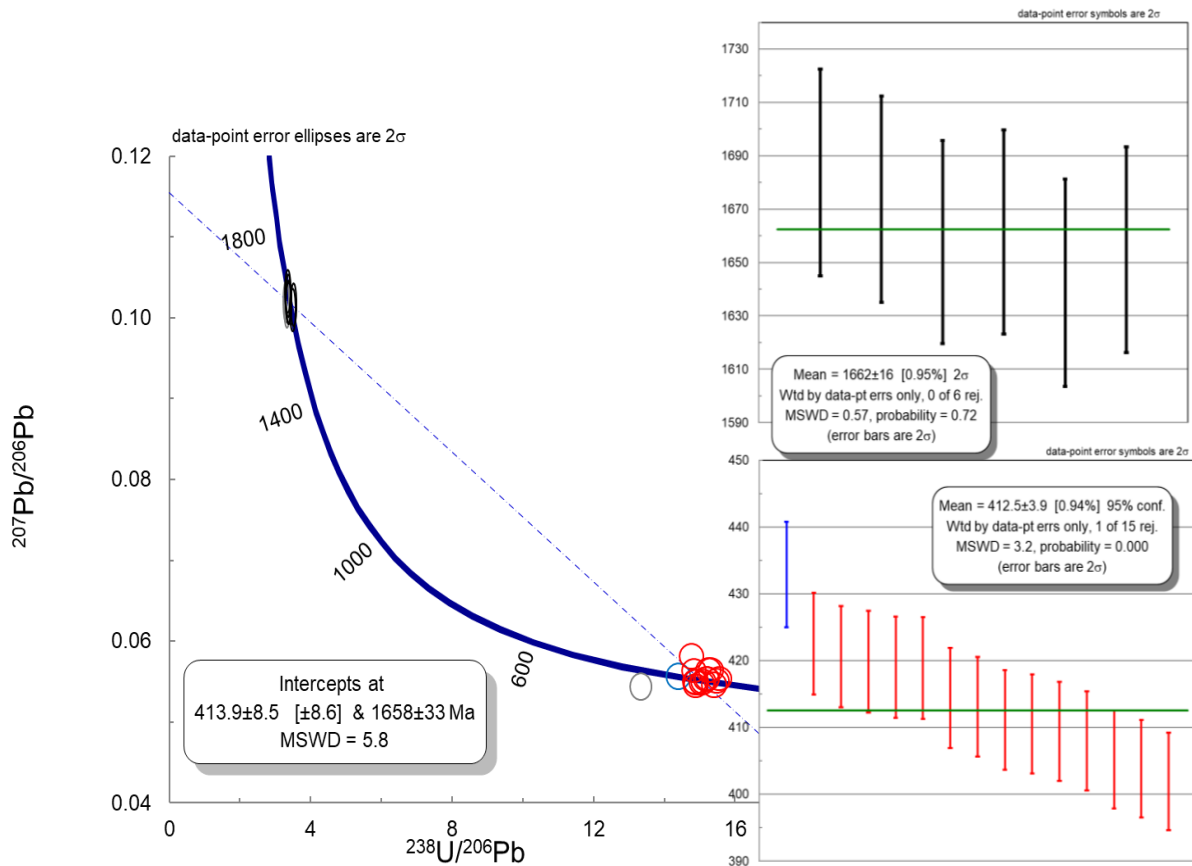
Figure 5.50: *TW plot of U-Pb isotopic data from sample 127894L. The black error ellipses correspond with the core analyses weighted average $^{207}Pb/^{206}Pb$ age, shown on the upper right-hand side. The red error ellipses mark the rims and metamorphic grain analyses, the blue error ellipse mark the statistical outlier, corresponding to the weighted average $^{206}Pb/^{238}U$ age Shown on the lower -hand side. The grey error ellipses mark the reverse discordant analyses for both groups.*

5.2.22   Sample: 127895L

In this sample 24 analyses were made on 24 separate zircons. The grains are between 150 -and 325 μm in size, all are tabular, sub-angular in shape. In CL-images, most of the grains display a dark core, interpreted to be magmatic, transected by CL-bright rims or mantles with diffuse irregular features. A few grains are CL-bright, with internal features like the rims, but lack cores. The CL-bright rims and grains are interpreted to be metamorphic.

A regression through all twenty-four analyses from this sample, yield an upper intercept age of 1690 ± 49 Ma, and a lower intercept age of 384 ± 6 Ma, with an MSWD of 1.6 (Figure 5.51). Most of the data fall in two groups, one at ca. 1700 Ma and another at ca. 400 Ma. The older group consist of three analyses that target cores with Th/U > 0.2, whereas the younger group consists of twenty-one analyses that target the rims and metamorphic grains, with a Th/U range <0.05.

The three analyses targeting the cores are scattered. The analysis scatter would render a weighted average ^{207}Pb/^{206}Pb age biased. The age yielded though a linear regression with all samples, of 1690 ± 49 Ma, is interpreted to best reflect the crystallization age of the protolith to the host gneiss.

The twenty-one analyses targeting the rims and metamorphic grains all fall in a relatively collected cluster at the concordia. The calculated weighted average ^{206}Pb/^{308}U age yield an age of 399 ± 2 Ma, (Figure 5.51 inset, MSWD = 1.4), interpreted to reflect the age of the high-grade metamorphism and migmatisation.
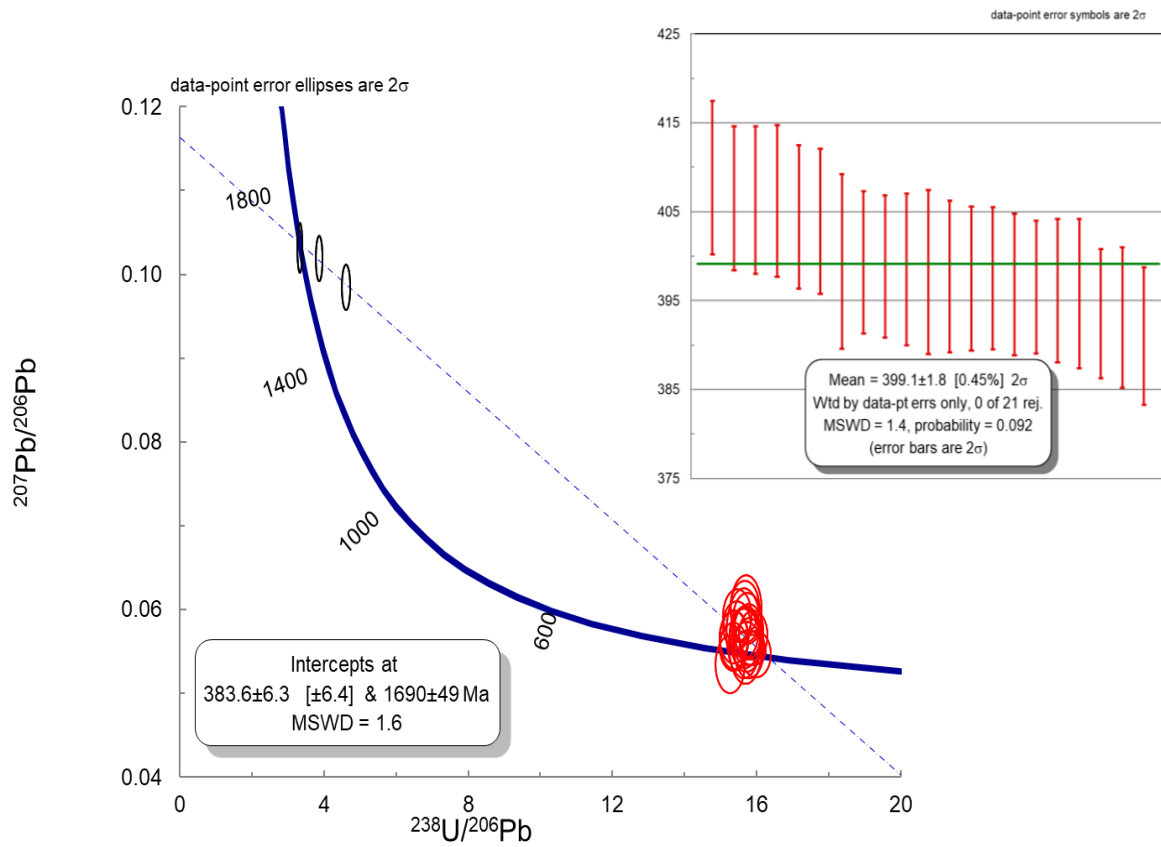
Figure 5.51: *TW plot of U-Pb isotopic data from sample 127895L. The black error ellipses mark the analyses targeting the cores. The red error ellipses mark the rim and metamorphic grain analyses corresponding to the weighted average $^{206}Pb/^{238}U$ age shown in the right-hand side.*

5.2.23 Sample: 197578L

In this sample 24 analyses were made on 23 zircons. The grains are between 100 and 175µm in size, and vary in shape from tabular to round, the edges being sub-angular to rounded. In CL-images, most of the grains display a dark core, interpreted to be magmatic. transected by rims or mantles with diffuse irregular features. The rims can appear both as CL-brighter and darker than the cores. A few grains have internal features like the rims and lack cores. These grains and the rims are interpreted to be metamorphic.

A regression through all twenty-four analyses from this sample, yield an upper intercept age of 1672 ± 15 Ma, and a lower intercept age of 407 ± 4 Ma, with an MSWD of 0.60 (Figure 5.52). The U – Pb isotopic data can be divided into in two groups, one at ca. 1700 Ma and another at ca. 400 Ma. The older group consist of twelve analyses that target zircon cores with Th/U > 0.3, whereas the younger group consists of the remaining twelve analyses that target the rims or grains interpreted to be metamorphic, with a Th/U generally <0.1.

In both groups most of the analyses cluster close to the concordia, but some six analyses fall evenly distributed along the indicated discordia, thus, the most precise estimate would be from the initial linear regression. Yielding an age of 1672 ± 15 Ma interpreted to reflect the crystallisation age of the protolith to the host gneiss. And an age of 407 ± 4 Ma interpreted to reflect the age of the high-grade metamorphism and migmatisation.
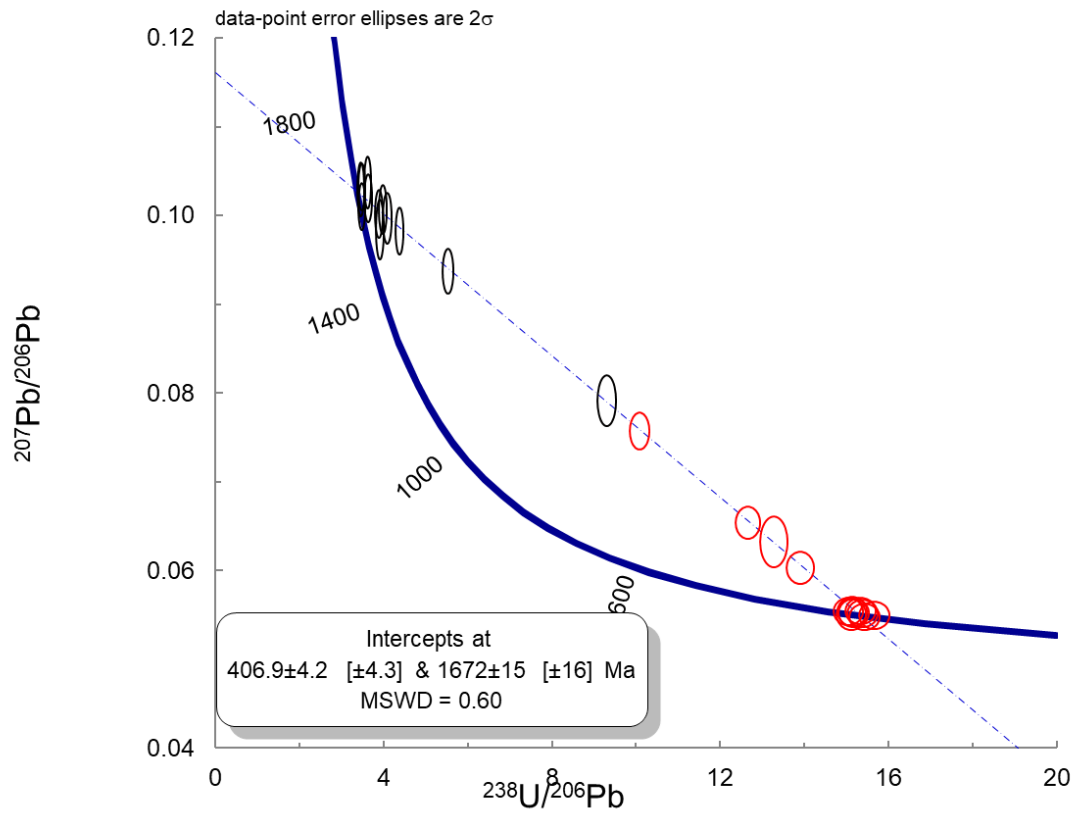
Figure 5.52: *TW plot of U-Pb isotopic data from sample 197578L. The black error ellipses mark the cores, and the red error ellipses mark the rims and metamorphosed grains. The precise distinction is based on the Th/U ratio for each analysis.*

5.2.24   Sample: 200998

In this sample 24 analyses were made on 23 zircons. The grains are between 100 and 200 μm in size, all having a tabular, sub-angular shape. In CL - images, some of the grains display an oscillatory zoning, interpreted to be magmatic. CL-bright rims can be observed on some grains, thought they are too thin to be analysed separately.

A regression though all twenty-four analyses from this sample yield an upper intercept age of 1675 ± 12 Ma, and a lower intercept age of 435 ± 75 Ma, with a MSWD of 0.68. The analysis U – Pb isotopic data all fall within one group at ca. 1700 Ma. With a lack of distinct mantles all analyses target the cores, which all have a Th/U ratio > 0.4.

Two analyses are removed as statistical outliers by Isoplot, excluding these analyses the remaining twenty-two analyses yield a weighted average ^{207}Pb/^{206}Pb age of 1660 ± 9 Ma (Figure 5.53 inset, MSWD = 1.4), interpreted to reflect the crystallization age of the protolith to the host gneiss.
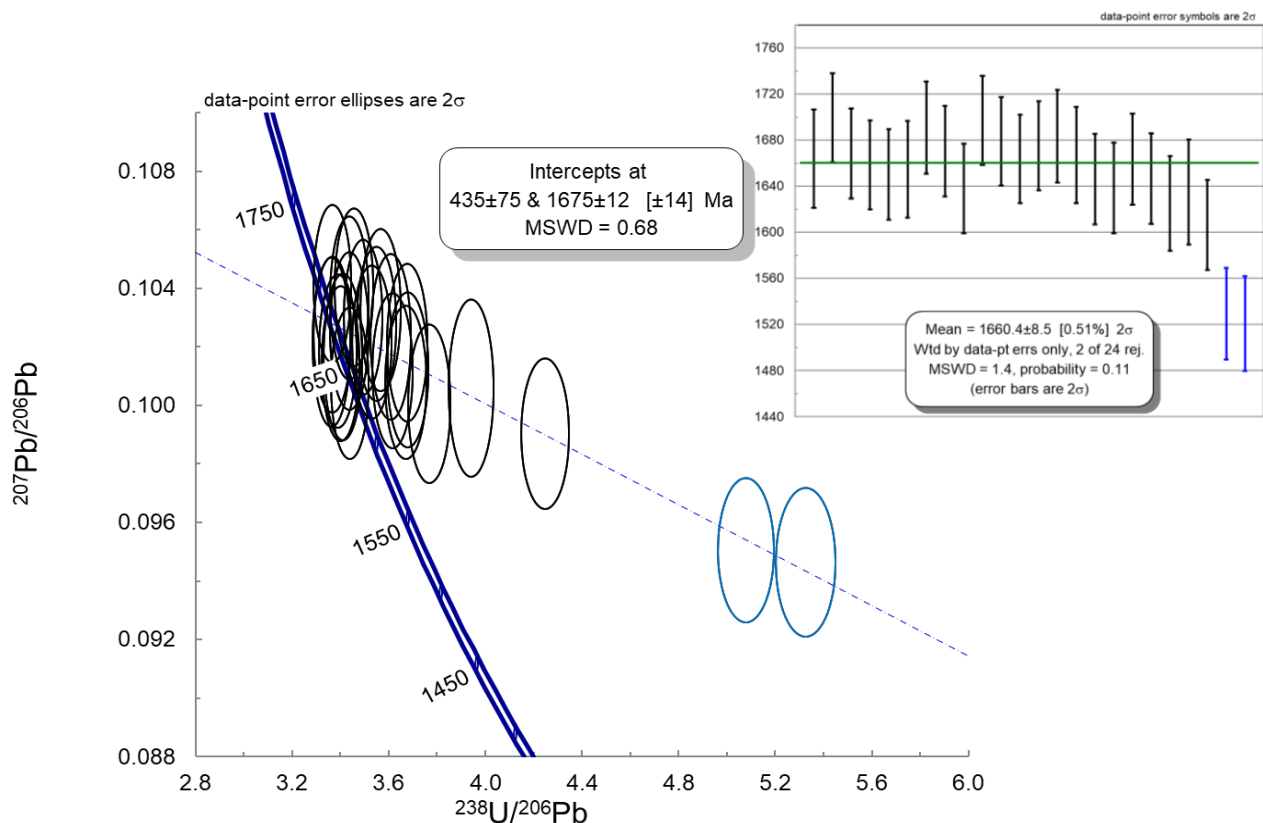
Figure 5.53: *TW plot of U-Pb isotopic data from sample 200998. The black error ellipses mark the core analyses, and the blue error ellipses mark the statistical outliers, both corresponding with the weighted average ^{207}Pb/^{206}Pb age, shown on the right-hand side.*

5.3 Geochemistry

5.3.1 Analytical and sampling procedure

The Major and trace elements were determined by use of the ALS Chemex laboratories in Sweden. The exact procedures and analytical methods used are given in the Methods section *4.4 Geochemistry*. The full dataset, with all 68 samples, from the analytical results are given in Appendix C.

One sample was taken from the allochthonous quarts-muscovite schist, and eight samples are from intrusive mafic bodies in the autochthonous basement. The main bulk of the samples (21 samples) were collected from metamorphosed granitic – granodioritic lithologies in the autochthonous basement with variable degree of migmatisation. Larger sections of leucosome have been cut out from these samples during preparation to get a representative analysis of the of the mesosome, interpreted to represent the igneous photolith. An additional 38 analyses, provided by Trond Slagstad, of the granitic to granodioritic basement is added to supplement the dataset. The additional samples are all collected in different locations within the WGR outside the mapped field area. The samples collected outside the field area will be marked in a light grey colour in the following plots. For simplicity, the collective group will be referred to as Precambrian basement gneisses.

5.3.2 Granitic- granodioritic basement.

The basement gneisses range in SiO_2 from 56.1 to 76.9 wt%. In the TSI- diagram (Irvine and Baragar, 1971), Figure 5.54 A, all but one sample fall well within the sub-alkaline range. They follow a calc-alkaline trend in the AFM-diagram (Irvine and Baragar, 1971) in Figure 5.54 C. Most of the samples fall to the left-hand side ins this diagram, indicating a well evolved composition. In the ASI-diagram, the basement samples fall in a cluster around the border between the metaluminous and peraluminous, Figure 5.54 B.
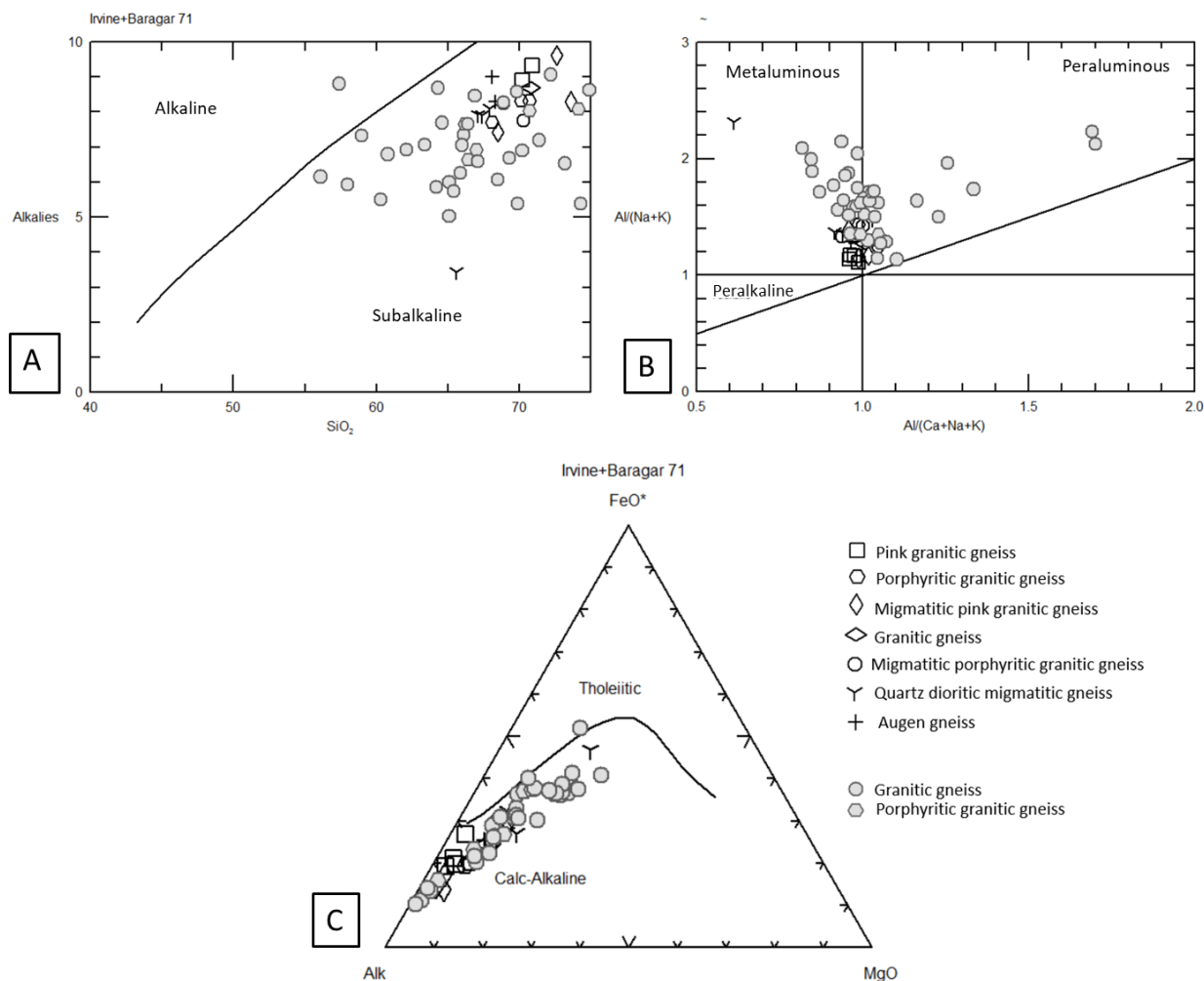
Figure 5.54: *A) The total alkalis versus silica index (TSI) -plot with analysed basement granites samples B) The alumina saturation indices (ASI) -plot with analysed basement granites samples C) trivariate AFM diagram (FeO + Fe_2O_3 vs. K_2O + Na_2O vs. MgO) with analysed basement granites samples. The legend given right-hand side corresponds with the Precambrian basement gneisses collected within the field area and are given in black. The additional samples provided by Trond Slagstad are given in grey.*

In the Harker diagrams, Figure 5.55 and 5.56, the major trends are negative compared to SiO_2 for all except K_2O, which has a positive trend. There is some scatter in all plots, but it is especially prominent in the Na_2O values, where the scatter makes the trend hard to interpret with certainty. Some scatter is also visible in the K_2O and P_2O_5 values, though here the trends are still prominent. Potassium, K, is mobile in granulite facies metamorphism (Allen et al., 1985) which can explain the observed scatter for this element, thought the visible trend indicates limited influence of any secondary processes. The linear trend in the major element Harker diagrams, Figure 5.55 and 5.56, could be interpreted to reflect the pre-metamorphic and magmatic origin, indicating the approximate igneous composition of the gneiss suite. The linear trends for the major elements in the basement gneisses, especially in K_2O, supports this interpretation. Thus, the variation is thought to reflect the magmatic evolution rather than later element mobility.

In the rock/chondrite REE plot, Figure 5.57 A, righthand side, some anomalies occur, but most of the samples fall within the same trend of a slight decrease towards the heavier REE, and a small Eu anomaly. In the primitive mantle-normalized diagram, Figure 5.57 A left-hand side, the trace-element trends are consistent with typical of magmatic arcs (Brown et al., 1984), with negative Nb, Ti and P anomalies in the basement gneiss suite. The samples plot primarily in the volcanic-arc granites in Figure 5.58, with some samples falling in the within plate granites in the Rb - (Y-NB) tectonic discrimination diagram (Pearce et al., 1984). The main cluster coinciding with the calc-alkali and trance element composition.

◇ Granitic gneiss   □ Pink granitic gneiss   ⦿ Granitic gneiss
○ Migmatitic porphyritic granitic gneiss   ○ Porphyritic granitic gneiss   ⦿ Porphyritic granitic gneiss
Y Quartz dioritic migmatitic gneiss   ◊ Migmatitic pink granitic gneiss
+ Augen gneiss
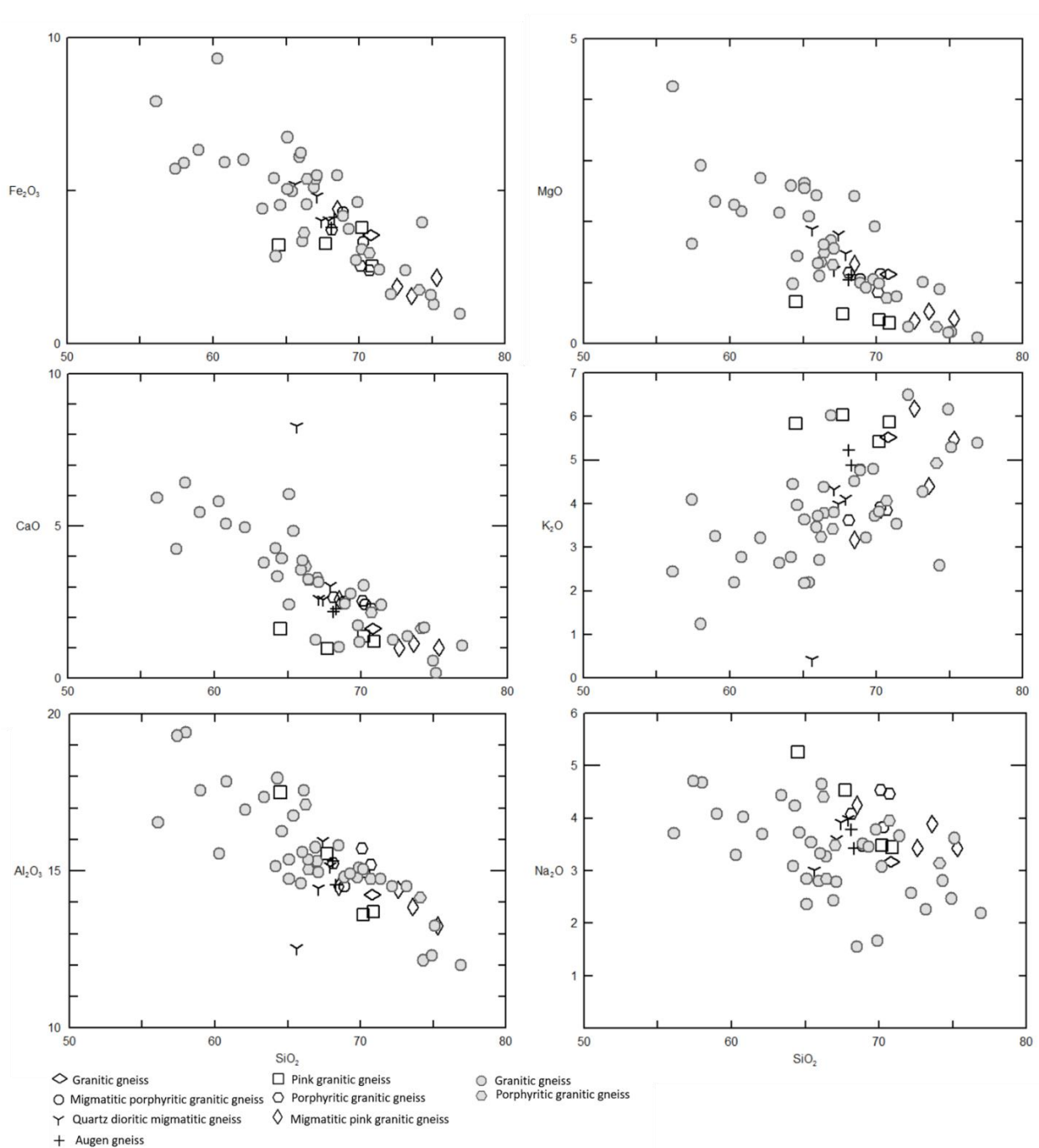
Figure 5.55: *Harker diagram of major elements in the basemen gneiss suite. Plotting a selection of the major oxides against SiO₂.*
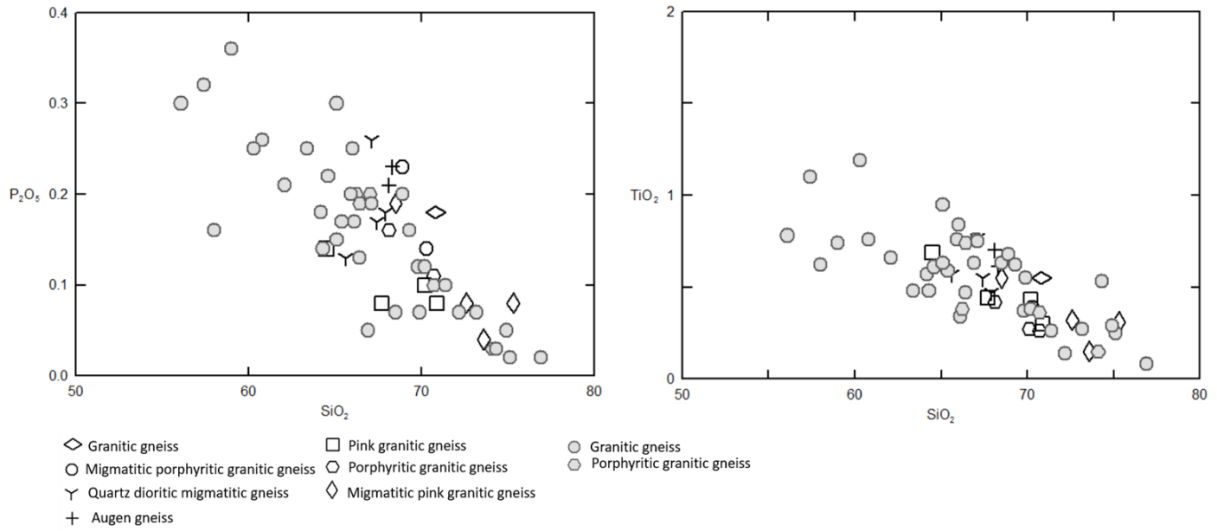
Figure 5.56: Harker diagram of major elements in the basemen gneiss suite continued. Plotting a selection of the major oxides against SiO₂.
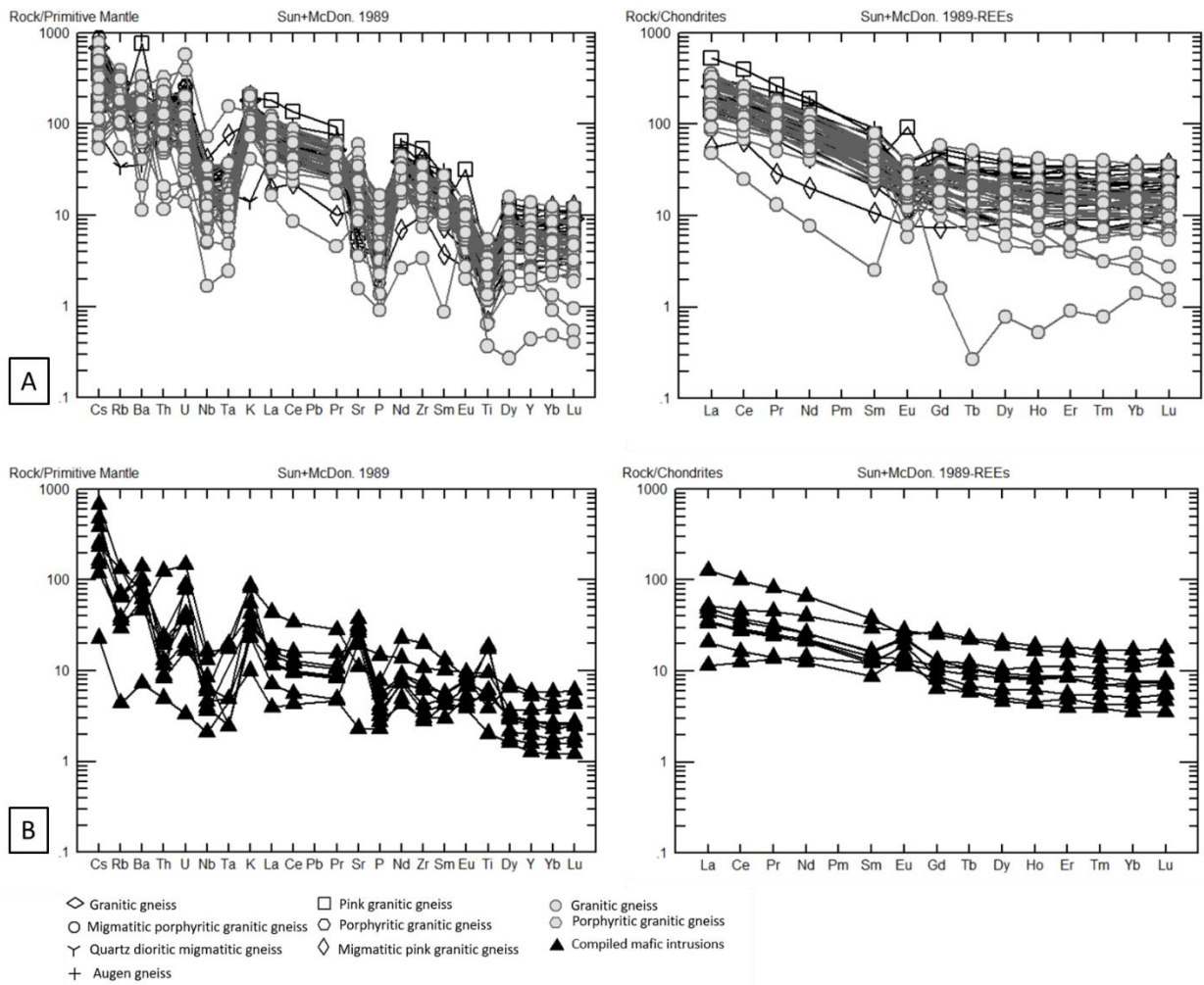
Figure 5.57: Primitive mantle and chondrite-normalized trace element diagrams A) of the basement gneiss samples collected in the WGR, B) of the mafic intrusion samples collected in the field area.

114
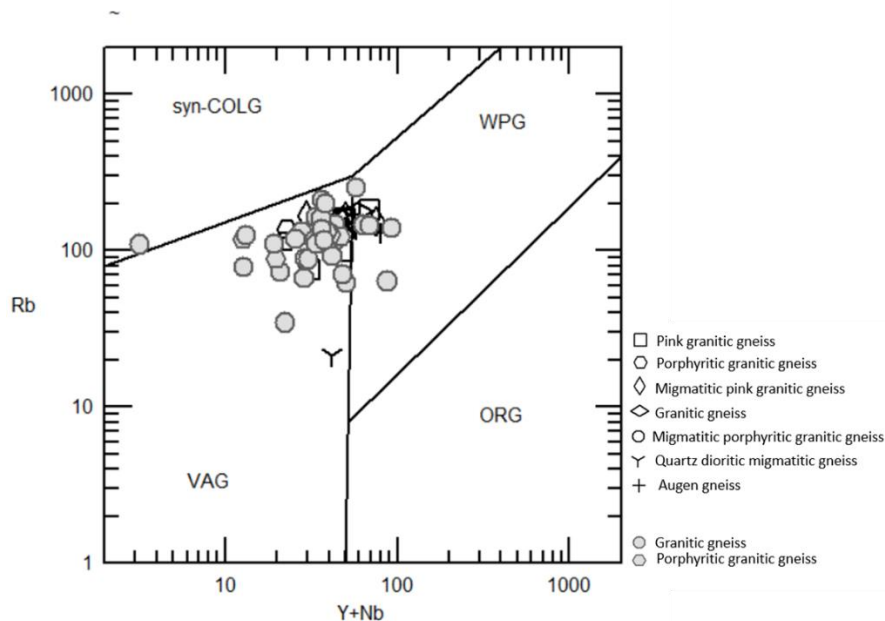
Figure 5.58: *The Rb-(Y-NB) discrimination diagram for granites (Pearce et al., 1984) showing the field of syn-collisional granites (syn-COLG), within-plate granites (WPG), volcanic-arc granites (VAG) and ocean-ridge granites (ORG). The samples place primarily in the VAG domain, with some samples crossing the border to the WPG domain.*

5.3.3 Additional samples

Eight samples were collected from a variety of mafic intrusions centred around Rausand, three of which contain high amounts of ore minerals. The FeO content in some of these samples is as high as 38.2 wt%. Thus, with a few samples collected within a restricted area, and a high proportion of ore minerals the major element chemistry for these samples are not deemed to be representative for the area at large. The same goes for the one allochthonous quarts-muscovite schist, where only one sample was analysed, with an expected high SiO_2 content of 90.5 wt%.

The rock/chondrite REE plot for the mafic samples Figure 5.57 B the same trend as in the basement gneisses can be observed, with a slight decrease towards the heavier REE. The small Eu anomaly, however, is positive in the primitive mantle-normalized diagram. The trace-element patterns show negative Nb and P anomalies but a small positive Ti anomaly. This last anomaly is to be expected as the ores in the area are iron-titanium oxides. The mafic samples cannot easily be compared to a tectonic setting, as with the basement gneisses, however note can be made of the relative spread in chemistry, which for these samples is rather small. This could indicate a correlation between the mafic bodies in the area. So, the smaller, usually more deformed and altered dikes, and the larger less altered bodes may be related.

6 Discussion

The data presented in this study can be used to give new and extended information about the Proterozoic protoliths within the WGR, and further information on the later metamorphic history of these protoliths.

The following discussion will be divided into five sections; I: Use the interpretation of the resulting data to assume the tectonostratigraphic environment of the protoliths. II: Discuss the extent of the Sveconorwegian Orogeny's influence within the WGR. III: Compare the acquired data with priory collected data and published works with protoliths of Proterozoic age within the Baltic Shield, here with special focus on units within south Sweden. IV: Timing of Caledonian migmatisation within the WGR. V: Compare this obtained data with earlier publications and discuss the timing of the Caledonian migmatisation and what impact that might have had on the rheology of the subducting slab.

6.1 The Western Gneiss Region protoliths

The data presented in section *5.2 Geochronological data* give both a simple overview, in Table 5.1, and a more in-depth introduction to each analysis in section *5.2.1 - 5.2.24*. As described, the analysed zircons are dominantly characterised by a core interpreted to reflect the crystallization of the protolith, and a mantle, interpreted to have grown during later metamorphic events. The cores yielded ages ranging from 1691 ± 22 Ma to 1589 ± 19 Ma. Figure 6.1 below show a weighted average plot for all samples, illustrating the age distribution.
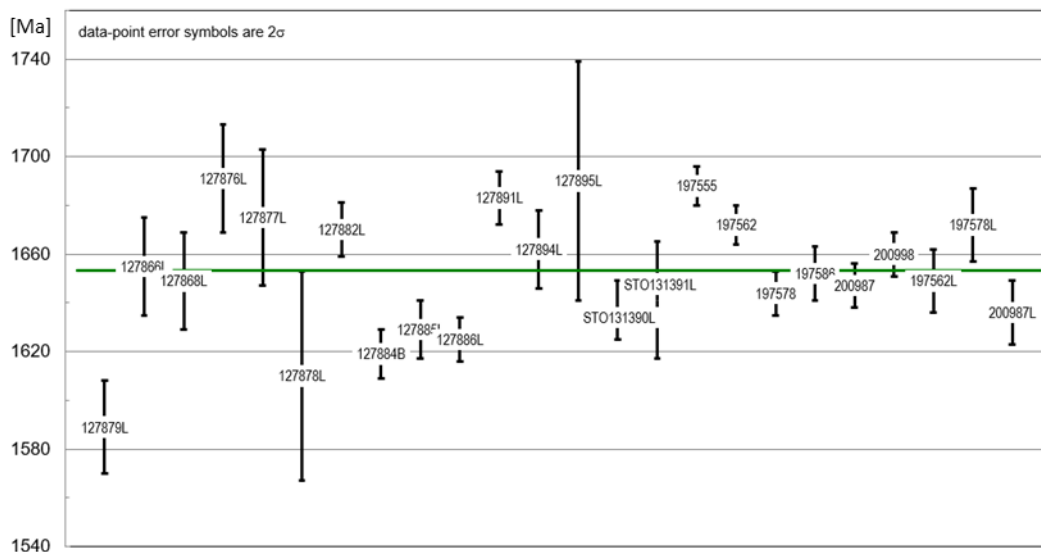
Figure 6.1: *Age distribution of protolith ages, all samples.*

Figure 6.2 below illustrate the different photolith ages acquired in this study at their acquired geographical location.

The protolith ages appear to have a geographical distribution, with the youngest samples located to the south-south-west. Some younger samples are also located in the upper northern section. The older samples are located more within the central parts of the WGR. Note however that this apparent distribution should be interpreted with caution, as younger protolith ages also do occur within the central parts of the region. Skar and Pedersen (2003) interpreted a gradual younging of WRG protoliths towards south and west. Though no distinct pattern of this nature is observed in this data or by Røhr et al., (2013), it is noted that the two youngest samples both are located on the southern section of the region. The conclusion is, however, that the age distribution does not appear to be distinctly gradual in any given direction.

The geochemistry is used to define the tectonic setting of protolith formation. As noted in section *5.3 Geochemistry*, the overall setting is interpreted to reflect an active margin setting, probably a volcanic arc. This interpretation is compatible with that of (Røhr et al., 2013, and others). Hf/Nb isotope analyses of zircons (By Trond Slagstad not yet published) indicate a juvenile, depleted-mantle sources. Thus, by these results one can interpret that the WGR photoliths are formed in an island-arc setting with recorded activity over a ~ 100 Ma period from 1691 ± 22 Ma to 1589 ± 19 Ma.
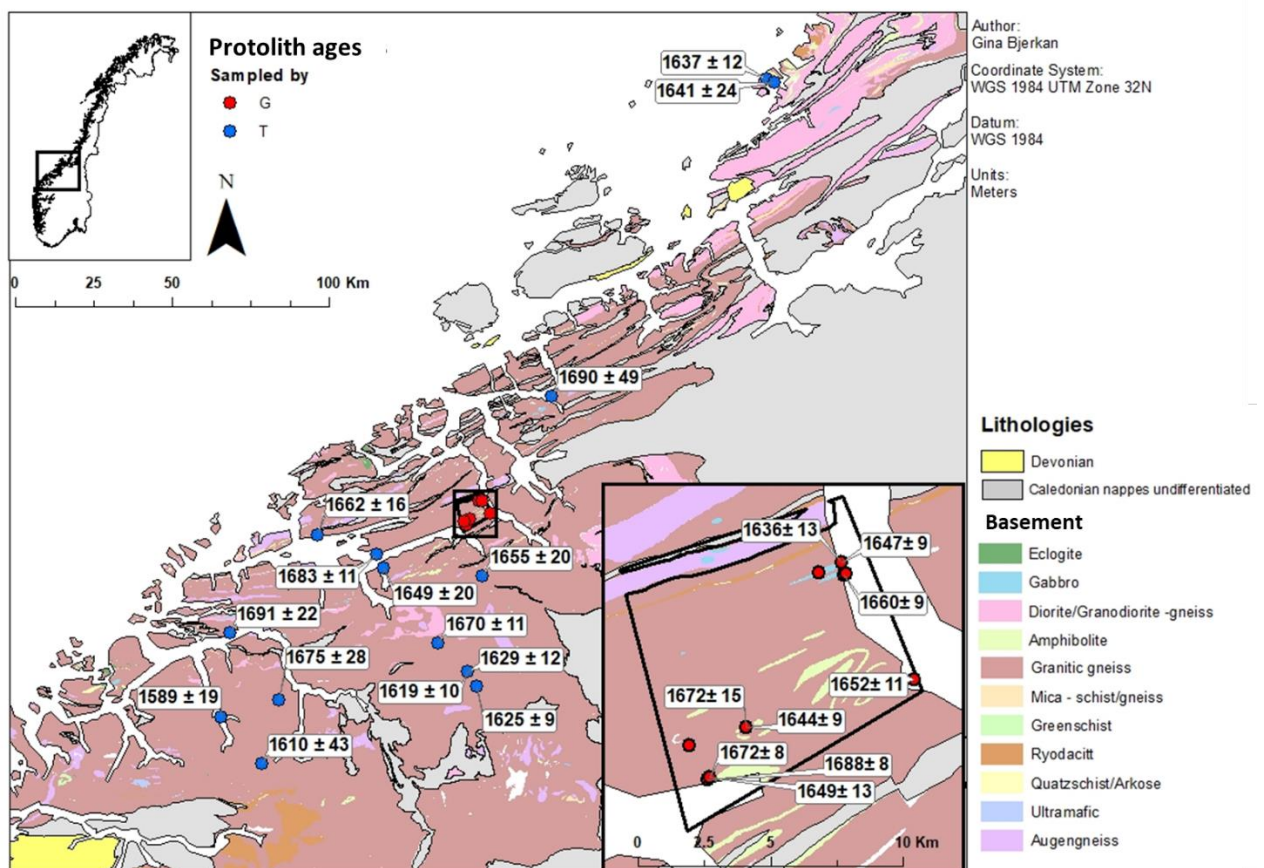
Figure 6.2: *Resulting protolith ages from U-Pb geochronological dating of zircon cores predominantly collected from leucosomes within the WGR basement gneisses, summarised list in Table 5.1, complete dataset given in Appendix D3.*

6.2 Sveconorwegian influence in the Western Gneiss Region

Of the leucosomes analysed in this study, a few analyses yielded ages within the Sveconorwegian range, from 1.15 to 0.9 Ga. All these samples have in common that the ~1000 Ma age came from the mantle on the zircons. Thus, the ages are interpreted to be related to Sveconorwegian metamorphosis. Two samples (127879L and 127886L) only have indications of Sveconorwegian influence, and one (127877L) has a large uncertainty. The only sample yielding a well-defined Sveconorwegian age is sample 127884B, which yielded an age of 962 ±11 Ma. The geographical location of these samples is given in Table 5.1 in section *5.2 Geochronological data* and is illustrated in Figure 6.3 below.
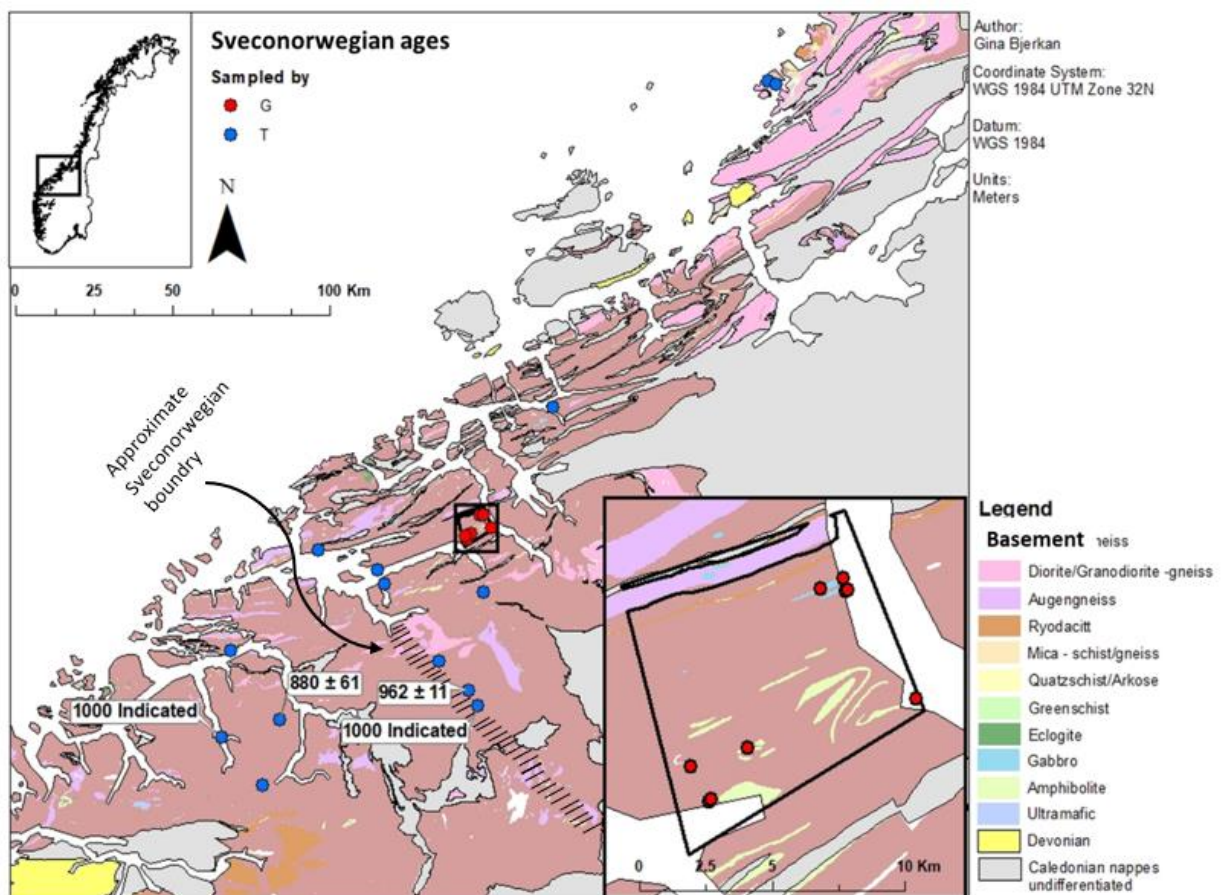
Figure 6.3: *Sveconorwegian ages from U-Pb geochronological dating of zircon mantles collected from leucosomes within the WGR basement gneisses, summarized in Table 5.1, complete dataset given in Appendix D3. The approximate Sveconorwegian boundary from (Tucker et al., 1990).*

The approximate Sveconorwegian boundary first set by Tucker et al. (1990) was based on multiple U-Pb dates of zircon and titanite in magmatic rock in the WGR. The north-west trending boundary does not correspond to any known structures but is an expression of the northernmost extent of known Sveconorwegian metamorphism within the WGR. Following Tucker several authors have published data with Sveconorwegian ages that confirm to the boundary (Skar and Pedersen, 2003, Røhr et al. 2004, Corfu,

1980, and Kylander-Clark et al., 2008). Analyses by Tucker et al., (2004, 1990) and Kylander-Clark et al. (2008) resulted in U-Pb titanite data with no evident resetting between the Proterozoic protolith age and the later Scandian orogeny north of this indicated boundary, which support the assumption of a lack of Sveconorwegian metamorphism in the northern part of the WGR. Note that any pe-Caledonian structures are usually altered, the Caledonian overprint increasing northwards, thus isotopic analyses are the most reliable method to provide further constraints.

Though there is evidence of both Sveconorwegian magnetism and metamorphism in the southern parts of the WGR these are not dominating features. This is consistent with the few Sveconorwegian dates obtained from zircon mantle U-Pb analyses in this project.

6.3 Linkage between the Wester Gneiss Regions and rock suites in southern Sweden

It is natural to explore the possibility of a possible linkage between the WGR and other exposed Proterozoic domains with the same characteristics. Looking at the obtained data together with relevant literature, whereof some is cited in *section 2.1 The evolution of the Fennoscandian Shield*, there are some striking indicators supporting a possible correlation between the WGR and the Proterozoic lithologies in the southern part of Sweden. The Photolith ages yielded by U-Pb dating of the zircon cores in the WGR yield an age range which overlaps with both the late TIB (1.86 to 1.66 Ga) and the early Gothian events (1.66 to 1.52 Ga). With the age ranges overlapping, additional geochemical and isotopic data can be used to further indicate any apparent lithological continuity between the regions in Sweden and the WGR.

Two main interpretations are considered here. Skar and Pedersen (2003) and Austrheim et al. (2003) suggest a correlation between the WGR and the Idefjorden Terrain when including Proterozoic felsic magnetism in the WGR as part of the "Gothian-event", whereas Tucker et al. (1990) and Gorbatschev and Bogdanova, (1993) proposes a correlation between the WGR and the Eastern Segment.

Figure 6.5 below shows all published U-Pb geochronological data between 1.4 and 2.0 Ga from the southern part of the Baltic Shield. What can readily be observed is the apparent age correlation between the Eastern Segment and the WGR. This also correspond with the protolith ages obtained in this thesis. Furthermore Røhr et al., (2013) point out how both the magmatic and metamorphic events in the WGR largely overlap with the ones in the Eastern Segment. This can also be observed when correlating the data given in this thesis and the record illustrated in Figure 6.4. This figure illustrates the magmatic and metamorphic events recorded on the southwestern margins of the Fennoscandian Shield. High magmatic activity in the Paleoproterozoic era and metamorphic activity in Neoproterozoic as recorded in the Eastern Segment correlates with the records from the WGR.

As mentioned in section *6.2 Sveconorwegian influence in the Western Gneiss Region* above several authors have published data on Sveconorwegian magmatism and metamorphism within the WGR. The metamorphism is dated using both zircon and monazite and give ages between 0.99 to 0.95 Ga (Rhør et al., 201, and references therein). In the Idefjorden Terrain the metamorphic activity place between 1.05 to 1.02 Ga, and in the Eastern Segment it places between 0.99 to 9.8 Ga (Möller et al., 2015). In Figure 6.4 below, the approximate location of the Sveconorwegian metamorphic activity in the WGR is placed comparatively to the metamorphic record in the Idefjorden Terrain and in the Eastern Segment.
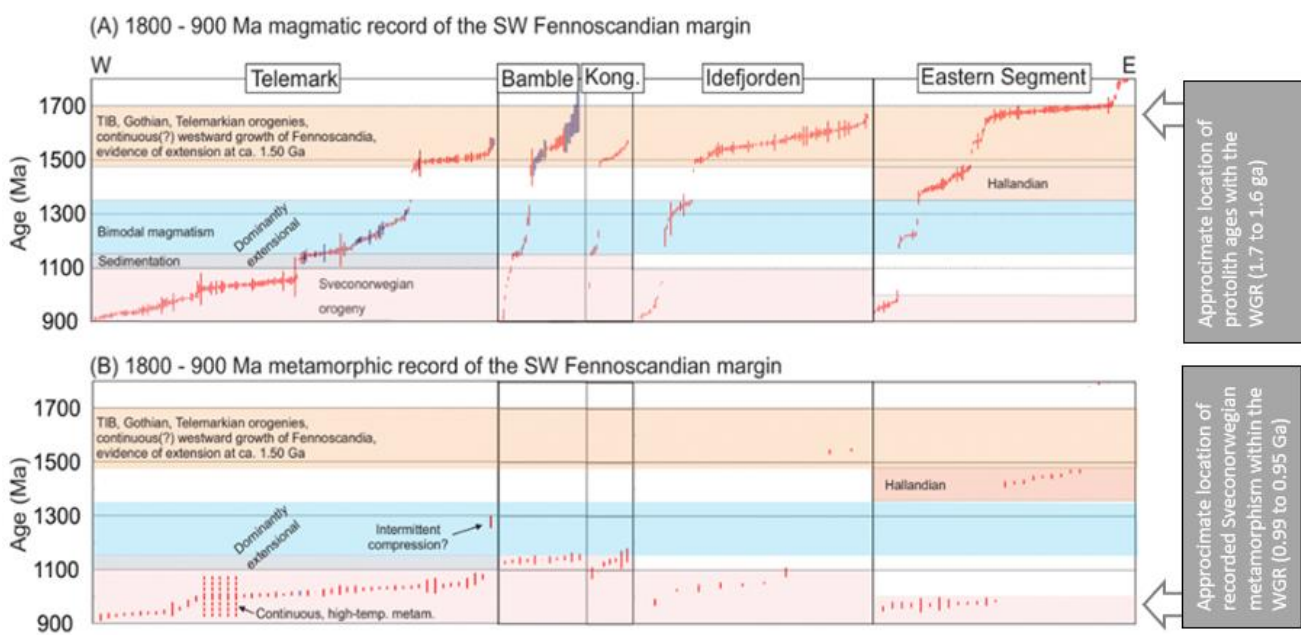
Figure 6.4: *Records of magmatic and metamorphic activity of the SW Fennoscandia margin (Slagstad et al., unpublished), with additions indicating the placement of similar records from within the WGR.*

The geochemistry presented in section *5.3 Geochemistry*, indicates that protolith composition in the WGR are consistent with formation in a magmatic arc. Which is similar both to the Idefjorden lithotectonic unit and the Eastern Segment. Hf-isotope distribution in the WGR (Provided by Trond Slagstad) give εHf values between 0 to 10. This range from very juvenile (εHf ~10) to significantly less juvenile (εHf ~0) are trends that overlap with the variation observed in the Eastern Segment, with reported εHf values ranging from 0 to 5 (Pettersson et al. 2015). The trends in Idefjorden Terrain are also juvenile, but much less variable then the two mentioned above.
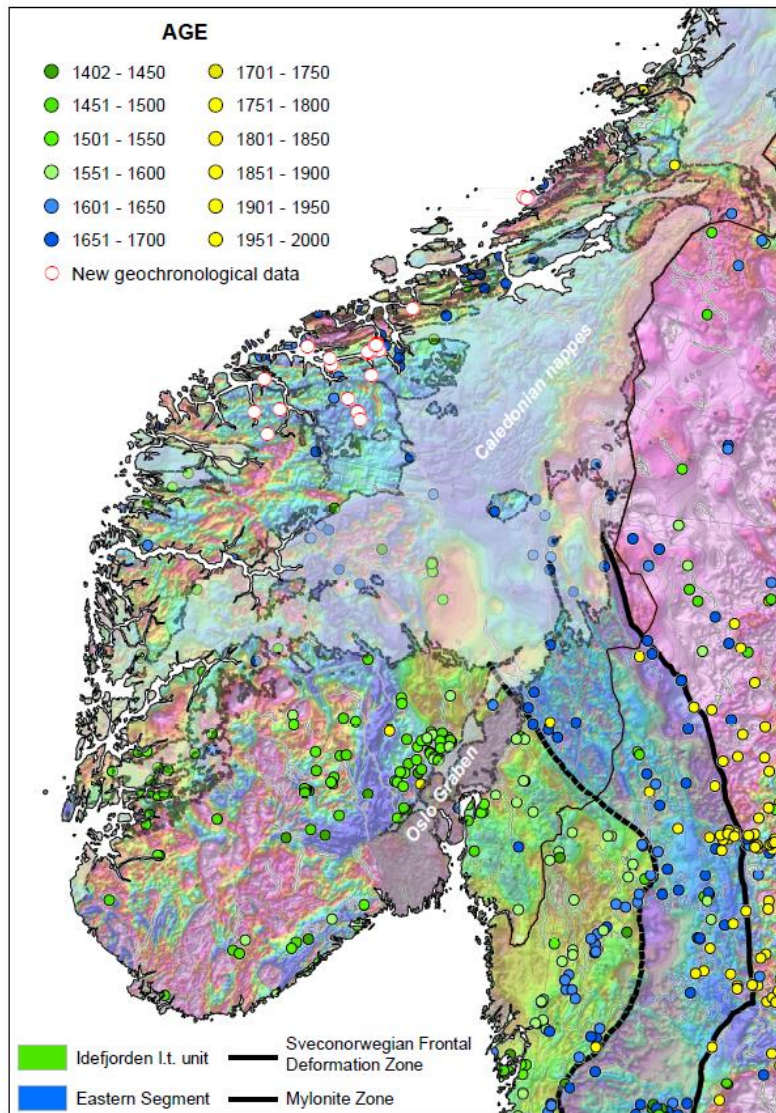
Figure 6.5: *Magnetic anomaly map, Norway and adjacent areas; Scale 1:3 mill. Geological Survey of Norway. (Assembled by Trond Slagstad using; Bingen and Solli, (2009), and the Swedish bedrock geochronology database (SGU))*

Dividing the two areas is what is known as the Mylonite Zone, (MZ). An ongoing debate is whether the MZ is a suture zone resulted from later accretion of a magmatic arc onto the Fennoscandian Shield (Petersson et al., 2015b), or if there was continuous growth along the Fennoscandian shield and the MZ is the results of a later deformational zone related to Sveconorwegian tectonics (Åhäll and Connelly, 2008). Figure 6.6 below shows a simplified illustration of the two proposed theories.
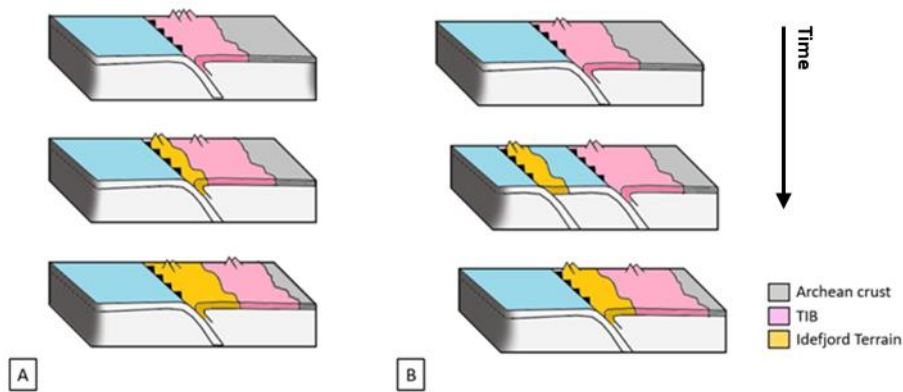
Figure 6.6: *Simplified illustration comparing two proposed theories involving the Idefjorden Terrain regarding the initial growth of the Fennoscandian shield. A) continuous growth along a long-lived subduction zone, thus indicating a later event causing the MZ. B) Later accretion of an arc system into Fennoscandia, making the MZ an accretion suture.*

A possible way of testing witch theory is the best fit is by testing Hf-isotopes and interpreting the juvenility distribution. Weather it is abrupt, indicating an accrediting arc, as illustrated in Figure 6.6 B, or gradual indicating continuous growth as illustrated in Figure 6.6 A. Reginal geophysics, both gravimetric and magmatic, could also be used as aids to extrapolate the interpretation boundaries below the Caledonian Nappes in Norway. Such data could be further used to I: supplement in the discussion of the MZ. II: Further relate the Norwegian basement windows to exposed Proterozoic crust westwards on the Baltic Shield, and how the WGR might place in relation to this.

There are obviously many different interpretations to these questions, and to make a conclusionary remark on this subject is outside the scope of this thesis. However, the correlation of the WGR with the Proterozoic units in Sweden can be useful to better constrain the Evolution of the Fennoscandian margin. To better place the WGR in a Fennoscandia setting, Zircon U-Pb and Hf- isotopes analysed in the same manner as by Petersson et al. (2015) would be useful. And as mentioned above could Hf- isotope analysis of this manner also be used to better correlate the WGR relationship with other Proterozoic units, such as the exposed windows further north in Norway.

6.4 Caledonian migmatisation during subduction and high- to ultrahigh-pressure metamorphism of the WGR

As described above, the analysed zircons are dominantly characterised by a core interpreted to reflect the crystallization of the protolith, and a mantle, interpreted to have grown during later metamorphic events. The mantles yield both Sveconorwegian ages of ~ 1000 Ma as discussed in section *6.2 Sveconorwegian ages*, and Caledonian ages of ~ 400 Ma, see presented data in section *5.2 Geochronological data* thus, indicating the presence of two metamorphic events which resulted in migmatisation of the basement gneisses.

Of the leucosomes analysed in this study, most of the analysed zircon mantles yielded Caledonian ages. Twenty of the total twenty-four samples had indications of mantles with Caledonian ages. Of these, two samples, sample 127884B and sample 200987L, only had an indication of a Caledonian age at the lower intercept, see section *5.2.3 Sample 127884B* and section *5.2.17 Sample 200987L.* Figure 6.7 below presents the age distribution of the remaining 18 samples. The ages range from 423 ± 10 Ma to 392 ± 3 Ma, and has, with a few exceptions, precise uncertainties of ~ 5 Ma. The geographical location of these samples is given in Table 5.1 in section *5.2 Geochronological data*. Precise ages and their geographic locations are illustrated in Figure 6.8 on the following page.
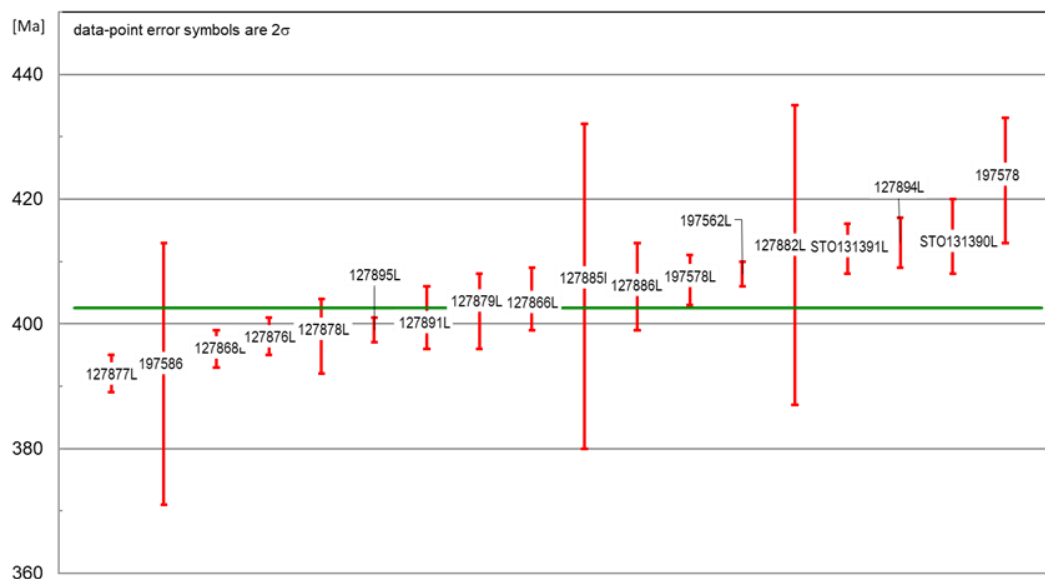
Figure 6.7: *Age distribution of the 18 Caledonian samples. Ages ranging from 392 ± 3 Ma to 423 ± 10 Ma.*

Figure 6.8 illustrates the same samples as in Figure 6.9, but with a colour coding used to better illustrate the age distribution in correlation with the geographical position of the samples. The isotherms and titanite line, distinguishing concordant and discordant ages are taken from Kylander-Clark et al. (2008). The eclogite isobars and the UHP domains are taken from Hacker et al. (2010).
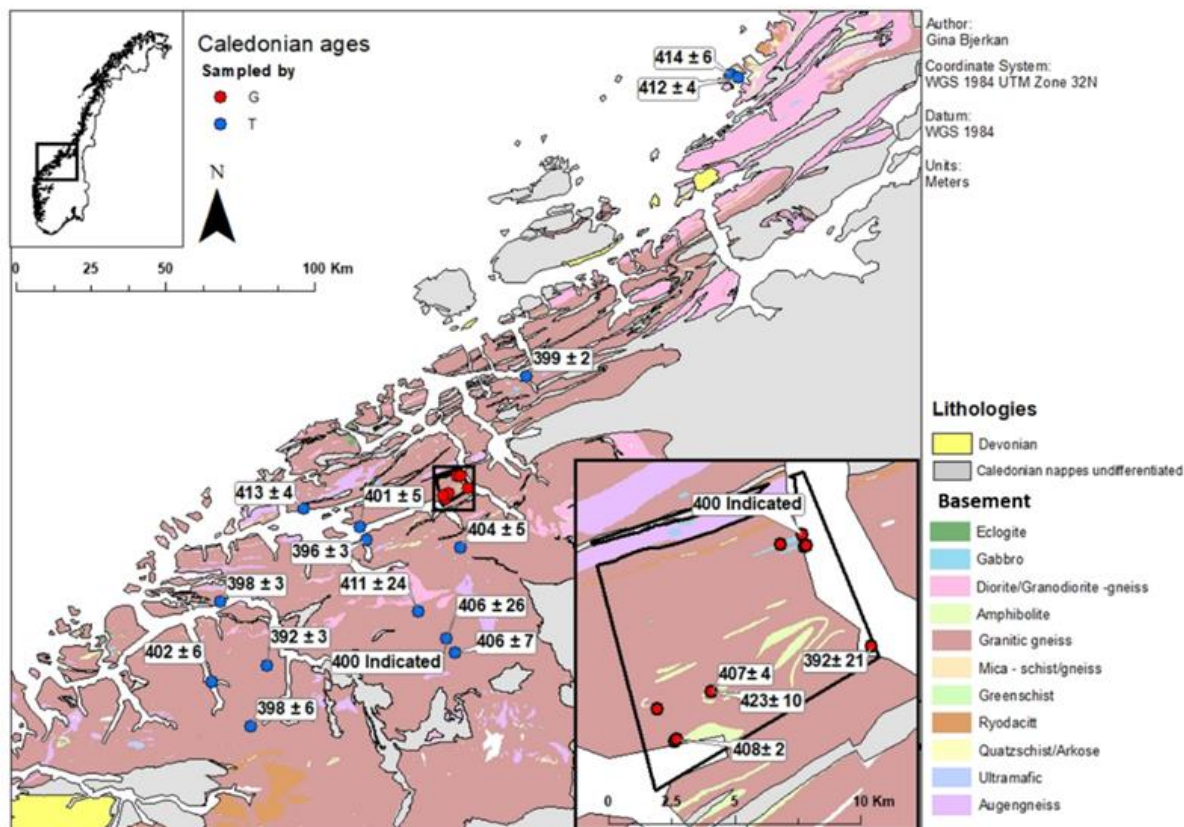
Figure 6.8: *Resulting Caledonian ages from U-Pb geochronological dating of zircon mantles predominantly collected from leucosomes within the WGR basement gneisses, summarised list in Table 5.1 – 5.3, complete dataset given in Appendix D*.

There is no clear observable trend in the geographical distribution of the Caledonian ages, see Figure 6.8. The only indication could be a collection of younger ages of < 400 Ma towards the southern part of the region. However, samples yielding ages within the same range can also be observed in the middle section of the region.

The lack of a systematic east-west geographical distribution sets the leucosome U-Pb ages apart form $^{40}Ar/^{39}Ar$ ages from white mica, Th/Pb monazite, U/Pb of rutile and titanite (Hacker, 2007, Walsh et al., 2007, Kylander-Clark et al., 2008, Schärer and Labrousse, 2003). These mineral ages exhibit a geographical distribution with ages younging westwards, which has been interpreted to reflect the cooling ages, related to the exhumation of the subducted slab below Laurentia, see section *2.2.1 The Western Gneiss Region*. If the leucosome zircons where to reflect the same event one would expect indication of the same geographical trend with slightly older ages, as the temperature for closure of diffusion of U-Pb in zircon is ~> 750°C (Cherniak and Watson, 2003) and the following minerals have successively lower closure temperatures, were monazite Th-Pb and titanite is ~< 750 °C (Walsh et al., 2013) and Ar-Ar in white mica is ~< 400°C (Harrison et al., 2009). However, as stated above, this is not the case. Notably the majority of the leucosome ages do fall in line with the ages found in the eclogites, see Figure 6.10.

124
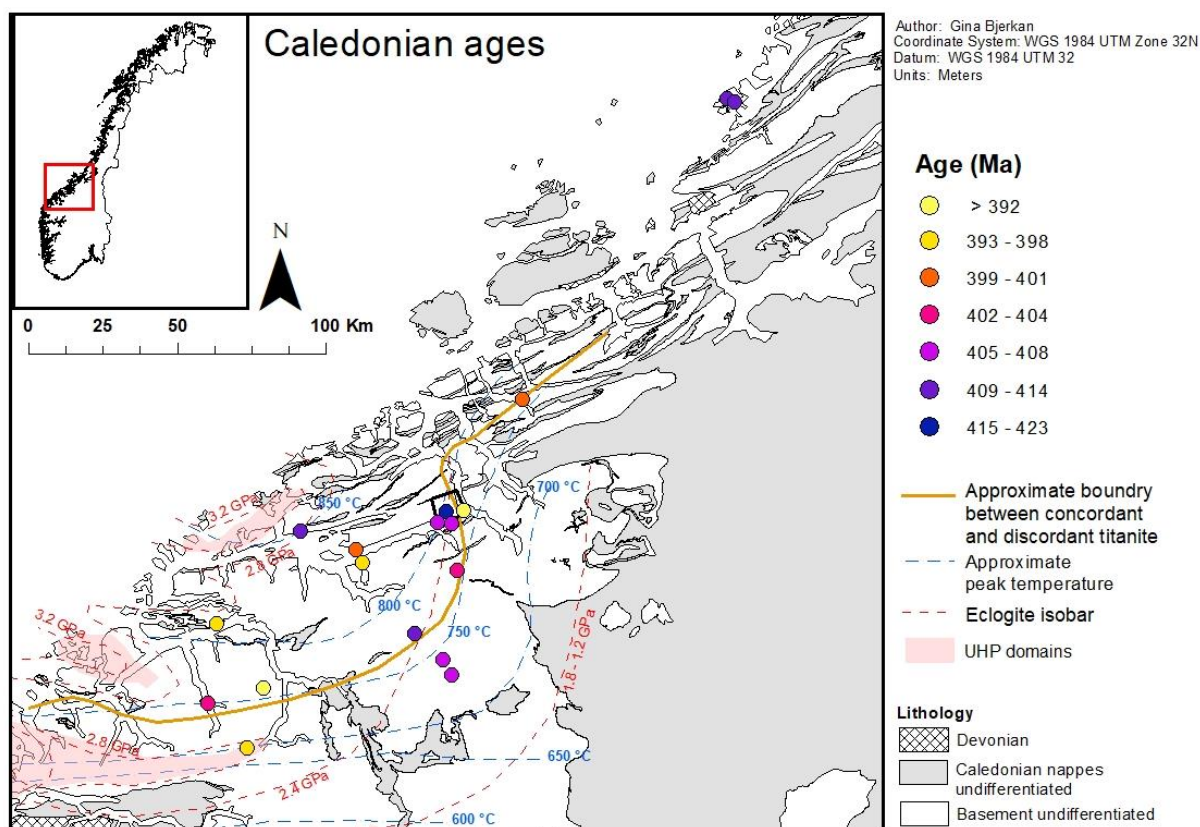
Figure 6.9: *Resulting Caledonian ages from U-Pb geochronological dating of zircon mantles predominantly collected from leucosomes within the WGR basement gneisses, summarised list in Table 5.1, complete dataset given in Appendix D3. Approximate peak temperature and titanite boundary from Kylander-Clark et al., (2008) fig 1 & 5. Eclogite isobars and the UHP domains from Hacker et al. (2010) and references therein*.

The lack of any apparent geographical younging westwards makes the leucosome ages incomparable with the westward progression of exhumation in the WGR inferred in other datasets (Hacker et al., 2015, Kylander-Clark et al., 2008, Walsh et al., 2007). Combined with the overlap of UHP and HP- ages of ~420 to 400 Ma this could indicate that the migmatisation of the basement gneisses is not related to the exhumation of the WGR, but rather to the prograde subduction and HP metamorphism.

In Figure 6.10 on the following page zircon ages from collected from eclogites by various authors (Krogh et al., 2011, Kylander-Clark et al., 2013, Krogh et al., 1974, Carswell et al., 2003, Root et al., 2004, Gebauer et al., 1985, Young et al., 2007, Walsh et al., 2007) presented in a compiled summary table by (DesOrmeau et al., 2015) can be compared to the U-Pb ages yielded in the leucosome zircons. Along with ^{40}Ar/^{39}Ar Muscovite ages from (Walsh et al., 2007) and (Root et al., 2005), titanite and rutile ages from (Kylander-Clark et al., 2008) and compiled titanite ages from (Spencer et al., 2013).
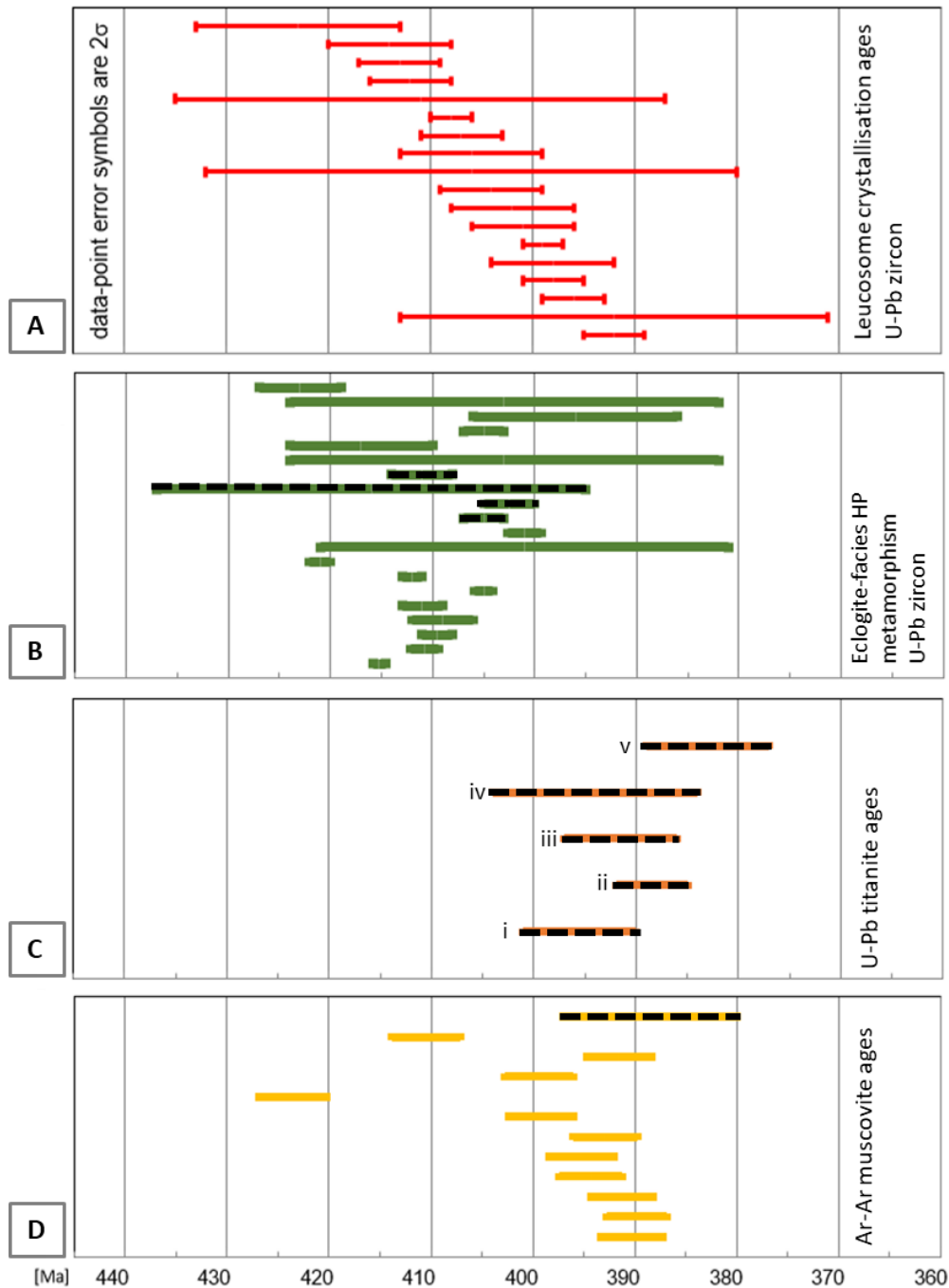
Figure 6.10: *A) Illustrates the U-Pb ages for leucosome crystallisation obtained in this project, from Figure 6.7. B) Illustrates eclogite zircon ages from a number of authors. The data is compiled by (DesOrmeau et al., 2015) in a Geochronological summary of various Scandian (U)HP eclogites from the Western Gneiss Region, see (DesOrmeau et al., 2015, table 1) for complete summary. C) Illustrate titanite datesfrom; i) concordant titanite, ii) concordant rutile from (Kylander-Clark et al., 2008). iii) Retrogressed eclogites, iv) concordant deformed and discordant nondeformed-leucosomes, v) mylonites and mylonitic gneiss from (Spencer et al., 2013). D) Illustrates $^{40}Ar/^{39}Ar$ Muscovite ages from (Walsh et al., 2007, and Root et al., 2005). For all diagrams reported uncertainties are given at 2σ or 95% confidence level unless otherwise stated, lines with black stipples are a collection of ages given in a "from – to" format.*

Field observations of the leucosomes can be used in correlation with the obtained zircon ages. Figure 6.11 below illustrate two different types of leucosomes, one parallel to the foliation, and one cross cutting. Both types have been analysed, see section *5.2 geochronological data: 5.2.3 Sample 127884B & 5.2.4 Sample 127885L,* yielding Caledonian and Sveconorwegian ages, respectively. The relative placement of the two leucosome types clearly indicates two separate events of migmatisation, which in turn is confirmed by the zircon ages. The younger Caledonian age leucosome takes the form of a tension gash with an indicated top to the east movement. This structural constraint of the leucosome fall in line with the interpretation of migmatisation during prograde subduction. Within the study area leucosomes crosscutting the foliation and with an indication of a directional sense of shear was only observed at one location. See section *5.1.3 Structural feature figure 5.24*. Here also, a top to the east sense of movement is observed.

These examples correspond to sample 127884B and sample 200987L respectively, and as mentioned in the beginning of this section, both samples only have indicated Caledonian ages. However, the structural relationship of the migmatites with their host rock do indicate a top to the east movement, which would correspond with the progressional subduction.
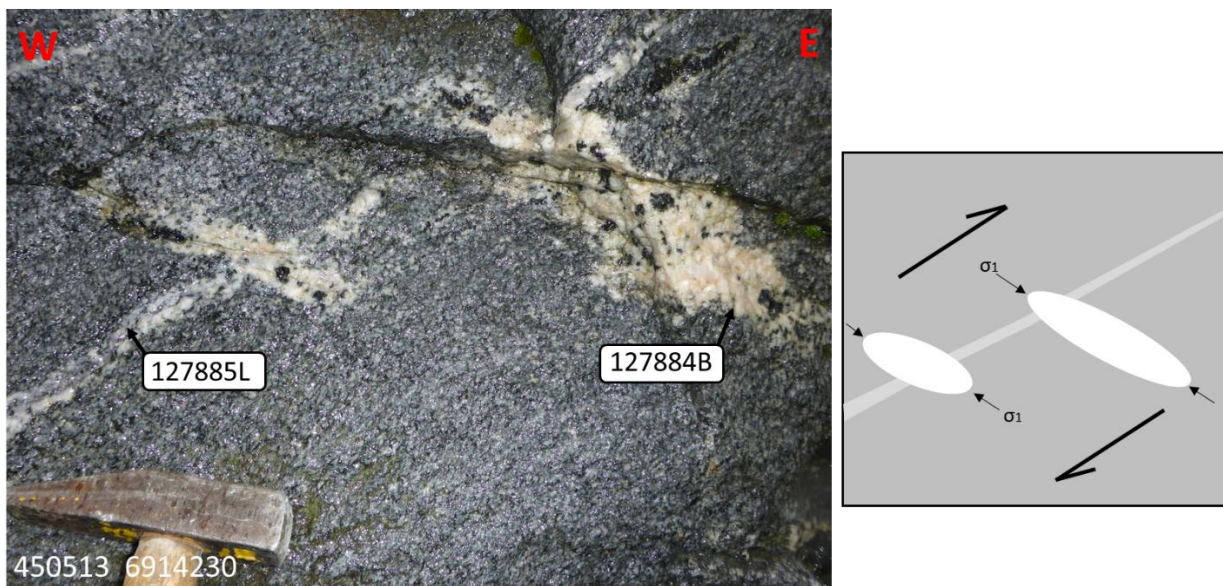
Figure 6.11: *Cross cutting leucosomes in the southern WGR. Figure on the right-hand side illustrate the indicated stress field and corresponding interpretation. Coordinates indicate the approximate location, field observation made by Trond Slagstad.*

127

6.5 UHP-melt and subducted continental slab rheology

Partial melting of continental crust in UHP units would first be associated with decompression melting related to exhumation. The distinctive pressure-temperature (P-T) path related to the subduction and exhumation of the UHP terrain in the WGR would be an indicator of such a situation. However, melting of dry felsic rock at mantle or crustal, level would require temperatures that are not recorded in the WGR. For migmatisation to be possible in a prograde continent-slab subduction setting fluid would have had to be present in the system. Studies done both in the field and experimentally coincide with models that suggest that melting can occur under UHP condition of continental slab subduction (Auzanneau et al., 2006, Liu et al., 2012, and additional references given in Gordon et al., 2013). P-T constrains in the WGR illustrated both by Labrousse et al. (2011) and Gordon et al., (2013, 2016) constructed by the use of experimental data by a series of authors, indicate that melting of the gneisses surrounding the eclogites in the WGR could have melted at UHP conditions within a fluid-present system. Labrousse et al., (2011) constructed P-T diagram illustrated in Figure 6.12 below.
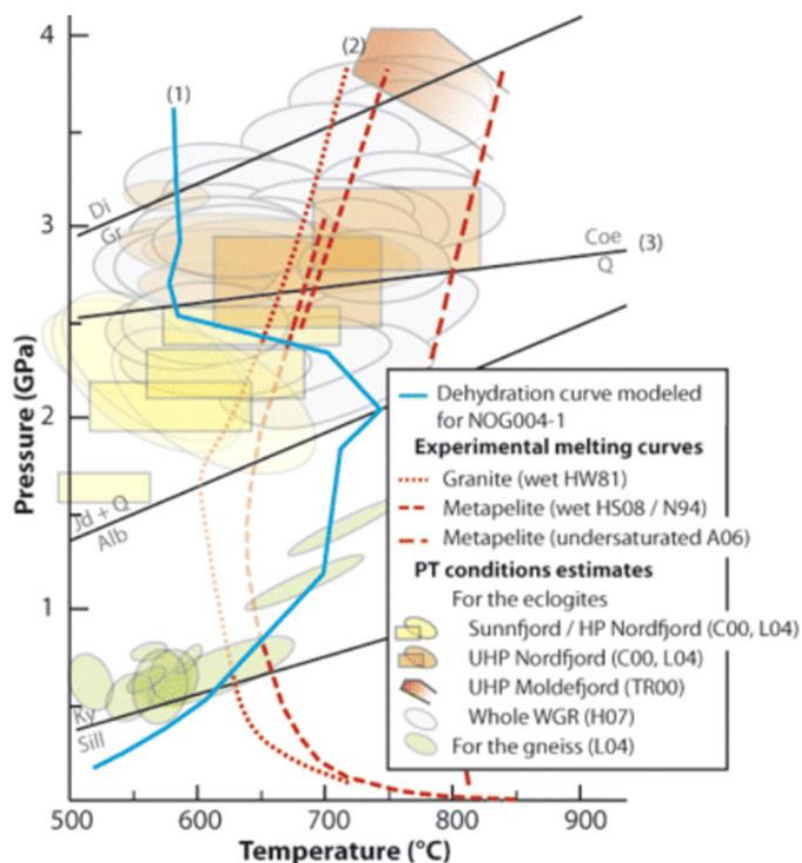
Figure 6.12: *The diagram is constructed by using a wealth of experiments (Labrousse et al., 2011, and references therein) to use as a supplement to constrain the P-T history in the WGR.*

The work done by Gordon et al. (2013) with the combined use of geochronology and trace element geochemistry in the zircons can be used to relate the zircons in the migmatites to a P-T setting. Here the method was used on different structured migmatites all in proximity to the UHP eclogites in the WGR, exploring the relationship from UHP to lower-P conditions. Labrousse et al. (2011) added complete leucosome geochemistry to try and correlate the natural diversity of leucosomes in the UHP and HP domains in proximity to the eclogites. Both these studies exemplify the use eclogites as a P-T reference while studying leucosomes within the WGR. The WGR gneisses in and of themselves are such poor constrainers of P-T indicators that this is necessary. Though neither can state exactly when the initial migmatisation did take place, both discuss the relevance of a melt-present system to the rheology of the down going continental slab. A melt fraction of > 10 to 15 % would decrease the viscosity of the downgoing slab drastically, and in turn changing the overall deformation regime (Rosenberg and Handy, 2005). A partially melted crust could initiate a dynamic instability with an upwards driving force in the slab. Partially melted crust could also be sufficiently weakened that it could decouple from the down going slab in favour of its ascent by buoyancy forces, as stated by Labrousse et al. (2011).

The discussion of the timing of the partial melting in the WGR is significant. As the presence of melt, or lack thereof, in a continental subduction would greatly affect the rheology of the subducting continental crust. And by extension, the later subsequent exhumation. Further study of the WRG migmatites would provide an opportunity to better understand partial melting in an UHP setting. And if it is possible to extrapolate the chemical, whole rock geochemistry of the leucosomes and the trace elements in the zircons, from the migmatites proximate to the UHP eclogite terrain to the more distal migmatites in the region. Which would be useful both for further rheological and partial-melt interpretations.

Though the U-Pb zircon geochronology presented in this thesis is indicative, further analysis is needed to make more certain interpretations. Where some examples are given in the above discussion. It is however also important to note that complicated nature of such a large system. Where factors such as the level of dehydration, mineral distribution and stress regime is likely to vary throughout the region. Such that if studies from one area to another is contradicting, the results should be considered as only parts of a region setting.

7 Conclusion

- The majority of the leucosome zircons have distinct cores and mantles interpreted to represent inheritance from the protoliths and later metamorphic growth, respectively. This is confirmed by the obtained U-Pb geochronological data from the zircons. The cores and rims can be used for dating both the protoliths and migmatisation events respectively over large areas in the WGR.

- Geochemical data from the protoliths to the basement gneiss are used to determine the tectonic setting of formation. The geochemical and geochronological data are consistent with formation in a magmatic arc system between 1691 ± 22 and 1589 ± 19 Ma.

- Sveconorwegian migmatisation of the basement gneisses is confirmed in the southern WGR. Obtained leucosome ages fall in line with previous observation made in the region by Tucker et al, (1990).

- The combined age and geochemical data from the protoliths make it plausible to correlate the WGR with other exposed Proterozoic units on the Baltic Shield. The ~1000 Ma migmatisation can also be used in these correlations. Extrapolation between the WGR and the Sveconorwegian Eastern Segment in Sweden is argued for here.

- The Caledonian ages for the majority of leucosomes indicate that the migmatisation took place during the 423 ± 10 to 392 ± 3 Ma time interval. These observations indicate that the migmatisation was mostly an effect of prograde metamorphism during subduction of the Baltic margin below Laurentia. The lack of any observable westward younging in the zircon ages, as well as observed top-to-east thrust structures in some leucosomes, substantiates this interpretation.

- Extensive and widespread partial melting during subduction would have affected the rheology of the downgoing slab, which in turn may have facilitated the slab break-off and resulting rapid exhumation.

Refrences

ÅHÄLL, K.-I. & CONNELLY, J. 1998. Intermittent 1.53–1.13 Ga magmatism in western Baltica; age constraints and correlations within a postulated supercontinent. Precambrian Research, 92, 1-20.

ÅHÄLL, K.-I. & CONNELLY, J. N. 2008. Long-term convergence along SW fennoscandia: 330 m.y. of proterozoic crustal growth. Precambrian Research, 161, 452-474.

ALLEN, P., CONDIE, K. C. & NARAYANA, B. L. 1985. The geochemistry of prograde and retrograde charnockite-gneiss reactions in southern India. Geochimica et Cosmochimica Acta, 49, 323-336.

AUZANNEAU, E., VIELZEUF, D. & SCHMIDT, M. 2006. Experimental evidence of decompression melting during exhumation of subducted continental crust. Contributions to Mineralogy and Petrology, 152, 125-148.

BERGSTRÖM, U., STEPHENS, M. B. & WAHLGREN, C.-H. 2020. Chapter 16 Polyphase (1.6–1.5 and 1.1–1.0 Ga) deformation and metamorphism of Proterozoic (1.7–1.1 Ga) continental crust, Idefjorden terrane, Sveconorwegian orogen. Geological Society, London, Memoirs, 50, 397-434.

BINGEN, B. & SOLLI, A. 2009. Geochronology of magmatism in the Caledonian and Sveconorwegian Belts of Baltica; synopsis for detrital zircon provenance studies. Norsk Geologisk Tidsskrift,Norwegian Journal of Geology, 89, 267-290.

BINGEN, B., ANDERSSON, J., SODERLUN, U. & MOLLER, C. 2008. The Mesoproterozoic in the Nordic countries. Episodes, 31, 29.

BOGDANOVA, S., BINGEN, B., GORBATSCHEV, R., KHERASKOVA, T., KOZLOV, V., PUCHKOV, V. & VOLOZH, Y. A. 2008. The East European Craton (Baltica) before and during the assembly of Rodinia. Precambrian Research, 160, 23-45.

BROWN, G. C., THORPE, R. S. & WEBB, P. C. 1984. The geochemical characteristics of granitoids in contrasting arcs and comments on magma sources. Journal of the Geological Society, 141, 413-426.

CARSWELL, D. A., TUCKER, R. D., O'BRIEN, P. J. & KROGH, T. E. 2003. Coesite micro-inclusions and the U/Pb age of zircons from the Hareidland Eclogite in the Western Gneiss Region of Norway. LITHOS, 67, 181-190.

CHERNIAK, D. J. & WATSON, E. B. 2003. Diffusion in zircon. Reviews in mineralogy and geochemistry, 53, 113-143.

CORFU, F., ARMITAGE, P. E., KULLERUD, K. & BERGH, S. G. 2003. Preliminary U-Pb geochronology in the West Troms Basement Complex, North Norway: Archaean and Palaeoproterozoic events and younger overprints. NORGES GEOLOGISKE UNDERSOKELSE, 441, 61-72.

CUTHBERT, S. J., CARSWELL, D. A., KROGH-RAVNA, E. J. & WAIN, A. 2000. Eclogites and eclogites in the Western Gneiss Region, Norwegian Caledonides. LITHOS, 52, 165-195.

DESORMEAU, J. W., GORDON, S. M., KYLANDER-CLARK, A. R., HACKER, B. R., BOWRING, S. A., SCHOENE, B. & SAMPERTON, K. M. 2015. Insights into (U) HP metamorphism of the Western Gneiss Region, Norway: A high-spatial resolution and high-precision zircon study. Chemical Geology, 414, 138-155.

DESORMEAU, J. W., GORDON, S. M., KYLANDER-CLARK, A. R., HACKER, B. R., BOWRING, S. A., SCHOENE, B. & SAMPERTON, K. M. 2015. Insights into (U) HP metamorphism of the Western Gneiss Region, Norway: A high-spatial resolution and high-precision zircon study. Chemical Geology, 414, 138-155.

FROST, B. R., BARNES, C. G., COLLINS, W. J., ARCULUS, R. J., ELLIS, D. J. & FROST, C. D. 2001. A Geochemical Classification for Granitic Rocks. Journal of Petrology, 42, 2033-2048.

GEBAUER, D., LAPPIN, M. A., GRÜNENFELDER, M. & WYTTENBACH, A. 1985. The age and origin of some Norwegian eclogites: AU□ Pb zircon and REE study. Chemical Geology: Isotope Geoscience section, 52, 227-247.

GEE, D. 1975. A tectonic model for the central part of the Scandinavian Caledonides. American Journal of Science, 275, 468-515.

GEE, D. G., FOSSEN, H., HENRIKSEN, N., HIGGINS, A. K. & LADENBERGER, A. 2008. From the early Paleozoic platforms of Baltica and Laurentia to the Caledonide Orogen of Scandinavia and Greenland. Episodes, 31, 44-51.

GORDON, S. M., WHITNEY, D. L., TEYSSIER, C. & FOSSEN, H. 2013. U-Pb dates and trace-element geochemistry of zircon from migmatite, Western Gneiss Region, Norway: Significance for history of partial melting in continental subduction. Lithos, 170-171, 35-53.

GORDON, S. M., WHITNEY, D. L., TEYSSIER, C., FOSSEN, H. & KYLANDER-CLARK, A. 2016. Geochronology and geochemistry of zircon from the northern Western Gneiss Region: Insights into the Caledonian tectonic history of western Norway. Lithos, 246-247, 134-148.

HACKER, B. 2007. Ascent of the ultrahigh-pressure Western Gneiss region, Norway. SPECIAL PAPERS-GEOLOGICAL SOCIETY OF AMERICA, 419, 171.

HACKER, B. R. 2006. Pressures and Temperatures of Ultrahigh-Pressure Metamorphism: Implications for UHP Tectonics and H2O in Subducting Slabs. International Geology Review, 48, 1053-1066.

HACKER, B. R., ANDERSEN, T. B., JOHNSTON, S., KYLANDER-CLARK, A. R. C., PETERMAN, E. M., WALSH, E. O. & YOUNG, D. 2010. High-temperature deformation during continental-margin subduction & exhumation: The ultrahigh-pressure Western Gneiss Region of Norway. Tectonophysics, 480, 149-171.

HACKER, B. R., KYLANDER-CLARK, A. R., HOLDER, R., ANDERSEN, T. B., PETERMAN, E. M., WALSH, E. O. & MUNNIKHUIS, J. K. 2015. Monazite response to ultrahigh-pressure subduction from U–Pb dating by laser ablation split stream. Chemical Geology, 409, 28-41.

HARRISON, T. M., CÉLÉRIER, J., AIKMAN, A. B., HERMANN, J. & HEIZLER, M. T. 2009. Diffusion of 40Ar in muscovite. Geochimica et Cosmochimica Acta, 73, 1039-1051.

HÖGDAHL, K., ANDERSSON, U. B. & EKLUND, O. 2004. The transscandinavian Igneous Belt (TIB) in Sweden: A review of its character and evolution. Special Paper of the Geological Survey of Finland, 1-125.

HOLDER, R. M., HACKER, B. R., KYLANDER-CLARK, A. R. C. & COTTLE, J. M. 2015. Monazite trace-element and isotopic signatures of (ultra)high-pressure metamorphism: Examples from the Western Gneiss Region, Norway. Chemical Geology, 409, 99-111.

HOSKIN, P. 2003. The Composition of Zircon and Igneous and Metamorphic Petrogenesis. Reviews in Mineralogy & Geochemistry - REV MINERAL GEOCHEM, 53, 27-62.

HYNES, A. & RIVERS, T. 2010. Protracted continental collision evidence from the Grenville Orogen This article is one of a series of papers published in this Special Issue on the theme Lithoprobe parameters, processes, and the evolution of a continent. Canadian Journal of Earth Sciences, 47, 591-620.

IRVINE, T. N. & BARAGAR, W. R. A. 1971. A Guide to the Chemical Classification of the Common Volcanic Rocks. Canadian Journal of Earth Sciences, 8, 523-548.

KAEPPELER, J. & MORACH, M. 2016. High purity silicon sizing by high voltage pulse power technology. In: L. NYGÅRD, B. P., I. B. PAGE, H. ROGN, M. TENGSTAD, H. TVEIT (ed.) Silicon for the Chemical and Solar Industry XIII. N-7491 Trondheim Norway: NTNU.

KORJA, A., LAHTINEN, R. & NIRONEN, M. 2006. The Svecofennian orogen: a collage of microcontinents and island arcs. Geological Society, London, Memoirs, 32, 561-578.

KRILL, A. G. 1980. Tectonics of the Oppdal area, central Norway. Geologiska Föreningen i Stockholm Förhandlingar, 102, 523-530.

KRILL, A., GEE, D. & STURT, B. 1985. Relationships between the Western Gneiss Region and the Trondheim Region–Stockwerk—Tectonics reconsidered. The Caledonide Orogen—Scandinavia and Related Areas, Wiley, Chichester, 475, 484.

KROGH RAVNA, E. J. & TERRY, M. P. 2004. Geothermobarometry of UHP and HP eclogites and schists – an evaluation of equilibria among garnet–clinopyroxene–kyanite–phengite–coesite/quartz. Journal of Metamorphic Geology, 22, 579-592.

KROGH, T. E., KAMO, S. L., ROBINSON, P., TERRY, M. P. & KWOK, K. 2011. UPb zircon geochronology of eclogites from the Scandian Orogen, northern Western Gneiss Region, Norway: 1420 million years between eclogite crystallization and return to amphibolite-facies conditions This article is one of a series of papers published in this Special Issue on the theme of Geochronology in honour of Tom Krogh. Canadian Journal of Earth Sciences, 48, 441-472.

KROGH, T. E., MYSEN, B. O. & DAVIS, G. L. 1974. A Paleozoic Age for the Primary Minerals of a Norwegian Eclogite. Year Book - Carnegie Institution of Washington, 73, 575-576.

KYLANDER-CLARK, A. R. C., HACKER, B. R. & COTTLE, J. M. 2013. Laser-ablation split-stream ICP petrochronology. Chemical Geology, 345, 99-112.

KYLANDER-CLARK, A. R. C., HACKER, B. R., JOHNSON, C. M., BEARD, B. L., MAHLEN, N. J. & LAPEN, T. J. 2007. Coupled Lu–Hf and Sm–Nd geochronology constrains prograde

and exhumation histories of high- and ultrahigh-pressure eclogites from western Norway. Chemical Geology, 242, 137-154.

KYLANDER-CLARK, A., HACKER, B. & MATTINSON, J. 2008. Slow exhumation of UHP terranes: titanite and rutile ages of the Western Gneiss Region, Norway. Earth and Planetary Science Letters, 272, 531-540.

LABROUSSE, L., PROUTEAU, G. & GANZHORN, A. C. 2011. Continental exhumation triggered by partial melting at ultrahigh pressure.(Author abstract)(Report). Geology, 39, 1171.

LAW, R., BUTLER, R., HOLDSWORTH, R., KRABBENDAM, M. & STRACHAN, R. 2010. Continental tectonics and mountain building. The legacy of Peach and Horne: an introduction. Geological Society, London, Special Publications, 335, 715 - 737.

LIU, F. L., ROBINSON, P. T. & LIU, P. H. 2012. Multiple partial melting events in the Sulu UHP terrane: zircon U–Pb dating of granitic leucosomes within amphibolite and gneiss. Journal of Metamorphic Geology, 30, 887-906.

LUDWIG, K.R. 2003. Isoplot 3.00, A Geochronological Toolkit for Microsoft Excel.Berkley GeochronologyCenter, Special Publication,4, 1-74

LUNDMARK, A. M. & LAMMINEN, J. 2016. The provenance and setting of the Mesoproterozoic Dala Sandstone, western Sweden, and paleogeographic implications for southwestern Fennoscandia. Precambrian Research, 275, 197-208.

LUTRO, O. & TVETEN, E. 1998. Geologisk kart over Noreg, berggrunskart ÅRDAL. Noregs Geologiske Undersøkning.

MÖLLER, C., ANDERSSON, J., DYCK, B. & LUNDIN, I. A. 2015. Exhumation of an eclogite terrane as a hot migmatitic nappe, Sveconorwegian orogen. Lithos, 226, 147-168.

MURPHY, J. B., NANCE, R. D. & CAWOOD, P. A. 2009. Contrasting modes of supercontinent formation and the conundrum of Pangea. Gondwana Research, 15, 408-420.

NASUTI, A., PASCAL, C., EBBING, J. & TONNESEN, J. F. 2011. Geophysical characterisation of two segments of the More-Trondelag Fault Complex, Mid Norway. Solid Earth, 2, 125-134.

PEARCE, J. A., HARRIS, N. B. & TINDLE, A. G. 1984. Trace element discrimination diagrams for the tectonic interpretation of granitic rocks. Journal of petrology, 25, 956-983.

PETERSSON, A., SCHERSTÉN, A., BINGEN, B., GERDES, A. & WHITEHOUSE, M. J. 2015. Mesoproterozoic continental growth: U–Pb–Hf–O zircon record in the Idefjorden Terrane, Sveconorwegian Orogen. Precambrian Research, 261, 75-95.

ROBERTS, D. & GEE, D. G. 1985. An introduction to the structure of the Scandinavian Caledonides. The Caledonide orogen–Scandinavia and related areas, 1, 55-68.

ROBERTS, D. 2003. The Scandinavian Caledonides: event chronology, palaeogeographic settings and likely modern analogues. Tectonophysics, 365, 283-299.

ROBERTS, N. M. W. & SLAGSTAD, T. 2014. Continental growth and reworking on the edge of the Columbia and Rodinia supercontinents; 1.86–0.9 Ga accretionary orogeny in southwest Fennoscandia. International Geology Review, 57, 1582-1606.

ROBINSON, P. 1995. Extension of Trollheimen tectono-stratigraphic sequence in deep synclines near Molde and Brativag, Western Gneiss Region, southern Norway. Norsk Geologisk Tidsskrift, 75, 181-197.

RØHR, T. S., CORFU, F., AUSTRHEIM, H. & ANDERSEN, T. B. 2004. Sveconorwegian U-Pb zircon and monazite ages of granulite-facies rocks, Hisarøya, Gulen, Western Gneiss Region, Norway. Norwegian Journal of Geology/Norsk Geologisk Forening, 84.

ROLLINSON, H. R. 1993. Using Geochemical Data: Evaluation, Presentation, Interpretation, Florence, UNITED KINGDOM, Routledge.

RØNNING, J. S., BARANWAL, V. & BRÖNNER, M. 2019. Grunnundersøkelser ved Raudsand, Nesset kommune i Møre og Romsdal. Supplerende.

ROOT, D. B., HACKER, B. R., MATTINSON, J. M. & WOODEN, J. L. 2004. Zircon geochronology and ca. 400 Ma exhumation of Norwegian ultrahigh-pressure rocks: an ion microprobe and chemical abrasion study. Earth and Planetary Science Letters, 228, 325-341.

ROOT, D., HACKER, B., GANS, P., EIDE, E., DUCEA, M. & MOSENFELDER, J. 2005. High-pressure allochthons overlie the ultrahigh-pressure Western Gneiss Region, Norway. Journal of Metamorphic Geology, 23, 45-61.

ROSENBERG, C. L. & HANDY, M. R. 2005. Experimental deformation of partially melted granite revisited: implications for the continental crust. Journal of Metamorphic Geology, 23, 19-28.

SCHALTEGGER, U., SCHMITT, A. K. & HORSTWOOD, M. S. A. 2015. U–Th–Pb zircon geochronology by ID-TIMS, SIMS, and laser ablation ICP-MS: Recipes, interpretations, and opportunities. Chemical Geology, 402, 89-110.

SCHÄRER, U. & LABROUSSE, L. 2003. Dating the exhumation of UHP rocks and associated crustal melting in the Norwegian Caledonides. Contributions to Mineralogy and Petrology, 144, 758-770.

SCHOENE, B. 2014. 4.10 - U–Th–Pb Geochronology. In: HOLLAND, H. D. & TUREKIAN, K. K. (eds.) Treatise on Geochemistry (Second Edition). Oxford: Elsevier.

Scientific algorithms in this program are described in: Allmendinger, R. W., Cardozo, N. C., and Fisher, D., 2013,

SKAR, O. & PEDERSEN, R. 2003. Relations between granitoid magmatism and migmatization: U-Pb geochronological evidence from the Western Gneiss Complex, Norway. J. Geol. Soc., 160, 935-946.

SLAGSTAD, T., ROBERTS, N. M. W., MARKER, M., RØHR, T. S. & SCHIELLERUP, H. 2013. A non-collisional, accretionary Sveconorwegian orogen. Terra Nova, 25, 30-37.

SPENCER, K. J., HACKER, B. R., KYLANDER-CLARK, A. R. C., ANDERSEN, T. B., COTTLE, J. M., STEARNS, M. A., POLETTI, J. E. & SEWARD, G. G. E. 2013. Campaign-style titanite U–Pb dating by laser-ablation ICP: Implications for crustal flow, phase transformations and titanite closure. Chemical Geology, 341, 84-101.

Structural Geology Algorithms: Vectors & Tensors: Cambridge, England, Cambridge University Press, 289 pp.

SAWYER, E. W. 2008. Atlas of migmatites, NRC Research press.

TERRY, M. P., ROBINSON, P., HAMILTON, M. A. & JERCINOVIC, M. J. 2000. Monazite geochronology of UHP and HP metamorphism, deformation, and exhumation, Nordøyane, Western Gneiss Region, Norway. American Mineralogist, 85, 1651-1664.

TORSVIK, T. H., SMETHURST, M. A., MEERT, J. G., VAN DER VOO, R., MCKERROW, W. S., BRASIER, M. D., STURT, B. A. & WALDERHAUG, H. J. 1996. Continental break-up and collision in the Neoproterozoic and Palaeozoic — A tale of Baltica and Laurentia. Earth Science Reviews, 40, 229-258.

TUCKER, R., KROGH, T. & RÅHEIM, A. 1990. Proterozoic evolution and age-province boundaries in the central part of the Western Gneiss Region, Norway: Results of U-Pb dating of accessory minerals from Trondheimsfjord to Geiranger. Mid-Proterozoic Laurentia-Baltica, 38, 149-173.

TUCKER, R., ROBINSON, P., SOLLI, A. & GEE, D. 2004. Thrusting and extension in the Scandian hinterland, Norway: New U-Pb ages and tectonostratigraphic evidence. American Journal of Science, 304, 477-532.

TVETEN, E., LURO, O. & THORSNES, T. 1998 Ålesund. Berggrunnskart Ålesund, Map, 1:250 000 trykt i farger, Norges geologiske undersøkelse, Almquist & Wiksell AWT Tryckeri, Uppsal

TVETEN, E., LUTRO, O. & THORSNES, T. 1998. Geologisk kart over Norge, berggrunnskart Ålesund, 1: 250.000. Geological Survey of Norway, Trondheim.

VAN ACHTERBERG, E., RYAN, C.G., JACKSON, S.E. & GRIFFIN, W.L. 2001. LA-ICP-MS in the Earth Sciences-Appendix 3, data reduction software for LA-ICP-MS.In: Sylvester, P.J. (ed)Short Course volume 29:St.John's, Mineralogical Association of Canada,, 239-243

VRIJMOED, J., VAN ROERMUND, H. & DAVIES, G. 2006. Evidence for diamond-grade ultra-high pressure metamorphism and fluid interaction in the Svartberget Fe–Ti garnet peridotite–websterite body, Western Gneiss Region, Norway. Mineralogy and Petrology, 88, 381-405.

WALSH, A., RAIMONDO, T., KELSEY, D., HAND, M., PFITZNER, H. & CLARK, C. 2013. Duration of high-pressure metamorphism and cooling during the intraplate Petermann Orogeny. Gondwana Research, 24, 969-983.

WALSH, E., HACKER, B., GANS, P., GROVE, M. & GEHRELS, G. 2007. Protolith ages and exhumation histories of(ultra)high-pressure rocks across the Western Gneiss Region, Norway. Geological Society of America. Geological Society of America Bulletin, 119, 289.

WHITE, W. M. 2015. Isotope Geochemistry, Hoboken, UNITED KINGDOM, John Wiley & Sons, Incorporated.

WINTER, J. D. 2001. An Introduction to Igneous and Metamorphic Petrology, Prentice-Hall Inc.

YOUNG, D. J., HACKER, B. R., ANDERSEN, T. B. & CORFU, F. 2007. Prograde amphibolite facies to ultrahigh-pressure transition along Nordfjord, western Norway: Implications for exhumation tectonics. Tectonics, 26.

ZHANG, S., LI, Z.-X., EVANS, D. A. D., WU, H., LI, H. & DONG, J. 2012. Pre-Rodinia supercontinent Nuna shaping up: A global synthesis with new paleomagnetic results from North China. Earth and Planetary Science Letters, 353-354, 145-155.

Appendix

Appendix A – Sample list

Sample nr:	UTM_E	UTM_N	Description	Geochem	Geochron	Thinsection
197562	450 011	6 960 762	Quarts diorite with leucosome	x	x	x
197578	451 403	6 962 671	Pink grantic gneiss with leucosome	x	x	x
200987	454 984	6 968 894	Pink granitic gneiss with leucomsome crossing foliation	x	x	x
200976	454 129	6 968 513	Pegmatitic metagabbro	x	x	x
200955	449 245	6 961 979	Gabbro (away from contact)	x	x	x
200960	455 165	6 968 440	Meta gabbro	x	x	x
197586	457 734	6 964 449	Quarts diorite with leucosome	x	x	x
200998	455 072	6 968 397	Phenochrystic granite with dike	x	x	x
197555	449 940	6 960 684	Pink granitic gniess	x	x	x
197556	449 956	6 960 711	Pink granitic gniess	x	-	-
200965	451 128	6 965 070	Pink granitic gniess with leuksosome	x	-	x
197590	455 648	6 967 143	Light granitic gneiss	x	-	x
200996	454 671	6 970 564	Augengneiss	x	-	x
197569	454 058	6 962 877	Quarts diorite with leucosome	x	-	x
200962	455 099	6 968 566	Grey granitic gneiss	x	-	-
200963	455 133	6 963 487	Quarts diorite with mafic layers	x	-	x
197551	455 658	6 967 099	Granite with leukosome	x	-	x
201000	455 086	6 967 548	Migmatitic pink granitic gneiss	x	-	x
200994	453 943	6 962 992	Granitic gniess with pegmatitic leucosome	x	-	x
200982	454 797	6 969 939	Quarts shicht with mica	x	-	x
200986	454 792	6 970 110	Granite with dike	x	-	x
200992	455 020	6 968 718	Pink granitic gneiss	x	-	-
200981	454 633	6 971 033	Augengneiss	x	-	-
200966	451 457	6 962 659	Pink granitic gneiss with leucomsome	x	-	-
200973	454 245	6 968 520	Meta grbbro with ore	x	-	x
200974	454 246	6 968 518	Foliated metagabbro with felsic material	x	-	x
200975	454 247	6 968 504	Mafic metagabbro	x	-	x
200959	455 209	6 964 413	Metagrabbro with ore	x	-	x
197554	455 650	6 967 229	Amphibolite with ore	x	s	x
200985	454 805	6 970 042	Amphibolite	x	-	-

7.1 Appendix B – Field map with sample location and structural measurements
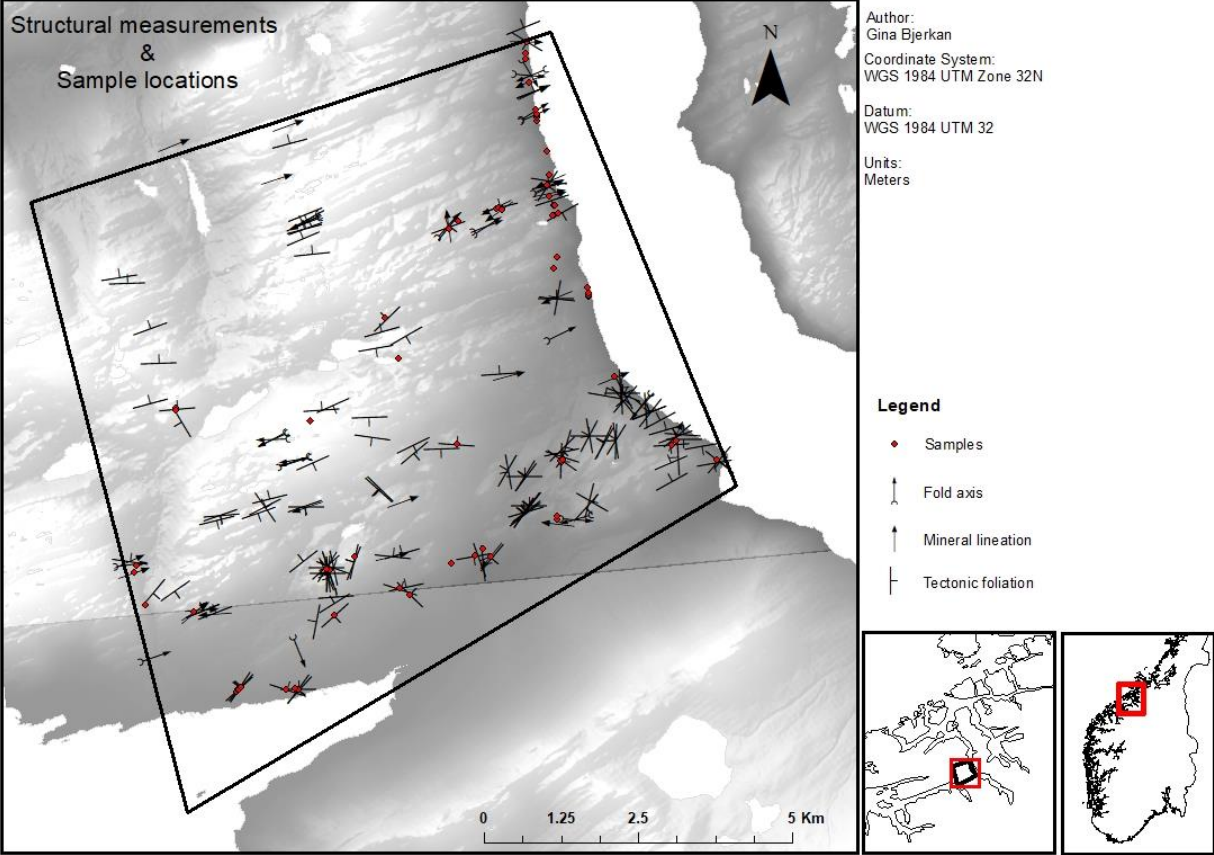
Appendix C - Geochemical data

C1: Whole-rock major elements

SAMPLE	SiO2	Al2O3	Fe2O3	CaO	MgO	Na2O	K2O	Cr2O3	TiO2	MnO	P2O5	SrO	BaO	LOI	Total
	%	%	%	%	%	%	%	%	%	%	%	%	%	%	%
197551	70.3	14.95	3.32	2.42	1.14	3.82	3.92	0.003	0.39	0.08	0.14	0.03	0.11	0.36	100.98
197554	48.3	16.25	14.35	10.2	6.51	2.43	0.72	0.009	1.14	0.16	0.07	0.05	0.04	0.94	101.17
197555	13.7	2.55	1.22	0.34	3.45	5.87	<0.002	0.3	0.07	0.08	0.02	0.1	0.26	98.86	98.86
197556	70.2	13.6	3.8	1.38	0.39	3.49	5.42	<0.002	0.43	0.1	0.1	0.01	0.09	0.29	99.3
197562	15.15	4.03	3.04	1.48	3.99	4.12	0.003	0.47	0.09	0.18	0.04	0.13	0.63	101.25	101.25
197569	67.1	14.45	4.83	2.62	1.21	3.6	4.33	0.003	0.77	0.11	0.26	0.02	0.12	0.72	100.14
197578	13.25	2.16	1.01	0.41	3.43	5.47	0.003	0.31	0.07	0.08	0.01	0.07	0.3	101.87	101.87
197586	15.95	4.02	2.59	1.79	3.92	3.99	0.004	0.55	0.08	0.17	0.03	0.1	0.54	101.13	101.13
197590	68.1	15.25	3.72	2.65	1.16	4.08	3.61	0.004	0.42	0.09	0.16	0.02	0.09	0.41	99.76
200955	16.6	14.2	8.85	6.95	3.07	0.9	0.007	2.05	0.2	0.32	0.04	0.05	1.05	99.69	99.69
200959	31.5	14.5	38.2	5.86	3.11	2.27	0.7	0.002	4	0.17	0.06	0.04	0.08	0.35	100.84
200960	16.65	5.21	5.63	5.16	4.58	2.47	0.025	0.44	0.11	0.13	0.07	0.06	0.63	100.67	100.67
200962	70.1	15.7	2.54	2.53	0.84	4.54	3.78	0.002	0.27	0.07	0.12	0.08	0.13	0.45	101.15
200963	65.6	12.55	5.21	8.28	1.88	3.01	0.43	0.011	0.57	0.08	0.13	0.06	0.03	1.52	99.36
200965	68.5	14.5	4.4	2.59	1.31	4.25	3.17	0.003	0.55	0.12	0.19	0.01	0.05	0.67	100.31
200966	72.6	14.4	1.87	1	0.38	3.43	6.18	0.002	0.32	0.04	0.08	0.02	0.07	0.65	101.04
200973	34.3	15.55	32.4	5.89	2.72	2.67	1.65	0.002	3.73	0.19	0.08	0.06	0.11	0.21	99.56
200974	43.8	16.25	19.2	7.53	4.46	3	1.27	<0.002	2.03	0.15	0.12	0.06	0.08	0.96	98.91
200975	45.8	10	18	9.98	11.5	1.22	0.3	0.089	1.33	0.19	0.05	<0.01	0.01	1.41	99.88
200976	18.3	11.9	8.44	4.51	3.91	1.04	0.002	1.17	0.16	0.09	0.08	0.08	1.29	100.27	100.27
200981	68.1	15.3	3.79	2.19	1.05	3.78	5.23	0.002	0.7	0.08	0.21	0.03	0.16	0.56	101.18
200982	90.5	4.25	0.82	0.05	0.27	0.61	2.13	0.004	0.16	<0.01	0.01	<0.01	0.05	0.34	99.19
200985	62.3	15	6.63	4.98	4.4	2.26	2.6	0.02	0.84	0.08	0.17	0.01	0.04	1.5	100.83
200986	70.8	14.25	3.55	1.63	1.14	3.17	5.52	0.004	0.55	0.06	0.18	0.01	0.1	0.46	101.42
200987	17.5	3.22	1.63	0.69	5.26	5.84	<0.002	0.69	0.1	0.14	0.01	0.58	0.49	100.65	100.65
200992	67.7	15.55	3.28	0.98	0.49	4.53	6.03	0.002	0.44	0.1	0.08	<0.01	0.07	0.29	99.54
200994	68.9	14.5	4.29	2.52	1.06	3.47	4.78	0.003	0.67	0.09	0.23	0.01	0.12	0.41	101.05
200996	68.3	14.55	4.13	2.29	1.13	3.43	4.87	0.002	0.61	0.08	0.23	0.03	0.11	0.6	100.36
200998	15.2	2.39	2.29	0.75	4.47	3.85	0.002	0.26	0.07	0.11	0.08	0.13	0.25	100.55	100.55
201000	73.6	13.85	1.56	1.14	0.53	3.89	4.4	<0.002	0.15	0.04	0.04	0.02	0.1	0.34	99.66

C2: Whole-rock major elements: additional samples

SAMPLE	SiO2	Al2O3	Fe2O3	CaO	MgO	Na2O	K2O	Cr2O3	TiO2	MnO	P2O5	SrO	BaO	LOI	Total
	%	%	%	%	%	%	%	%	%	%	%	%	%	%	%
090346	75.1	13.25	1.28	0.18	0.19	3.62	5.29	0.003	0.25	0.02	0.02	<0.01	0.01	0.47	99.68
133123	64.3	17.95	2.86	3.35	0.98	4.24	4.44	0.003	0.48	0.06	0.14	0.08	0.15	0.68	99.71
133124	69.8	14.8	2.72	1.74	1.05	3.78	4.79	0.006	0.37	0.07	0.12	0.03	0.08	0.42	99.78
133128	58	19.4	5.91	6.42	2.92	4.68	1.24	0.006	0.62	0.12	0.16	0.07	0.03	0.82	100.4
133129	63.4	17.35	4.41	3.79	2.15	4.43	2.64	0.008	0.48	0.09	0.25	0.07	0.13	0.52	99.72
127866M	64.2	15.15	5.41	4.26	2.59	3.09	2.77	0.018	0.57	0.1	0.18	0.04	0.12	0.81	99.31
127867	64.6	16.25	4.52	3.93	1.44	3.72	3.97	0.003	0.61	0.1	0.22	0.05	0.17	0.72	100.3
127868M	62.1	16.95	6.01	4.96	2.71	3.7	3.21	0.004	0.66	0.1	0.21	0.05	0.12	0.58	101.36
127869	69.9	15.1	4.62	1.19	1.92	1.67	3.71	0.011	0.55	0.12	0.07	<0.01	0.09	1.74	100.69
127870	68.5	15.8	5.5	1.02	2.42	1.55	4.51	0.015	0.63	0.13	0.07	0.01	0.11	0.65	100.92
127871	68.9	14.8	4.17	2.44	1	3.51	4.76	0.003	0.68	0.1	0.2	0.02	0.14	0.5	101.22
127872	57.4	19.3	5.71	4.25	1.64	4.71	4.09	<0.002	1.1	0.12	0.32	0.08	0.3	0.6	99.62
127873	74.1	14.15	1.77	1.65	0.28	3.14	4.93	0.008	0.15	0.04	0.03	0.05	0.21	0.49	101
127874	66.1	17.55	3.34	3.78	1.11	4.65	2.7	0.003	0.34	0.07	0.17	0.12	0.19	0.64	100.76
127875	66.2	17.1	3.64	3.67	1.34	4.41	3.23	0.005	0.38	0.08	0.2	0.1	0.21	0.57	100.14
127876M	60.8	17.85	5.93	5.07	2.17	4.02	2.77	0.003	0.76	0.12	0.26	0.06	0.09	0.62	100.52
127877M	65.1	15.35	6.74	2.42	2.63	2.36	3.64	0.008	0.95	0.09	0.3	0.05	0.1	1.11	100.85
127878M	69.3	14.9	3.75	2.77	0.92	3.46	3.22	0.002	0.62	0.1	0.16	0.02	0.08	0.46	99.76
127879M	65.9	14.6	6.1	3.56	2.43	2.8	3.46	0.01	0.76	0.13	0.2	0.02	0.11	0.96	101.04
127880	72.2	14.5	1.61	1.26	0.28	2.57	6.49	0.002	0.14	0.01	0.07	0.04	0.2	0.41	99.78
127881	66.9	15.75	5.11	1.27	1.69	2.43	6.02	0.01	0.63	0.07	0.05	0.02	0.11	0.78	100.84
127882M	74.3	12.15	3.97	1.66	0.89	2.81	2.58	0.006	0.53	0.09	0.03	0.01	0.09	0.89	100.01
127883	67	15.3	5.37	3.29	1.29	3.49	3.42	0.002	0.76	0.13	0.2	0.02	0.12	0.39	100.78
127884M	60.3	15.55	9.3	5.81	2.28	3.3	2.19	0.002	1.19	0.24	0.25	0.01	0.05	0.52	100.99
127885M	65.4	16.75	4.98	4.84	2.09	3.54	2.19	0.002	0.59	0.1	0.17	0.03	0.05	0.68	101.41
127886M	70.2	15.05	3.09	3.05	0.99	3.08	3.81	<0.002	0.38	0.07	0.12	0.02	0.09	0.37	100.32
127887	70.7	14.75	2.97	2.17	0.75	3.95	4.07	0.004	0.36	0.09	0.1	<0.01	0.11	0.41	100.43
127888	66.4	15.05	5.38	3.22	1.49	2.85	3.78	0.004	0.74	0.09	0.19	0.01	0.11	0.41	99.72
127889	66.4	15.35	4.55	3.24	1.62	3.27	4.38	0.002	0.47	0.08	0.13	0.04	0.11	0.6	100.24
127890	73.2	14.5	2.4	1.39	1.01	2.26	4.27	0.007	0.27	0.06	0.07	0.01	0.1	0.76	100.31
127891M	67.1	14.95	5.5	3.16	1.56	2.79	3.8	0.005	0.75	0.09	0.19	0.01	0.11	0.37	100.39
127892	66	15.6	6.23	3.87	1.32	3.33	3.72	0.002	0.84	0.11	0.25	0.01	0.14	0.48	101.9
127893	76.9	12	0.97	1.07	0.1	2.19	5.39	0.005	0.08	0.01	0.02	0.01	0.2	0.26	99.21
127894M	56.1	16.55	7.92	5.93	4.22	3.71	2.44	0.014	0.78	0.16	0.3	0.07	0.1	0.99	99.28
127895M	71.4	14.75	2.43	2.41	0.77	3.66	3.53	0.006	0.26	0.05	0.1	0.03	0.14	0.46	100
STO131390M	59	17.55	6.33	5.46	2.33	4.08	3.25	0.004	0.74	0.13	0.36	0.06	0.15	0.42	99.86
STO131391M	74.9	12.3	1.6	0.57	0.18	2.47	6.16	0.003	0.29	0.04	0.05	<0.01	0.02	0.23	98.81
STO131392	65.1	14.75	5.04	6.04	2.55	2.85	2.18	0.016	0.63	0.08	0.15	0.03	0.06	0.49	99.97

C3: Whole-rock minor elements

SAMPLE	Pass2mm %	Pass75um %	Ba ppm	Ce ppm	Cr ppm	Cs ppm	Dy ppm	Er ppm	Eu ppm	Ga ppm	Gd ppm	Hf ppm	Ho ppm	La ppm	Lu ppm	Nb ppm
197551			931	91.7	10	5.74	4.4	2.85	1.09	17	4.82	6.6	0.95	49.4	0.44	14.3
197554		856	325	17.5	50	0.94	2.37	1.44	0.78	19.2	2.35	1.4	0.51	8.5	0.2	2.8
197555	92.7		72.7	<10	1.44	6.81	4.18	1.24	19.2	6.19	7.1	1.38	33.9	0.6	15.5	33.6
197556	77.4	95.3	722	145	10	2.86	9.25	5.49	1.7	22.1	9.69	9.9	1.94	70.3	0.87	19.8
197562		1095	71.9	20	5.45	7.65	5.07	1.84	20	7.9	6.3	1.61	31.9	0.82	14.3	37.6
197569			950	122	10	4.58	6.99	4.1	1.84	16.2	7.74	9.5	1.4	62.4	0.63	17.7
197578		585	112.5	20	1.95	5.38	3.43	0.64	16.6	5.12	8.1	1.11	52.7	0.56	18.5	38.4
197586		773	103	20	3.81	4.77	2.85	1.35	16.1	5.76	6.3	0.97	48.7	0.47	16.7	43
197590			813	101	20	7.05	5.08	3.2	1.18	17.7	5.24	7.4	1.03	54.7	0.51	16.5
200955		427	28.5	50	1.29	4.81	2.67	1.61	21.6	5.16	3.2	0.95	12.3	0.35	6.1	18.7
200959			685	10	<10	1.18	1.31	0.82	0.88	30.4	1.31	0.9	0.26	4.9	0.12	3.3
200960		522	17.7	180	1.82	1.18	0.66	0.65	18.5	1.67	1.9	0.25	7.9	0.09	4.3	10.2
200962			1150	68.2	10	2.88	2.12	1.35	1.02	16.8	2.71	4.4	0.41	37.6	0.23	9.9
200963			255	68.3	70	0.63	4.94	3.08	1.15	15.8	5.51	8.3	1.01	33.1	0.44	13.7
200965			417	80.9	10	5.84	7.39	5.5	0.82	18.8	5.75	8.1	1.63	32.8	0.95	29.8
200966			653	76.1	10	2.15	3.03	2.06	0.66	14.4	2.46	6.5	0.71	33.3	0.38	20.2
200973			986	16.8	<10	2.01	1.58	0.92	1.13	30.2	1.79	1.2	0.35	8.4	0.14	4.7
200974			680	21.3	<10	3.07	2.68	1.89	1.35	25.4	2.65	2.3	0.63	10.3	0.32	9.4
200975			50.5	7.6	630	0.18	2.14	1.41	0.69	15.9	2.08	1	0.46	2.7	0.18	1.5
200976		718	23.3	10	3.77	2.24	1.4	1.31	21.9	2.67	2	0.48	11.6	0.19	2.6	12.3
200981			1530	169	10	3.07	9.75	5.92	2.21	18.2	10.95	9.6	1.96	73.9	0.8	24.9
200982	78.5	94.1	423	21.1	20	0.61	2.2	1.38	0.56	5.1	2.16	5.8	0.46	11.8	0.23	4.8
200985	78.2	88.2	332	60.3	130	5.31	5.28	3.02	1.44	17.3	5.57	6.6	1.07	30.1	0.45	11.7
200986			910	125	20	5.41	6.97	4.41	1.41	15.9	7.2	9.1	1.4	61.5	0.68	21
200987		5410	74.2	<10	1.27	3.94	2.23	5.34	18.7	4.83	10.6	0.79	39.8	0.35	10.3	32.6
200992			596	242	10	4	6.33	3.65	1.26	17.2	8.34	13.4	1.25	124.5	0.5	16.7
200994			1040	140.5	10	4.93	6.96	4.32	1.85	16.5	7.53	8.9	1.48	73.6	0.67	18.5
200996			985	125	10	3.12	6.62	3.94	1.53	16.6	7.16	7.6	1.34	62.4	0.61	19.3
200998		1100	65.8	10	2.88	2.01	1.2	0.88	19	2.67	4.3	0.43	35.5	0.22	11.5	25
201000			873	39.5	<10	4.18	2.03	1.52	0.45	15.2	1.51	3.5	0.43	13.4	0.25	15.3

SAMPLE	Nd	Pr	Rb	Sm	Sn	Sr	Ta	Tb	Th	Tm	U	V	W	Y	Yb	Zr
	ppm	ppm	ppm	ppm	ppm	ppm	ppm	ppm	ppm	ppm	ppm	ppm	ppm	ppm	ppm	ppm
197551	36.4	10.35	150	5.95	2	307	0.9	0.79	13.1	0.41	4.3	37	<1	26	2.86	233
197554	10.5	2.38	22.9	2.21	1	557	0.1	0.4	1.84	0.22	0.88	481	<1	12.8	1.32	47
197555	9.03	161	6.65	2	189.5	1	1.06	10.55	0.57	3.23	15	1	34.1	3.76	272	70.9
197556	62.2	17.5	182	11.05	3	135	1.3	1.52	17.4	0.83	3.72	17	2	49.4	5.43	394
197562	9.43	140.5	8.01	4	451	1.4	1.22	13.3	0.7	5.17	70	2	43.4	4.91	239	67.9
197569	55	14.6	143	8.96	2	246	1	1.2	12.75	0.59	3.36	53	<1	39.1	4.01	392
197578	11.55	166	6.24	2	99.1	1	0.83	16.2	0.49	2.11	27	2	31.5	3.43	316	75.3
197586	12.4	151.5	7.03	2	320	1.1	0.82	14.8	0.44	3.65	66	1	27.7	3.01	249	67.4
197590	40.5	11.5	158	6.64	3	320	1	0.87	14.5	0.45	5.32	43	<1	29.4	3.17	262
200955	4.28	18.8	4.51	2	410	0.1	0.82	0.7	0.36	0.35	243	2	24.1	2.23	121	45.4
200959	5.8	1.36	24.7	1.33	1	443	0.2	0.22	0.75	0.11	1.88	1850	<1	7.2	0.75	34
200960	2.44	84.9	1.97	1	642	<0.1	0.22	0.98	0.1	0.43	83	1	5.8	0.6	68	59.5
200962	28.3	7.81	114.5	3.97	1	772	0.6	0.4	10.7	0.17	4.66	27	<1	12.4	1.34	150
200963	32.4	8.48	21.6	5.74	2	617	0.7	0.85	10.25	0.43	3.23	67	<1	27.8	2.73	317
200965	31.9	8.56	154	6.24	4	176.5	3.1	1.1	18.2	0.87	4.66	51	<1	45.1	6.14	263
200966	20.2	6.31	165.5	3.22	2	189	1.5	0.44	14.7	0.35	1.36	18	<1	20	2.44	245
200973	9.8	2.27	41.2	1.87	1	658	0.2	0.26	1.12	0.14	0.83	1220	<1	9	0.87	40
200974	12.2	2.91	45.8	2.51	2	598	0.8	0.46	2.06	0.27	1.63	659	<1	16.7	1.87	74
200975	6.7	1.3	2.8	1.88	1	48.8	<0.1	0.34	0.42	0.18	0.07	512	<1	11.5	1.14	31
200976	3.06	42.3	2.49	1	788	<0.1	0.4	1.66	0.18	0.76	439	2	12.7	1.25	83	49.3
200981	79.3	21	129.5	13.9	3	357	1.3	1.74	12.45	0.81	2.72	46	<1	55.3	5.32	415
200982	12.1	3.01	65.4	2.3	1	28.7	0.3	0.35	2.86	0.21	0.88	11	<1	12.7	1.37	215
200985	30.8	7.78	84.6	5.77	2	230	0.7	0.86	10.6	0.44	3.07	142	1	26.7	2.89	224
200986	52.8	14.4	178	8.82	2	219	1.3	1.18	14.6	0.63	2.71	44	<1	37.9	4.26	343
200987	8.86	75.9	5.5	1	164.5	0.4	0.67	5.2	0.33	1.46	14	1	20.7	1.91	603	64.5
200992	88.9	25.3	98.4	11.85	1	86.6	0.6	1.18	11.3	0.47	3.8	10	<1	31.6	3.12	604
200994	57.2	15.75	149	9.3	2	250	1	1.16	14.35	0.59	3.56	49	9	38.6	3.91	355
200996	53.8	14.95	147	8.94	2	294	1.1	1.16	13.35	0.53	3.38	52	<1	36.1	3.76	279
200998	7.41	135.5	3.62	2	726	0.6	0.38	11.15	0.19	5.5	29	1	11.3	1.42	157	70.7
201000	9.4	2.74	167.5	1.65	2	253	0.7	0.29	10.5	0.23	1.76	11	<1	14.2	1.61	112

SAMPLE	Pass2mm	Pass75um	Ba	Ce	Cr	Cs	Dy	Er	Eu	Ga	Gd	Hf	Ho	La	Lu	Nb
	%	%	ppm	ppm	ppm	ppm	ppm	ppm	ppm	ppm	ppm	ppm	ppm	ppm	ppm	ppm
090346			79.4	87	10	2.38	5.37	3.55	0.34	14.9	4.7	6.5	1.14	42.9	0.64	24.9
133123			1190	77.4	10	2.65	3.21	1.68	1.26	17.6	3.82	7.7	0.61	40.4	0.28	11
133124			639	78.6	30	6.22	3.42	2.2	0.71	15.9	3.53	5.3	0.69	37.9	0.37	15.5
133128			289	41.8	30	1.99	2.87	1.6	1.02	18.2	3.46	3.9	0.57	20.5	0.27	5.7
133129			1065	58.5	40	2.57	3.37	1.87	1.25	16.6	3.47	3	0.66	29.4	0.3	9.8
127866M			1035	152.5	130	1.33	3.49	1.86	1.39	17.5	4.67	5.4	0.68	84.4	0.2	12
127867			1425	133.5	<10	0.63	4.78	2.66	1.68	17.8	5.94	6.3	0.96	65.8	0.34	15.9
127868M			985	98.1	10	1.68	2.87	1.73	1.23	17.6	3.86	6.5	0.61	51.4	0.22	8.8
127869			766	126.5	70	2.8	5.07	2.95	1.4	16.8	5.73	6.7	1.09	62.9	0.43	12.5
127870			946	141	100	3.2	5.19	3.18	1.51	19.6	6.24	7.7	1.15	70.6	0.42	14
127871			1215	157	10	2.24	6.29	3.89	1.68	18	7.37	7.9	1.38	73.2	0.59	23.4
127872			2350	69.9	<10	6.16	5	3.8	2.25	17.8	4.58	2.3	1.2	32.9	0.61	52.3
127873			1815	120.5	50	2.47	1.18	0.81	0.89	13.6	2.02	4.4	0.25	64.5	0.17	4.8
127874			1615	76	10	2.6	2.02	1.16	1.11	18.4	2.91	4	0.42	38.7	0.17	8.5
127875			1700	74.6	20	3.12	2.15	1.22	1.12	17.7	2.98	4.3	0.42	39.5	0.16	7.6
127876M			736	131.5	10	2.06	5.2	2.93	1.91	19.8	6.77	7.3	1.08	64.1	0.43	12.5
127877M			909	139.5	50	1.5	4.9	2.32	1.74	21	6.96	8.9	0.89	66	0.28	16.6
127878M			664	92.4	<10	3.31	8.41	5.42	1.62	16.7	7.03	9.1	1.9	34.4	0.73	19
127879M			883	124	60	1.56	5.57	3.13	1.64	18.7	6.36	7.5	1.19	58.1	0.36	14.5
127880			1600	86.1	<10	0.49	2.52	0.66	1.12	13.2	4.32	3.5	0.38	40.3	0.04	3.6
127881			810	92.8	30	0.9	3.46	2.38	1.18	16.8	4.63	6	0.72	44	0.38	12.9
127882M			741	98.1	30	1.6	5.94	4.08	1.04	15.3	5.54	9	1.39	44.9	0.62	10.8
127883			1050	116	<10	3	5.53	3.19	1.62	17.5	6.43	6.7	1.12	58.3	0.4	16.1
127884M			437	104.5	<10	0.86	11.6	6.57	2.31	21.1	12.1	6.4	2.39	43.5	0.92	24.1
127885M			433	50.9	10	1.19	5.46	2.91	1.24	19.9	5.88	3.3	1.11	22	0.33	11.1
127886M			758	66.2	<10	2.39	2.01	1.17	0.92	15.9	2.48	4.6	0.42	31.1	0.14	8
127887			972	90.1	20	2.6	4.37	2.64	1.16	17.6	5.15	6.4	0.96	39.8	0.41	13.5
127888			917	156.5	10	3.75	5.09	2.75	1.91	18	7.36	7.2	0.98	78.2	0.31	11.9
127889			1010	82.3	<10	4.03	4.13	2.44	1.17	16.9	4.93	5.2	0.87	39.8	0.31	11.5
127890			913	96.1	40	1.92	4.46	2.57	1.18	13.8	4.9	5	0.88	44.9	0.33	6.8
127891M			930	123.5	10	4.12	4.6	2.33	1.73	17.6	6.19	9.2	0.95	62.1	0.28	11.5
127892			1270	95.1	<10	0.51	5.08	3.45	2.12	19.6	5.97	9.1	1.1	44.8	0.47	15.2
127893			1780	15.2	10	0.55	0.2	0.15	1.72	13.1	0.33	1.1	0.03	11.4	0.03	1.2
127894M			832	65.8	70	4.76	3.99	2.32	1.42	20.1	5.09	3.7	0.76	30.8	0.36	10
127895M			1140	77.7	20	0.59	1.57	0.77	1.01	15.6	2.89	2.8	0.26	40.7	0.07	3.7
STO131390M			1210	74.2	<10	3.9	4.63	2.76	1.64	19.5	5.45	3.3	0.94	35.5	0.38	10.6
STO131391M			146	110.5	<10	0.9	4.69	2.3	0.46	13.7	5.84	9.3	0.85	52.5	0.35	14.9
STO131392			482	59.9	90	0.43	3.25	1.94	1.08	17.2	3.9	5.9	0.62	30.6	0.24	9.1

SAMPLE	Nd	Pr	Rb	Sm	Sn	Sr	Ta	Tb	Th	Tm	U	V	W	Y	Yb	Zr
	ppm	ppm	ppm	ppm	ppm	ppm	ppm	ppm	ppm	ppm	ppm	ppm	ppm	ppm	ppm	ppm
090346	34.1	9.62	250	5.91	3	33.1	1.5	0.8	19.6	0.59	4.06	12	2	33.3	4.58	220
133123	32.3	8.81	130.5	4.63	1	678	0.7	0.49	7.92	0.28	2.51	51	2	16.9	1.78	307
133124	29.1	8.2	211	4.67	2	294	1	0.56	16.15	0.35	2.96	40	1	21.1	2.42	194
133128	18.8	4.83	34.5	3.51	1	642	0.4	0.41	7.5	0.25	1.67	117	<1	16.6	1.72	149
133129	27.8	6.91	89.2	4.69	1	623	0.7	0.54	4.11	0.29	4.29	81	<1	19.4	2.03	134
127866M	53.1	15.55	88	6.86	2	485	0.4	0.73	11.3	0.25	1.56	86	<1	18.6	1.57	211
127867	51	14.7	98.5	7.87	1	542	1	0.84	7.89	0.42	1.22	63	<1	25.7	2.42	246
127868M	36.3	10.35	119	5.24	1	597	0.2	0.55	8.37	0.25	0.87	120	1	16.9	1.63	242
127869	47.9	13.8	111.5	7.39	2	180.5	0.7	0.89	16.15	0.43	2.93	61	1	29.8	3.01	244
127870	53.9	15.4	146.5	8.46	3	214	0.6	0.92	17.35	0.44	2.42	78	<1	29.8	3.12	259
127871	61.6	17.4	145.5	9.45	2	346	1.4	1.14	13	0.64	3	50	<1	40.4	4.16	333
127872	30.2	8.08	139	5.34	3	737	6.4	0.74	13.2	0.65	12.15	24	1	40.5	4.51	83
127873	35.3	11.4	119	3.92	<1	592	0.6	0.23	28.1	0.15	8.14	18	1	7.8	1.07	145
127874	30.9	8.8	72.7	4.17	1	1275	0.6	0.36	4.49	0.18	1.32	45	2	12.6	1.38	164
127875	28.9	8.26	88	4.55	1	1005	0.3	0.43	4.88	0.17	1.5	50	1	12	1.08	185
127876M	54	14.95	95.8	8.69	2	609	0.6	0.96	11.5	0.44	1.54	99	1	29.1	2.81	279
127877M	58.4	16.05	128	8.98	3	567	0.6	0.9	16.9	0.34	0.75	99	<1	23.6	1.99	334
127878M	37.8	10.05	144.5	7.92	3	222	1.5	1.27	11.1	0.84	2.36	44	<1	50.2	5.36	356
127879M	50.2	13.95	117.5	8.39	2	303	0.6	0.99	17.4	0.45	2.18	85	1	30	2.8	276
127880	32.7	9.35	125	5.22	<1	356	0.2	0.48	20.5	0.08	0.7	18	<1	9.7	0.45	117
127881	38.8	10.55	164	6.55	1	202	0.3	0.63	14.75	0.35	0.79	67	<1	20.6	2.64	211
127882M	38.9	11	62.2	6.98	3	278	0.7	0.93	18.25	0.64	1.38	41	1	40.1	4.2	366
127883	45.3	12.6	123	7.1	1	321	0.8	1	10.95	0.46	1.03	48	1	30.4	2.94	274
127884M	55.8	13.5	63.7	12.1	3	280	1.5	1.9	6.69	1.02	0.87	164	1	63.5	6.16	250
127885M	28.4	6.69	91.8	6.53	2	466	0.4	0.92	1.47	0.43	0.3	79	<1	30.9	2.51	122
127886M	23.6	7.01	110.5	3.71	1	378	0.5	0.35	9.14	0.18	1.83	42	1	11.4	1.18	166
127887	37.2	10.6	127.5	6.33	2	323	0.9	0.7	10.75	0.42	3.18	34	2	27.3	2.79	238
127888	60.5	17	133	8.91	2	268	0.6	0.9	23	0.35	1.85	84	1	27	2.25	284
127889	34.3	9.52	160	6.13	2	533	0.8	0.76	12.15	0.36	4.24	83	1	24.8	2.25	207
127890	39	10.7	115.5	6.25	1	246	0.4	0.77	14.75	0.4	1.99	26	<1	26.4	2.52	181
127891M	49.7	13.7	137.5	7.73	2	262	0.5	0.87	18.15	0.35	1.76	85	1	25.1	2.1	332
127892	43	11.5	70.4	6.88	<1	206	0.6	0.89	0.99	0.51	0.47	70	<1	33	3.14	400
127893	3.6	1.25	109	0.39	<1	183	0.1	0.01	1.76	0.02	0.5	<5	<1	2	0.24	38
127894M	30.7	7.9	110	5.81	1	806	0.7	0.66	9.91	0.34	2.94	161	<1	23.9	2.31	133
127895M	28.6	8.4	78.3	4.13	1	516	<0.1	0.31	7.35	0.08	0.3	26	<1	9.1	0.65	110
STO131390M	35.6	9.13	116.5	6.49	2	727	0.6	0.79	7.14	0.4	2.97	107	<1	27.4	2.67	120
STO131391M	43.7	12.7	200	7.79	2	76.3	0.4	0.81	19.3	0.35	1.55	6	<1	23.6	2.56	290
STO131392	25.6	6.85	66.3	4.69	2	500	0.6	0.51	10.9	0.26	2.57	96	<1	19.7	1.81	223

7.2 Appendix D - Zircon geochronology

D1: BS-images and zircon on tape

127886L
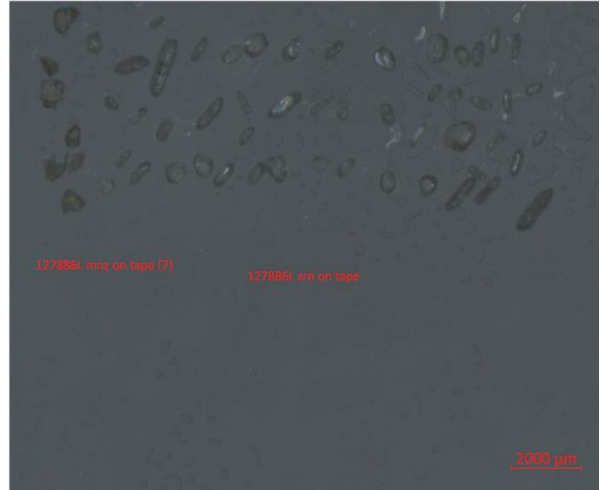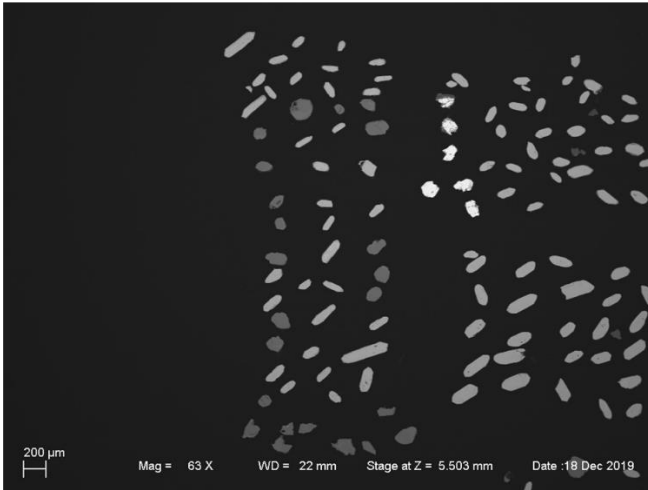
127876L
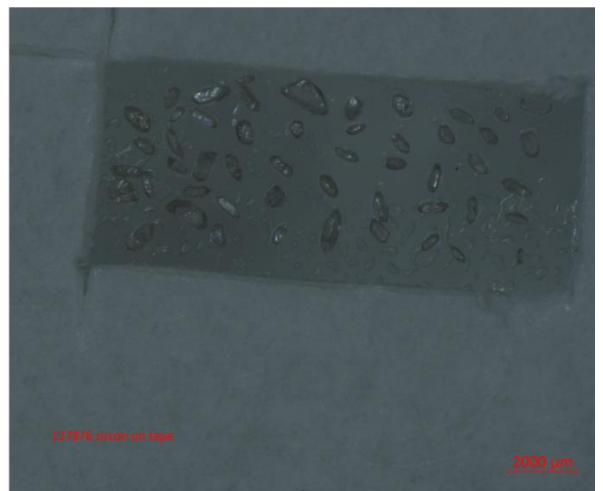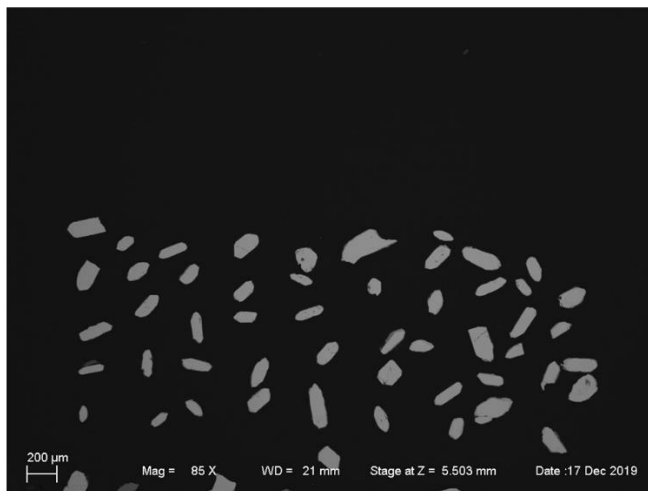
127868L
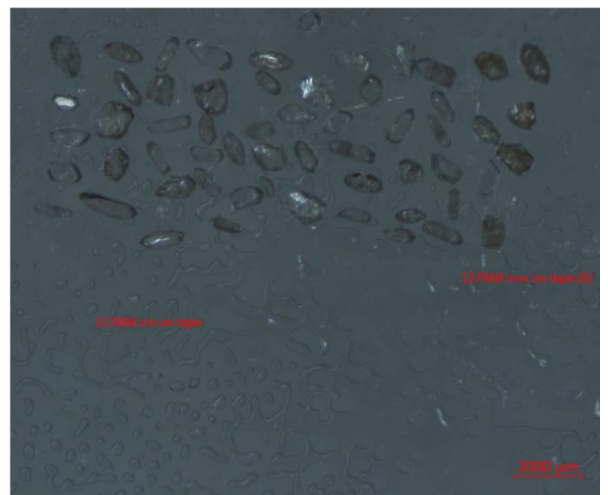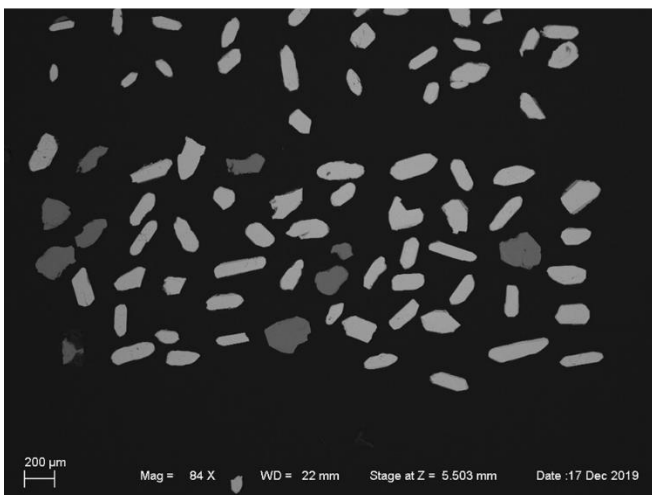
127882L

127878L

127885L

148
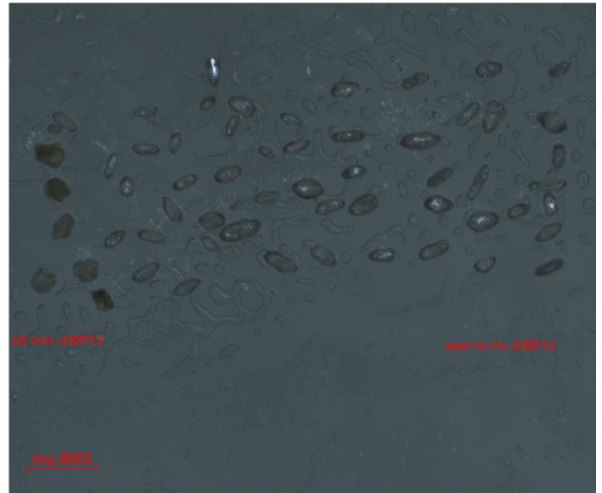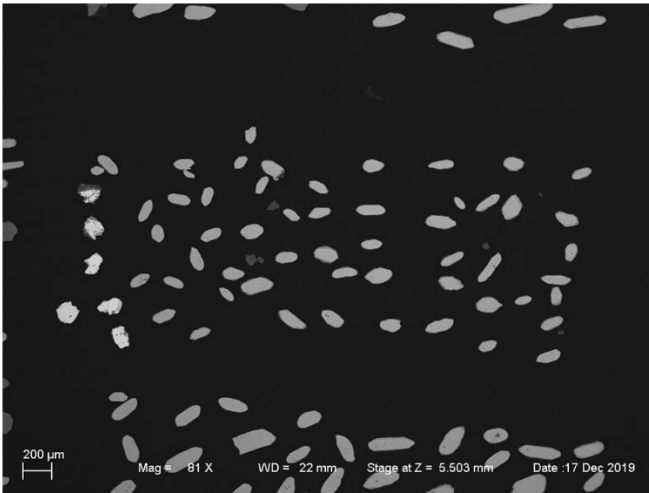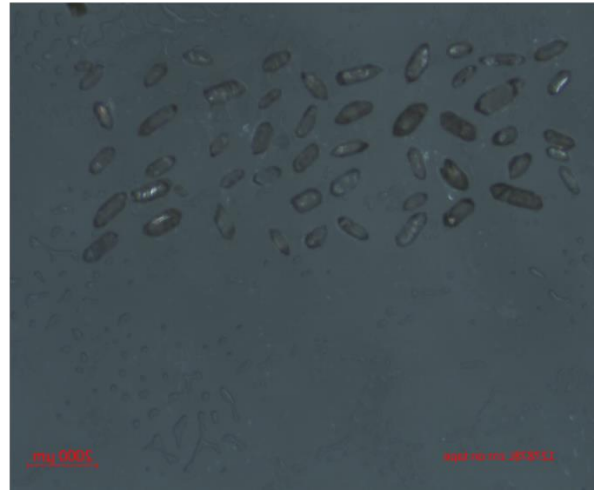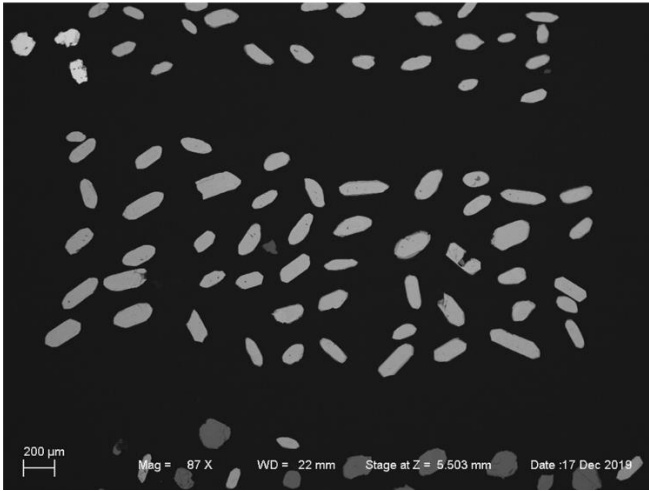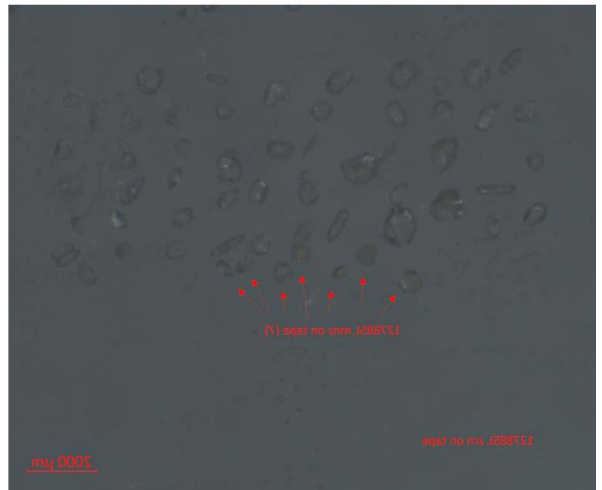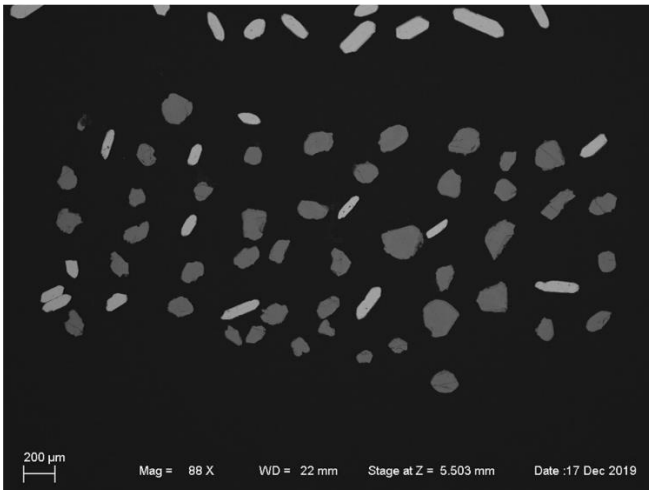
127877L
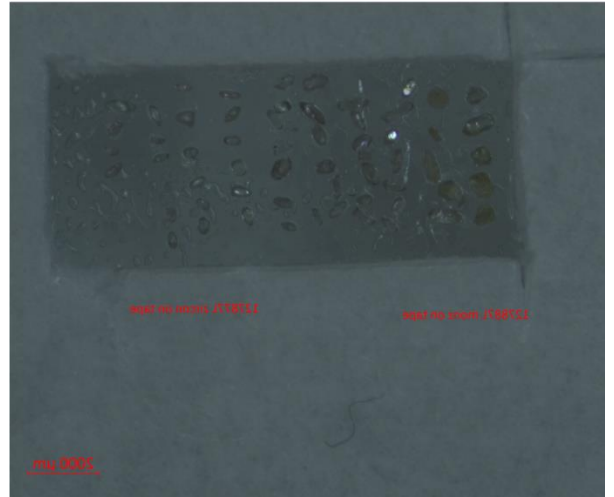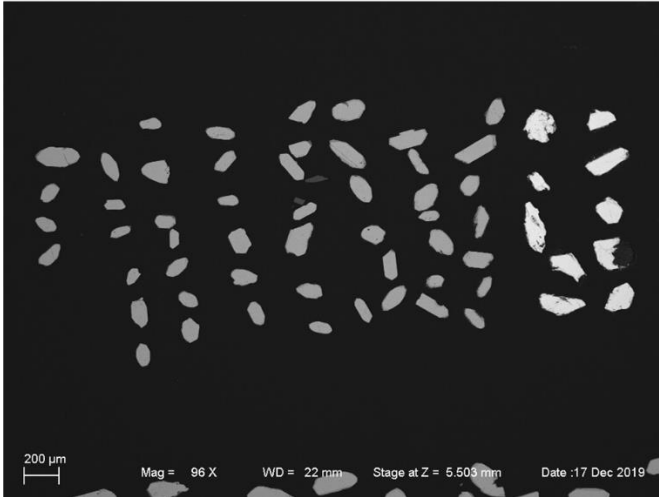
127866L
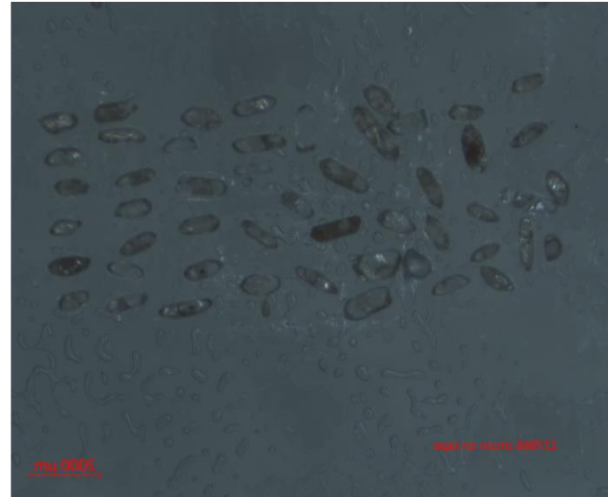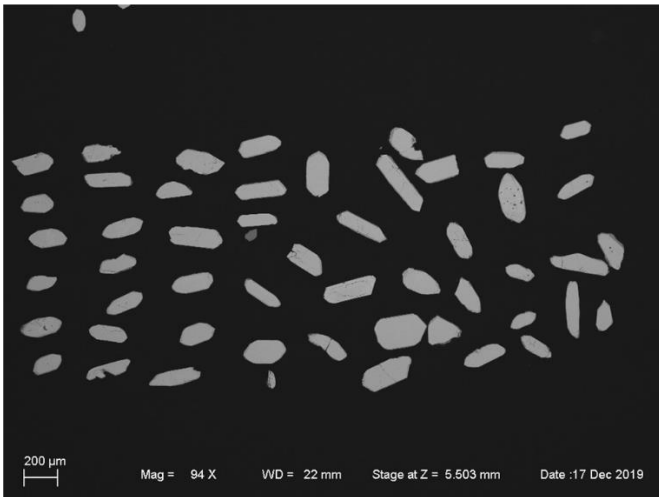
127884B
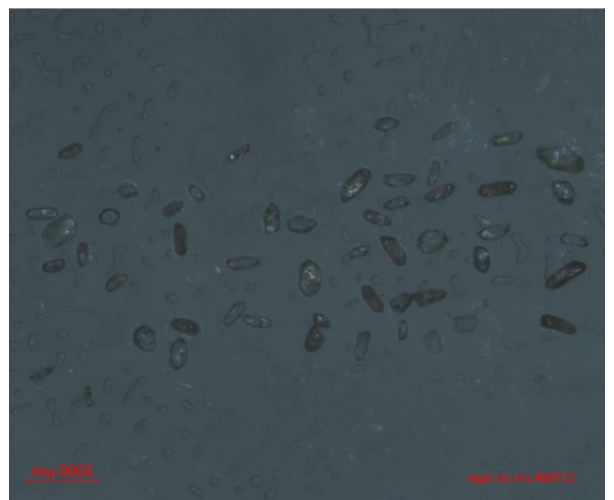
127879L
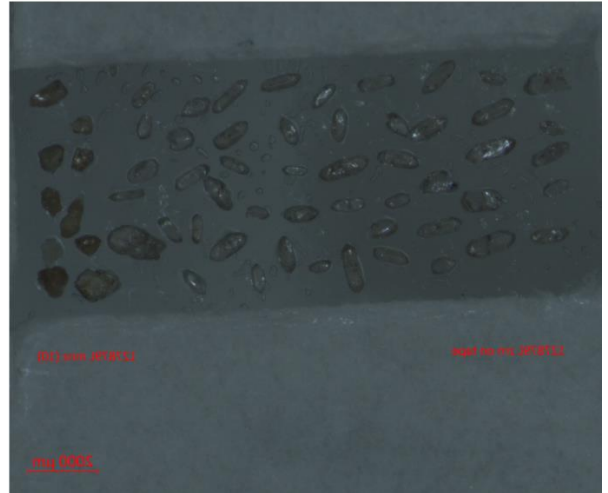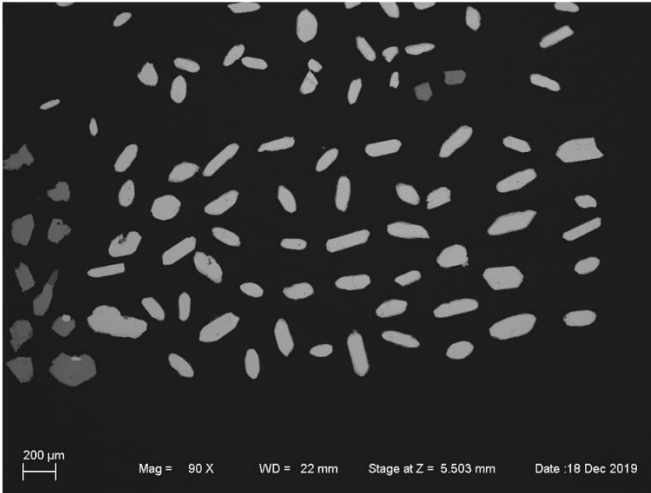
197555
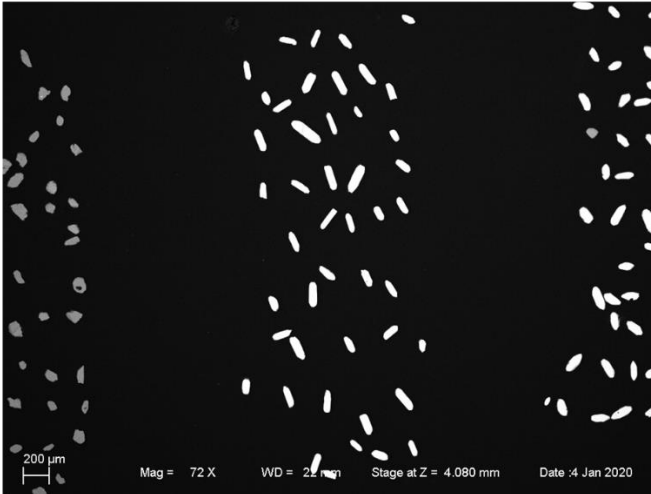
197586
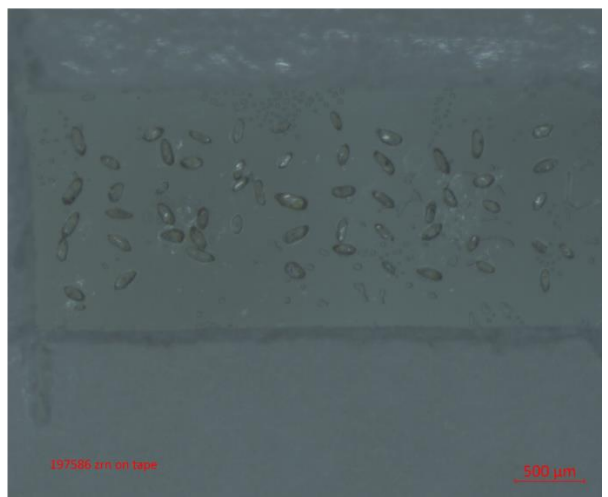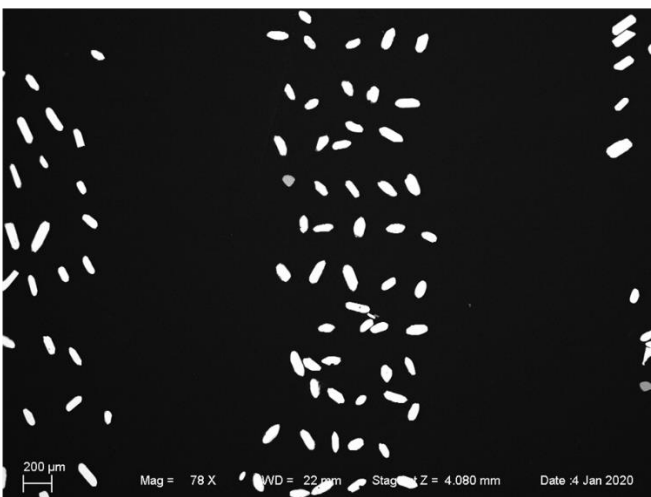
200987

197578

127891L

151
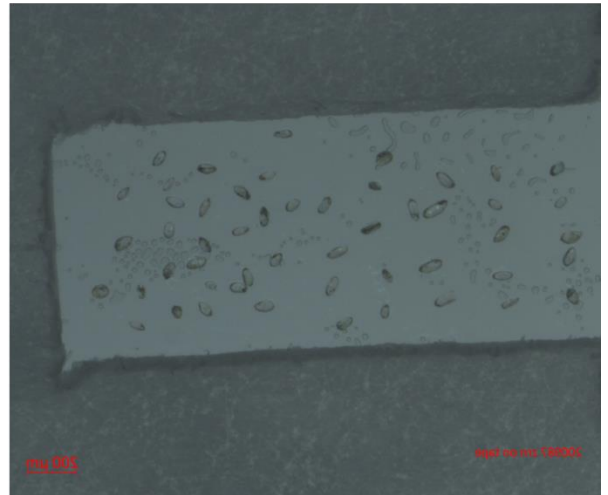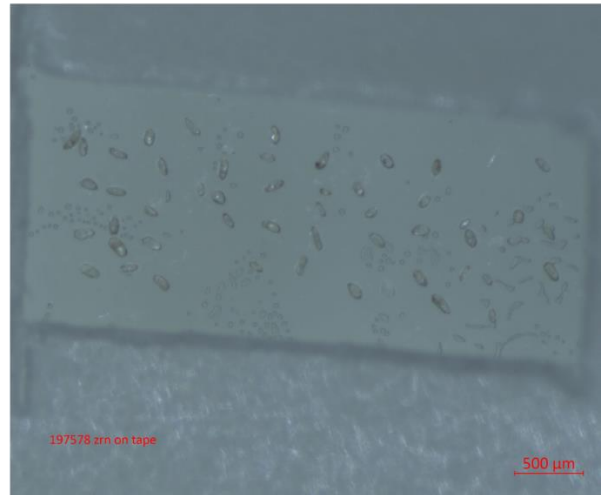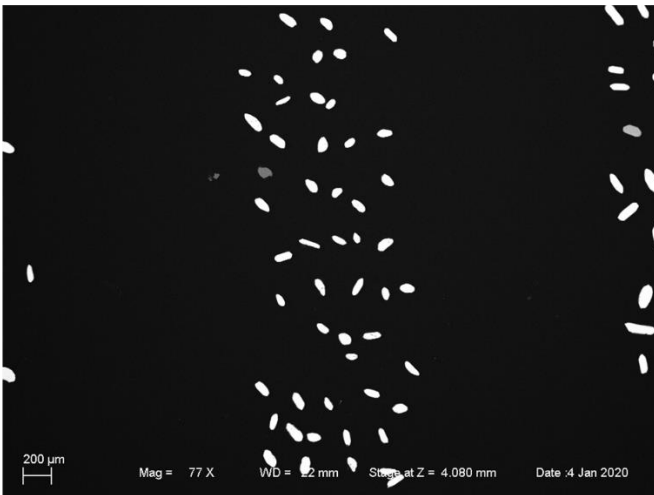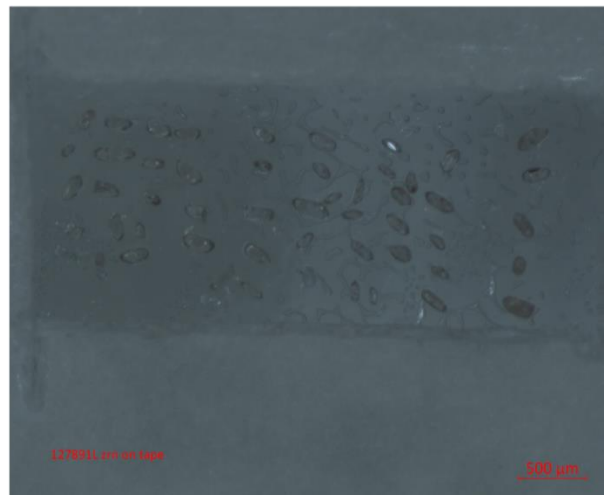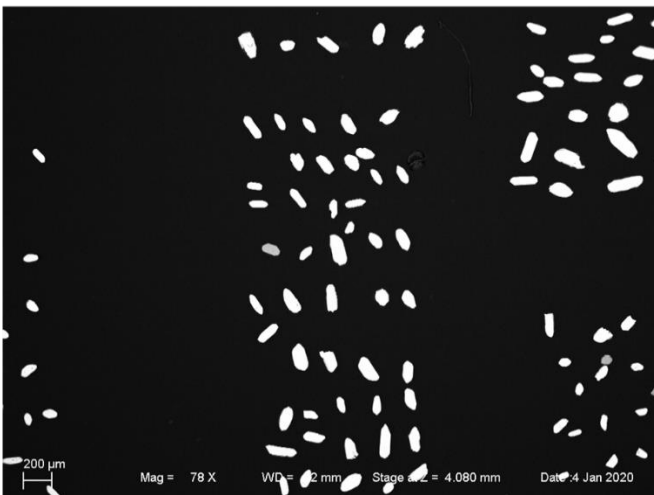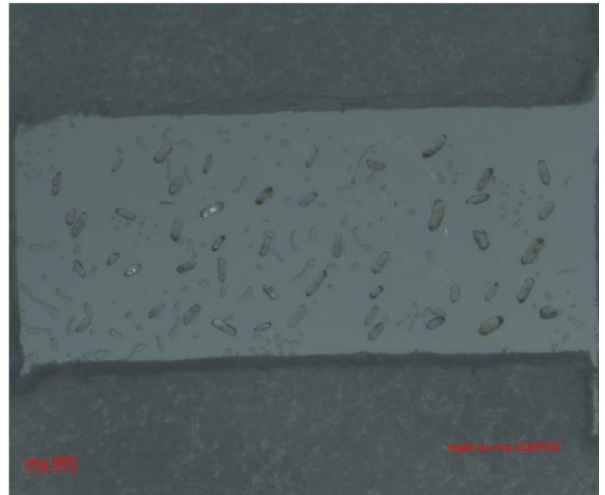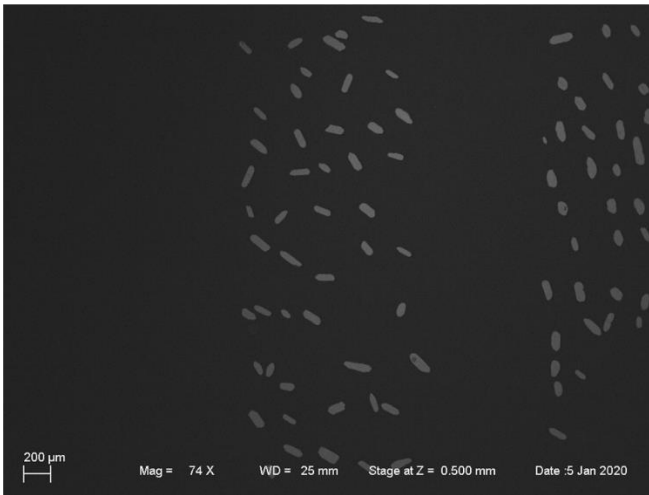
197562L

197562
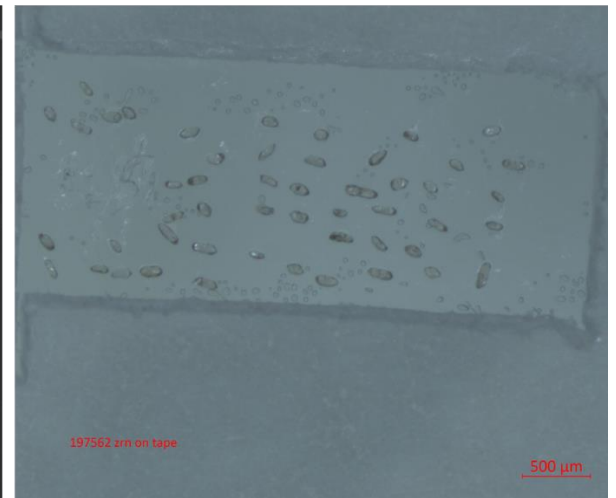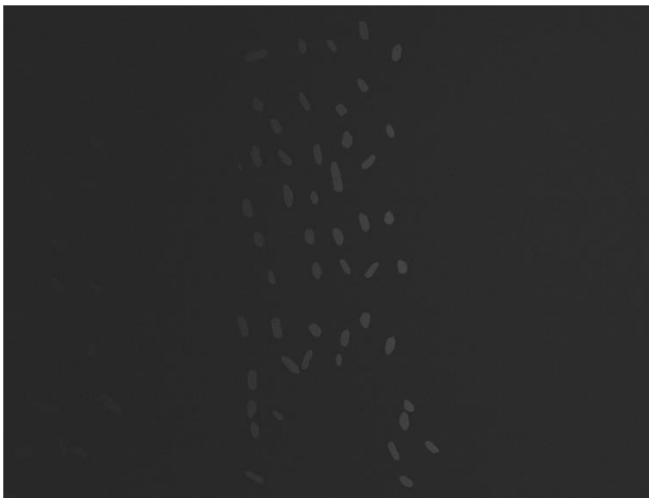
200987L
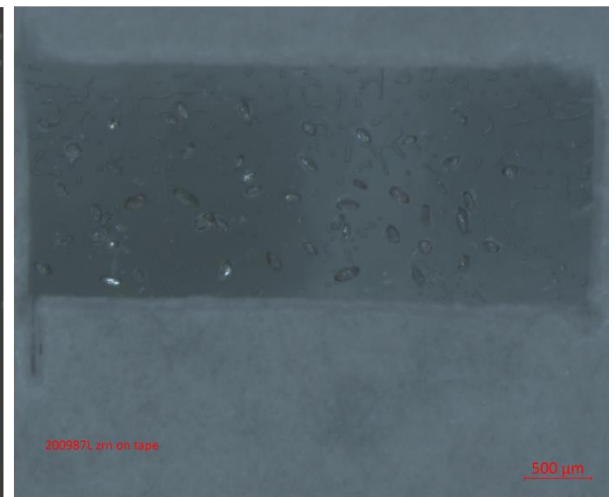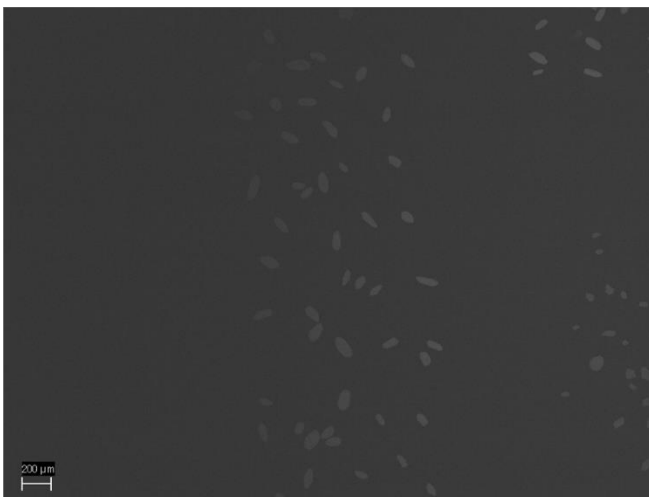
STO 131391L
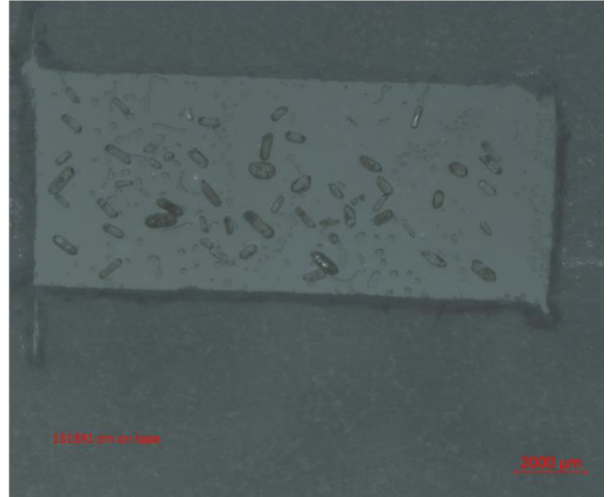
STO 131390L

127895L

153
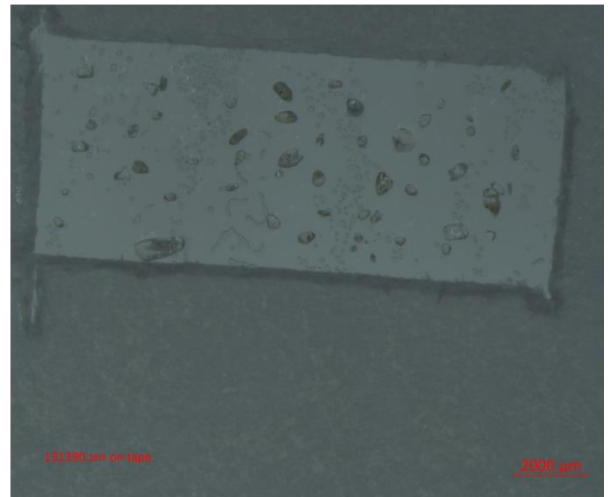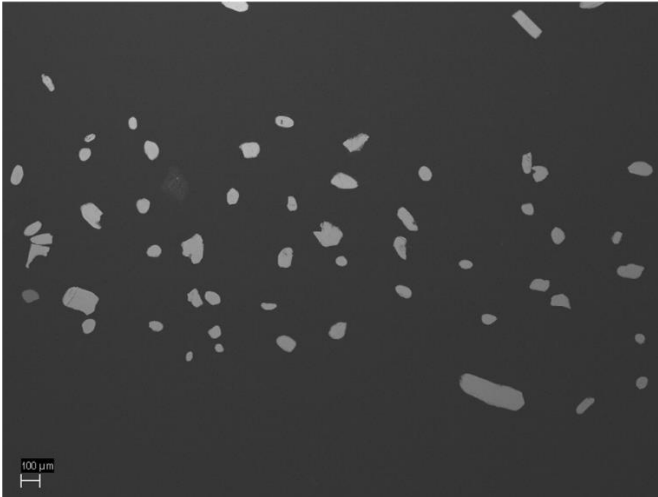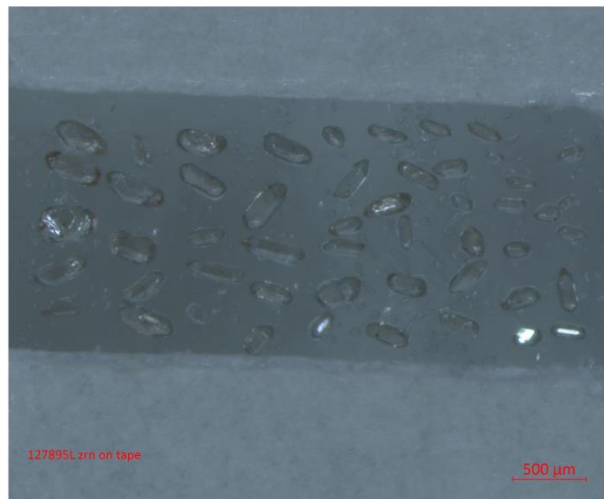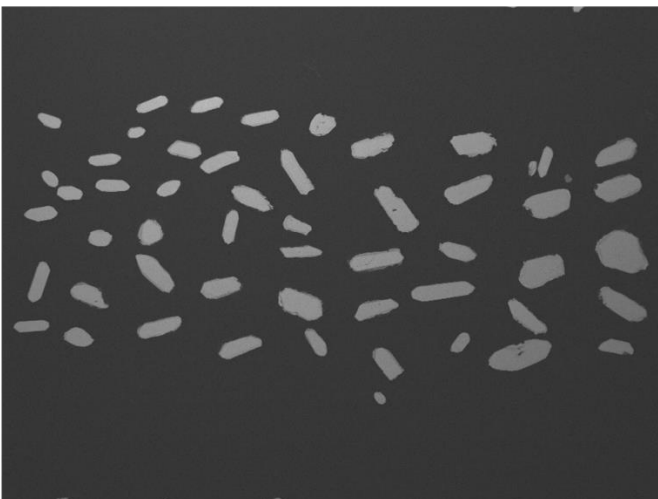
127894L
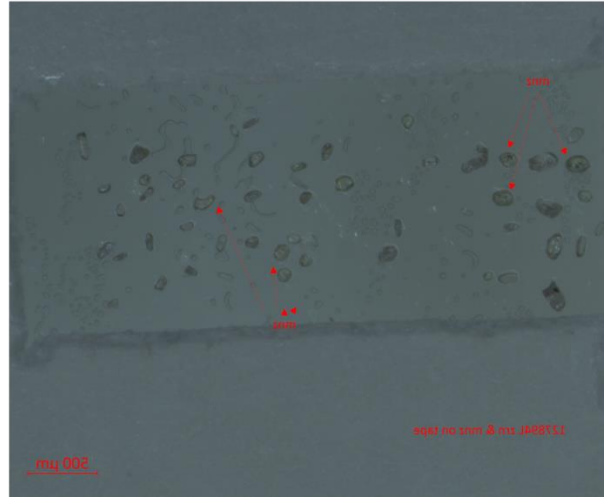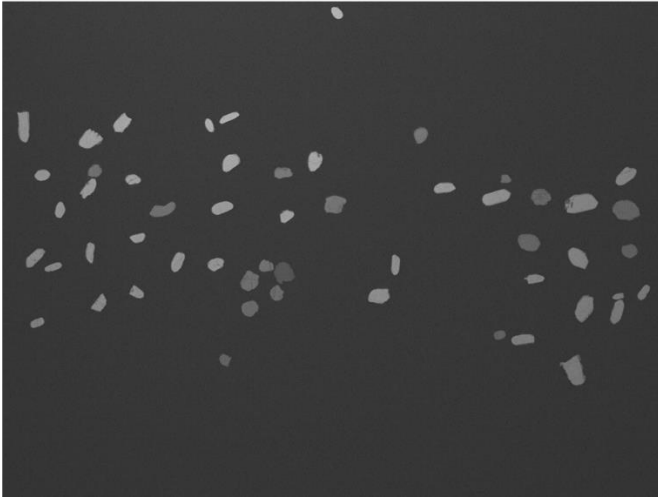
200998
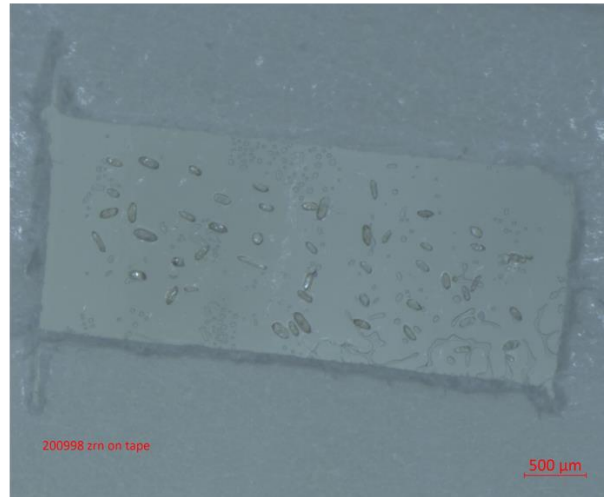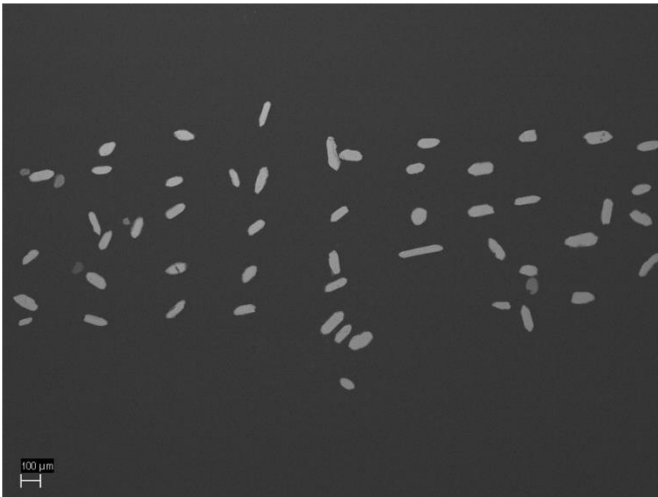
197578L
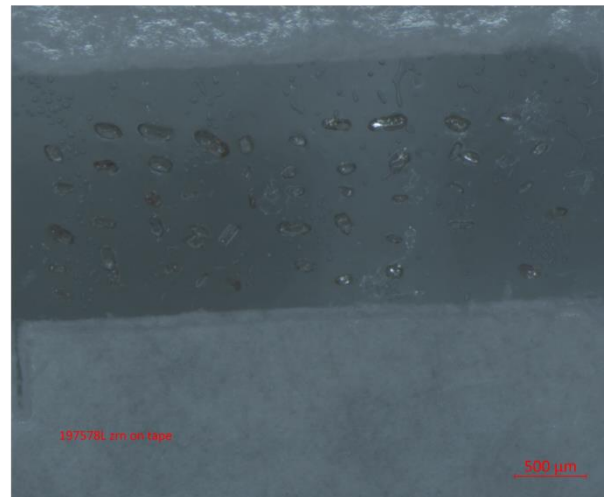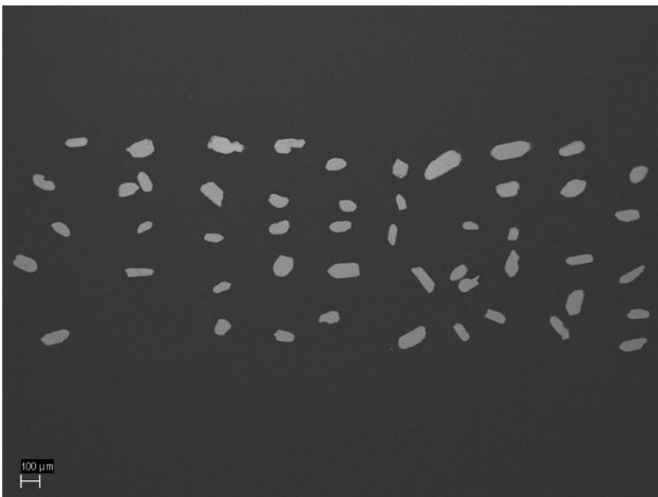
D2: CL-images with laser spots

Sample: 197555

Mount: WGR18_GB_2

Sample: STO 131390L

Mount: WGR18_GB_2

131390L _24
131390L _23
131390L _22
131390L _18
131390L _20
131390L _19
131390L _17
131390L _21
131390L _16
131390L _15
131390L _11
131390L _13
131390L _10
131390L _12
131390L _14
131390L _09
131390L _06
131390L _08
131390L _07
131390L _05
131390L _04
131390L _03
131390L _01
131390L _02

1 mm

Magnification | Accelerating Voltage | Working Distance | Horizontal Field Width
300 x | 15 kV | 25.3 mm | 4.4 mm

Sample: 197586

Mount: WGR18_GB_2

197586_01
197586_02
197586_03
197586_01
197586_05
197586_06
197586_07
197586_08
197586_12
197586_09
197586_11
197586_10
197586_13
197586_14
197586_15
197586_16
197586_18
197586_17
197586_19
197586_20
197586_21
197586_23
197586_22
197586_24
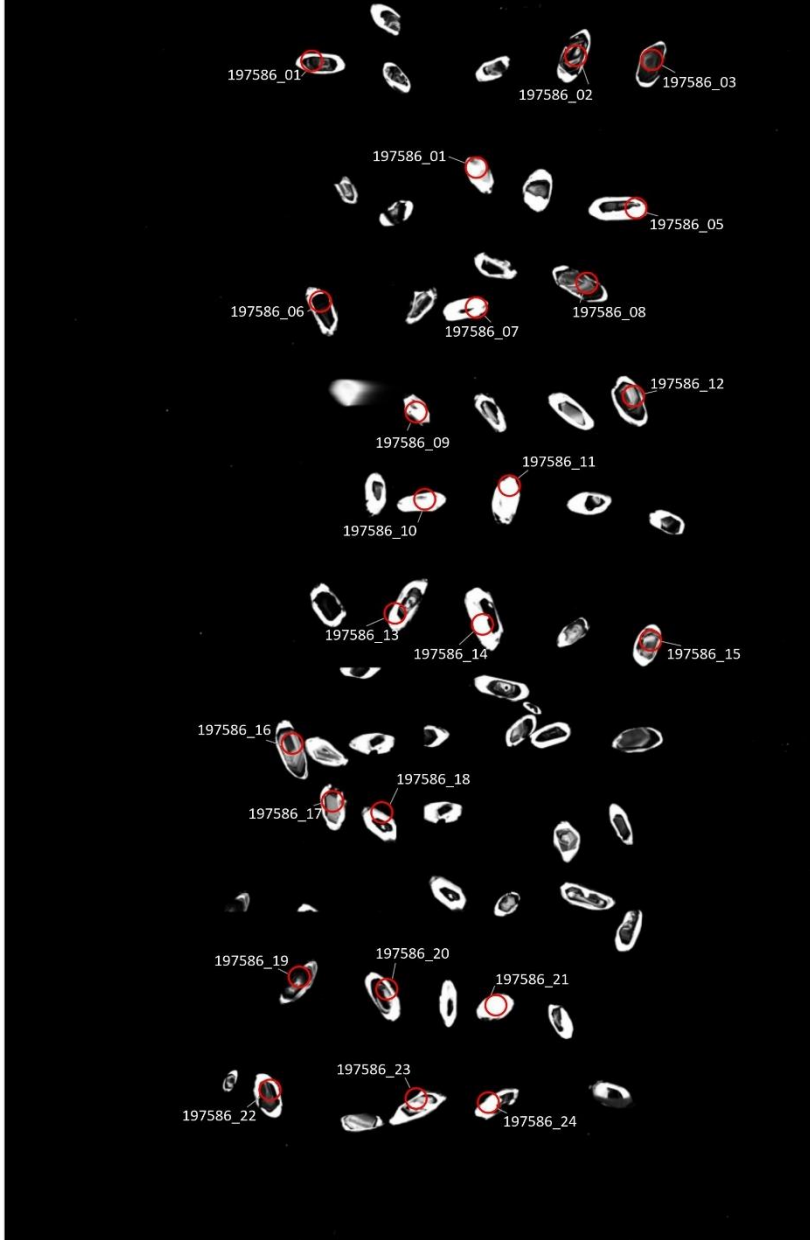
| Magnification | Accelerating Voltage | |
| 300 x | 20 kV | —500 μm— |

Sample: 200987

Mount: WGR18_GB_2

200987_02
200987_01
200987_03
200987_05
200987_04
200987_06
200987_07
200987_08
200987_09
200987_10
200987_11
200987_12
200987_13
200987_14
200987_15
200987_16
200987_17
200987_18
200987_20
200987_19
200987_21
200987_22
200987_23
200987_24
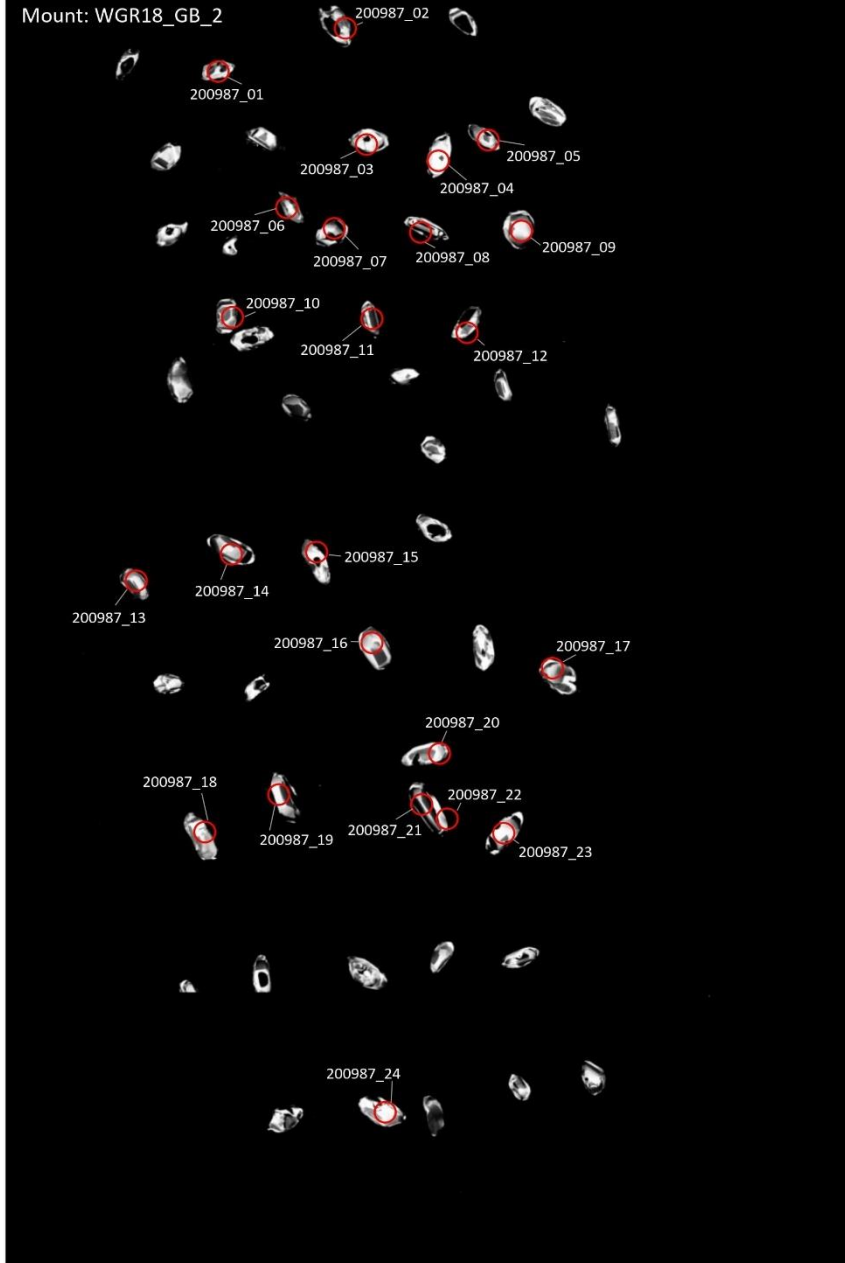
Magnification	Accelerating Voltage	
300 x	20 kV	—500 µm—

Sample: 197578

Mount: WGR18_GB_2
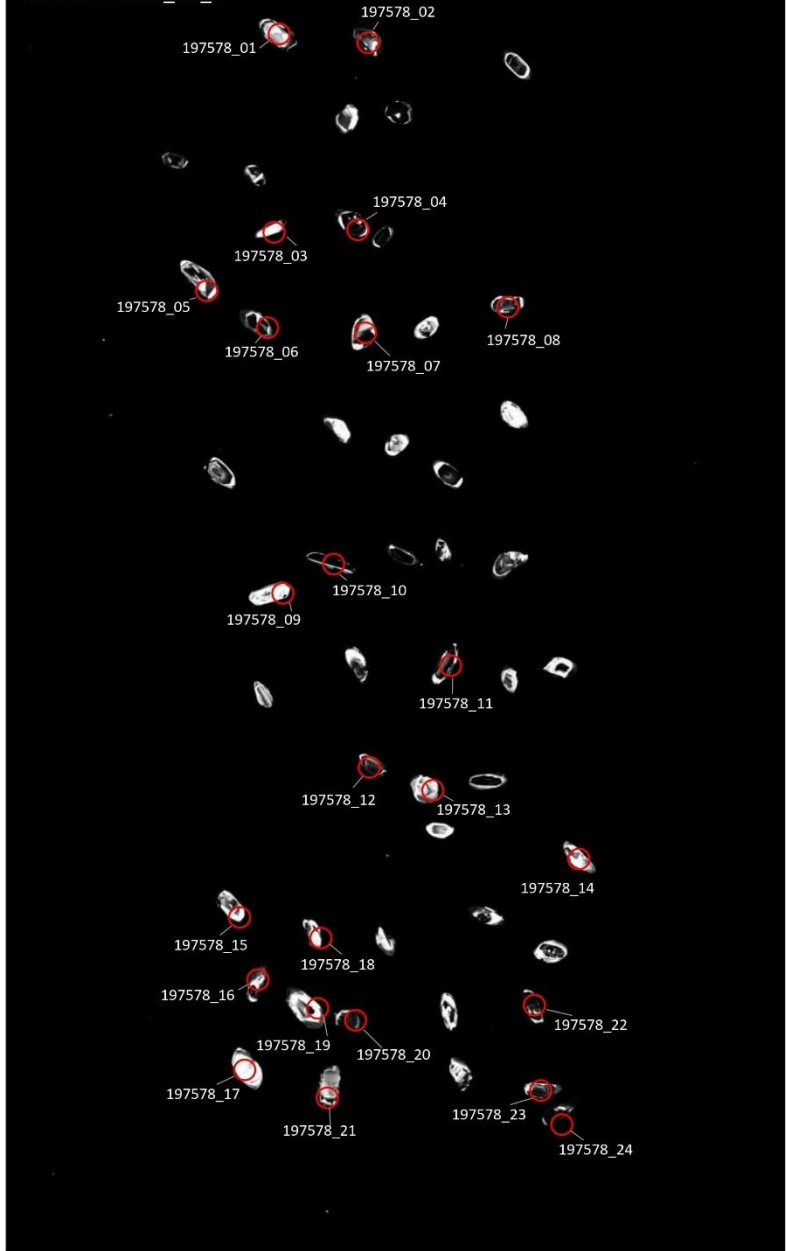
Sample: 127891L

Mount: WGR18_GB_2

127891L_01
127891L_02
127891L_04
127891L_06
127891L_03
127891L_05
127891L_09
127891L_10
127891L_07
127891L_08
127891L_11
127891L_12
127891L_13
127891L_16
127891L_14
127891L_15
127891L_19
127891L_17
127891L_20
127891L_18
127891L_21
127891L_22
127891L_23
127891L_24

Magnification
300 x   —500 µm—
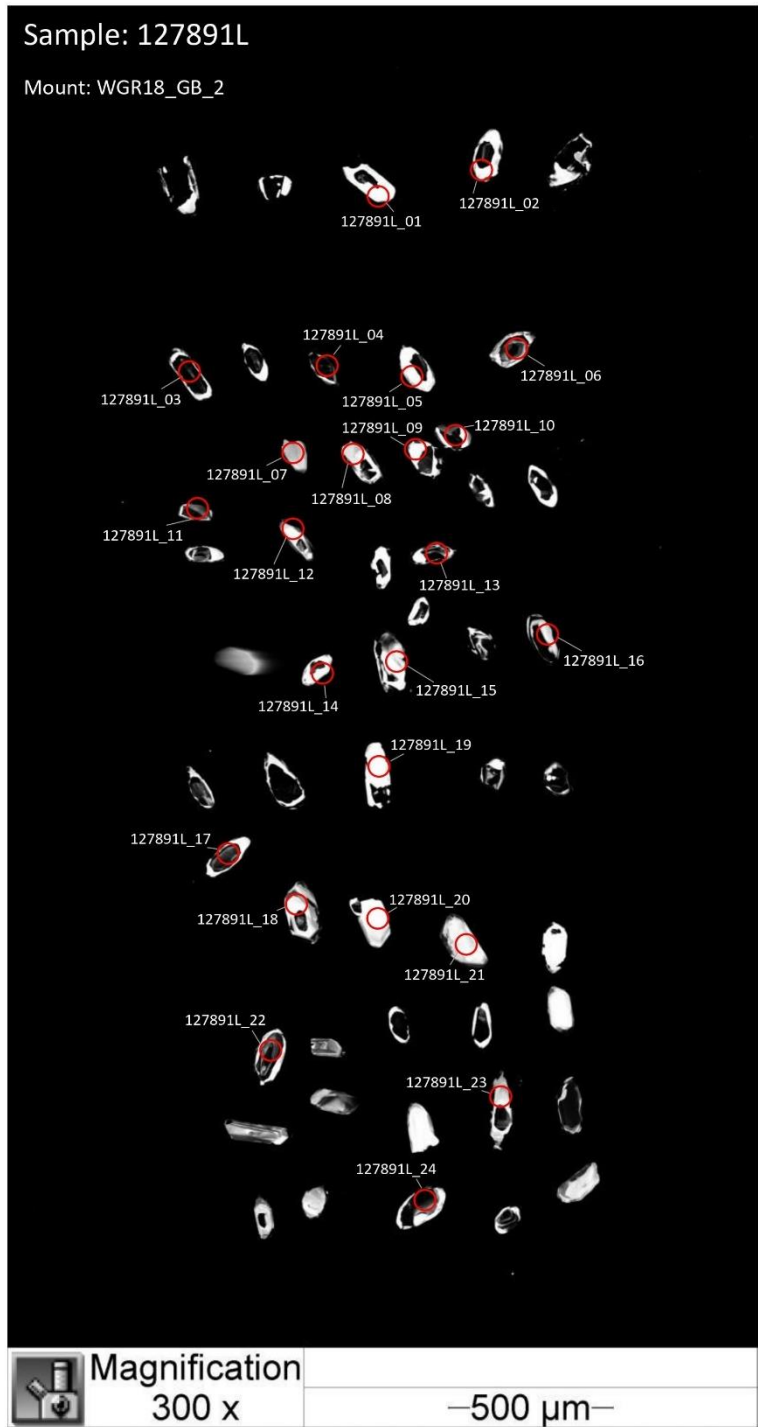
Sample: 197562L

Mount: WGR18_GB_2

Magnification 300 x | Working Distance 25 mm | —500 µm—

Sample: 197562

Mount: WGR18_GB_2

197562_01
197562_04
197562_06
197562_05
197562_03
197562_02
197562_12
197562_07
197562_10
197562_11
197562_08
197562_09
197562_14
197562_13
197562_16
197562_15
197562_20
197562_19
197562_17
197562_18
197562_21
197562_22
197562_24
197562_23
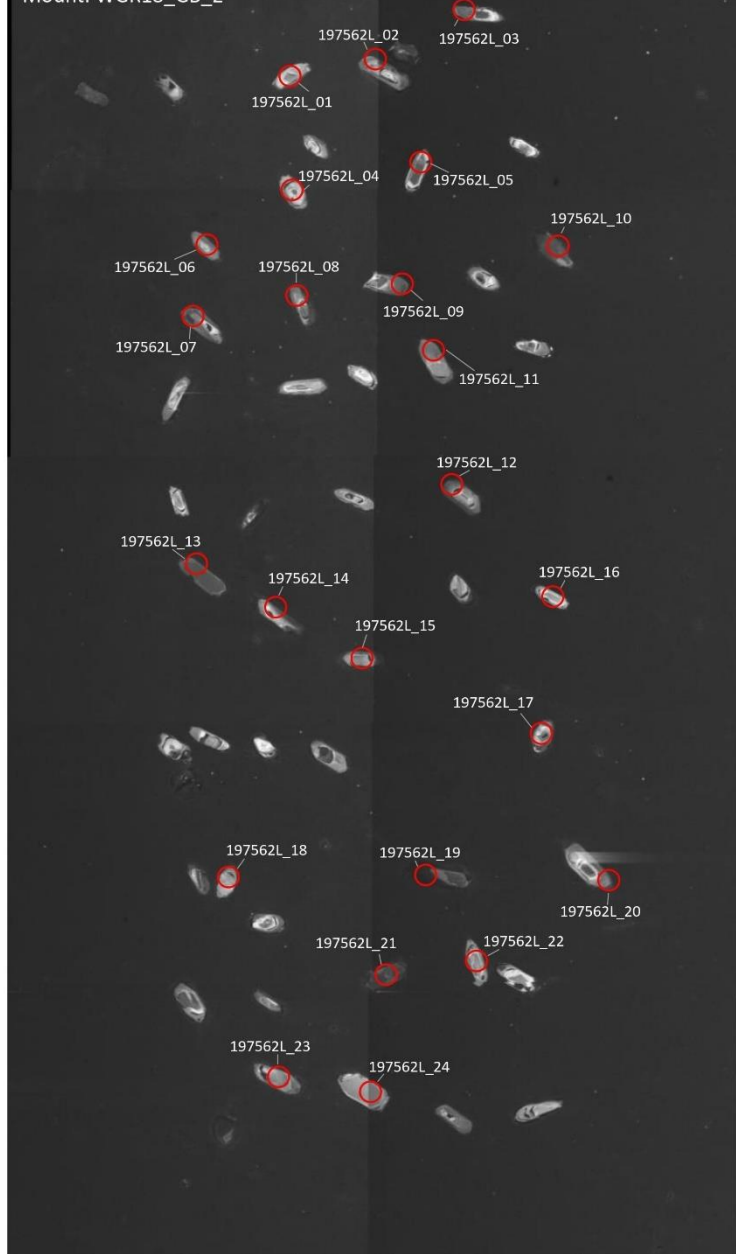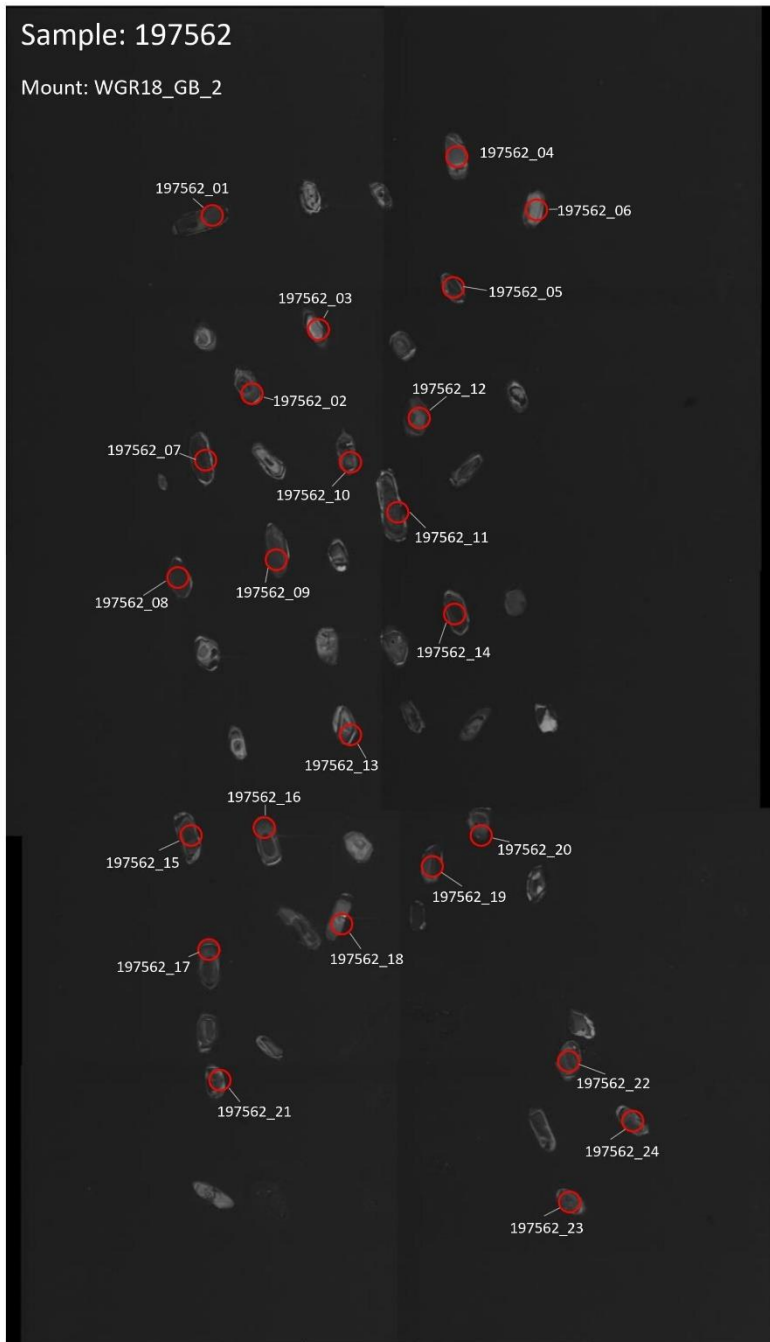
Magnification	Working Distance	
300 x	25 mm	—500 µm—

Sample: 200987L

Mount: WGR18_GB_2

Magnification 300 x | Working Distance 25.2 mm | —500 µm—

163
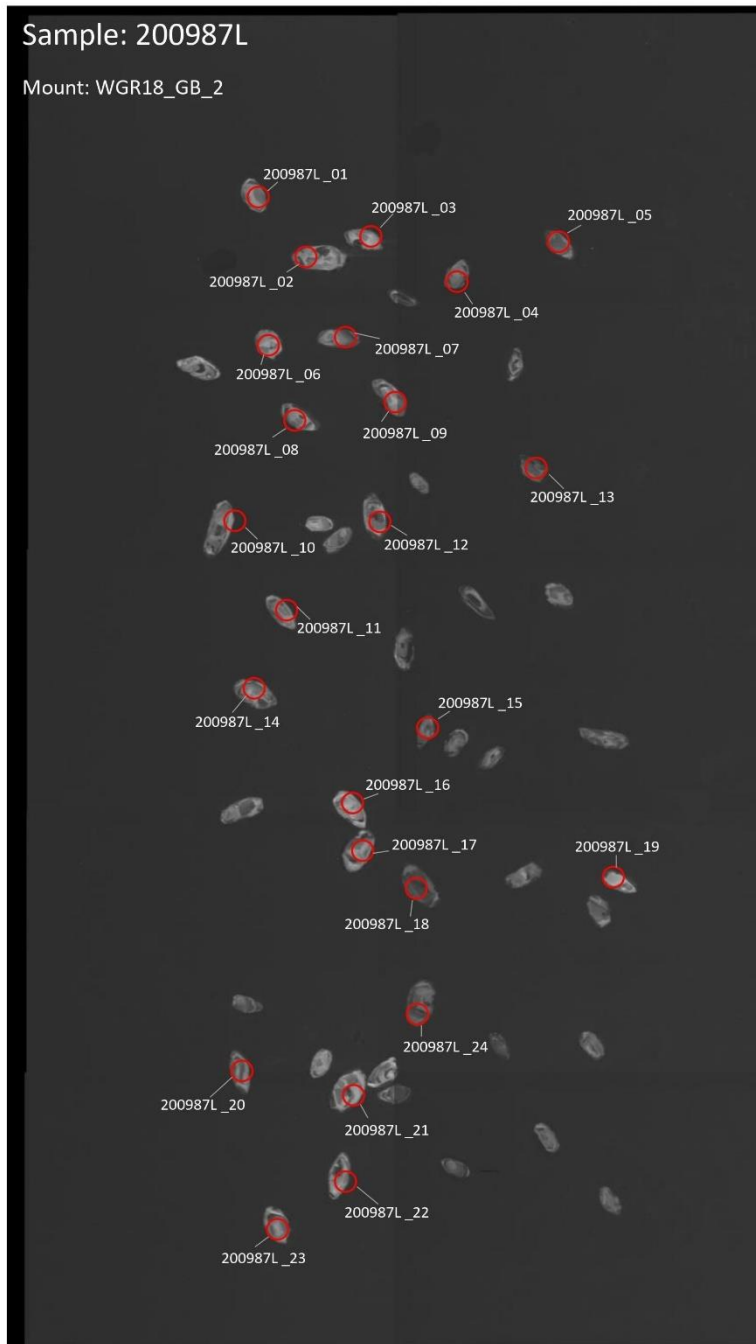
Sample: STO 131391L

Mount: WGR18_GB_2

131391L _24
131391L _23
131391L _21
131391L _22
131391L _20
131391L _17
131391L _18
131391L _19
131391L _16
131391L _14
131391L _13
131391L _15
131391L _11
131391L _12
131391L _10
131391L _09
131391L _08
131391L _06
131391L _07
131391L _05
131391L _03
131391L _04
131391L _01
131391L _02

1 mm

Magnification | Accelerating Voltage | Working Distance | Horizontal Field Width
300 x | 15 kV | 25.3 mm | 4.4 mm

Sample: 127895L

Mount: WGR18_GB_2
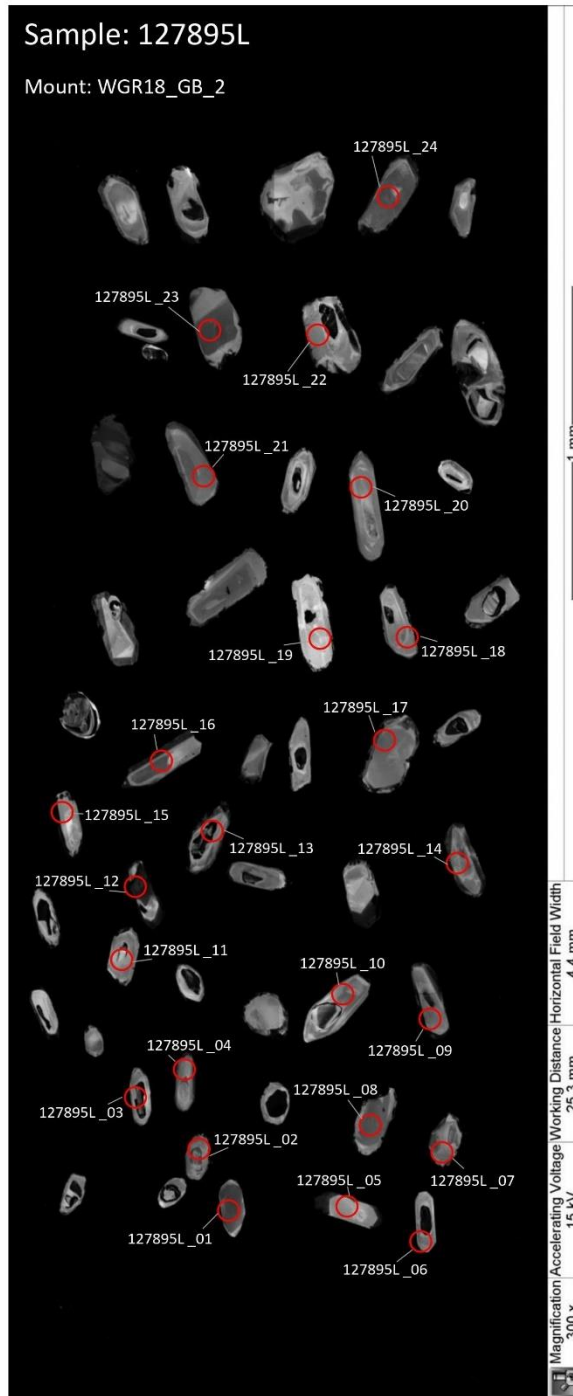
Sample: 127894L

Mount: WGR18_GB_2
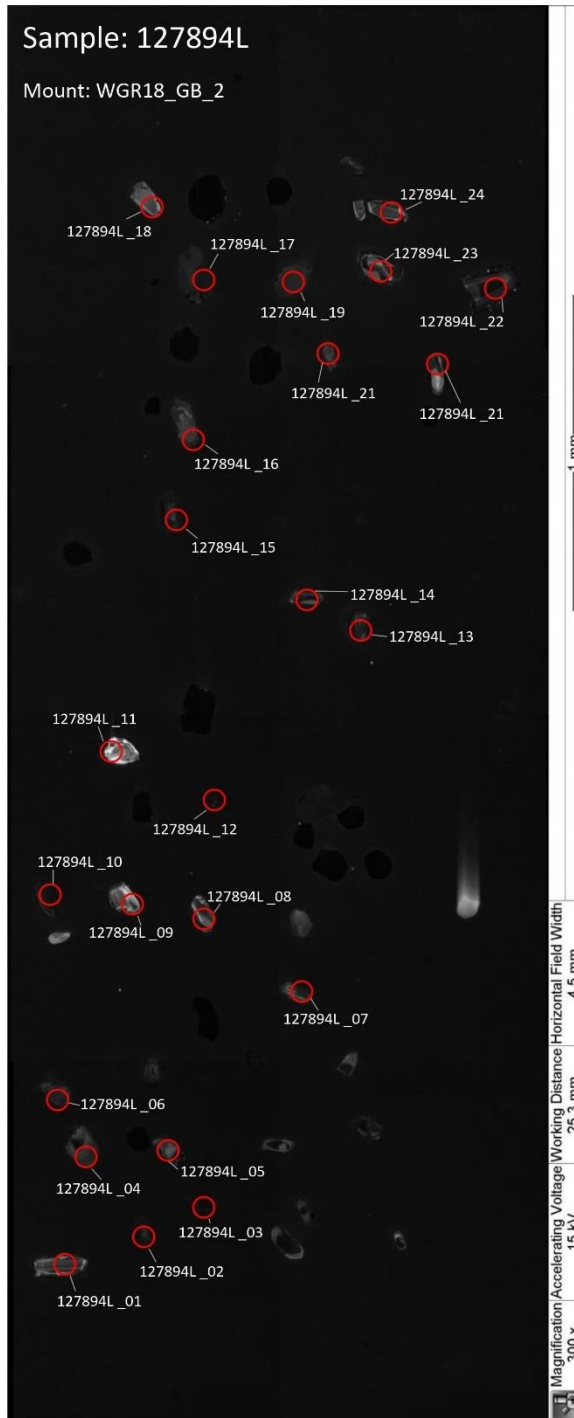
Sample: 200998

Mount: WGR18_GB_2
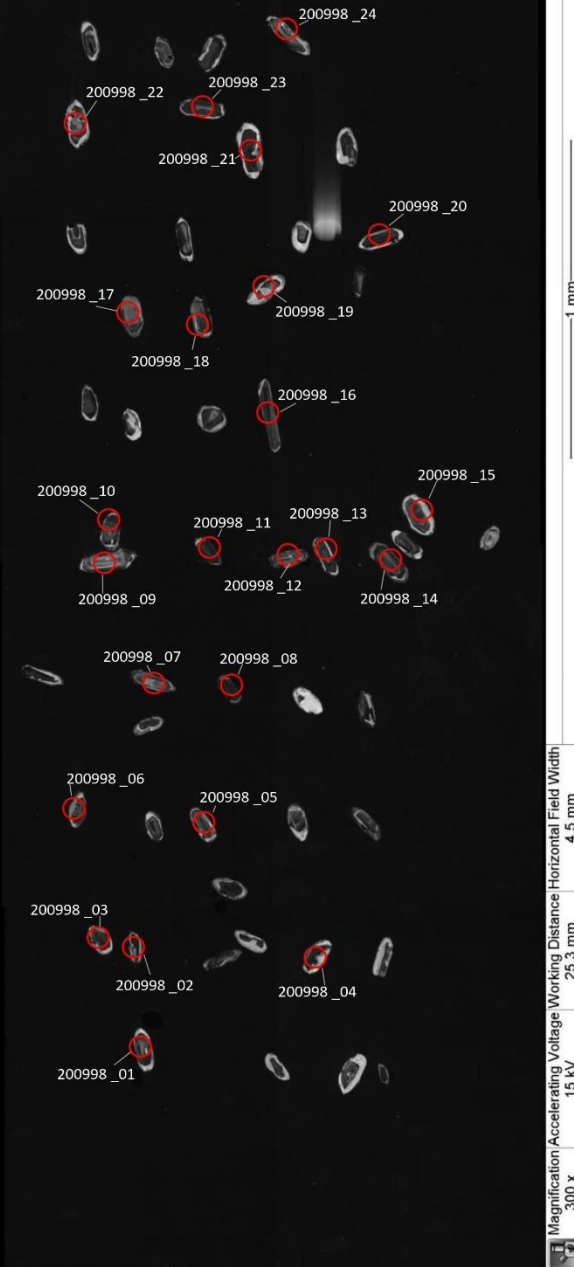
Sample: 197578L

Mount: WGR18_GB_2

Sample: 127886L

Mount: WGR18_GB_1

Magnification	Working Distance	
300 x	21.8 mm	—500 μm—
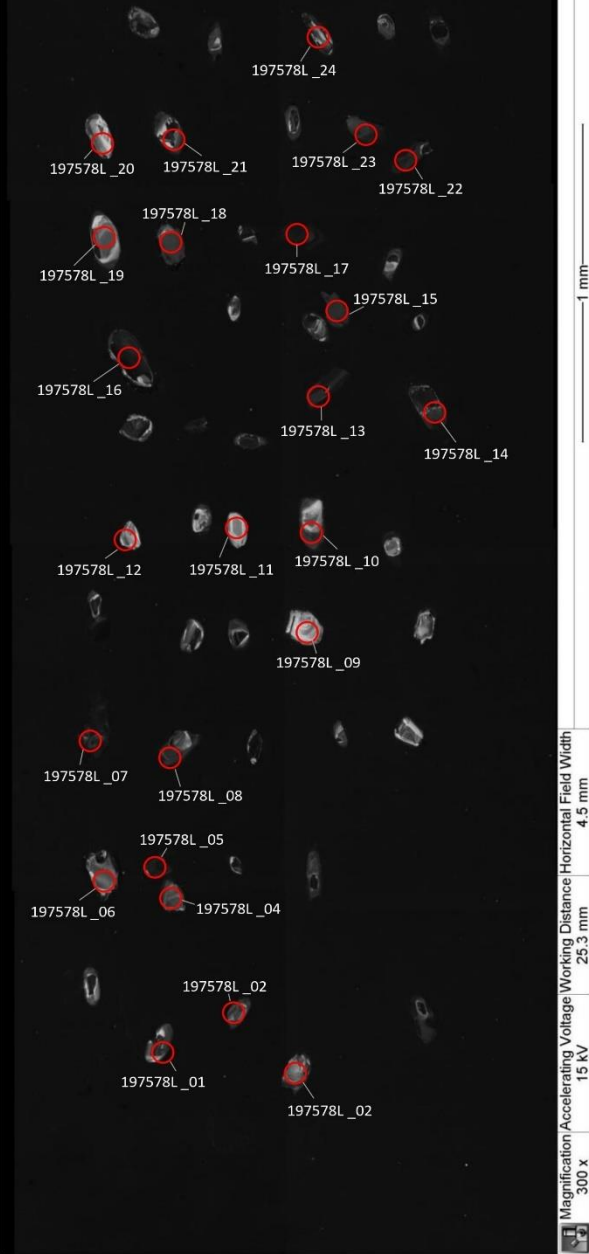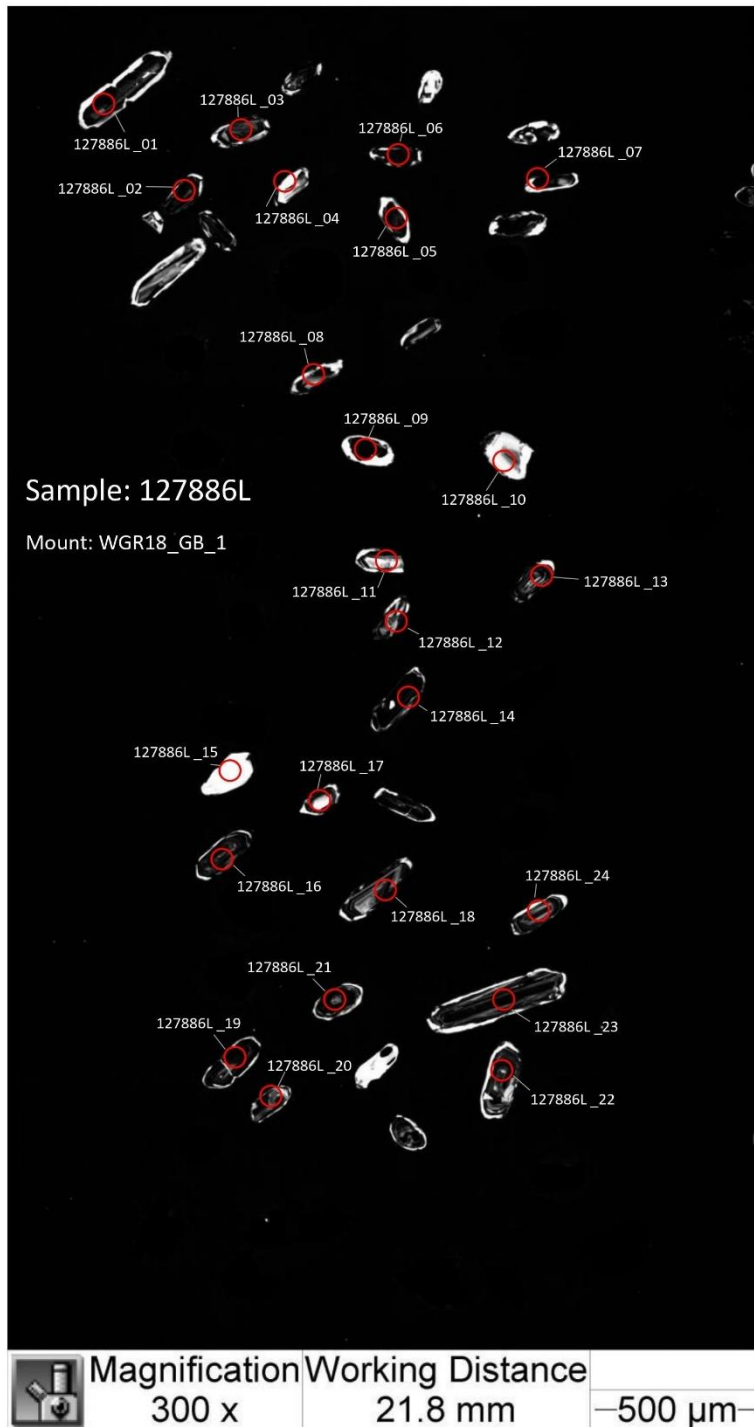
Sample: 127876L

Mount: WGR18_GB_1

127876L _23   127876L _24
127876L _18   127876L _19
127876L _20
127876L _22
127876L _21
127876L _17   127876L _16
127876L _14
127876L _15
127876L _13
127876L _12
127876L _11
127876L _10   127876L _09
127876L _08
127876L _07
127876L _06
127876L _01   127876L _04
127876L _05
127876L _02   127876L _03

Magnification | Accelerating Voltage | Working Distance | Horizontal Field Width
300 x | 20 kV | 21.2 mm | 4.5 mm

1 mm

170

Sample: 127868L

Mount: WGR18_GB_1

127868L_24
127868L_23
127868L_21
127868L_20
127868L_22
127868L_18
127868L_19
127868L_17
127868L_15
127868L_16
127868L_13
127868L_12
127868L_10
127868L_02
127868L_14
127868L_08
127868L_11
127868L_09
127868L_06
127868L_01
127868L_04
127868L_07
127868L_05
127868L_03

Magnification | Accelerating Voltage | Working Distance | Horizontal Field Width
300 x | 20 kV | 21.8 mm | 4.2 mm

1 mm

Sample: 127882L

Mount: WGR18_GB_1

127882L_24
127882L_22
127882L_23
127882L_21
127882L_20
127882L_19
127882L_18
127882L_16
127882L_17
127882L_12
127882L_13
127882L_15
127882L_14
127882L_10
127882L_08
127882L_09
127882L_05
127882L_07
127882L_05
127882L_04
127882L_03
127882L_02
127882L_01

Magnification | Accelerating Voltage | Working Distance | Horizontal Field Width
300 x | 20 kV | 21.8 mm | 4.5 mm

1 mm
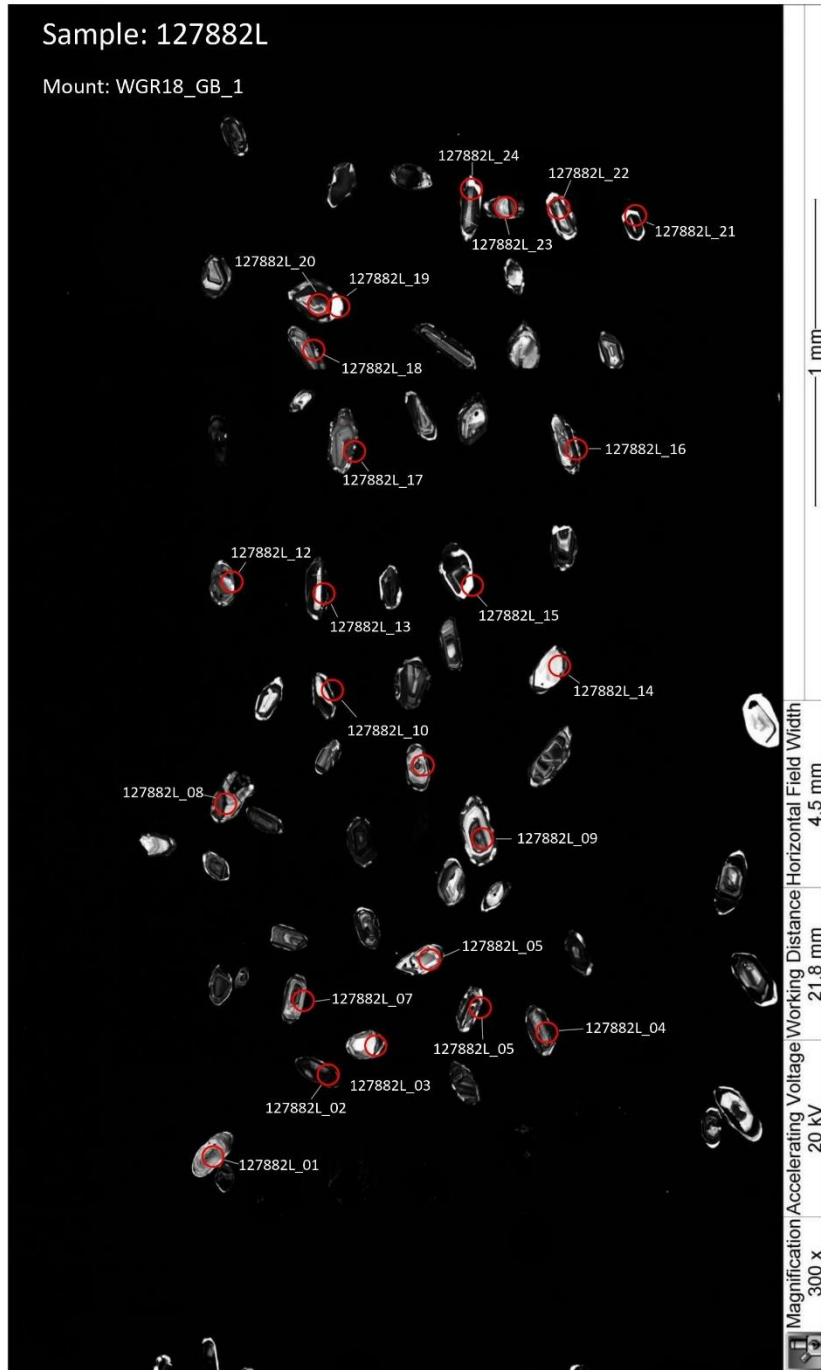
Sample: 127878L

Mount: WGR18_GB_1

Sample: 127877L

Mount: WGR18_GB_1
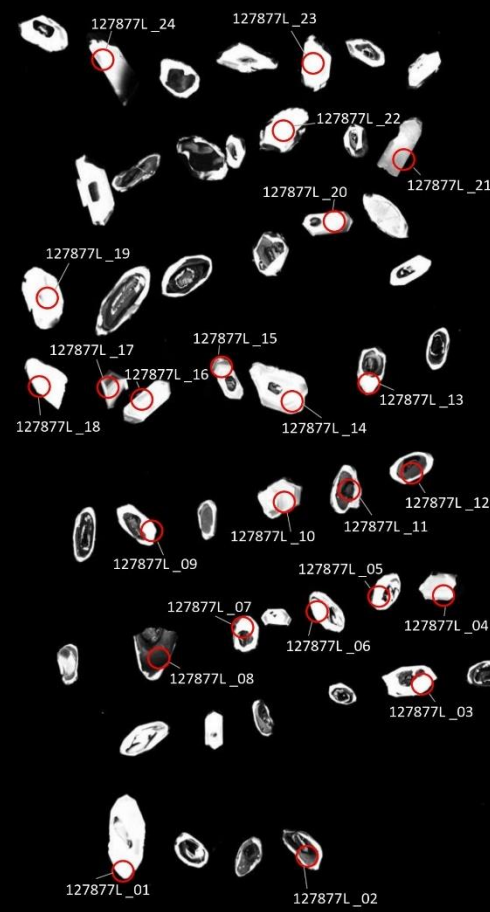
Sample: 127866L

Mount: WGR18_GB_1
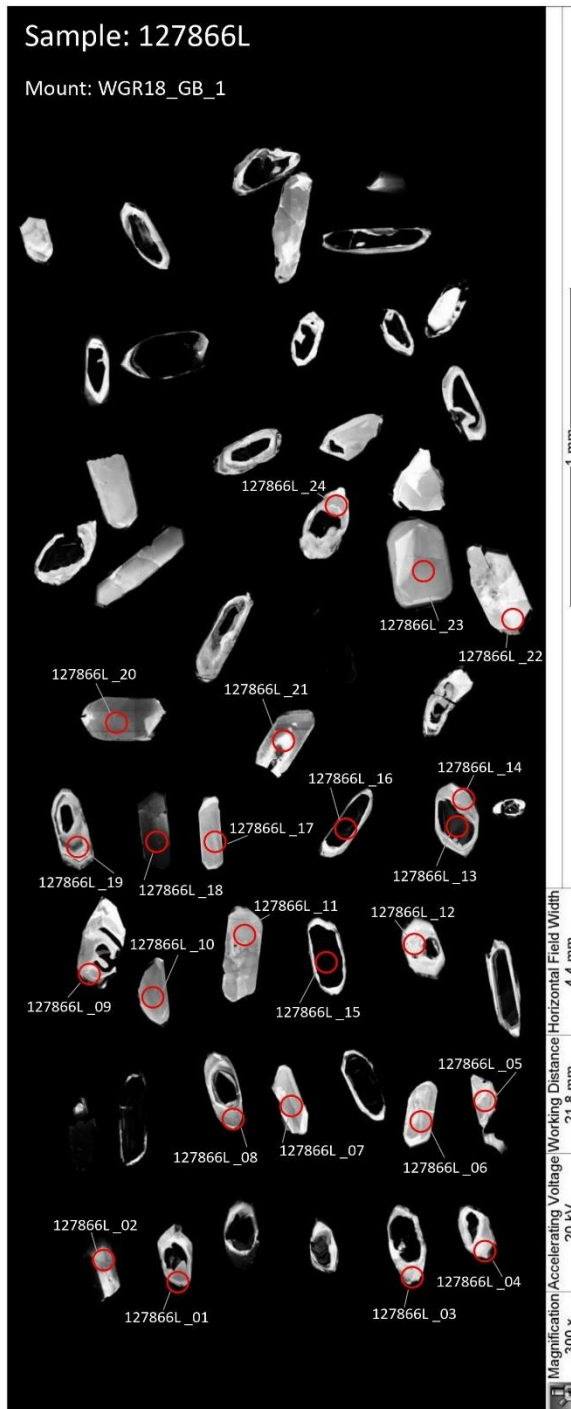
Sample: 127884B

Mount: WGR18_GB_1
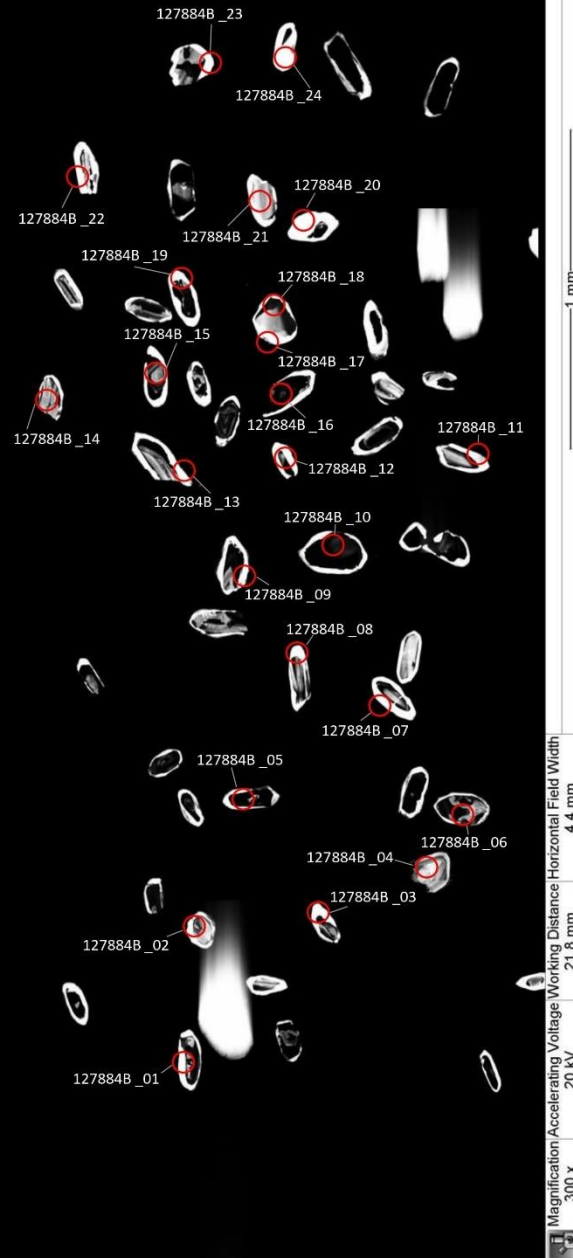
Sample: 127879L

Mount: WGR18_GB_1

127879L _24
127879L _21
127879L _23
127879L _20
127879L _22
127879L _18
127879L _19
127879L _15
127879L _17
127879L _16
127879L _14
127879L _11
127879L _13
127879L _10
127879L _12
127879L _O8
127879L _09
127879L _07
127879L _05
127879L _01
127879L _03
127879L _06
127879L _02
127879L _04

Magnification | Accelerating Voltage | Working Distance | Horizontal Field Width
300 x | 20 kV | 21.8 mm | 4.4 mm

1 mm

D3: U-Pb data

Table groups: *Isotope ratios* — Concordia output (Pb207/U235, 1s%, Pb206/U238, 1s%) and Tera-Wasserburg output (roh, 238/206, 1s%, 207/206, 1s%); *Age estimates (ma)* (Pb207/Pb206, 1s, Pb207/U235, 1s, Pb206/U238, 1s, conc); *Concentrations* (ThU, U*, Th*, Pb*, Phtot*, Pb com. >LLD (%)).

Analysis #	Pb207 U235	1s%	Pb206 U238	1s%	roh	238/206	1s%	207/206	1s%	Pb207 Pb206	1s	Pb207 U235	1s	Pb206 U238	1s	conc	ThU	U*	Th*	Pb*	Phtot*	Pb com. >LLD (%)
1278661_01	0.64	7.89	0.06693	2.27	0.07	14.94098312	2.27	0.06935	8.06	909.3	157.81	502.3	31.27	417.6	9.16	45.9	0.01	25	0	0	2	56
1278661_02	0.49995	2.24	0.06445	1.23	0.29	15.5159038	1.23	0.05626	2.22	461.9	48.95	411.7	7.60	402.6	4.77	87.2	0.01	62	0	0	4	16
1278661_03	4.00657	1.22	0.28448	1.14	0.56	3.515185602	1.14	0.10215	1.11	1663.5	20.33	1635.5	9.89	1613.9	16.26	97.0	0.44	204	90	0	71	1
1278661_04	0.63599	8.25	0.06402	2.05	0.06	15.62011871	2.05	0.07205	8.37	987.5	161.56	499.8	32.55	400	7.93	40.5	0.00	21	0	0	1	-
1278661_05	0.49678	4.34	0.06497	1.43	0.14	15.39171926	1.43	0.05546	4.38	430.4	94.87	409.5	14.64	405.8	5.64	94.3	0.01	27	0	0	2	63
1278661_06	0.52863	6.24	0.07113	1.62	0.09	14.05876564	1.62	0.0539	6.31	366.8	135.87	430.9	21.93	443	6.92	120.8	0.02	23	0	0	2	-
1278661_07	0.536	11.11	0.0632	2.44	0.05	15.82278481	2.44	0.06151	11.27	657.1	224.85	435.8	39.36	395.1	9.37	60.1	0.00	21	0	0	2	266
1278661_08	0.52437	12.98	0.06772	3.01	0.04	14.76608636	3.01	0.05616	13.19	458.3	269.19	428.1	45.33	422.4	12.32	92.2	0.01	25	0	0	2	51
1278661_09	3.3634	2.45	0.23735	1.38	0.28	4.21318728	1.38	0.10277	2.44	1674.8	44.5	1495.9	19.14	1372.9	17.11	82.0	0.29	37	11	0	11	10
1278661_10	0.51289	6.83	0.06452	1.69	0.08	15.49407006	1.69	0.05765	6.90	516.2	145.08	420.4	23.51	403.1	6.58	78.1	0.01	23	0	0	1	104
1278661_11	0.51853	10.55	0.06555	2.04	0.05	15.25553013	2.04	0.05737	10.65	505.5	218.92	424.2	36.56	409.3	8.12	81.0	0.00	21	0	0	-	-
1278661_12	0.48885	5.58	0.06579	1.63	0.10	15.6764831	1.63	0.05558	5.65	435.2	121.43	404.1	18.59	398.7	6.28	91.6	0.01	27	0	0	2	86
1278661_13	4.05158	1.42	0.28729	1.17	0.48	3.48080369	1.17	0.10228	1.34	1665.9	24.58	1644.6	11.60	1628	16.88	97.7	0.47	72	34	0	25	-
1278661_14	0.53327	6.86	0.06909	1.69	0.08	14.47387466	1.69	0.05598	6.93	451.2	147.42	434	24.24	430.7	7.08	95.5	0.00	23	0	0	2	60
1278661_15	3.91425	1.17	0.27992	1.13	0.58	3.572490271	1.13	0.10142	1.06	1630.2	19.45	1616.6	9.50	1591	15.96	96.4	0.83	287	239	0	105	-
1278661_16	3.66853	1.20	0.26368	1.13	0.57	3.79247573	1.13	0.1009	1.08	1640.8	19.94	1564.5	9.54	1508.7	15.27	91.9	0.87	149	129	0	52	-
1278661_17	0.51515	4.10	0.06254	1.41	0.15	15.9897665	1.41	0.05974	4.13	594	87.33	421.9	14.16	391.1	5.37	65.8	0.01	27	0	0	2	-
1278661_18	0.48148	2.12	0.06395	1.20	0.31	15.6372166	1.20	0.05461	2.09	396.2	45.89	399.1	7.00	399.6	4.66	100.9	0.01	53	0	0	4	15
1278661_19	0.49622	1.93	0.06429	1.18	0.34	15.5545186	1.18	0.05598	1.89	451.2	41.17	409.1	6.50	401.7	4.63	89.0	0.01	59	0	0	4	-
1278661_20	0.49997	7.88	0.06541	1.79	0.07	15.2881822	1.79	0.05544	7.95	429.6	168.54	411.7	26.66	408.4	7.09	95.1	0.00	22	0	0	2	-
1278661_21	0.4829	13.74	0.06239	2.63	0.04	16.0282096	2.63	0.05613	13.90	457.2	282.15	400.1	45.42	390.2	9.92	85.3	0.00	21	0	0	1	-
1278661_22	0.47631	5.38	0.06355	1.51	0.11	15.7356412	1.51	0.05436	5.43	385.9	117.2	395.5	17.62	397.2	5.85	102.9	0.01	25	0	0	2	-
1278661_23	0.48918	4.43	0.06492	1.48	0.13	15.4035736	1.48	0.05465	4.48	397.9	96.92	404.3	14.78	405.5	5.83	101.9	0.00	31	0	0	2	-
1278661_24	0.52035	6.08	0.06804	1.69	0.09	14.6972369	1.69	0.05546	6.17	430.6	131.96	425.4	21.12	424.4	6.94	98.6	0.02	25	1	0	2	65

Analysis #	Pb207 U235	1s%	Pb206 U238	1s%	roh	238/206	1s%	207/206	1s%	Pb207 Pb206	1s	Pb207 U235	1s	Pb206 U238	1s	conc	ThU	U*	Th*	Pb*	Phtot*	Pb com. >LLD (%)
1278681_01	5.27514	1.46	0.37931	1.18	0.48	2.63656033	1.18	0.10086	1.37	1640	25.22	1864.8	12.43	2073.1	20.95	126.4	0.07	32	2	0	14	-
1278681_02	0.47848	5.22	0.0628	1.58	0.11	15.92356688	1.58	0.05525	5.29	422.4	113.49	397	17.15	392.6	6.01	92.9	0.01	27	0	0	2	43
1278681_03	0.60873	11.75	0.06295	2.45	0.04	15.88562351	2.45	0.07014	11.90	932.3	226.89	482.8	45.15	393.5	9.32	42.2	0.01	20	0	0	1	412
1278681_04	4.01488	1.17	0.28779	1.13	0.59	3.474758988	1.13	0.10118	1.05	1645.9	19.39	1637.2	9.52	1630.5	16.29	99.1	0.77	245	188	0	92	-
1278681_05	1.96149	3.85	0.06011	2.10	0.13	16.636167	2.10	0.23666	4.15	3097.7	64.57	1102.4	25.92	376.3	7.66	12.1	0.15	22	3	0	2	120
1278681_06	0.40683	6.60	0.06225	1.61	0.08	16.064257	1.61	0.0474	6.67	68.9	151.94	346.6	19.39	389.3	6.08	565.0	0.01	24	0	0	2	69
1278681_07	0.57304	8.89	0.06416	2.01	0.06	15.5860349	2.01	0.06477	9.00	766.9	178.94	460	32.87	400.9	7.81	52.3	0.03	21	1	0	2	115
1278681_08	0.47459	2.50	0.06413	1.23	0.26	15.5933261	1.23	0.05367	2.48	357	55.24	394.4	8.17	400.7	4.80	112.2	0.00	42	0	0	3	-
1278681_09	0.51223	6.29	0.06692	1.70	0.08	14.94321578	1.70	0.05551	6.38	432.7	136.31	419.9	21.63	417.6	6.89	96.5	0.00	24	0	0	2	92
1278681_10	0.52276	3.85	0.06469	1.41	0.16	15.4583977	1.41	0.05861	3.89	552.6	82.81	427	13.44	404.1	5.52	73.1	0.01	28	0	0	2	-
1278681_11	4.09781	1.18	0.2907	1.13	0.58	3.43997248	1.13	0.10223	1.07	1665	19.54	1653.9	9.63	1645.1	16.44	98.8	0.84	181	152	0	69	-
1278681_12	0.56141	4.80	0.0633	1.55	0.12	15.79778831	1.55	0.06432	4.87	752.2	99.52	452.4	17.51	395.7	5.96	52.6	0.01	24	0	0	2	78
1278681_13	0.4946	4.94	0.06383	1.52	0.11	15.66661444	1.52	0.0562	5.00	459.3	107.96	408	16.61	398.9	5.88	86.8	0.00	25	0	0	2	-
1278681_14	0.47239	4.41	0.06273	1.43	0.13	15.94133588	1.43	0.05461	4.45	396.4	96.29	392.8	14.37	392.2	5.49	98.9	0.00	27	0	0	2	42
1278681_15	0.4492	5.79	0.06244	1.59	0.10	16.01574476	1.59	0.05217	5.85	292.9	128.23	376.7	18.22	390.5	5.98	133.3	0.01	24	0	0	2	42
1278681_16	0.46121	3.77	0.06284	1.37	0.22	15.91343094	1.37	0.05323	3.79	338.4	83.63	385.1	12.07	392.9	5.21	116.1	0.01	29	0	0	2	26
1278681_17	0.45984	2.87	0.06309	1.28	0.58	15.85037248	1.28	0.05286	2.88	322.7	63.96	384.1	9.17	394.4	4.90	122.2	0.00	46	0	0	3	21
1278681_18	3.99998	1.17	0.28602	1.13	0.58	3.496259003	1.13	0.10135	1.06	1648.9	19.44	1663.6	9.53	1621.6	16.21	98.3	0.42	243	102	0	84	-
1278681_19	0.33242	19.96	0.06184	2.75	0.02	16.17076326	2.75	0.03899	20.08	0.1	39.54	291.4	50.56	386.8	10.31	398800.0	0.01	21	0	0	1	141
1278681_20	0.50988	4.04	0.06646	1.41	0.15	15.0466446	1.41	0.05564	4.08	437.8	88.33	418.4	13.86	414.8	5.66	94.7	0.01	27	0	0	2	-
1278681_21	3.73897	1.21	0.26958	1.14	0.57	3.709473997	1.14	0.10059	1.09	1635	20.2	1579.8	9.67	1538.7	15.55	94.1	0.39	270	106	0	88	-
1278681_22	0.56561	23.02	0.06938	3.85	0.02	14.41337561	3.85	0.05913	23.25	571.8	438.89	455.2	84.45	432.4	16.08	75.6	0.02	20	0	0	1	274
1278681_23	0.52062	8.07	0.06477	1.88	0.06	15.4392466	1.88	0.0583	8.16	540.3	169.86	425.6	28.04	404.6	7.39	74.9	0.02	21	0	0	2	204
1278681_24	0.48642	4.00	0.06387	1.41	0.15	15.6568029	1.41	0.05523	4.04	421.6	87.37	402.5	13.28	399.1	5.43	94.7	0.00	27	0	0	2	31

12786L

Analysis #	Pb207/U235	1s%	Pb206/U238	1s%	roh	238/206	1s%	207/206	1s%	Pb207/Pb206	1s	Pb207/U235	1s	Pb206/U238	1s	conc	Th/U	U*	Th*	Pbtot*	Pb com. >LLD (%)
	Concordia output				Tera-Wasserburg output					Age estimates (ma)							Concentrations				
12786L_01	0.45408	6.48	0.06483	1.64	0.09	15.4249576	1.64	0.0508	6.54	231.7	144.27	380.1	20.53	404.9	6.40	174.8	0.03	23	1	2	112
12786L_02	0.47726	4.72	0.06323	1.49	0.12	15.8152776	1.49	0.05474	4.77	401.7	102.96	396.2	15.48	395.2	5.68	98.4	0.01	26	0	2	32
12786L_03	3.60424	1.18	0.25952	1.13	0.58	3.85326757	1.13	0.10072	1.06	1637.4	19.61	1550.5	9.37	1487.4	15.03	90.8	1.11	220	245	80	1
12786L_04	0.47586	4.21	0.06451	1.41	0.15	15.50147264	1.41	0.0535	4.24	349.8	93.13	395.2	13.80	403	5.53	115.2	0.02	27	0	2	28
12786L_05	0.50624	5.38	0.06497	1.62	0.10	15.3917926	1.62	0.05651	5.45	471.7	117.02	415.9	18.35	405.8	6.33	86.0	0.01	25	0	2	83
12786L_06	0.50086	2.57	0.06351	1.24	0.25	15.74555188	1.24	0.05719	2.55	498.5	55.93	412.3	8.69	396.9	4.82	79.6	0.02	39	1	3	-
12786L_07	4.08409	1.19	0.28801	1.13	0.57	3.472101663	1.13	0.10384	1.07	1676	19.63	1651.1	9.67	1631.6	16.32	97.4	1.03	196	203	77	-
12786L_08	0.49454	5.02	0.06429	1.52	0.12	15.5545186	1.52	0.05579	5.07	443.7	65.84	408	16.88	401.6	5.93	90.5	0.03	25	1	2	104
12786L_09	0.47711	2.98	0.06435	1.29	0.20	15.5400155	1.29	0.05377	2.99	361.3	65.84	396.1	9.77	402	5.02	111.3	0.01	35	0	2	-
12786L_10	0.46907	3.55	0.06344	1.34	0.17	15.7629256	1.34	0.05362	3.58	355.2	78.55	390.5	11.51	396.5	5.17	111.6	0.01	30	0	2	47
12786L_11	0.4783	3.60	0.06373	1.35	0.17	15.6911972	1.35	0.05443	3.62	388.7	78.62	396.9	11.82	398.3	5.22	102.5	0.02	29	0	2	25
12786L_12	0.4752	3.54	0.06215	1.35	0.18	16.0901046	1.35	0.05545	3.55	430.1	77.32	394.8	11.56	388.7	5.10	90.4	0.01	30	0	2	-
12786L_13	3.35527	1.20	0.24245	1.13	0.57	4.12456177	1.13	0.10036	1.09	1630.8	20.13	1494	9.41	1399.4	14.27	85.8	0.70	198	139	63	-
12786L_14	0.4688	4.04	0.06371	1.40	0.14	15.6961231	1.40	0.05337	4.08	344.3	89.49	390.4	13.10	398.1	5.41	115.6	0.02	28	0	2	83
12786L_15	3.4987	1.28	0.24654	1.15	0.53	4.05613694	1.15	0.10236	1.18	1667.4	21.65	1522.7	10.09	1420.6	14.61	85.2	0.55	116	64	36	49
12786L_16	0.48392	2.91	0.06411	1.28	0.21	15.5981906	1.28	0.05474	2.92	401.7	63.26	400.8	9.64	400.6	4.97	99.7	0.01	35	0	2	29
12786L_17	0.47885	5.07	0.06321	1.52	0.11	15.8202816	1.52	0.05494	5.13	409.8	110.53	397.3	16.67	395.1	5.80	96.4	0.01	25	0	2	83
12786L_18	0.48449	4.86	0.06345	1.50	0.12	15.7604413	1.50	0.05538	4.91	427.3	105.77	401.2	16.10	396.5	5.77	92.8	0.01	25	0	2	49
12786L_19	0.49246	3.92	0.06445	1.40	0.16	15.5159038	1.40	0.05542	3.95	428.8	85.86	406.6	13.14	402.6	5.47	93.9	0.01	27	0	2	-
12786L_20	0.52869	3.94	0.06325	1.42	0.14	15.8102767	1.42	0.06062	3.99	625.8	83.7	430.9	13.84	395.3	5.47	63.2	0.01	27	0	2	32
12786L_21	0.45165	5.08	0.06249	1.55	0.11	16.0025604	1.55	0.05241	5.15	303.4	113.03	378.4	16.05	390.8	5.87	128.8	0.02	27	0	2	-
12786L_22	0.501	3.49	0.06362	1.35	0.17	15.7183276	1.35	0.05711	3.52	495.4	76.17	412.4	11.81	397.6	5.23	80.3	0.01	30	0	2	-
12786L_23	3.17098	1.34	0.22956	1.15	0.51	4.35615961	1.15	0.10017	1.25	1627.3	23.05	1450.1	10.35	1332.2	13.90	81.9	0.68	85	58	25	-
12786L_24	0.51405	4.52	0.06391	1.49	0.12	16.6470036	1.49	0.05833	4.58	541.5	97.59	421.2	15.57	399.4	5.73	73.8	0.01	26	0	2	26

12877L

Analysis #	Pb207/U235	1s%	Pb206/U238	1s%	roh	238/206	1s%	207/206	1s%	Pb207/Pb206	1s	Pb207/U235	1s	Pb206/U238	1s	conc	Th/U	U*	Th*	Pbtot*	Pb com. >LLD (%)
	Concordia output				Tera-Wasserburg output					Age estimates (ma)							Concentrations				
12877L_01	0.46142	2.87	0.06237	1.28	0.22	16.0333494	1.28	0.05365	2.87	356.2	63.61	385.2	9.21	390	4.83	109.5	0.02	36	1	2	35
12877L_02	3.4907	1.24	0.25545	1.14	0.55	3.9146604	1.14	0.0991	1.14	1607.2	21.07	1525.1	9.82	1466.5	14.95	91.2	0.57	186	105	59	-
12877L_03	0.52822	5.73	0.0647	1.68	0.10	14.4559505	1.68	0.05921	5.81	574.9	121.71	430.6	20.12	404.1	6.59	70.3	0.02	24	0	2	66
12877L_04	0.47444	2.03	0.06279	1.19	0.33	15.9261029	1.19	0.0548	1.99	403.9	43.76	394.3	6.63	392.6	4.55	97.2	0.02	56	1	4	19
12877L_05	0.48153	3.11	0.06123	1.32	0.20	16.3318635	1.32	0.05703	3.12	492.1	68.1	399.1	10.25	383.1	4.91	77.9	0.02	38	1	2	-
12877L_06	4.09769	1.63	0.28916	1.21	0.42	3.45829299	1.21	0.10277	1.57	1674.7	28.6	1653.8	13.27	1637.4	17.47	97.8	1.46	34	50	15	4
12877L_07	0.48573	2.29	0.06366	1.23	0.28	15.7084511	1.23	0.05533	2.28	425.4	49.42	402	7.61	397.9	4.71	93.5	0.01	47	1	3	-
12877L_08	1.55556	1.36	0.1567	1.15	0.50	6.38162093	1.15	0.07199	1.26	985.7	25.56	952.7	8.38	938.4	10.02	95.2	0.09	151	14	26	-
12877L_09	1.34812	1.98	0.14435	1.22	0.33	6.92760651	1.22	0.06773	1.95	860.2	39.84	866.7	11.53	869.2	9.91	101.0	0.05	96	5	15	19
12877L_10	0.50825	2.10	0.06328	1.20	0.30	15.8027813	1.20	0.05825	2.08	538.5	45.3	417.3	7.18	395.5	4.63	73.4	0.01	53	1	4	-
12877L_11	2.5384	1.38	0.20982	1.15	0.49	4.7659899	1.15	0.08773	1.29	1376.6	24.62	1283.1	10.05	1227.9	12.92	89.2	0.06	199	12	46	14
12877L_12	3.10096	1.23	0.23726	1.14	0.55	4.21478547	1.14	0.09478	1.12	1523.7	20.91	1432.9	9.41	1372.5	14.04	90.1	0.23	222	52	61	-
12877L_13	1.46479	1.48	0.14491	1.16	0.45	6.900835	1.16	0.07331	1.40	1022.4	28.14	916	8.92	872.4	9.47	85.3	0.06	129	8	20	-
12877L_14	0.50491	3.69	0.06278	1.40	0.16	15.9286397	1.40	0.05833	3.74	541.4	80.3	415	12.58	392.5	5.35	72.5	0.01	32	0	2	-
12877L_15	0.47278	1.72	0.06279	1.16	0.38	15.9261029	1.16	0.0546	1.67	395.9	36.51	393.1	5.59	392.6	4.45	99.2	0.02	86	2	6	-
12877L_16	0.49059	2.37	0.0633	1.23	0.28	15.7977883	1.23	0.05621	2.35	459.8	51.82	405.3	7.92	395.6	4.72	86.0	0.03	43	1	3	19
12877L_17	0.46462	1.65	0.06329	1.17	0.40	15.8002844	1.17	0.05323	1.60	338.7	35.5	387.5	5.32	395.6	4.46	116.8	0.02	102	2	7	-
12877L_18	0.44751	3.49	0.06104	1.36	0.17	16.3826999	1.36	0.05317	3.52	336	77.7	375.5	10.94	381.9	5.02	113.7	0.01	35	0	2	-
12877L_19	0.47475	3.25	0.06488	1.33	0.18	15.4130703	1.33	0.05307	3.28	331.6	72.58	394.5	10.63	405.2	5.20	122.2	0.02	35	1	3	19
12877L_20	0.44791	2.73	0.06213	1.27	0.23	16.0952841	1.27	0.05228	2.74	297.6	60.92	375.8	8.56	388.6	4.77	130.6	0.01	47	1	3	-
12877L_21	0.64487	1.65	0.07789	1.17	0.41	12.8386186	1.17	0.06004	1.58	605.1	33.97	505.3	6.56	483.5	5.43	79.9	0.05	75	3	6	-
12877L_22	1.35377	1.48	0.14052	1.16	0.46	7.11642471	1.16	0.06986	1.40	924.3	28.57	869.2	8.64	847.6	9.20	91.7	0.11	96	10	15	3
12877L_23	0.45191	3.23	0.0635	1.31	0.20	15.7480315	1.31	0.05161	3.24	268	72.6	378.6	10.19	396.9	5.02	148.1	0.01	32	0	2	-
12877L_24	0.47039	3.35	0.0618	1.33	0.18	16.1812298	1.33	0.0552	3.37	420.1	73.11	391.5	10.88	386.5	4.99	92.0	0.01	31	0	2	-

180

Isotope ratios / Age estimates (ma) / Concentrations / Pb com.

Analysis #	Pb207 U235	1s %	Pb206 U238	1s %	roh	238/206	1s %	207/206	1s %	Pb207 Pb206	1s	Pb207 U235	1s	Pb206 U238	1s	conc	Th/U	U*	Th*	Pbtot*	>LLD (%)
127878L_01	3.70347	1.36	0.26882	1.25	0.50	3.71996131	1.16	0.09991	1.27	1622.4	23.44	1572.1	10.87	1534.8	15.80	94.6	0.62	180	112	61	2
127878L_02	3.67804	1.22	0.27174	1.18	0.56	3.67998822	1.13	0.09815	1.11	1589.3	20.63	1566.6	9.74	1549.7	15.63	97.5	0.99	138	137	51	1
127878L_03	0.46358	4.06	0.06352	1.24	0.15	15.743073	1.40	0.05292	4.10	325.4	90.42	386.7	13.07	397	5.38	122.0	0.00	28	0	2	-
127878L_04	0.51324	6.30	0.06206	1.20	0.08	16.1134386	1.85	0.09997	6.42	602.5	133.16	420.6	21.71	388.2	6.95	64.4	0.00	27	0	2	35
127878L_05	3.68524	1.23	0.27284	1.21	0.55	3.66515174	1.14	0.09795	1.12	1585.5	20.94	1568.2	9.86	1555.2	15.71	98.1	1.31	139	182	54	-
127878L_06	0.49279	1.91	0.06592	1.19	0.35	15.1699029	1.18	0.05421	1.86	379.5	41.49	406.8	6.40	411.6	4.73	108.5	0.00	112	0	8	-
127878L_07	0.52196	5.27	0.06223	1.20	0.11	16.0694199	1.61	0.06082	5.34	632.9	111.21	426.5	18.36	389.2	6.09	61.5	0.01	25	0	2	84
127878L_08	3.74105	1.23	0.27178	1.20	0.55	3.67944661	1.14	0.09982	1.12	1620.7	20.75	1580.2	9.85	1549.8	15.65	95.6	0.67	119	79	41	-
127878L_09	0.57453	5.70	0.07143	1.20	0.10	13.99972	1.69	0.08833	5.78	541.3	122.36	460.9	21.10	444.8	7.30	82.2	0.00	25	0	2	89
127878L_10	3.79376	1.24	0.27896	1.20	0.55	3.58474333	1.14	0.09862	1.14	1598.2	21	1591.4	9.96	1586.1	15.99	99.2	0.73	118	86	42	-
127878L_11	0.49912	3.54	0.06202	1.21	0.17	16.123831	1.37	0.05836	3.58	543.2	76.31	411.1	11.98	387.9	5.16	71.4	0.01	31	0	2	-
127878L_12	0.48785	1.65	0.06326	1.19	0.40	15.8077774	1.17	0.05592	1.59	448.9	34.59	403.4	5.49	395.4	4.46	88.1	0.00	89	0	6	-
127878L_13	3.59883	1.22	0.26224	1.25	0.55	3.81330079	1.13	0.09952	1.12	1615.1	20.57	1549.3	9.70	1501.3	15.19	93.0	0.48	163	78	52	-
127878L_14	2.55404	1.21	0.19754	1.24	0.56	5.06226587	1.13	0.09376	1.10	1503.3	20.67	1287.6	8.84	1162.1	12.04	77.3	0.14	282	41	64	-
127878L_15	0.45783	4.40	0.06524	1.19	0.13	15.3280196	1.44	0.05089	4.44	235.7	99.36	382.8	14.03	407.4	5.70	172.8	0.00	29	0	2	-
127878L_16	0.48463	3.57	0.06267	1.20	0.17	15.9565981	1.37	0.05608	3.60	455.2	77.83	401.2	11.82	391.8	5.22	86.1	0.01	32	0	2	-
127878L_17	0.51665	2.53	0.06674	1.21	0.25	14.9835181	1.26	0.05614	2.53	457.4	55.11	422.9	8.76	416.5	5.06	91.1	0.01	53	0	4	-
127878L_18	1.1868	1.32	0.11032	1.19	0.51	9.06453952	1.14	0.07801	1.23	1147.1	24.15	794.5	7.26	674.6	7.32	58.8	0.12	289	34	36	21
127878L_19	3.66961	1.30	0.27344	1.19	0.52	3.657710942	1.14	0.09732	1.20	1573.3	22.29	1564.8	10.35	1558.3	15.86	99.0	0.83	157	130	57	1
127878L_20	3.7763	1.34	0.27627	1.23	0.51	3.61964745	1.15	0.09912	1.24	1607.7	22.99	1587.7	10.72	1572.5	16.08	97.8	0.67	112	75	39	1
127878L_21	0.49422	2.34	0.06426	1.20	0.27	15.5617803	1.23	0.05577	2.33	442.9	50.57	407.8	7.85	401.5	4.78	90.7	0.00	48	0	3	-
127878L_22	3.05732	1.26	0.23147	1.19	0.54	4.32021428	1.14	0.09578	1.16	1543.5	21.7	1422.1	9.67	1342.2	13.81	87.0	0.50	107	53	31	-
127878L_23	0.46305	2.32	0.06259	1.20	0.27	15.9769931	1.23	0.05365	2.31	356.1	51.25	386.4	7.45	391.4	4.65	109.9	0.00	75	0	5	-
127878L_24	0.47673	1.47	0.06266	1.19	0.45	15.9591446	1.15	0.05517	1.40	418.9	30.63	395.8	4.82	391.8	4.37	93.5	0.00	152	0	10	-

Analysis #	Pb207 U235	1s %	Pb206 U238	1s %	roh	238/206	1s %	207/206	1s %	Pb207 Pb206	1s	Pb207 U235	1s	Pb206 U238	1s	conc	Th/U	U*	Th*	Pbtot*	>LLD (%)
1278821_01	4.06029	1.25	0.2876	1.18	0.58	3.47705146	1.18	0.1024	1.11	1668	20.42	1646.4	10.21	1629.5	16.90	97.7	0.55	156	86	56	1
1278821_02	4.57903	1.18	0.30856	1.16	0.61	3.240860773	1.16	0.10763	1.03	1759.7	18.65	1745.5	9.87	1733.6	17.69	98.5	0.89	309	274	126	-
1278821_03	4.39941	1.24	0.30724	1.17	0.59	3.25478453	1.17	0.10385	1.10	1694.1	20.09	1712.2	10.27	1727.1	17.77	101.9	0.64	63	41	24	-
1278821_04	4.1423	1.19	0.29207	1.17	0.60	3.42383675	1.17	0.10286	1.04	1676.4	19.12	1662.7	9.77	1651.9	16.98	98.5	0.88	194	171	75	-
1278821_05	4.17683	1.20	0.29548	1.17	0.60	3.38432381	1.17	0.10253	1.05	1670.3	19.28	1669.5	9.84	1668.8	17.15	99.9	0.49	289	141	105	-
1278821_06	4.19847	1.21	0.2942	1.17	0.60	3.399024827	1.17	0.10351	1.06	1687.9	19.47	1673.7	9.93	1662.5	17.12	98.5	1.16	113	131	46	-
1278821_07	4.40122	1.19	0.3059	1.16	0.61	3.26904217	1.16	0.10435	1.03	1703	18.98	1712.6	9.85	1720.5	17.59	101.0	0.74	201	149	79	-
1278821_08	3.99855	1.20	0.28988	1.17	0.61	3.44970333	1.17	0.10005	1.05	1624.9	19.31	1633.9	9.72	1640.9	16.89	101.0	0.04	323	12	104	-
1278821_09	4.24814	1.20	0.30002	1.17	0.61	3.333111126	1.17	0.1027	1.04	1673.4	19.2	1683.4	9.85	1691.4	17.35	101.1	0.55	214	118	79	-
1278821_10	3.98401	1.21	0.28373	1.17	0.61	3.524477496	1.17	0.10184	1.05	1658	19.4	1630.9	9.78	1610.1	16.63	97.1	0.87	148	129	56	-
1278821_11	4.06365	1.23	0.28711	1.17	0.60	3.482985615	1.17	0.10265	1.08	1672.6	19.92	1647	10.03	1627.1	16.84	97.3	0.51	77	39	27	-
1278821_12	4.20896	1.21	0.29762	1.17	0.60	3.359489248	1.17	0.10257	1.06	1671.2	19.51	1675.8	9.94	1679.5	17.28	100.5	0.88	135	118	53	-
1278821_13	4.4764	1.25	0.31262	1.17	0.59	3.198771672	1.17	0.10385	1.10	1694.1	20.18	1726.6	10.34	1753.6	18.02	103.5	0.51	91	47	35	-
1278821_14	4.19039	1.24	0.29313	1.17	0.59	3.411455668	1.17	0.10368	1.10	1691	20.12	1672.1	10.19	1657.1	17.15	98.0	1.20	67	80	28	-
1278821_15	4.32487	1.19	0.30007	1.17	0.62	3.33255574	1.17	0.10453	1.03	1706.1	18.98	1698.1	9.83	1691.6	17.34	99.2	1.89	293	554	137	-
1278821_16	4.24386	1.19	0.30375	1.17	0.61	3.29218107	1.17	0.10133	1.04	1648.7	19.07	1682.5	9.78	1709.9	17.50	103.7	1.20	297	357	126	-
1278821_17	4.19281	1.20	0.29357	1.16	0.61	3.40634261	1.16	0.10358	1.03	1689.3	19.14	1672.6	9.82	1659.3	17.07	98.2	1.04	187	195	75	-
1278821_18	4.0524	1.21	0.28987	1.17	0.61	3.449822334	1.17	0.10139	1.06	1649.8	19.42	1644.8	9.82	1640.9	16.92	99.5	0.69	138	95	52	-
1278821_19	4.03387	1.19	0.29585	1.17	0.61	3.403096818	1.17	0.09956	1.04	1615.9	19.24	1641.1	9.71	1660.7	17.07	102.8	0.08	240	20	79	-
1278821_20	4.09413	1.20	0.29076	1.17	0.61	3.43926262	1.17	0.10212	1.04	1663.1	19.17	1653.1	9.76	1645.3	16.94	98.9	0.34	197	67	68	-
1278821_21	0.50211	1.25	0.06566	1.17	0.59	15.2299726	1.17	0.05546	1.10	430.7	24.34	413.1	4.23	410	4.64	95.2	0.01	964	10	67	1
1278821_22	4.16478	1.19	0.29024	1.16	0.61	3.44542448	1.16	0.10407	1.04	1698	18.94	1667.1	9.74	1642.7	16.90	96.7	0.39	314	121	109	-
1278821_23	4.20155	1.20	0.29943	1.17	0.61	3.33967872	1.17	0.10177	1.05	1656.7	19.31	1674.3	9.86	1688.5	17.34	101.9	0.43	162	69	59	-
1278821_24	3.80233	1.19	0.27427	1.17	0.61	3.64604222	1.17	0.10055	1.04	1634.2	19.21	1593.2	9.61	1562.4	16.18	95.6	0.22	376	82	119	-

Table 1

Analysis_#	Isotope ratios								Age estimates (ma)							Concentrations				Pb com.
	Concordia output				Tera-Wasserburg output															
	Pb207_U235	1s%	Pb206_U238	1s%	roh	238/206	207/206	1s%	Pb207_Pb206	1s	Pb207_U235	1s	Pb206_U238	1s	conc	Th/U	U*	Th*	Phtot*	>LLD (%)
127879L_01	3.70014	1.19	0.2718	1.16	0.61	3.6791758565	0.09874	1.04	1600.5	19.36	1571.4	9.55	1549.9	16.02	96.8	0.33	369	121	119	-
127879L_02	2.79004	1.26	0.21974	1.17	0.58	4.550832602	0.09209	1.12	1469.2	21.29	1352.9	9.42	1280.5	13.60	87.2	0.44	114	50	30	-
127879L_03	0.56695	24.88	0.07175	3.44	0.02	13.93728223	0.05731	3.44	503.1	473.52	456	91.40	446.7	14.88	88.8	0.00	16	0	1	73
127879L_04	1.47838	1.55	0.14501	1.20	0.46	6.896076133	0.07395	1.46	1040	29.09	921.6	9.38	872.9	9.79	83.9	0.03	58	2	9	-
127879L_05	0.51779	2.50	0.06735	1.28	0.27	14.84780995	0.05576	2.47	442.6	53.77	423.7	8.64	420.2	5.17	94.9	0.01	32	0	2	-
127879L_06	0.51634	1.64	0.06655	1.19	0.44	15.02629602	0.05628	1.55	462.5	34.21	422.7	5.66	415.3	4.80	89.8	0.01	97	1	7	-
127879L_07	0.48423	1.96	0.06316	1.22	0.35	15.83280557	0.0556	1.91	436.3	41.3	401	6.48	394.8	4.68	90.5	0.01	98	1	7	-
127879L_08	0.53167	4.58	0.06224	1.51	0.13	16.06683805	0.06195	4.63	672.5	96.09	432.9	16.15	389.3	5.73	57.9	0.02	20	0	1	94
127879L_09	0.76653	3.96	0.06443	1.61	0.15	15.5207202	0.08629	4.04	1344.6	76	577.8	17.43	402.5	6.28	29.9	0.03	24	1	2	53
127879L_10	3.58336	1.20	0.2674	1.16	0.61	3.739715782	0.0972	1.05	1571	19.57	1545.9	9.54	1527.6	15.84	97.2	0.71	150	106	51	-
127879L_11	0.4786	2.02	0.06421	1.23	0.35	15.57389815	0.05406	1.96	373.6	43.76	397.1	6.65	401.2	4.77	107.4	0.01	85	0	6	-
127879L_12	2.28883	1.52	0.19787	1.20	0.47	5.053823217	0.0839	1.43	1290.1	27.49	1208.8	10.76	1163.9	12.82	90.2	1.19	84	100	24	-
127879L_13	3.20881	1.21	0.23951	1.16	0.60	4.175191015	0.09717	1.06	1570.5	19.8	1459.3	9.38	1384.2	14.52	88.1	0.85	153	130	49	-
127879L_14	1.56553	1.40	0.13168	1.18	0.51	7.594167679	0.08623	1.29	1343.3	24.65	956.7	8.66	797.5	8.90	59.4	0.22	80	18	13	-
127879L_15	1.77457	1.33	0.15194	1.18	0.54	6.581545347	0.08471	1.20	1308.8	23.19	1036.2	8.62	911.8	10.02	69.7	0.17	103	17	18	-
127879L_16	3.89769	1.95	0.29088	1.30	0.38	3.43784378	0.09719	1.88	1570.8	34.93	1613.2	15.73	1645.9	18.84	104.8	1.56	31	48	13	-
127879L_17	0.69299	2.12	0.08091	1.25	0.33	12.3594117	0.06212	2.08	678.4	43.63	534.6	8.79	501.5	6.00	73.9	0.02	32	1	3	-
127879L_18	3.70908	1.36	0.27106	1.19	0.53	3.6892201	0.09925	1.24	1610	22.94	1573.3	10.89	1546.2	16.35	96.0	1.01	65	66	24	-
127879L_19	0.49369	1.58	0.06447	1.19	0.46	15.5110904	0.05554	1.48	433.8	32.22	407.4	5.29	402.7	4.64	92.8	0.01	84	1	6	-
127879L_20	3.4685	1.22	0.25685	1.17	0.60	3.89332295	0.09794	1.07	1585.3	19.89	1520.1	9.60	1473.7	15.38	93.0	0.59	126	74	40	-
127879L_21	0.51625	1.82	0.06407	1.22	0.39	15.6079288	0.05844	1.75	546.2	37.72	422.6	6.28	400.4	4.70	73.3	0.01	50	0	3	20
127879L_22	0.49271	2.21	0.06422	1.25	0.31	15.5714731	0.05565	2.17	438.1	47.13	406.8	7.40	401.2	4.84	91.6	0.00	44	0	3	-
127879L_23	0.48761	3.90	0.06355	1.46	0.16	15.7356412	0.05565	3.94	438	85.4	403.3	12.98	397.2	5.65	90.7	0.01	34	0	2	-
127879L_24	0.49862	2.04	0.06289	1.22	0.34	15.9007791	0.0575	1.98	510.5	43.43	410.8	6.89	393.2	4.69	77.0	0.00	42	0	3	-

Table 2

Analysis_#	Isotope ratios								Age estimates (ma)							Concentrations				Pb com.
	Concordia output				Tera-Wasserburg output															
	Pb207_U235	1s%	Pb206_U238	1s%	roh	238/206	207/206	1s%	Pb207_Pb206	1s	Pb207_U235	1s	Pb206_U238	1s	conc	Th/U	U*	Th*	Phtot*	>LLD (%)
197555_01	4.27425	1.05	0.2947	1.02	0.50	3.393281303	0.10518	1.02	1717.5	18.96	1688.4	8.63	1665	14.91	96.9	0.55	163	89	60	-
197555_02	4.10402	1.05	0.28807	1.02	0.49	3.471378484	0.10332	1.02	1684.6	19.14	1655.1	8.60	1631.9	14.67	96.9	0.42	135	56	48	-
197555_03	4.30714	1.16	0.30284	1.04	0.45	3.302073702	0.10315	1.04	1681.5	21.26	1694.7	9.60	1706.4	15.52	101.4	0.33	111	37	40	-
197555_04	4.11167	1.04	0.2872	1.02	0.50	3.48189415	0.10383	1.03	1693.6	18.86	1656.6	8.50	1627.5	14.60	96.1	0.39	243	95	85	-
197555_05	4.19591	1.04	0.29151	1.02	0.50	3.430414051	0.10439	1.03	1703.5	18.88	1673.2	8.55	1649.1	14.78	96.8	0.26	253	66	87	-
197555_06	4.12156	1.10	0.29231	1.03	0.47	3.421025623	0.10226	1.10	1665.5	20.05	1658.6	8.98	1653.1	14.94	99.3	0.40	96	38	34	-
197555_07	4.31045	1.11	0.30343	1.03	0.48	3.295653034	0.10302	1.10	1679.3	20.19	1695.4	9.14	1708.3	15.41	101.7	0.40	164	66	60	-
197555_08	3.76547	1.05	0.26668	1.02	0.49	3.763926528	0.10279	1.04	1675	19.04	1585.4	8.41	1518.8	13.76	90.7	0.30	430	128	136	-
197555_09	3.93073	1.04	0.27667	1.02	0.51	3.61441284	0.10304	1.02	1679.5	18.79	1620	8.39	1574.6	14.19	93.8	0.43	378	163	128	-
197555_10	4.29734	1.06	0.30728	1.02	0.49	3.254360844	0.10142	1.05	1650.3	19.3	1692.9	8.72	1727.3	15.44	104.7	0.36	294	105	109	-
197555_11	4.2037	1.07	0.29245	1.02	0.49	3.41938793	0.10424	1.02	1701	19.33	1674.7	8.75	1653.8	14.89	97.2	0.36	274	98	96	-
197555_12	4.27257	1.06	0.29856	1.02	0.49	3.349410504	0.10379	1.02	1692.9	19.28	1688.1	8.75	1684.1	15.12	99.5	0.41	130	53	47	-
197555_13	4.12561	1.09	0.29038	1.02	0.48	3.443763345	0.10304	1.02	1679.6	19.79	1659.4	8.90	1643.4	14.86	97.8	0.29	162	46	56	-
197555_14	4.19085	1.06	0.29005	1.02	0.50	3.447681434	0.10379	1.02	1692.9	19.13	1664.4	8.64	1641.8	14.77	97.0	0.33	159	52	55	-
197555_15	4.20647	1.05	0.29295	1.02	0.50	3.413551801	0.10411	1.02	1698.7	18.98	1675.1	8.61	1656.2	14.87	97.5	0.40	167	67	59	-
197555_16	4.18562	1.04	0.29575	1.02	0.51	3.38123415	0.10264	1.02	1672.4	18.84	1671.2	8.51	1670.2	14.96	99.9	0.35	297	103	105	-
197555_17	4.30458	1.06	0.30368	1.02	0.49	3.29293994	0.1028	1.05	1675.3	19.28	1694.2	8.75	1709.5	15.33	102.0	0.55	142	78	54	-
197555_18	4.18519	1.06	0.29378	1.02	0.49	3.40390769	0.10332	1.02	1684.5	19.13	1671.1	8.65	1660.4	14.93	98.6	0.37	141	52	50	-
197555_19	4.20657	1.04	0.29424	1.02	0.50	3.398586119	0.10368	1.02	1691	18.73	1675.3	8.50	1662.7	14.90	98.3	0.54	429	233	159	-
197555_20	4.25919	1.10	0.2937	1.03	0.48	3.40483487	0.10517	1.09	1717.3	19.96	1685.5	9.08	1660	15.04	96.7	0.37	68	25	24	-
197555_21	4.21594	1.08	0.29588	1.02	0.49	3.37974855	0.10333	1.06	1684.9	19.5	1677.1	8.83	1670.9	15.06	99.2	0.42	92	39	33	-
197555_22	4.03943	1.04	0.28552	1.02	0.51	3.50238162	0.1026	1.02	1671.8	18.86	1642.2	8.47	1619.1	14.57	96.8	0.17	407	70	134	-
197555_23	3.88695	1.05	0.27584	1.02	0.50	3.62529002	0.1022	1.04	1664.4	19.09	1611	8.49	1570.4	14.21	94.4	0.45	172	78	59	-
197555_24	4.2007	1.04	0.29155	1.02	0.51	3.42994341	0.10449	1.02	1705.4	18.78	1674.2	8.54	1649.3	14.81	96.7	0.37	311	114	110	-

Isotope ratios / Age estimates (Concentrations) — 127884B

Analysis_#	Pb207_U235	1s%	Pb206_U238	1s%	roh	238/206	1s%	207/206	1s%	Pb207_Pb206	1s	Pb207_U235	1s	Pb206_U238	1s	conc	Th/U	U*	Th*	Phot*	>LLD (%)
	Concordia output					Tera-Wasserburg output				Age estimates (ma)							Concentrations				Pb com.
127884B_01	3.80499	1.22	0.27495	1.17	0.60	3.63702914	1.17	0.10037	1.08	1631	19.85	1593.8	9.84	1565.9	16.28	96.0	0.25	161	41	52	-
127884B_02	4.13017	1.22	0.29382	1.17	0.60	3.403444286	1.17	0.10195	1.07	1659.9	19.74	1660.3	9.99	1660.6	17.14	100.0	0.66	123	81	46	-
127884B_03	3.74405	1.21	0.27427	1.17	0.61	3.646042221	1.17	0.09901	1.05	1605.5	19.54	1580.8	9.67	1562.4	16.22	97.3	0.12	299	35	93	-
127884B_04	1.5779	1.41	0.163	1.19	0.51	6.134969325	1.19	0.07021	1.30	934.5	26.29	961.5	8.77	973.4	10.73	104.2	0.48	88	42	17	-
127884B_05	3.7951	1.19	0.27786	1.17	0.62	3.598934715	1.17	0.09906	1.03	1606.5	19.05	1591.7	9.53	1580.6	16.34	98.4	0.05	989	46	306	-
127884B_06	3.78393	1.19	0.26996	1.17	0.61	3.704252482	1.17	0.10166	1.04	1654.6	19.14	1589.3	9.60	1540.6	15.99	93.1	0.06	355	22	107	-
127884B_07	2.23984	1.31	0.19316	1.18	0.56	5.177055291	1.18	0.0841	1.18	1294.8	22.82	1193.6	9.23	1138.5	12.32	87.9	0.06	395	24	84	-
127884B_08	3.73606	1.28	0.27444	1.18	0.57	3.6437837	1.18	0.09873	1.14	1600.3	21.23	1579.1	10.29	1563.3	16.38	97.7	0.77	155	118	55	-
127884B_09	3.75727	1.19	0.276	1.17	0.62	3.62318841	1.17	0.09873	1.03	1600.3	19.21	1583.7	9.56	1571.2	16.27	98.2	0.18	418	75	133	-
127884B_10	3.7832	1.19	0.27937	1.17	0.62	3.579948241	1.17	0.09821	1.03	1590.5	19.17	1589.2	9.55	1588.2	16.42	99.9	0.17	624	108	199	-
127884B_11	3.79888	1.20	0.27752	1.17	0.62	3.6033439	1.17	0.09928	1.04	1610.6	19.3	1592.5	9.62	1578.9	16.35	98.0	0.29	274	81	90	-
127884B_12	3.47424	1.25	0.25593	1.18	0.58	3.90731841	1.18	0.09845	1.04	1595	19.3	1521.4	9.43	1469	15.34	92.1	0.12	520	64	151	-
127884B_13	4.12007	1.25	0.29337	1.18	0.58	3.40866483	1.18	0.10185	1.11	1658.2	20.41	1658.5	10.25	1658.3	17.20	100.0	0.46	150	69	54	-
127884B_14	2.21401	1.28	0.19186	1.17	0.58	5.21213385	1.17	0.08369	1.11	1285.2	21.45	1185.5	8.75	1131.5	12.18	88.0	0.76	110	83	27	-
127884B_15	1.57601	1.20	0.16156	1.18	0.57	6.1896509	1.18	0.07075	1.14	950.2	23.14	960.8	7.94	965.4	10.53	101.6	0.46	144	66	27	-
127884B_16	3.61123	1.40	0.2637	1.17	0.61	3.79218809	1.17	0.09932	1.05	1611.4	19.36	1552	9.55	1508.7	15.72	93.6	0.06	497	28	146	-
127884B_17	2.40562	1.23	0.19579	1.20	0.52	5.10751315	1.20	0.08911	1.28	1406.5	24.23	1244.3	10.02	1152.6	12.59	81.9	0.25	76	19	17	-
127884B_18	3.94877	1.27	0.28689	1.17	0.59	3.48565652	1.17	0.09983	1.08	1620.8	19.94	1623.7	9.95	1626	16.85	100.3	0.58	96	56	34	-
127884B_19	3.35772	1.89	0.24549	1.18	0.58	4.07348568	1.18	0.0992	1.13	1609.1	20.86	1494.6	9.92	1415.2	14.97	87.9	0.69	189	129	59	-
127884B_20	0.57304	1.24	0.06597	1.23	0.38	15.1584053	1.23	0.063	1.83	708.3	38.32	460	6.98	411.8	4.89	58.1	0.01	44	0	3	-
127884B_21	4.07795	2.60	0.29311	1.17	0.59	3.41168844	1.17	0.1009	1.09	1640.8	20.11	1649.9	10.10	1657	17.16	101.0	0.62	81	50	30	-
127884B_22	0.90574	1.23	0.09712	1.32	0.26	10.2965404	1.32	0.06764	2.59	857.5	52.73	654.8	12.53	597.5	7.55	69.7	0.01	28	0	3	-
127884B_23	3.2799	1.49	0.24698	1.17	0.59	4.04891084	1.17	0.09631	1.08	1553.9	20.04	1476.3	9.53	1422.9	14.96	91.6	0.26	176	46	51	-
127884B_24	1.56779		0.15974	1.20	0.49	6.26017278	1.20	0.07118	1.38	962.7	27.9	957.6	9.22	955.3	10.63	99.2	0.03	107	3	18	3

Isotope ratios / Age estimates (Concentrations) — 127885L

Analysis_#	Pb207_U235	1s%	Pb206_U238	1s%	roh	238/206	1s%	207/206	1s%	Pb207_Pb206	1s	Pb207_U235	1s	Pb206_U238	1s	conc	Th/U	U*	Th*	Phot*	>LLD (%)
	Concordia output					Tera-Wasserburg output				Age estimates (ma)							Concentrations				Pb com.
127885L_01	3.7306	1.21	0.27514	1.17	0.61	3.63451334	1.17	0.09834	1.05	1592.8	19.5	1578	9.65	1566.9	16.27	98.4	0.30	253	77	82	-
127885L_02	0.50205	1.92	0.06611	1.23	0.38	15.1263046	1.23	0.05508	1.85	415.4	40.69	413.1	6.52	412.6	4.88	99.3	0.01	46	0	3	-
127885L_03	3.91357	1.20	0.2828	1.17	0.61	3.53606789	1.17	0.10036	1.05	1630.8	19.25	1616.5	9.70	1605.5	16.61	98.4	0.42	445	185	151	-
127885L_04	4.0709	1.21	0.29203	1.17	0.61	3.42430572	1.17	0.1011	1.06	1644.4	19.5	1648.5	9.88	1651.7	17.06	100.4	0.49	172	84	61	-
127885L_05	0.4717	1.66	0.06353	1.20	0.43	15.740595	1.20	0.05385	1.58	364.5	35.58	392.4	5.42	397.1	4.62	108.9	0.01	66	0	4	0
127885L_06	3.77515	1.20	0.27448	1.17	0.61	3.6432527	1.17	0.09975	1.04	1619.4	19.23	1587.5	9.61	1563.5	16.23	96.5	0.28	704	195	226	-
127885L_07	3.8863	1.21	0.27995	1.17	0.61	3.57206644	1.17	0.10068	1.05	1636.7	19.39	1610.8	9.74	1591.1	16.50	97.2	0.51	289	148	100	0
127885L_08	2.37219	1.24	0.19876	1.17	0.59	5.03119934	1.17	0.08656	1.10	1350.6	21.02	1234.3	8.88	1168.7	12.55	86.5	0.45	181	82	43	-
127885L_09	3.93123	1.23	0.28457	1.17	0.60	3.51407387	1.17	0.10019	1.08	1627.6	19.84	1620.1	9.92	1614.3	16.76	99.2	0.55	127	70	45	-
127885L_10	3.97452	1.21	0.28776	1.17	0.61	3.47511815	1.17	0.10017	1.06	1627.3	19.5	1629	9.82	1630.3	16.87	100.2	0.30	233	71	79	-
127885L_11	3.82696	1.27	0.27518	1.18	0.58	3.63398503	1.18	0.10086	1.12	1640	20.73	1598.4	10.21	1567	16.41	95.5	0.22	155	34	49	-
127885L_12	4.11921	1.20	0.29591	1.17	0.61	3.3794059	1.17	0.10096	1.04	1641.8	19.23	1658.1	9.80	1671	17.22	101.8	0.91	597	541	235	-
127885L_13	3.81911	1.22	0.27607	1.17	0.60	3.62226971	1.17	0.10033	1.07	1630.2	19.76	1596.8	9.84	1571.6	16.36	96.4	0.27	176	47	57	-
127885L_14	0.67354	10.43	0.06698	2.43	0.05	14.9298298	2.43	0.07293	10.60	1012	201.15	522.9	42.62	417.9	9.85	41.3	0.00	17	0	1	-

Isotope ratios

Analysis_#	Concordia output Pb207 U235	1s%	Pb206 U238	1s%	roh	Tera-Wasserburg output 238/206	1s%	207/206	1s%	Age estimates (ma) Pb207 Pb206	1s	Pb207 U235	1s	Pb206 U238	1s	conc	Concentrations Th/U	U*	Th*	Phtot*	Pb com. >LLD (%)
127886L_01	4.02464	1.22	0.29298	1.17	0.61	3.41320227	1.17	0.09962	1.06	1617.1	19.72	1639.2	9.92	1656.4	17.13	102.4	0.72	306	221	115	1
127886L_02	3.89644	1.21	0.27931	1.17	0.61	3.58025133	1.17	0.10117	1.05	1645.7	19.34	1612.9	9.74	1587.9	16.48	96.5	0.53	573	304	197	-
127886L_03	3.66816	1.23	0.27227	1.18	0.60	3.67282477	1.18	0.09771	1.07	1580.8	20.04	1564.5	9.82	1552.3	16.20	98.2	0.40	337	135	110	-
127886L_04	1.57275	1.55	0.15992	1.21	0.47	6.25312656	1.21	0.07133	1.44	966.8	29.28	959.5	9.62	956.3	10.72	98.9	0.01	116	1	20	-
127886L_05	3.8019	1.21	0.27483	1.17	0.61	3.63861296	1.17	0.10033	1.05	1630.1	19.4	1593.1	9.70	1565.3	16.28	96.0	0.69	450	310	158	-
127886L_06	3.84371	1.21	0.2811	1.17	0.61	3.55745286	1.17	0.09917	1.05	1608.5	19.44	1602	9.72	1596.9	16.57	99.3	0.54	500	270	175	-
127886L_07	4.12304	1.20	0.29494	1.17	0.61	3.39052011	1.17	0.10138	1.05	1649.6	19.28	1658.9	9.84	1666.2	17.19	101.0	0.70	765	538	290	-
127886L_08	3.99145	1.24	0.28836	1.18	0.60	3.46788736	1.18	0.10039	1.09	1631.2	20.13	1632.5	10.07	1633.3	16.97	100.1	0.20	242	49	81	-
127886L_09	3.98948	1.21	0.29767	1.17	0.61	3.35942487	1.17	0.0972	1.05	1571	19.56	1632.1	9.81	1679.7	17.32	106.9	0.81	1221	994	469	-
127886L_10	0.49803	1.50	0.06557	1.19	0.48	15.2508769	1.19	0.05508	1.40	415.4	30.58	410.4	5.07	409.4	4.73	98.6	0.01	97	1	7	-
127886L_11	4.15826	1.27	0.29855	1.18	0.58	3.34952269	1.18	0.10101	1.13	1642.8	20.76	1665.8	10.41	1684.1	17.51	102.5	0.50	79	40	29	2
127886L_12	3.99183	1.23	0.28833	1.18	0.60	3.46824819	1.18	0.10041	1.09	1631.6	19.99	1632.5	10.03	1633.2	16.96	100.1	0.63	240	150	87	-
127886L_13	4.00561	1.22	0.28928	1.17	0.61	3.45685841	1.17	0.10042	1.06	1631.9	19.57	1635.3	9.88	1638	16.96	100.4	0.60	303	182	109	-
127886L_14	3.8625	1.23	0.28234	1.18	0.60	3.541829	1.18	0.09921	1.08	1609.4	19.9	1605.9	9.90	1603.1	16.67	99.6	0.89	505	451	188	-
127886L_15	0.49624	1.62	0.06421	1.20	0.45	15.5738981	1.20	0.05605	1.52	453.9	33.19	409.2	5.45	401.2	4.67	88.4	0.00	74	0	5	-
127886L_16	3.96334	1.21	0.28799	1.17	0.60	3.47234279	1.17	0.09981	1.06	1620.5	19.57	1626.7	9.84	1631.5	16.90	100.7	0.79	354	281	132	-
127886L_17	4.40661	1.26	0.30775	1.18	0.59	3.24939074	1.18	0.10384	1.11	1693.9	20.34	1713.6	10.42	1729.6	17.90	102.1	0.76	73	55	29	-
127886L_18	3.52763	1.22	0.2577	1.17	0.61	3.88048118	1.17	0.09928	1.06	1610.6	19.67	1533.4	9.64	1478	15.50	91.8	0.74	429	319	142	-
127886L_19	3.80617	1.21	0.27718	1.17	0.61	3.60776391	1.17	0.09956	1.05	1615.9	19.49	1593.8	9.73	1577.1	16.40	97.6	1.04	899	936	338	-
127886L_20	4.08182	1.24	0.2976	1.18	0.60	3.36021505	1.18	0.09947	1.09	1614.2	20.05	1650.7	10.08	1679.4	17.39	104.0	0.95	175	167	70	-
127886L_21	3.94789	1.22	0.28877	1.17	0.61	3.4629636	1.17	0.09915	1.06	1608.2	19.62	1623.6	9.85	1635.4	16.95	101.7	0.59	541	319	194	-
127886L_22	3.97274	1.22	0.28436	1.17	0.60	3.51666901	1.17	0.10132	1.07	1648.5	19.59	1628.6	9.89	1613.3	16.75	97.9	0.58	448	258	158	-
127886L_23	3.30233	1.22	0.24289	1.17	0.61	4.11709004	1.17	0.0986	1.05	1597.8	19.64	1481.6	9.47	1401.7	14.78	87.7	0.98	608	597	200	-
127886L_24	4.00465	1.23	0.29055	1.17	0.60	3.44174841	1.17	0.09996	1.07	1623.3	19.79	1635.1	9.96	1644.3	17.05	101.3	0.49	214	104	76	-

Analysis_#	Concordia output Pb207 U235	1s%	Pb206 U238	1s%	roh	Tera-Wasserburg output 238/206	1s%	207/206	1s%	Age estimates (ma) Pb207 Pb206	1s	Pb207 U235	1s	Pb206 U238	1s	conc	Concentrations Th/U	U*	Th*	Phtot*	Pb com. >LLD (%)
197562_04	4.0009	1.07	0.2843	1.03	0.50	3.51741119	1.03	0.10206	1.05	1662	19.32	1634.4	8.69	1613	14.66	97.1	0.59	130	77	47	-
197562_05	4.08392	1.06	0.2854	1.03	0.50	3.50385424	1.03	0.10378	1.04	1692.8	18.98	1651.1	8.61	1618.5	14.68	95.6	1.02	221	226	87	-
197562_06	4.06008	1.13	0.28577	1.04	0.48	3.49931763	1.04	0.10304	1.12	1679.6	20.52	1646.3	9.24	1620.4	14.88	96.5	0.52	123	64	44	-
197562_07	3.81408	1.05	0.27327	1.02	0.50	3.65938449	1.02	0.10122	1.04	1646.6	19.03	1595.7	8.47	1557.4	14.19	94.6	0.85	353	299	129	-
197562_08	4.19919	1.05	0.2924	1.03	0.50	3.41997264	1.03	0.10415	1.04	1699.4	18.93	1673.9	8.65	1653.5	14.96	97.3	0.98	217	214	87	-
197562_09	4.19243	1.06	0.29407	1.03	0.51	3.40055089	1.03	0.10339	1.03	1685.9	18.97	1672.5	8.66	1661.8	15.04	98.6	1.03	213	220	86	-
197562_10	3.89399	1.10	0.28067	1.03	0.49	3.56290305	1.03	0.10062	1.07	1635.5	19.86	1612.4	8.85	1594.7	14.59	97.5	0.68	203	139	73	-
197562_11	4.26049	1.06	0.29802	1.03	0.50	3.3554795	1.03	0.10368	1.04	1691	19.05	1685.8	8.72	1681.5	15.21	99.4	0.38	182	68	65	-
197562_12	4.07166	1.09	0.29149	1.03	0.50	3.43064942	1.03	0.1013	1.07	1648.2	19.73	1648.6	8.89	1649	15.01	100.0	0.58	84	48	31	-
197562_13	4.32272	1.08	0.30313	1.03	0.50	3.29891466	1.03	0.10342	1.05	1686.4	19.41	1697.7	8.90	1706.8	15.45	101.2	0.67	139	93	54	-
197562_14	4.13284	1.05	0.28898	1.02	0.51	3.46044709	1.03	0.10372	1.03	1691.7	18.84	1660.8	8.59	1636.4	14.83	96.7	0.80	318	254	121	-
197562_15	4.15249	1.06	0.29196	1.03	0.51	3.42512673	1.03	0.10315	1.04	1681.5	19.11	1664.7	8.70	1651.3	14.98	98.2	0.91	368	334	144	-
197562_16	4.0621	1.06	0.29079	1.03	0.51	3.4389078	1.03	0.10131	1.04	1648.2	19.12	1646.7	8.63	1645.5	14.92	99.8	0.69	194	133	73	-
197562_17	4.13898	1.07	0.29571	1.03	0.50	3.38169152	1.03	0.10151	1.04	1651.9	19.29	1662	8.75	1670	15.15	101.1	0.75	136	102	52	-
197562_18	4.20997	1.07	0.29941	1.03	0.50	3.33990181	1.03	0.10198	1.05	1660.4	19.35	1676	8.81	1688.4	15.30	101.7	0.74	121	90	47	-
197562_19	3.97337	1.09	0.28298	1.03	0.49	3.53381864	1.03	0.10183	1.07	1657.8	19.7	1628.8	8.85	1606.3	14.69	96.9	0.90	161	145	61	-
197562_20	4.13913	1.16	0.29164	1.05	0.47	3.42888493	1.05	0.10293	1.15	1677.6	21.06	1662.1	9.52	1649.7	15.22	98.3	0.56	105	58	38	-
197562_21	4.06247	1.07	0.28753	1.03	0.50	3.47789796	1.03	0.10247	1.04	1669.3	19.18	1646.8	8.69	1629.2	14.82	97.6	0.49	201	98	71	1
197562_22	4.29081	1.07	0.30086	1.03	0.50	3.32380509	1.03	0.10343	1.05	1686.6	19.26	1691.6	8.83	1695.6	15.37	100.5	0.91	230	209	93	1
197562_23	4.2583	1.07	0.29782	1.03	0.51	3.35773286	1.03	0.1037	1.04	1691.3	19.16	1685.3	8.78	1680.5	15.24	99.4	0.70	149	104	57	1
197562_24	4.02394	1.14	0.28811	1.04	0.48	3.47089653	1.04	0.10129	1.12	1647.9	20.62	1639	9.25	1632.1	15.01	99.0	0.57	147	83	53	2

Table: Sample 197562L

	Isotope ratios									Age estimates (ma)							Concentrations				Pb com.
	Concordia output					Tera-Wasserburg output															
Analysis #	Pb207 U235	1s%	Pb206 U238	1s%	roh	238/206	1s%	207/206	1s%	Pb207 Pb206	1s	Pb207 U235	1s	Pb206 U238	1s	conc	Th/U	U*	Th*	Phtot*	>LLD (%)
197562L_04	4.40005	1.06	0.31028	1.01	0.48	3.222895449	1.01	0.10284	1.06	1676.1	19.48	1712.4	8.78	1742.1	15.43	103.9	0.66	85	56	34	2
197562L_05	4.16256	1.05	0.29542	1.01	0.48	3.385011171	1.01	0.10219	1.05	1664.2	19.29	1666.7	8.60	1668.6	14.83	100.3	0.46	130	60	47	
197562L_06	0.50161	2.14	0.06587	1.11	0.23	15.18141794	1.11	0.05823	2.17	421.4	47.36	412.8	7.27	411.2	4.41	97.6	0.00	122	0	8	
197562L_07	0.516	1.62	0.06517	1.06	0.31	15.34448366	1.06	0.05742	1.64	507.3	36.12	422.5	5.60	407	4.15	80.2	0.00	134	0	9	
197562L_08	0.48677	1.37	0.06619	1.03	0.35	15.10802336	1.03	0.05443	1.40	389	30.75	409.5	4.64	413.1	4.12	106.2	0.00	134	0	9	
197562L_09	0.49827	1.19	0.06537	1.01	0.42	15.2975371	1.01	0.05528	1.19	423.2	26.28	410.5	4.02	408.2	4.02	96.5	0.00	207	0	14	
197562L_10	0.53119	1.21	0.06736	1.02	0.42	14.8456057	1.02	0.05719	1.21	498.5	26.72	432.6	4.14	420.2	4.14	84.3	0.00	296	1	21	
197562L_11	0.49172	1.21	0.06436	1.03	0.41	15.53760099	1.03	0.05541	1.23	428.6	26.89	406.1	3.97	402.1	3.97	93.8	0.00	152	0	10	
197562L_12	0.46391	1.34	0.06451	1.02	0.37	15.50147264	1.02	0.05552	1.35	433	29.28	407.6	4.01	402	4.01	93.1	0.00	165	0	11	
197562L_13	0.52209	1.14	0.06614	1.01	0.45	15.1194436	1.01	0.05725	1.14	500.6	25.18	426.5	3.97	412.9	4.05	82.5	0.01	223	1	16	
197562L_14	0.49416	2.17	0.06552	1.11	0.22	15.26251526	1.11	0.0547	2.21	400.1	48.28	407.7	4.40	409.1	4.40	102.2	0.00	101	0	7	
197562L_15	3.97933	1.06	0.28782	1.01	0.48	3.474393718	1.01	0.10027	1.06	1629.1	19.45	1630	8.57	1630.6	14.56	100.1	0.54	169	92	61	
197562L_16	3.69061	1.06	0.26383	1.01	0.48	3.790319524	1.01	0.10145	1.05	1650.8	19.42	1569.3	8.44	1509.4	13.61	91.4	0.57	176	100	59	1
197562L_17	3.66273	1.06	0.26902	1.01	0.48	3.773300128	1.01	0.10023	1.06	1628.4	19.49	1563.3	8.44	1515.5	13.66	93.1	0.46	137	64	45	
197562L_18	4.28948	1.11	0.30031	1.02	0.46	3.329892444	1.02	0.10359	1.11	1689.4	20.34	1691.3	9.15	1692.8	15.20	100.2	0.71	97	69	38	
197562L_19	0.48761	1.04	0.06478	1.00	0.48	15.4386623	1.00	0.05459	1.04	395.3	22.94	403.3	3.46	404.6	3.95	102.4	0.00	1252	2	86	1
197562L_20	0.50151	1.27	0.06564	1.02	0.39	15.23461304	1.02	0.05541	1.28	428.4	28.16	412.7	4.31	409.9	4.06	95.7	0.00	170	0	12	
197562L_21	0.49519	1.22	0.06454	1.02	0.42	15.49426712	1.02	0.05564	1.22	437.8	26.5	408.4	4.09	403.2	3.99	92.1	0.00	223	0	15	
197562L_22	3.66023	1.07	0.26349	1.01	0.48	3.795210444	1.01	0.10075	1.06	1637.9	19.65	1562.7	8.52	1507.7	13.63	92.1	0.55	96	53	32	
197562L_23	4.1005	1.06	0.29355	1.01	0.48	3.406574689	1.01	0.1013	1.01	1648.2	19.47	1654.4	8.65	1659.3	14.82	100.7	0.53	104	55	38	
197562L_24	3.8054	1.07	0.27352	1.01	0.48	3.650039778	1.01	0.1009	1.06	1640.7	19.61	1593.9	8.58	1558.6	14.04	95.0	0.68	94	64	33	2

Table: Sample 197578

	Isotope ratios									Age estimates (ma)							Concentrations				Pb com.
	Concordia output					Tera-Wasserburg output															
Analysis #	Pb207 U235	1s%	Pb206 U238	1s%	roh	238/206	1s%	207/206	1s%	Pb207 Pb206	1s	Pb207 U235	1s	Pb206 U238	1s	conc	Th/U	U*	Th*	Phtot*	>LLD (%)
197578_04	3.83666	1.04	0.27511	1.02	0.51	3.63490967	1.02	0.10114	1.02	1645.2	18.83	1600.5	8.36	1566.7	14.17	95.2	0.40	520	209	174	-
197578_05	3.42568	1.11	0.24632	1.03	0.47	4.05975966	1.03	0.10086	1.10	1640	20.22	1510.3	8.71	1419.5	13.11	86.6	0.45	191	87	58	-
197578_06	3.79177	1.05	0.27455	1.02	0.50	3.6423238	1.02	0.10016	1.03	1627	19.03	1591	8.40	1563.9	14.17	96.1	0.50	346	171	117	-
197578_07	3.91204	1.07	0.27985	1.03	0.49	3.57334286	1.03	0.10138	1.06	1649.5	19.47	1616.2	8.67	1590.6	14.44	96.4	0.62	104	65	37	-
197578_08	4.0826	1.06	0.29351	1.02	0.50	3.40703894	1.02	0.10088	1.04	1640.3	19.23	1650.8	8.63	1659	14.95	101.1	0.72	182	132	70	-
197578_09	0.67279	1.51	0.07829	1.06	0.35	12.7730234	1.06	0.06233	1.51	685.3	32.02	522.4	6.15	485.9	4.96	70.9	0.04	127	6	11	-
197578_10	3.8587	1.04	0.2785	1.02	0.50	3.59066427	1.02	0.10048	1.03	1633.1	18.89	1605.1	8.39	1583.8	14.32	97.0	0.36	446	159	149	-
197578_11	3.96056	1.05	0.28254	1.02	0.50	3.53932187	1.02	0.10166	1.03	1654.6	19.02	1626.2	8.51	1604.2	14.51	97.0	0.69	212	147	78	-
197578_12	3.90928	1.06	0.27729	1.02	0.50	3.60633272	1.02	0.10224	1.05	1665.3	19.16	1615.6	8.56	1577.7	14.32	94.7	0.56	283	158	99	-
197578_13	4.2597	1.16	0.30158	1.04	0.46	3.31586975	1.04	0.10244	1.15	1668.7	21.1	1685.6	9.54	1699.1	15.53	101.8	1.17	87	102	38	-
197578_14	3.75007	1.12	0.26962	1.03	0.47	3.70892367	1.03	0.10087	1.11	1640.2	20.41	1582.1	8.98	1538.9	14.14	93.8	0.70	129	91	45	-
197578_15	3.88328	1.12	0.28059	1.03	0.47	3.56391889	1.03	0.10037	1.11	1630.9	20.36	1610.2	9.01	1594.4	14.58	97.8	0.95	177	168	68	-
197578_16	0.51699	1.32	0.06726	1.04	0.40	14.8676777	1.04	0.05574	1.31	441.9	28.61	423.1	4.57	419.6	4.22	95.0	0.00	212	1	15	-
197578_17	4.06075	1.48	0.28556	1.10	0.37	3.50189102	1.10	0.10313	1.48	1681.2	27.22	1646.5	12.09	1619.3	15.77	96.3	0.99	53	52	21	-
197578_18	0.7321	1.19	0.08154	1.03	0.44	12.2639195	1.03	0.06511	1.18	778	24.57	557.8	5.09	505.3	5.02	64.9	0.04	229	9	21	-
197578_19	3.45961	1.09	0.24987	1.03	0.48	4.00208108	1.03	0.10041	1.08	1631.7	19.79	1518.1	8.57	1437.8	13.25	88.1	0.28	328	93	97	-
197578_20	4.06444	1.05	0.28845	1.02	0.51	3.46680534	1.02	0.10219	1.05	1664.3	18.92	1647.2	8.53	1633.8	14.76	98.2	0.48	287	139	103	-
197578_21	4.14418	1.17	0.29656	1.04	0.46	3.37199892	1.04	0.10134	1.15	1648.6	21.3	1663.1	9.56	1674.2	15.37	101.5	0.65	85	56	32	-
197578_22	3.6028	1.05	0.26415	1.02	0.50	3.78572781	1.02	0.09891	1.03	1603.8	19.03	1550.1	8.31	1511.1	13.77	94.2	0.44	455	200	147	-
197578_23	3.98505	1.06	0.28542	1.03	0.50	3.50360872	1.03	0.10126	1.05	1647.3	19.3	1631.2	8.64	1618.6	14.68	98.3	1.04	242	251	95	-
197578_24	3.85668	1.05	0.27444	1.02	0.51	3.6437837	1.03	0.10192	1.03	1659.3	18.96	1604.7	8.46	1563.3	14.20	94.2	0.37	465	170	154	-

Table — Analyses 197586

Analysis #	Pb207 U235	1s%	Pb206 U238	1s%	roh	238/206	1s%	207/206	1s%	Pb207 Pb206	1s	Pb207 U235	1s	Pb206 U238	1s	conc	Th/U	U*	Th*	Phtot*	>LLD (%)
197586_04	3.76776	1.26	0.26527	1.06	0.43	3.76974403	1.06	0.10301	1.25	1679	22.92	1585.9	10.13	1516.8	14.37	90.3	0.68	154	105	53	
197586_05	3.14001	1.14	0.23188	1.04	0.48	4.31257547	1.04	0.09821	1.12	1590.4	20.85	1442.6	8.80	1344.4	12.64	84.5	0.68	130	88	40	
197586_06	4.09235	1.06	0.2899	1.03	0.51	3.44946533	1.03	0.10238	1.04	1667.7	19.08	1652.8	8.67	1641	14.93	98.4	0.65	221	143	82	
197586_07	2.92168	1.06	0.21759	1.03	0.51	4.59579944	1.03	0.09738	1.04	1574.5	19.29	1387.5	8.03	1269.1	11.87	80.6	0.49	310	151	84	
197586_08	3.97147	1.07	0.2867	1.03	0.50	3.48796652	1.03	0.10046	1.06	1632.7	19.39	1628.4	8.72	1625	14.83	99.5	0.84	139	118	53	
197586_09	1.28876	1.15	0.1146	1.04	0.47	8.72600349	1.04	0.08156	1.13	1234.9	22.06	840.7	6.58	699.4	6.89	56.6	0.03	474	16	60	
197586_10	3.48879	2.83	0.26202	1.43	0.23	3.81650256	1.43	0.09657	2.87	1558.8	52.94	1524.7	22.35	1500.2	19.11	96.2	1.12	47	53	17	9
197586_11	0.53991	3.33	0.06641	1.31	0.15	15.0579732	1.31	0.05897	3.39	565.8	72.23	438.4	5.23	414.5	5.23	73.3	0.01	37	0	3	
197586_12	4.12374	1.08	0.29411	1.03	0.50	3.4000884	1.03	0.10169	1.06	1655.1	19.5	1659	8.86	1662	15.16	100.4	0.77	107	83	41	
197586_13	3.80637	1.09	0.27307	1.04	0.50	3.66206467	1.04	0.10109	1.07	1644.3	19.68	1594.1	8.78	1556.4	14.33	94.7	0.85	216	184	79	
197586_14	2.04928	1.60	0.16757	1.11	0.34	5.96765531	1.11	0.0887	1.61	1397.6	30.5	1132.1	10.93	998.7	10.24	71.5	0.12	43	5	8	
197586_15	3.73504	1.08	0.27055	1.03	0.50	3.69617446	1.03	0.10012	1.06	1626.4	19.58	1578.9	8.69	1543.6	14.21	94.9	1.08	134	146	51	
197586_16	3.99457	1.09	0.2848	1.04	0.50	3.51123596	1.04	0.10172	1.06	1655.8	19.53	1633.1	8.82	1615.5	14.80	97.6	0.83	107	89	41	
197586_17	4.08659	1.08	0.29212	1.03	0.50	3.42325072	1.03	0.10146	1.05	1650.9	19.46	1651.6	8.83	1652.1	15.09	100.1	0.61	117	71	43	
197586_18	3.79765	1.07	0.27561	1.03	0.51	3.62831537	1.03	0.09993	1.04	1622.8	19.28	1592.2	8.60	1569.2	14.39	96.7	0.57	242	137	84	
197586_19	3.96911	1.08	0.28482	1.04	0.50	3.5109894	1.04	0.10107	1.06	1643.8	19.48	1627.9	8.78	1615.6	14.80	98.3	0.73	123	90	46	
197586_20	4.07862	1.07	0.28797	1.03	0.51	3.47258395	1.03	0.10272	1.04	1673.8	19.16	1650	8.73	1631.4	14.90	97.5	1.06	173	182	69	
197586_21	3.59775	1.23	0.2613	1.06	0.45	3.82701875	1.06	0.09986	1.21	1621.5	22.4	1549	9.77	1496.5	14.14	92.3	0.83	76	63	26	
197586_22	3.91868	1.10	0.28007	1.04	0.49	3.57053594	1.04	0.10148	1.07	1651.3	19.7	1617.5	8.86	1591.7	14.64	96.4	0.91	146	133	55	
197586_23	4.05611	1.11	0.29209	1.04	0.49	3.42360231	1.04	0.10071	1.08	1637.3	19.96	1645.5	9.02	1652	15.15	100.9	0.93	83	77	33	
197586_24	0.58959	3.71	0.06998	1.37	0.12	14.2897971	1.37	0.0611	3.80	642.8	79.45	470.6	13.98	436	5.81	67.8	0.02	30	1	2	

Table — Analyses 200987

Analysis #	Pb207 U235	1s%	Pb206 U238	1s%	roh	238/206	1s%	207/206	1s%	Pb207 Pb206	1s	Pb207 U235	1s	Pb206 U238	1s	conc	Th/U	U*	Th*	Phtot*	>LLD (%)
200987_04	4.09691	1.19	0.292	1.04	0.43	3.42465753	1.04	0.10176	1.20	1656.4	21.97	1653.7	9.75	1651.5	15.10	99.7	0.62	39	24	14	
200987_05	3.89182	1.28	0.2789	1.05	0.41	3.58551452	1.05	0.1012	1.28	1646.2	23.67	1612	10.35	1585.8	14.78	96.3	0.51	54	28	19	
200987_06	4.05128	1.13	0.29147	1.03	0.46	3.43088483	1.03	0.1008	1.12	1638.9	20.71	1644.6	9.17	1648.9	14.91	100.6	0.51	51	26	18	4
200987_07	4.06842	1.22	0.2873	1.04	0.43	3.48068221	1.04	0.1027	1.22	1673.5	22.37	1648	9.93	1628	14.98	97.3	0.57	52	29	19	4
200987_08	3.9077	1.07	0.27993	1.01	0.49	3.57232165	1.01	0.10124	1.06	1647	19.56	1615.3	8.62	1591	14.32	96.6	0.58	97	56	34	
200987_09	4.12765	1.14	0.29559	1.03	0.45	3.38306438	1.03	0.10127	1.15	1647.6	21.03	1659.8	9.35	1669.4	15.13	101.3	0.61	44	27	16	
200987_10	4.03794	1.13	0.29047	1.03	0.46	3.44269632	1.03	0.10082	1.12	1639.2	20.74	1641.9	9.18	1643.9	14.89	100.3	0.73	48	36	18	
200987_11	3.91427	1.19	0.28614	1.03	0.43	3.49479276	1.03	0.09921	1.19	1609.3	21.94	1616.6	9.60	1622.2	14.85	100.8	0.65	52	34	19	
200987_12	2.85678	1.12	0.212	1.02	0.45	4.71698113	1.02	0.09773	1.13	1581.2	20.82	1370.6	8.45	1239.4	11.54	78.4	0.45	62	28	17	
200987_13	4.13749	1.16	0.29073	1.03	0.45	3.43961751	1.03	0.10321	1.15	1682.6	21.15	1661.7	9.45	1645.2	14.98	97.8	0.50	41	20	15	
200987_14	3.99852	1.15	0.28624	1.03	0.45	3.49357183	1.03	0.10131	1.15	1648.2	21.17	1633.9	9.36	1622.7	14.78	98.5	0.52	45	23	16	
200987_15	4.10307	1.13	0.29134	1.03	0.46	3.43241573	1.03	0.10214	1.13	1663.3	20.7	1654.9	9.22	1648.2	14.94	99.1	0.51	51	26	19	
200987_16	4.12466	1.13	0.29191	1.03	0.46	3.4257134	1.03	0.10247	1.12	1669.4	20.61	1659.2	9.20	1651.1	14.95	98.9	0.60	49	29	18	
200987_17	4.15598	1.16	0.29428	1.03	0.45	3.39812424	1.03	0.10242	1.16	1668.4	21.33	1665.4	9.53	1662.9	15.15	99.7	0.66	46	31	17	
200987_18	3.47037	1.14	0.25345	1.03	0.45	3.96118432	1.03	0.0997	1.14	1618.4	21.1	1520.5	9.02	1451.1	13.37	89.7	0.53	64	34	20	
200987_19	4.09294	1.15	0.29297	1.03	0.45	3.4131877	1.03	0.10132	1.14	1648.4	21.14	1652.9	9.40	1656.3	15.06	100.5	0.63	43	27	16	
200987_20	3.87256	1.14	0.27971	1.03	0.45	3.575131386	1.03	0.10041	1.14	1631.6	20.93	1608	9.18	1589.9	14.49	97.4	0.55	47	26	17	
200987_21	4.08359	1.09	0.29126	1.02	0.48	3.43338511	1.02	0.10168	1.08	1655	19.95	1651	8.89	1647.8	14.85	99.6	0.66	67	44	25	
200987_22	3.99178	1.07	0.28423	1.02	0.48	3.518277451	1.02	0.10185	1.06	1658.2	19.51	1632.5	8.67	1612.6	14.52	97.3	0.64	94	60	34	
200987_23	4.06853	1.13	0.28919	1.03	0.46	3.45793423	1.03	0.10203	1.13	1661.4	20.73	1648	9.23	1637.5	14.87	98.6	0.54	51	27	18	
200987_24	3.7087	1.16	0.26522	1.03	0.45	3.770454717	1.03	0.10141	1.15	1650.1	21.27	1573.2	9.26	1516.5	13.95	91.9	0.60	70	42	24	

Isotope ratios / **Age estimates (ma)** / **Concentrations** / **Pb com.**

Analysis #	Pb207 U235	1s%	Pb206 U238	1s%	roh	238/206	1s%	207/206	1s%	Pb207 Pb206	1s	Pb207 U235	1s	Pb206 U238	1s	conc	Th/U	U*	Th*	Phtot*	>LLD (%)
	Concordia output					Tera-Wasserburg output															
2009871_04	2.85722	1.34	0.21267	1.08	0.41	4.70212066	1.08	0.09744	1.33	1575.7	24.73	1370.7	10.09	1243	12.16	78.9	0.41	69	29	18	-
2009871_05	4.17663	1.17	0.29642	1.05	0.47	3.37359153	1.05	0.10219	1.14	1664.3	21.09	1669.4	9.59	1673.5	15.51	100.6	0.68	62	42	24	-
2009871_06	4.094	1.20	0.2903	1.06	0.46	3.44471237	1.06	0.10228	1.18	1665.9	21.67	1653.1	9.80	1643	15.33	98.6	0.71	45	32	17	-
2009871_07	3.98476	1.16	0.28804	1.05	0.48	3.47174004	1.05	0.10033	1.14	1630.3	21.03	1631.1	9.44	1631.7	15.14	100.1	0.43	86	36	30	-
2009871_08	4.11018	1.24	0.29241	1.06	0.45	3.41985568	1.06	0.10195	1.22	1659.8	22.39	1656.3	10.11	1653.5	15.51	99.6	0.66	52	34	19	-
2009871_09	4.22966	1.13	0.30036	1.05	0.49	3.32933813	1.05	0.10213	1.11	1663.2	20.35	1679.8	9.30	1693.1	15.58	101.8	0.60	59	35	22	-
2009871_10	3.65161	1.26	0.26637	1.07	0.44	3.754417652	1.07	0.09942	1.25	1613.3	23.05	1560.9	10.08	1522.3	14.47	94.4	0.58	88	51	30	-
2009871_11	3.68288	1.35	0.26979	1.08	0.42	3.7065866	1.08	0.099	1.33	1605.5	24.72	1567.7	10.78	1539.7	14.82	95.9	0.64	51	33	18	-
2009871_12	3.14931	1.07	0.23299	1.04	0.52	4.2920297	1.04	0.09803	1.04	1587.1	19.4	1444.8	8.28	1350.1	12.63	85.1	0.42	247	103	71	-
2009871_13	3.72666	1.19	0.27308	1.05	0.46	3.66193057	1.05	0.09897	1.17	1604.9	21.68	1577.1	9.55	1556.4	14.60	97.0	0.60	78	47	27	4
2009871_14	3.94835	1.32	0.28456	1.08	0.42	3.51419736	1.08	0.10063	1.31	1635.8	24.09	1623.7	10.71	1614.3	15.40	98.7	0.60	46	28	17	-
2009871_15	3.88069	1.27	0.28302	1.07	0.44	3.5333192	1.07	0.09945	1.26	1613.8	23.22	1609.7	10.29	1606.5	15.21	99.5	0.47	77	36	27	-
2009871_16	4.06779	1.16	0.2888	1.05	0.48	3.46260388	1.05	0.10215	1.14	1663.6	20.95	1647.9	9.49	1635.6	15.20	98.3	0.64	47	30	17	-
2009871_17	4.1272	1.28	0.29206	1.07	0.44	3.42395398	1.07	0.10249	1.26	1669.7	23.09	1659.7	10.44	1651.8	15.62	98.9	0.45	111	50	40	-
2009871_18	4.12163	1.10	0.29652	1.04	0.51	3.3724538	1.04	0.10081	1.06	1639.1	19.65	1658.6	8.95	1674	15.35	102.1	0.65	101	66	38	-
2009871_19	0.57452	6.61	0.06294	2.02	0.07	15.8881474	2.02	0.0662	6.78	812.6	135.8	460.9	24.50	393.5	7.71	48.4	0.00	26	0	2	-
2009871_20	4.18211	1.31	0.29473	1.08	0.42	3.39293591	1.08	0.10291	1.30	1677.3	23.78	1670.5	10.77	1665.1	15.84	99.3	0.61	49	30	18	-
2009871_21	4.04488	1.21	0.29865	1.06	0.47	3.34840114	1.06	0.09823	1.18	1590.8	21.99	1643.3	9.84	1684.6	15.71	105.9	0.60	96	57	36	4
2009871_22	3.54407	1.24	0.2589	1.06	0.45	3.86249517	1.06	0.09928	1.22	1610.6	22.46	1537.1	9.78	1484.2	14.10	92.2	0.43	64	27	20	-
2009871_23	4.10802	1.19	0.2928	1.06	0.47	3.41530055	1.06	0.10175	1.17	1656.4	21.5	1655.9	9.74	1655.5	15.45	99.9	0.61	51	31	19	-
2009871_24	3.87397	1.51	0.28172	1.11	0.38	3.54962374	1.11	0.09973	1.50	1619.1	27.77	1608.3	12.21	1600	15.80	98.8	0.62	74	46	27	5

Isotope ratios / **Age estimates (ma)** / **Concentrations** / **Pb com.**

Analysis #	Pb207 U235	1s%	Pb206 U238	1s%	roh	238/206	1s%	207/206	1s%	Pb207 Pb206	1s	Pb207 U235	1s	Pb206 U238	1s	conc	Th/U	U*	Th*	Phtot*	>LLD (%)
	Concordia output					Tera-Wasserburg output															
1278911_01	0.52186	3.18	0.06539	1.19	0.12	15.29288824	1.19	0.05788	3.27	525	70	426.4	11.07	408.3	4.73	77.8	0.00	34	0	2	-
1278911_02	4.21679	1.07	0.29695	0.94	0.36	3.3675070298	0.94	0.10298	1.15	1678.6	20.96	1677.3	8.76	1676.2	13.90	99.9	0.69	172	119	67	-
1278911_03	3.34438	0.95	0.24417	0.92	0.40	4.095507229	0.92	0.09934	1.03	1611.7	19.04	1491.5	7.41	1408.3	11.66	87.4	0.39	545	211	163	-
1278911_04	4.12783	0.97	0.28785	0.92	0.39	3.474031644	0.92	0.104	1.05	1696.7	19.15	1659.8	7.90	1630.8	13.32	96.1	0.61	177	109	66	-
1278911_05	0.52131	3.90	0.06263	1.34	0.09	15.96678908	1.34	0.06036	4.01	616.5	84.3	426	13.57	391.6	5.09	63.5	0.00	40	0	3	28
1278911_06	4.10108	0.96	0.28809	0.92	0.39	3.471137492	0.92	0.10324	1.05	1683.1	19.12	1654.5	7.86	1632	13.33	97.0	0.92	171	156	68	-
1278911_07	0.50732	1.31	0.06474	0.94	0.27	15.44640099	0.94	0.05683	1.39	484.1	30.6	416.6	4.48	404.4	3.72	83.5	0.00	78	0	5	-
1278911_08	0.48106	1.73	0.06315	0.98	0.20	15.83531275	0.98	0.05525	1.81	422	39.19	416.6	5.72	394.8	3.79	93.6	0.00	62	0	4	-
1278911_09	0.50439	3.78	0.06558	1.30	0.10	15.2485514	1.30	0.05578	3.87	443.1	83.96	414.7	12.86	409.5	5.12	92.4	0.00	31	0	2	-
1278911_10	4.17217	0.97	0.29207	0.93	0.40	3.42383675	0.93	0.1036	1.04	1689.5	19.16	1668.6	7.93	1651.9	13.51	97.8	0.90	188	169	76	-
1278911_11	4.20733	0.98	0.29638	0.93	0.39	3.37404683	0.93	0.10295	1.06	1678	19.46	1675.5	8.08	1673.4	13.70	99.7	0.83	126	105	50	-
1278911_12	0.50649	2.40	0.06636	1.07	0.15	15.0693189	1.07	0.05535	2.48	426.2	53.79	416.1	8.18	414.2	4.30	97.2	0.00	40	0	3	-
1278911_13	4.12759	0.97	0.29063	0.93	0.40	3.44080102	0.93	0.103	1.04	1678.9	19.14	1659.8	7.90	1644.7	13.46	98.0	0.74	160	119	62	-
1278911_14	4.05455	0.98	0.29261	0.93	0.39	3.4175182	0.93	0.10049	1.05	1633.2	19.56	1645.2	8.02	1654.5	13.58	101.3	0.70	134	94	51	-
1278911_15	3.72016	0.98	0.26186	0.93	0.39	3.81883449	0.93	0.10303	1.06	1679.5	19.41	1575.7	7.86	1499.3	12.44	89.3	0.65	114	74	39	-
1278911_16	4.17262	0.95	0.29419	0.92	0.40	3.39916381	0.92	0.10286	1.03	1676.4	18.91	1668.7	7.81	1662.4	13.57	99.2	0.69	374	257	144	-
1278911_17	3.77531	0.98	0.2671	0.93	0.39	3.74391614	0.93	0.10251	1.05	1670	19.3	1587.5	7.84	1526.1	12.64	91.4	0.70	138	96	49	-
1278911_18	0.48801	1.55	0.06245	0.98	0.24	16.0128102	0.98	0.05667	1.62	478	35.79	403.6	5.16	390.5	3.70	81.7	0.00	56	0	4	-
1278911_19	0.54248	3.05	0.06466	1.18	0.11	15.4655119	1.18	0.06085	3.14	633.8	66.15	440.1	10.88	403.9	4.63	63.7	0.01	28	0	2	-
1278911_20	0.50839	2.17	0.06407	1.05	0.17	15.6079288	1.05	0.06755	2.24	512.2	48.85	417.4	7.41	400.3	4.06	78.2	0.00	43	0	3	-
1278911_21	0.50987	1.65	0.06302	0.98	0.23	15.8679784	0.98	0.06967	1.72	555	37.77	418.4	5.67	394	3.78	71.0	0.00	45	0	3	-
1278911_22	4.32023	0.98	0.29706	0.93	0.40	3.3663233	0.93	0.10547	1.05	1722.6	19.26	1697.2	8.10	1676.7	13.77	97.3	1.02	142	145	60	-
1278911_23	0.50636	1.34	0.06511	0.95	0.29	15.3586239	0.95	0.05641	1.40	467.6	31.08	416	4.57	406.6	3.77	87.0	0.00	74	0	5	-
1278911_24	4.13381	0.97	0.28733	0.93	0.39	3.4803188	0.93	0.10434	1.04	1702.7	19.03	1661	7.91	1628.2	13.39	95.6	0.83	211	174	82	-

Table STO131390L

Analysis_#	Pb207_U235	1s%	Pb206_U238	1s%	roh	238/206	1s%	207/206	1s%	Pb207_Pb206	1s	Pb207_U235	1s	Pb206_U238	1s	conc	Th/U	U*	Th*	Ptot*	>LLD (%)
			Concordia output			Tera-Wasserburg output						Age estimates (ma)						Concentrations			Pb com.
STO131390L_04	0.52675	1.55	0.006748	0.98	0.24	14.8192057	0.98	0.05661	1.63	475.6	35.81	429.6	5.45	421	4.00	88.5	0.00	98	0	7	-
STO131390L_05	0.50808	0.98	0.006716	1.04	0.39	14.8898154	0.94	0.05487	1.06	406.8	23.09	417.2	3.36	419	3.79	103.0	0.01	1053	6	75	-
STO131390L_06	3.98068	1.07	0.28154	0.95	0.38	3.55189316	0.95	0.10254	1.13	1670.7	20.83	1630.3	8.67	1599.1	13.46	95.7	0.95	105	100	41	-
STO131390L_07	3.79551	0.98	0.27155	0.94	0.40	3.68256306	0.94	0.10137	1.05	1649.4	19.24	1591.8	7.84	1548.6	12.87	93.9	0.71	239	170	86	-
STO131390L_08	3.12617	1.03	0.23211	0.94	0.38	4.3083021	0.94	0.09768	1.10	1580.3	20.35	1439.2	7.91	1345.5	11.45	85.1	0.96	112	108	37	-
STO131390L_09	4.1797	0.97	0.29828	0.94	0.40	3.35255465	0.94	0.10163	1.04	1654	19.12	1670	7.96	1682.8	13.85	101.7	0.59	343	203	131	-
STO131390L_10	0.53797	1.34	0.06893	0.96	0.28	14.5074713	0.96	0.0566	1.41	475.3	31.11	437.1	4.77	429.7	4.01	90.4	0.00	127	0	9	-
STO131390L_11	4.11824	1.03	0.29395	0.95	0.39	3.40193911	0.95	0.10161	1.09	1653.7	20.09	1657.9	8.39	1661.2	13.84	100.5	0.88	68	60	27	-
STO131390L_12	4.05634	0.98	0.2936	0.94	0.40	3.40599455	0.94	0.1002	1.05	1627.8	19.27	1645.6	7.96	1659.5	13.71	101.9	0.25	523	133	180	-
STO131390L_13	1.12917	1.00	0.10508	0.94	0.40	9.51655881	0.94	0.07793	1.07	1145.2	21.01	767.4	5.38	644.1	5.75	56.2	0.14	461	67	54	-
STO131390L_14	3.44838	1.03	0.25392	0.95	0.39	3.93824827	0.95	0.09849	1.10	1595.8	20.38	1515.5	8.14	1458.7	12.35	91.4	0.77	109	84	37	-
STO131390L_15	0.49933	0.99	0.06476	0.94	0.40	15.4416306	0.94	0.05592	1.06	448.8	22.79	411.2	3.34	404.5	3.67	90.1	0.01	1255	17	86	-
STO131390L_16	1.05489	0.97	0.10409	0.93	0.41	9.6070708	0.93	0.0735	1.03	1027.7	20.78	731.3	5.05	638.3	5.69	62.1	0.15	5675	830	665	0
STO131390L_17	0.49941	1.05	0.06505	0.94	0.38	15.3727902	0.94	0.05568	1.11	439.3	24.14	411.3	3.56	406.3	3.71	92.5	0.02	1163	20	80	-
STO131390L_18	0.51777	1.60	0.06823	0.98	0.25	14.6563095	0.98	0.05504	1.65	413.6	36.35	423.7	5.52	425.5	4.07	102.9	0.00	155	0	11	7
STO131390L_19	3.39531	1.06	0.24666	0.95	0.38	4.05416363	0.95	0.09984	1.12	1621	20.72	1503.3	8.31	1421.2	12.14	87.7	0.05	239	11	66	-
STO131390L_20	4.07004	1.04	0.29269	0.95	0.39	3.4165841	0.95	0.10085	1.10	1639.8	20.24	1648.3	8.44	1655	13.85	100.9	0.86	67	58	26	-
STO131390L_21	0.49295	1.01	0.06504	0.94	0.39	15.3751538	0.94	0.05497	1.07	410.8	23.51	406.9	3.38	406.2	3.70	98.9	0.00	709	3	49	-
STO131390L_22	0.50727	1.00	0.06651	0.95	0.40	15.035333	0.95	0.05531	1.07	424.7	23.29	416.6	3.40	415.1	3.78	97.7	0.01	1046	8	74	-
STO131390L_23	0.50458	1.13	0.06591	0.96	0.36	15.1722045	0.96	0.05552	1.19	432.9	25.88	414.8	3.86	411.5	3.79	95.1	0.01	165	1	12	-
STO131390L_24	0.49305	1.07	0.06527	0.95	0.37	15.3209744	0.95	0.05478	1.13	403.4	24.81	407	3.58	407.6	3.73	101.0	0.01	280	2	19	-

....

Table STO131391L

Analysis_#	Pb207_U235	1s%	Pb206_U238	1s%	roh	238/206	1s%	207/206	1s%	Pb207_Pb206	1s	Pb207_U235	1s	Pb206_U238	1s	conc	Th/U	U*	Th*	Ptot*	>LLD (%)
			Concordia output			Tera-Wasserburg output						Age estimates (ma)						Concentrations			Pb com.
STO131391L_04	1.18177	1.00	0.10839	0.94	0.40	9.22594335	0.94	0.07908	1.06	1174.1	20.75	792.1	5.49	663.4	5.96	56.5	0.05	751	39	90	-
STO131391L_05	1.16272	1.04	0.10774	0.95	0.39	9.28160386	0.95	0.07827	1.10	1153.7	21.58	783.2	5.66	659.6	5.95	57.2	0.18	662	119	86	1
STO131391L_06	0.51314	1.03	0.06701	0.94	0.40	14.9231458	0.94	0.05554	1.08	433.8	23.99	420.6	3.55	418.1	3.84	96.4	0.02	794	13	56	-
STO131391L_07	3.94663	1.01	0.28867	0.95	0.41	3.46416323	0.95	0.09916	1.06	1608.4	19.66	1623.3	8.14	1634.9	13.69	101.6	1.32	464	612	201	-
STO131391L_08	0.50332	1.03	0.06537	0.95	0.39	15.2975371	0.95	0.05584	1.09	445.8	23.54	413.9	3.50	408.2	3.75	91.6	0.02	1049	24	73	-
STO131391L_09	1.2948	1.01	0.11597	0.95	0.41	8.62291972	0.95	0.08098	1.06	1220.9	20.78	843.4	5.78	707.3	6.35	57.9	0.15	602	92	83	-
STO131391L_10	1.97089	1.00	0.15666	0.95	0.42	6.38325035	0.95	0.09125	1.05	1451.6	19.97	1105.6	6.75	938.2	8.28	64.6	0.29	554	159	107	-
STO131391L_11	0.50994	1.02	0.06569	0.94	0.41	15.2230172	0.94	0.05631	1.07	463.7	23.76	418.4	3.50	410.1	3.77	88.4	0.03	857	23	60	-
STO131391L_12	0.50009	1.04	0.06481	0.96	0.41	15.4297176	0.96	0.05596	1.09	450.6	23.74	411.8	3.52	404.8	3.73	89.8	0.03	516	14	36	-
STO131391L_13	0.5061	1.04	0.06656	0.95	0.40	15.0240385	0.95	0.05515	1.09	418.2	23.95	415.8	3.53	415.4	3.82	99.3	0.03	857	25	61	-
STO131391L_14	0.47594	1.07	0.06162	0.96	0.39	16.2284972	0.96	0.05602	1.12	453	24.48	395.3	3.52	385.4	3.57	85.1	0.05	940	48	62	-
STO131391L_15	3.15239	1.04	0.23433	0.96	0.40	4.26748602	0.96	0.09757	1.10	1578.2	20.4	1445.6	8.05	1357.2	11.70	86.0	0.60	250	150	77	-
STO131391L_16	0.51496	1.04	0.06665	0.95	0.40	15.0037509	0.95	0.05604	1.09	453.6	23.68	421.8	3.58	415.9	3.83	91.7	0.03	1099	33	78	-
STO131391L_17	0.49875	1.05	0.06576	0.96	0.41	15.2068127	0.96	0.05501	1.09	412.6	24.15	410.9	3.54	410.6	3.79	99.5	0.05	920	46	65	-
STO131391L_18	0.48751	1.04	0.06372	0.96	0.40	15.6936598	0.96	0.05549	1.10	431.9	24.13	403.2	3.47	398.2	3.68	92.2	0.12	603	70	42	-
STO131391L_19	0.54182	1.05	0.06887	0.96	0.40	14.5201104	0.96	0.05706	1.10	493.3	24.4	439.6	3.75	429.4	3.96	87.0	0.02	1048	23	77	2
STO131391L_20	0.51364	1.08	0.06699	0.96	0.38	14.9276011	0.96	0.05561	1.13	436.5	24.49	420.9	3.72	418	3.87	95.8	0.02	1080	19	77	1
STO131391L_21	0.51548	1.04	0.06793	0.96	0.40	14.7210364	0.96	0.05504	1.09	413.7	23.85	422.1	3.58	423.7	3.91	102.4	0.01	1386	20	100	-
STO131391L_22	1.95429	1.01	0.15898	0.95	0.41	6.29009938	0.95	0.08916	1.07	1407.5	20.21	1099.9	6.82	951.1	8.43	67.6	0.50	580	287	124	-
STO131391L_23	0.50798	1.09	0.06548	0.96	0.39	15.2718887	0.96	0.05627	1.14	462.3	25.16	417.1	3.72	408.8	3.79	88.4	0.04	1219	50	85	1
STO131391L_24	0.4898	1.02	0.06517	0.95	0.42	15.3444837	0.95	0.05451	1.06	392.1	23.68	404.8	3.40	407	3.76	103.8	0.08	2150	171	151	-

....

188

Table: Analysis 1278941 — Isotope ratios, Age estimates, Concentrations

Analysis #	Concordia output Pb207/U235	1s%	Pb206/U238	1s%	roh	Tera-Wasserburg 238/206	1s%	207/206	1s%	Age Pb207/Pb206	1s	Pb207/U235	1s	Pb206/U238	1s	conc	Th/U	U*	Th*	Phot*	Pb com. >LLD (%)
1278941_01	4.16719	0.96	0.296677	0.93	0.41	3.369612831	0.93	0.10183	1.03	1657.7	19.05	1667.6	7.89	1675.3	13.73	101.1	1.16	263	304	112	-
1278941_02	0.50437	1.01	0.06716	0.94	0.38	14.88981537	0.94	0.05446	1.08	390.1	23.97	414.7	3.43	419	3.78	107.4	0.00	733	2	52	-
1278941_03	0.52374	0.98	0.06742	0.93	0.40	14.83239395	0.93	0.05633	1.05	464.7	23.22	427.6	3.42	430.6	3.79	90.5	0.00	1290	3	92	-
1278941_04	0.50188	1.02	0.06617	0.94	0.38	15.11258879	0.94	0.055	1.09	412.2	24.01	413	3.47	413.1	3.74	100.2	0.01	396	5	28	-
1278941_05	0.48821	1.07	0.06488	0.94	0.37	15.41307028	0.94	0.05457	1.14	394.7	25.25	403.7	3.57	405.2	3.68	102.7	0.00	292	1	20	-
1278941_06	0.50213	1.01	0.06575	0.93	0.38	15.20912548	0.93	0.05538	1.08	427.5	23.85	413.1	3.43	410.5	3.71	96.0	0.00	478	1	33	-
1278941_07	0.50177	1.01	0.0664	0.93	0.39	15.06024096	0.93	0.0548	1.08	404.2	23.7	412.9	3.42	414.4	3.74	102.5	0.00	547	1	38	-
1278941_08	4.26005	0.96	0.30276	0.93	0.40	3.302946228	0.93	0.10204	1.04	1661.6	19.05	1685.7	7.93	1705	13.96	102.6	1.65	298	492	143	-
1278941_09	4.21289	0.98	0.29744	0.93	0.40	3.362022593	0.93	0.10271	1.05	1673.7	19.28	1676.5	8.03	1678.6	13.81	100.3	1.15	138	159	59	-
1278941_10	0.50635	1.06	0.06714	0.94	0.37	14.89425082	0.94	0.05491	1.13	408.4	24.81	417.3	3.62	418.9	3.80	102.6	0.01	634	3	45	1
1278941_11	4.2445	0.99	0.29805	0.94	0.40	3.355141755	0.94	0.10327	1.06	1683.8	19.38	1682.7	8.11	1681.6	13.85	99.9	0.62	124	77	47	-
1278941_12	0.5429	0.97	0.06773	0.93	0.39	14.76450613	0.93	0.05813	1.05	534.1	23.17	440.3	3.47	422.5	3.81	79.1	0.02	2421	58	175	1
1278941_13	0.5101	1.07	0.06728	0.94	0.37	14.86325803	0.94	0.05498	1.13	411.4	24.95	418.5	3.66	419.8	3.81	102.0	0.00	387	2	28	-
1278941_14	0.53302	1.13	0.06947	0.94	0.35	14.39470275	0.94	0.05564	1.19	437.9	25.86	433.8	3.97	432.9	3.94	98.9	0.02	503	10	37	2
1278941_15	0.50829	1.03	0.06534	0.93	0.38	15.30456076	0.93	0.05641	1.10	467.9	24.42	417.3	3.54	408	3.70	87.2	0.01	600	6	42	-
1278941_16	0.50231	1.03	0.06585	0.94	0.38	15.18602885	0.94	0.05532	1.10	425.1	23.97	413.3	3.51	411.1	3.73	96.7	0.00	361	1	25	-
1278941_17	0.49107	0.99	0.06432	0.93	0.39	15.54726368	0.93	0.05536	1.07	426.7	23.42	405.6	3.32	401.9	3.64	94.2	0.06	746	46	51	-
1278941_18	4.2088	1.00	0.30075	0.94	0.39	3.325020781	0.94	0.10149	1.07	1651.5	19.71	1675.7	8.22	1695	13.99	102.6	0.88	153	134	62	-
1278941_19	0.49103	1.01	0.06465	0.93	0.37	15.4679041	0.93	0.05508	1.09	415.4	23.77	405.6	3.38	403.8	3.66	97.2	0.00	509	2	35	-
1278941_20	0.56211	1.19	0.07498	0.95	0.34	13.33688984	0.95	0.05437	1.25	386.2	28.03	452.9	4.36	466.1	4.26	120.7	0.00	299	1	24	-
1278941_21	3.998	0.98	0.28518	0.94	0.40	3.50655762	0.94	0.10167	1.05	1654.8	19.3	1633.8	7.95	1617.4	13.38	97.7	0.26	232	61	78	1
1278941_22	0.50999	0.98	0.06556	0.93	0.40	15.25320317	0.93	0.05641	1.05	467.8	23.29	418.4	3.37	409.4	3.70	87.5	0.01	971	10	68	-
1278941_23	3.99808	0.99	0.28652	0.94	0.39	3.490157755	0.94	0.10099	1.06	1642.4	19.45	1632.2	8.00	1624.1	13.44	98.9	1.14	282	320	116	1
1278941_24	4.16046	0.97	0.2957	0.93	0.40	3.381805884	0.93	0.10203	1.04	1660.4	19.11	1666.3	7.94	1670	13.74	100.5	1.16	232	270	99	-

Table: Analysis 1278951 — Isotope ratios, Age estimates, Concentrations

Analysis #	Concordia output Pb207/U235	1s%	Pb206/U238	1s%	roh	Tera-Wasserburg 238/206	1s%	207/206	1s%	Age Pb207/Pb206	1s	Pb207/U235	1s	Pb206/U238	1s	conc	Th/U	U*	Th*	Phot*	Pb com. >LLD (%)
1278951_04	0.5286	2.10	0.06465	1.05	0.18	15.4679041	1.05	0.05929	2.18	577.8	46.59	430.9	7.39	403.9	4.09	69.9	0.02	30	1	2	-
1278951_05	0.48727	2.14	0.0636	1.04	0.17	15.7232704	1.04	0.05556	2.21	434.6	48.16	403.1	7.13	397.5	4.01	91.5	0.02	34	1	2	-
1278951_06	0.51927	1.96	0.06475	1.02	0.19	15.4440154	1.02	0.05816	2.03	535.3	44.36	424.7	6.80	404.4	4.02	75.5	0.01	41	0	3	-
1278951_07	0.49816	2.58	0.06377	1.10	0.15	15.6813549	1.10	0.05665	2.65	477.1	57.76	410.5	8.70	398.5	4.25	83.5	0.04	27	1	2	-
1278951_08	0.50176	2.21	0.06361	1.05	0.18	15.7207986	1.05	0.0572	2.27	498.9	49.96	412.9	7.49	397.5	4.05	79.7	0.02	30	1	2	46
1278951_09	0.49897	2.03	0.06509	1.03	0.18	15.3633431	1.03	0.05559	2.10	435.8	45.61	411	6.86	406.5	4.06	93.3	0.01	40	1	3	-
1278951_10	0.50396	3.72	0.06391	1.27	0.10	15.6470036	1.27	0.05719	3.81	498.1	82.49	414.4	12.67	399.4	4.92	80.2	0.01	23	0	2	-
1278951_11	2.94294	1.06	0.21684	0.95	0.37	4.61169526	0.95	0.09843	1.13	1594.5	20.84	1393	8.01	1265.1	10.89	79.3	0.26	86	22	22	-
1278951_12	3.63173	1.26	0.25851	0.95	0.31	3.86832231	0.95	0.10188	1.32	1658.7	29.12	1556.5	8.10	1482.2	12.48	93.9	0.01	107	1	7	-
1278951_13	0.48254	2.56	0.06548	1.08	0.40	15.2718389	1.08	0.05345	2.64	347.7	58.51	399.8	8.46	408.8	4.32	117.6	0.60	174	104	58	-
1278951_14	0.4936	2.06	0.06288	1.03	0.14	15.9033079	1.03	0.05693	2.13	488	46.37	407.4	6.91	393.1	3.94	80.6	0.02	32	1	2	-
1278951_15	0.52738	2.65	0.06363	1.12	0.19	15.7158573	1.12	0.0601	2.73	607.3	57.81	430.1	9.28	397.7	4.28	65.5	0.02	33	1	2	-
1278951_16	0.51574	2.04	0.06349	1.04	0.13	15.7505119	1.04	0.05891	2.10	563.6	45.21	422.3	7.03	396.8	3.98	70.4	0.02	25	0	2	-
1278951_17	0.5069	2.43	0.06532	1.08	0.19	15.37279016	1.08	0.0564	2.50	467.6	55.01	415.7	8.29	406.2	4.26	86.9	0.02	33	1	2	-
1278951_18	0.4839	2.56	0.06337	1.09	0.15	15.79279848	1.09	0.05542	2.63	429	57.18	400.7	8.46	395.8	4.20	92.3	0.03	32	1	2	-
1278951_19	0.50195	2.20	0.06253	1.06	0.14	15.7803377	1.06	0.05744	2.26	508	49.54	413	7.47	396.1	4.03	78.0	0.02	30	1	2	-
1278951_20	0.47188	1.99	0.06506	1.02	0.18	15.99232368	1.02	0.05473	2.06	401.3	45.08	392.5	6.48	391	3.88	97.4	0.02	31	1	2	-
1278951_21	0.5089	2.19	0.0639	1.05	0.18	15.3704273	1.05	0.05673	2.26	480.3	49.45	417.7	7.50	406.3	4.15	84.6	0.02	36	1	2	-
1278951_22	0.50357	2.01	0.06506	1.03	0.17	15.64945227	1.03	0.05715	2.08	496.7	44.9	414.1	6.82	399.3	3.99	80.4	0.01	38	1	3	-
1278951_23	0.49043	3.32	0.06371	1.19	0.11	15.69612306	1.19	0.05582	3.40	445	73.95	405.2	11.09	398.2	4.60	89.5	0.01	35	0	2	-

189

Table 1

Analysis #	Concordia output					Tera-Wasserburg output				Age estimates (ma)							Concentrations				Pb com.
	Pb207 U235	1s%	Pb206 U238	1s%	roh	238/206	1s%	207/206	1s%	Pb207 Pb206	1s	Pb207 U235	1s	Pb206 U238	1s	conc	Th/U	U*	Th*	Pbtot*	>LLD (%)
197578L_04	3.551	1.02	0.257	0.95	0.39	3.89105058	0.95	0.1002	1.09	1627.9	20.01	1538.7	8.10	1474.5	12.48	90.6	0.80	113	90	39	2
197578L_05	3.99987	1.00	0.28718	0.94	0.41	3.48213664	0.94	0.10101	1.06	1642.7	19.5	1634.2	8.10	1627.4	13.56	99.1	0.77	501	387	191	0
197578L_06	3.8727	1.02	0.27547	0.95	0.40	3.63015936	0.95	0.10195	1.08	1660	19.93	1608	8.26	1568.5	13.19	94.5	0.84	108	90	40	2
197578L_07	0.48986	1.06	0.06481	0.94	0.38	15.4297176	0.94	0.05481	1.11	404.5	24.6	404.8	3.53	404.8	3.71	100.1	0.00	668	1	46	2
197578L_08	0.50493	1.15	0.06606	0.95	0.35	15.1377536	1.00	0.05543	1.21	429.3	26.59	415	3.91	412.4	3.80	96.1	0.00	258	0	18	-
197578L_09	3.46354	1.33	0.25525	1.00	0.31	3.91772772	1.00	0.09841	1.39	1594.1	25.69	1519	10.48	1465.5	13.11	91.9	0.72	46	33	16	7
197578L_10	0.50163	1.11	0.06592	0.96	0.36	15.1699029	0.96	0.05519	1.18	419.7	25.8	412.8	3.78	411.5	3.79	98.0	0.00	231	0	16	6
197578L_11	4.11039	1.14	0.28958	0.97	0.36	3.45327716	0.97	0.10294	1.18	1677.8	22.02	1656.4	9.34	1639.4	14.02	97.7	0.61	54	33	20	-
197578L_12	3.95209	1.08	0.2763	0.96	0.38	3.61925443	0.96	0.10373	1.20	1692	20.86	1624.4	8.75	1572.7	13.36	92.9	0.90	63	56	24	5
197578L_13	0.50196	1.23	0.06614	0.95	0.33	15.1194436	0.95	0.05504	1.29	413.8	28.37	413	4.18	412.8	3.84	99.8	0.00	312	1	22	3
197578L_14	0.71282	1.10	0.07906	0.95	0.36	12.6486213	0.95	0.06539	1.16	786.9	24.12	546.4	4.64	490.5	4.49	62.3	0.06	259	15	23	3
197578L_15	0.50759	1.09	0.06651	0.95	0.38	15.035333	0.95	0.05535	1.14	426.1	25.28	416.8	3.72	415.1	3.81	97.4	0.00	287	1	20	4
197578L_16	4.09191	1.00	0.28749	0.94	0.41	3.47838186	0.94	0.10322	1.06	1682.8	19.4	1652.7	8.14	1629	13.59	96.8	0.66	334	220	125	1
197578L_17	0.49848	1.04	0.06523	0.95	0.39	15.3303695	0.95	0.05542	1.10	428.9	24.28	410.7	3.52	407.4	3.73	95.0	0.00	546	2	38	-
197578L_18	1.03617	1.08	0.09925	0.95	0.38	10.0755668	0.95	0.07571	1.14	1087.4	22.69	722	5.58	610	5.54	56.1	0.09	172	16	20	-
197578L_19	0.65708	1.80	0.07534	1.02	0.21	13.2731617	1.02	0.06325	1.87	716.6	39.04	512.8	7.23	468.2	4.63	65.3	0.04	118	4	10	-
197578L_20	3.36756	1.12	0.24496	0.96	0.37	4.08229915	0.96	0.0997	1.17	1618.4	21.76	1496.9	8.77	1412.4	12.22	87.3	0.70	89	62	29	-
197578L_21	0.59903	1.16	0.07197	0.96	0.34	13.8946783	0.96	0.06036	1.23	616.5	26.13	476.6	4.42	448	4.14	72.7	0.01	148	1	11	6
197578L_22	0.49479	1.08	0.065	0.95	0.37	15.3846154	0.95	0.05521	1.14	420.4	24.95	408.2	3.61	406	3.73	96.6	0.00	353	1	24	3
197578L_23	0.48352	1.08	0.06383	0.96	0.37	15.6666144	0.96	0.05494	1.15	409.7	25	400.5	3.57	398.8	3.67	97.3	0.00	480	1	32	-
197578L_24	3.09485	1.03	0.22843	0.95	0.40	4.37770871	0.95	0.09826	1.09	1591.3	20.15	1431.4	7.88	1326.3	11.37	83.3	0.74	147	108	45	-

Table 2

Analysis #	Concordia output					Tera-Wasserburg output				Age estimates (ma)							Concentrations				Pb com.
	Pb207 U235	1s%	Pb206 U238	1s%	roh	238/206	1s%	207/206	1s%	Pb207 Pb206	1s	Pb207 U235	1s	Pb206 U238	1s	conc	Th/U	U*	Th*	Pbtot*	>LLD (%)
200998_04	4.03964	0.99	0.29079	0.94	0.40	3.438907803	0.94	0.10075	1.05	1637.9	19.39	1642.2	8.03	1645.5	13.64	100.5	0.83	269	224	106	-
200998_05	4.14326	0.99	0.29495	0.94	0.41	3.390405153	0.94	0.10187	1.05	1658.5	19.33	1662.9	8.07	1666.2	13.80	100.5	0.86	207	178	84	-
200998_06	4.26553	1.00	0.29701	0.94	0.41	3.366890004	0.94	0.10415	1.06	1699.4	19.41	1686.7	8.19	1676.4	13.90	98.6	0.79	185	147	74	-
200998_07	3.66158	1.05	0.2641	0.95	0.39	3.767755548	0.95	0.10005	1.11	1625	20.55	1563	8.37	1517.4	12.84	93.4	0.50	105	52	35	-
200998_08	3.99401	0.98	0.28178	0.94	0.40	3.548867911	0.94	0.10279	1.05	1675.1	19.24	1633	7.98	1600.3	13.31	95.5	0.84	306	258	117	-
200998_09	4.11254	1.01	0.29089	0.95	0.40	3.437725601	0.95	0.10253	1.07	1670.4	19.75	1656.8	8.26	1646	13.71	98.5	0.84	101	85	40	-
200998_10	3.99278	1.04	0.28046	0.95	0.39	3.565570848	0.95	0.10325	1.09	1683.3	20.14	1632.7	8.41	1593.7	13.39	94.7	0.67	161	108	59	-
200998_11	4.15904	1.03	0.29095	0.95	0.39	3.43701667	0.95	0.10367	1.10	1690.8	20.09	1666	8.47	1646.3	13.77	97.4	0.64	288	183	108	-
200998_12	3.83022	1.01	0.27195	0.95	0.39	3.677146534	0.95	0.10214	1.08	1663.4	19.74	1599.1	8.14	1550.7	13.01	93.2	0.69	185	127	66	-
200998_13	2.58105	1.00	0.1969	0.94	0.40	5.078720163	0.94	0.09506	1.06	1529.3	19.9	1295.3	7.32	1158.7	9.99	75.8	0.51	258	133	66	1
200998_14	4.18847	1.10	0.29732	0.96	0.37	3.363379524	0.96	0.10216	1.16	1663.8	21.27	1671.8	8.99	1678	14.17	100.9	0.84	135	113	55	-
200998_15	3.91086	1.08	0.27713	0.96	0.38	3.608414823	0.96	0.10234	1.13	1667	20.88	1615.9	8.69	1576.9	13.36	94.6	0.53	131	70	46	-
200998_16	4.06596	0.99	0.28626	0.94	0.41	3.493327744	0.94	0.10301	1.05	1679	19.26	1647.5	8.04	1622.8	13.49	96.7	1.45	280	405	121	-
200998_17	3.51832	1.17	0.25368	0.97	0.35	3.94197414	0.97	0.10058	1.23	1634.8	22.74	1531.3	9.27	1457.4	12.67	89.1	0.49	106	52	34	-
200998_18	4.14923	0.99	0.28926	0.94	0.40	3.45709742	0.94	0.10403	1.06	1697.2	19.33	1664.1	8.12	1637.8	13.62	96.5	1.39	209	291	92	-
200998_19	2.44958	1.03	0.18771	0.95	0.39	5.32736668	0.95	0.09464	1.10	1520.8	20.5	1257.3	7.44	1109	9.64	72.9	0.51	116	60	28	-
200998_20	3.78617	1.00	0.27245	0.94	0.40	3.67039824	0.94	0.10078	1.06	1638.5	19.59	1589.8	8.03	1553.2	13.01	94.8	0.67	299	200	106	-
200998_21	3.21575	0.99	0.23546	0.94	0.40	4.24700586	0.94	0.09904	1.06	1606.2	19.58	1461	7.70	1363.1	11.57	84.9	0.78	353	277	111	1
200998_22	4.10909	1.08	0.29312	0.96	0.38	3.41157205	0.96	0.10166	1.14	1654.7	21.06	1656.1	8.85	1657.1	13.99	100.1	0.74	114	85	44	-
200998_23	3.86068	1.00	0.27668	0.94	0.40	3.61428365	0.94	0.10119	1.07	1646.1	19.66	1605.5	8.10	1574.6	13.18	95.7	1.05	143	151	56	-
200998_24	4.11212	1.00	0.29404	0.94	0.40	3.40089784	0.94	0.10142	1.06	1650.3	19.63	1656.7	8.20	1661.7	13.82	100.7	0.79	147	116	58	-

7.3 Appendix E – Thinsections

E1: Petroligical description of additional samples

Sample: 1 – 22 (1Gn)   **Location:** 454 657, 6 971 125

**Rock name:** Augen gneiss *(Granititc biotite gneiss, with titanite porphyroclasts)*

Mineralogy:

Orthoclase, 0,5 – 4mm, mode of 25%. Plagioclase with distinctive twinning, 0,5 – 3mm, mode of 20%. Perthite lamella, myrmekite and major seritization observed in the feldspars. Quarts, ~ 0,5, mode of 15%. Biotite laths, ~ 1mm, mode of 15%. Titanite, 1 – 2 mm, mode of 10%. Chlorite, very altered, ~ 1mm, mode of 5%. Epidote, 0,5 – 1 mm, mode of ~5%. Opaque mineral interpreted to be oxides, 0,5 – 1 mm, mode of 5%. Observations of accessory muscovite.

Textures:

Granitic texture, with seriate, interbolate grains. Some nematoblastic foliation, mainly due to oriented titanite. Highly retrograde, loots of secondary alteration products distorting primary texture.
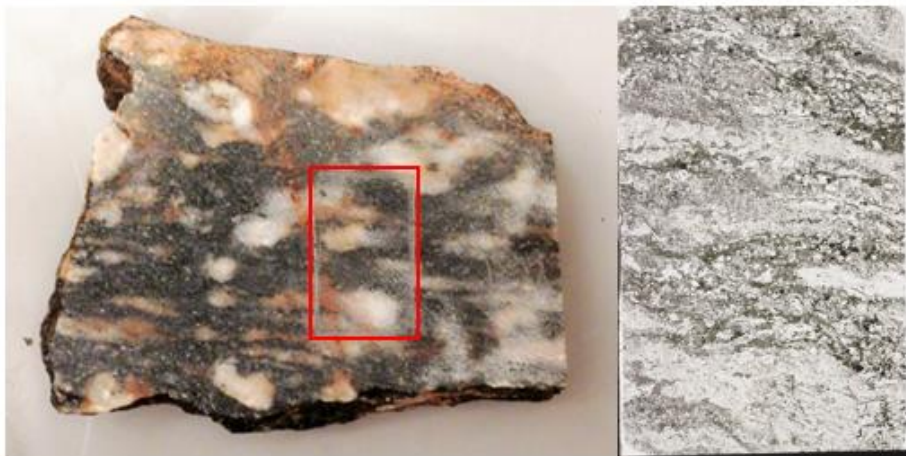
Figure E1: *Handsample collected at location 9. With red square marking location of made thinsection. Scan of thin section illustrated on the righthand side.*

Sample: 1 – 23 (3C)   **Location:** 454937, 6 968 691

Rock name: Mafic dike in porphyritic granitic gneiss (*amphibole biotite dike*)

Note: sample of dike and host-rock contact.

Mineralogy:

Quartz, 0,2 – 3 mm, mode of ~ 20%. Orthoclase, 0,5 – 5 mm, mode of 20%, with some secondary alteration and myrmekite. Biotite laths, 0,2 – 2mm, mode of 20%. Plagioclase, distinctive twinning 10%. Green amphibole, ~ 2mm, mode of 15%. Microcline, ~ 0,5mm, mode of 4%. Chlorite, alteration of primary biotite, mode of 4%. Epidote, ~ 0,5mm, mode of 4%. Opaque mineral interpreted to be oxide, ~ 0,1, mode of 2%. Zircon, ~ 0,2mm, mode of 1%. Apatite and clinozoisite observed as accessory phases.

Textures:

Inequigranular, interbolate grains. Mafic mineral likely to quench growth of the felsic minerals in darker areas. Slight nematoblastic foliation. Notably the presence of amphibole and zircon separating dike and host-rock.
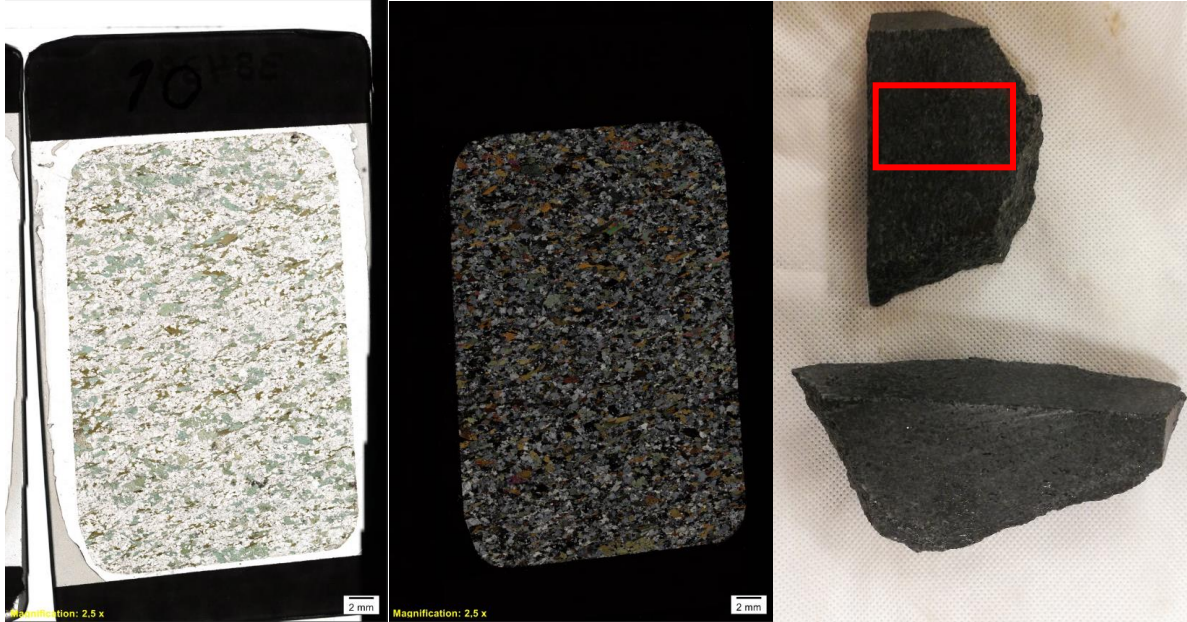

Figure 11: Handsample collected at location 10. With red square marking location of made thin-section. Scan of thin section illustrated on the righthand side.

E2: Remaining thinsections part 1: Normal light, cross-polarised & hand sample

Sample: 200960   **Location:** 455 165, 6 968 440
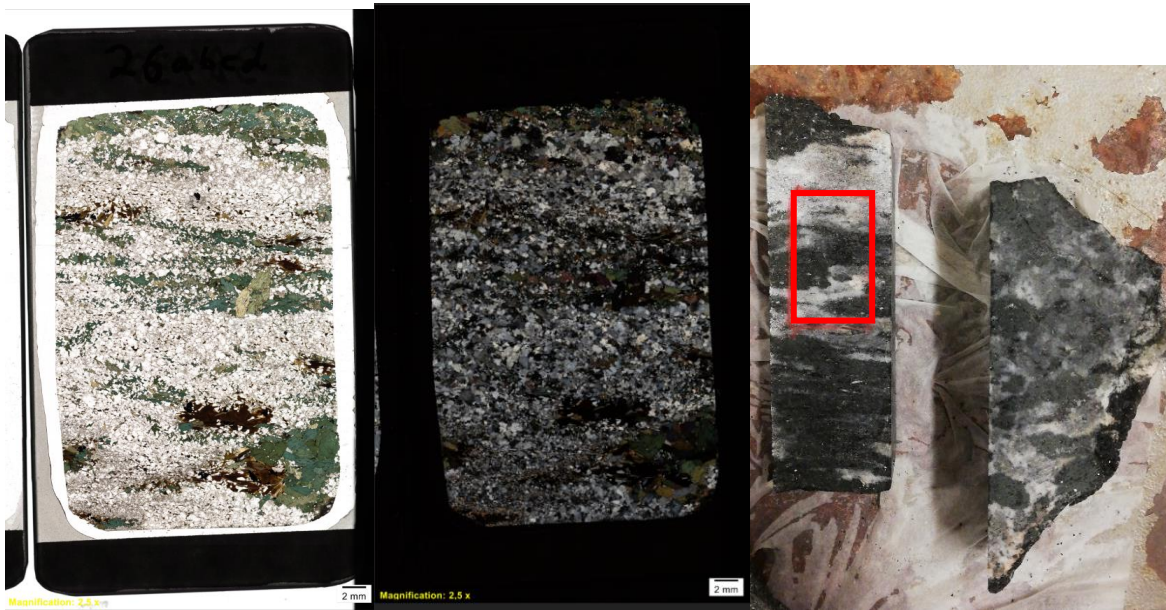

Sample: 200965   **Location:** 451 128, 6 965 070

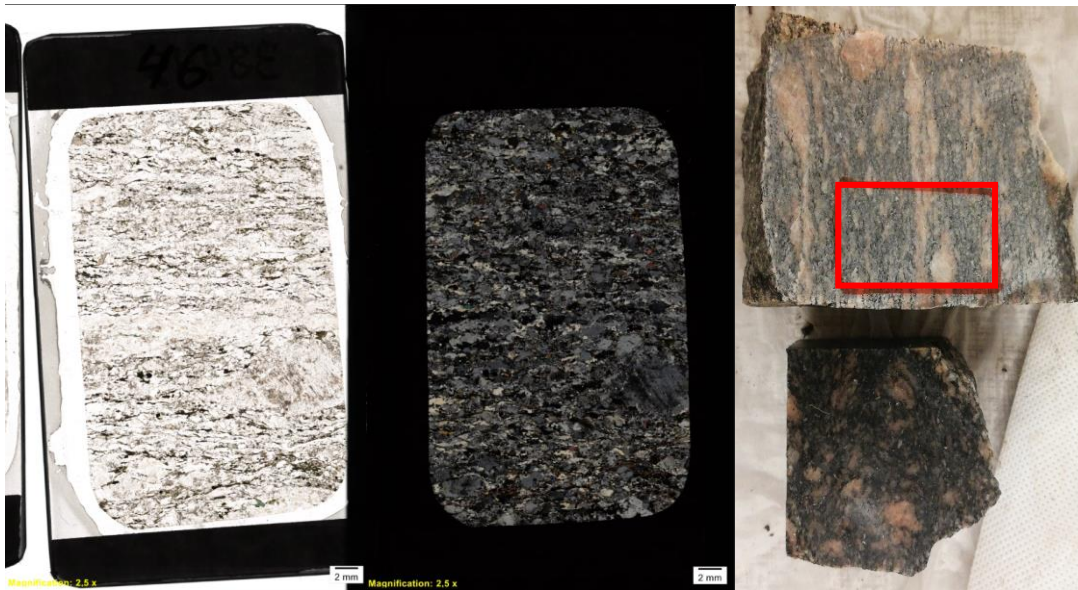**Sample:** 200976   **Location:** 454 129,   6 968 513

Sample: 200987   **Location:** 454 984,   6 968 894

Sample: 200996   **Location:** 454 671, 6 970 564

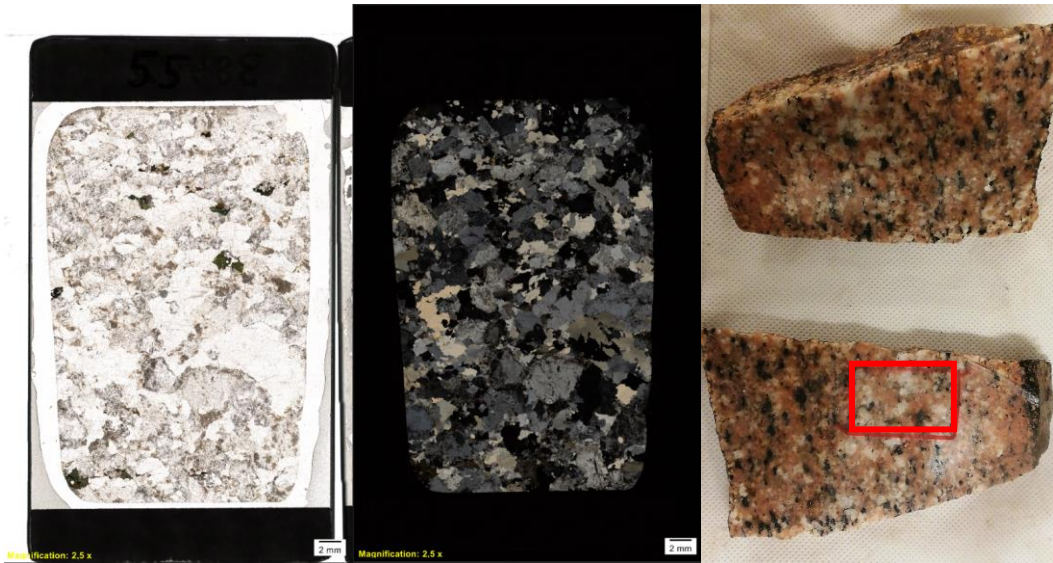**Sample:** 200998   **Location:** 455 072,   6 968 397

Sample: 197554   **Location:** 455 650, 6 967 229

Sample: 197555   **Location:** 449 940, 6 960 684

Sample: 197562

Location: 450 011, 6 960 762

Sample: 197578

Location: 451 403, 6 962 671

Sample: 197586   **Location:** 457 734, 6 964 449

Sample: 197590   **Location:** 455 648, 6 967 143

E3: Remaining thin sections part 2: Photograph & hand sample

Sample: 197551 **Location:** 455 658, 6 967 099

Sample: 200986 **Location:** 454 792, 6 970 110

Sample: 200959 **Location:** 455 209, 6 964 413

Sample: 200975   **Location:** 454 247, 6 968 504

Sample: 200973   **Location:** 454 245,   6 968 520

Sample: 197569   **Location:** 454 058, 6 962 877

Sample: 200994   **Location:** 453 943,   6 962 992

Sample: 200974   **Location:** 454 246,   6 968 518

Sample: 200955   **Location:** 449 245,   6 961 979
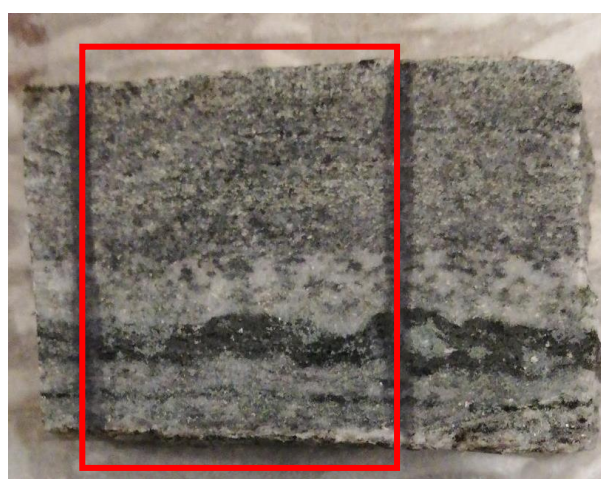
Sample: 201000   **Location:** 455 086, 6 967 548

Sample: 200963   **Location:** 455 133, 6 963 487

Sample: 200982   **Location:** 454 797, 6 969 939

202